Fabrication and Characterisation of Regular and Complex Shapes Alumina from Aluminium Foil by PEO Process

This dissertation submitted in partial fulfilment of the requirements for the degree of Doctor of Philosophy

by

Husein Meshreghi

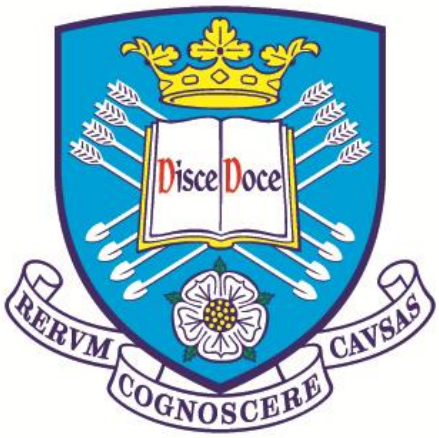

The University Of Sheffield.

Department of Materials Science and Engineering

November 2017

ABSTRACT

Alumina thick and thin films can be used for a variety of purposes, including the semiconductors, electronics, dielectric, piezoelectric and ferromagnetic devices. The films can be produced by conventional methods such as tape casting and roll compaction from ceramic slurry. However, these methods offer limited part geometries and cause defects in the film structure. Plasma electrolytic oxidation (PEO) is a surface engineering technique that converts the surface of light metals and alloys into oxide ceramics layers. In this study, ceramic alumina films were produced by conversion of different shapes aluminium foil (50 μm) substrate using PEO technique.

The influence of processing conditions, such as (treatment time, electrolyte composition, current density and sample shape), on the formation, growth behaviour and properties of PEO coatings were investigated. Optical emission spectroscopy was used to investigate the composition of plasma discharge and evolution of its main components during the PEO process. The plasma electron temperature was calculated using two independent peaks of aluminium in the near ultraviolet band.

COMSOL Multiphysics software was used to model the distribution of electric field in the electrolyser and investigate a possibility of achieving a uniform coating thickness on complex shape in several electrode configurations. The surface morphology and phase composition of ceramic coatings were analysed using SEM and XRD techniques. The breakdown voltages, thickness of ceramic coatings in different electrolyte were comparatively studied.

Depending on the treatment parameters the metal-to-ceramic conversion ratio varies from 10 to 80 %. However, after a treatment for 12 min, complete conversion of aluminium foil into alumina was successfully achieved.

The shape of working electrodes strongly influenced the coating thickness. Gamma alumina was the prominent phase in thin coatings, however formation of alpha-alumina was observed when treatments lasted longer than 6 min. Correlations have been studied between characteristics of plasma discharge, such as plasma electron temperature, and phase transitions in the surface layer to develop in situ diagnostic methods for the PEO processes.

The L and U shaped thin-walled 3D ceramic-metal composite structures were successfully fabricated using PEO treatments in specific electrolyte with uniform PEO coatings without cracks grown on the edges and corners at outer surfaces of L and U shape Al foil samples. However, the coating thickness at the inner surfaces was around 30 % lower.

ACKNOWLEDGMENTS

I would like to express my whole-hearted gratitude to my supervisor Dr. Aleksey Yerokhin and prof. Allan Matthews for their instructive and excellent supervision during my studies and research work, as well as their kindness and patience. Also i would like to express my deepest gratitude to Dr. Adrian Leyland for his advice and continuous support.

My sincere thanks also goes to my friend Mr. M. Gorbatkov and Prof. E.V. Parfenov at Ufa State Aviation Technical University-Russia who were involved in (Chapter 7) for their support, help and useful discussions.

Part of the work related to nuclear magnetic resonance experiments in (Chapter 5) has been performed with Department of Chemistry-University of Durham, UK. I would like to thank researchers at this department, D. Apperley and F. Markwell for their help

My gratitude also goes to members of the Research Centre in Surface Engineering (Dr. Chen Jui Liang, Dr. Fahima Indeir, Dr. Ming Sun, Dr. Chang Liu, Dr, Lian Liu, Dr, Lian Liu and N. Yaakop).

I would like to express my love and most sincere gratitude to my wife for her unlimited and unconditional support and encouragement; for her understanding and patience to share with me this experience. This work is dedicated to her, my sons Abdulalghani, Mohammed and my daughters Aisha, Asmaa and Eman.

I gratefully acknowledge the financial support for my doctoral study provided by the Ministry of Higher Education, Libyan Government.

I would like to thank Dr. Yerokhin again, you have been so supportive and patience of me from the start, and I am really grateful for giving me this opportunity.

Finally, above all I thank the Almighty God whom I believe is the ultimate guide for enabling me to finish the project and my life in general.

Husein Meshreghi

Sheffield

Nov-2017

Table of Contents

Figures List

Tables list

Chapter 1

1.1. Introduction

In industry ceramics, such as thick and thin alumina films, are considered one the most cost effective materials [1-4]. These are commonly used for a variety purposes in precision applications. A thin film is a layer of material which varies from fractions of a nanometre (monolayer) to a number of micrometres in thickness (although some references refer to 0.1 μm or less) while the thick films usually range from < 5 to 500 μm [5, 6]. Thin and thick alumina films have low cost productivity due to the small amounts of material used [6]. Such films can be produced from ceramic slurry by conventional methods, including tape casting and roll compaction. However, these methods offer limited part geometries and cause defects in the film structure [1, 7].

Plasma electrolytic oxidation (PEO) is a novel surface engineering technology, allowing relatively thin and thick oxide coatings to be formed on light metals [8-12]. It is used not only to avoid the drawbacks of traditional techniques such as flow forming or deep drawing, but also because the PEO process employs less material, so costs are reduced and their mechanical and chemical properties in many cases superior to the materials in a bulk form. PEO also allows implementation of design and microstructures with properties unavailable in bulk materials. PEO coatings can be formed on aluminium with a variety of thicknesses, offering attractive combination of chemical and thermal stability, good strength, wear resistance and interfacial adhesion, which makes them attractive for many engineering applications [9, 13, 14].

1.2. Aims and objectives

The principal aim of the present work is to explore a novel approach to fabricate a thin-walled 3D alumina structure with low thickness and various shapes by conversion of aluminium foil using a plasma electrolytic oxidation technique, with emphasis on the structural characteristics of produced layers including morphology, phase component, and composition. To achieve this aim, the following specific objectives have been identified.

1. Analysing the effect of process parameters such as treatment time and electrolyte composition on the characteristics and properties of the coatings formed in different regions of the foil substrate.

2. Study the degree of conversion of Al into its oxide and identify possible limitations in obtaining uniform coatings in different locations of thin-walled complex-shape substrates, such as inner and outer faces, edges and corners.

3. Study the characteristics of PEO process and coating formation on regular workpieces such as flat rectangular samples and complex geometry workpieces such as L and U shapes.
4. Study the effects of electric field and current density distribution over the surfaces of working electrodes during the PEO process on the characteristics of growth, microstructure and phase composition of resulting coatings.
5. Identify the composition of plasma discharge and monitor evolution of its main components during the PEO process in different electrolytes.

1.3. Thesis organisation

The dissertation is divided into nine chapters. **Chapter 1** gives introductory information on thin and thick alumina films, usage and production techniques and the aim of this work.

Chapter 2 covering the entire scope of the thesis. It provides a review of background literature on the PEO processes and its mechanisms, including the composition and morphology of PEO coatings, effects of electrolyte composition, treatment time and the current regimes, plasma discharge phenomena, chemical reactions during the PEO process, and the dielectric breakdown phenomena, effects of electric field and current density distribution over the working electrode on the PEO coatings. Also the mechanical properties of PEO coatings were reviewed.

Chapter 3 describes the experimental procedures and instrumentation used for PEO process. Also it was introduces the methods used to fix the samples during the PEO process. A COMSOL-Multiphysics software used for modelling the current density distribution during the PEO process is introduced.

Chapter 4 provides discussion of the main experimental results and analysis of the effects of treatment time on the PEO process and produced coatings. These include analysis of current

transients during the PEO process, studies of coating thickness, morphology and evaluation of oxide film growth efficiency. The mechanical properties of the oxide ceramic coatings produced by PEO process are evaluated by nanoindentation techniques.

Chapter 5 discusses the effects of electrolyte composition on the PEO process of Al foil. Nine different electrolytes compositions were formulated according to the design of experiments method. Influences of electrolyte characteristics on current density during potentiostatic PEO treatments and resulting coating characteristics are discussed. Statistical analysis is applied to model the relationship between the concentrations of electrolyte components and coating thickness, roughness and porosity.

Chapter 6 discusses electrochemical behaviour of Al in alkaline silicate/phosphate electrolyte. The processes accompanying the growth of PEO coatings and resulting in non-uniform thickness distributions of the oxide layer and residual aluminium along the sample length are studied. The distributions of electric field in the electrolyser and in the reaction layer at the electrode surface are investigated by combining experimental and modelling approach, with attempts made to link the results of theoretical and experimental studies of the PEO treatment of aluminium.

Chapter 7 presents an approach of electromagnetic modelling that considers nonlinear current-voltage diagrams which successfully developed to predict the current distribution on the surface of electrode (thin Al foil) in electrolyser. The results of the simulation have been validated by comparison to the experimental results and can be suggested as description of a new physical phenomenon.

Chapter 8 presents the results of the experiments on fabrication of 3D thin-walled ceramic-metal shapes using the PEO process. This chapter also discusses the effects of the shape of working electrode on distribution discharge characteristics, coating thickness and morphology across the complex shape substrates. Results of numerical simulations of electric field and current density distributions over the surface of working electrodes are discussed.

Finally **Chapter 9** provides the main conclusions derived from the work discussed in this thesis and suggestions for future work, which is followed by the list of References.

Chapter 2

Literature review

2.1. Alumina films

Alumina or aluminium oxide is a chemical compound with the chemical formula Al_2O_3. It has several forms in nature such as corundum, diaspore, and gibbsite ($Al_2O_3.3H_2O$). High chemical stability of ceramic alumina components makes them resistant to chemical corrosion and wear even at elevated temperatures and attains many other properties important for various applications. Alumina appears in several allotropic types different from each other in the crystal structure, physical and chemical properties [15, 16]. These properties depend on the degree of purity and porosity. Impurities also play crucial role in the performance of alumina ceramics. For instance alumina has melting point of about 2040 ^oC, however impurities and some alloying elements form secondary phases can melt at lower temperatures [15, 17]. There exists in a number of crystalline phases depending on purity and mechanical and physical properties, three of the most important being γ, θ, and α [17, 18]. The structures of hydrated alumina and alumina are shown in table 2.1 and 2.2. Corundum or α-phase alumina is transparent, uncoloured and it is the most suited phases for use in many high-temperature applications due to its thermodynamic stability. However α phase is stable at high temperatures while the other phases do not always exist in stable phase. For instance, at certain temperatures, γ and θ phases are transformed to the corundum phase. Shackelford and Doremus [19] when discussing the alumina structure stated that the α-phase is the only phase which is stable at all temperatures and ambient pressure of 1 atm. In addition there are a number of other interesting characteristics, for instance high hardness, wear resistance, chemical inertness and high-temperature diffusion barrier properties, that have made α alumina thin films important [20]. Selected physical and mechanical properties of alumina are collected in Table 2.1.

Table 2.1. Hydrated alumina phases [4]

Phase	Structure	Lattice parameters (Å)		
		a	b	c
Bayerite β-$Al(OH)_3$	Monoclinic	4.72	8.68	5.06
Gibbsite α-$Al(OH)_3$	Monoclinic	8.64	5.07	9.72
Boehmite α-AlOOH	Orthorhombic	2.87	12.23	3.70
Diaspore β-AlOOH	Orthorhombic	4.40	9.43	2.84

Table 2.2. Stable and unstable alumina phases [21]

Designation	Structure	Lattice Parameters (Å)		
		a	b	c
Corundum	Hexagonal	4.758		12.991
Eta	Cubic (spinel)	7.90		
Gamma	Tetragonal	7.95		7.79
Delta	Tetragonal	7.97		23.47
Theta	Monoclinic	5.63	2.95	11.86
Kappa	Orthorhombic	8.49	12.73	13.39

Table 2.3. Selected properties of α -, β -, and γ alumina [21]

	α- Al_2O_3	θ-Al_2O_3	γ- Al_2O_3
Density (kg/m^3)	3390-3980	3560-3600	3200-3700
Elastic modulus (GPa)	409-441	-	
Hardness (GPa)	28	-	
Bulk modulus (GPa)	239	-	
Band gap (eV)	8.8	7.4	
Melting point (°C)	2051	θ to α : 1050	γ to δ:700-800

Many attractive engineering properties along with availability and abundance have made alumina required for processes and industrial applications. [7].

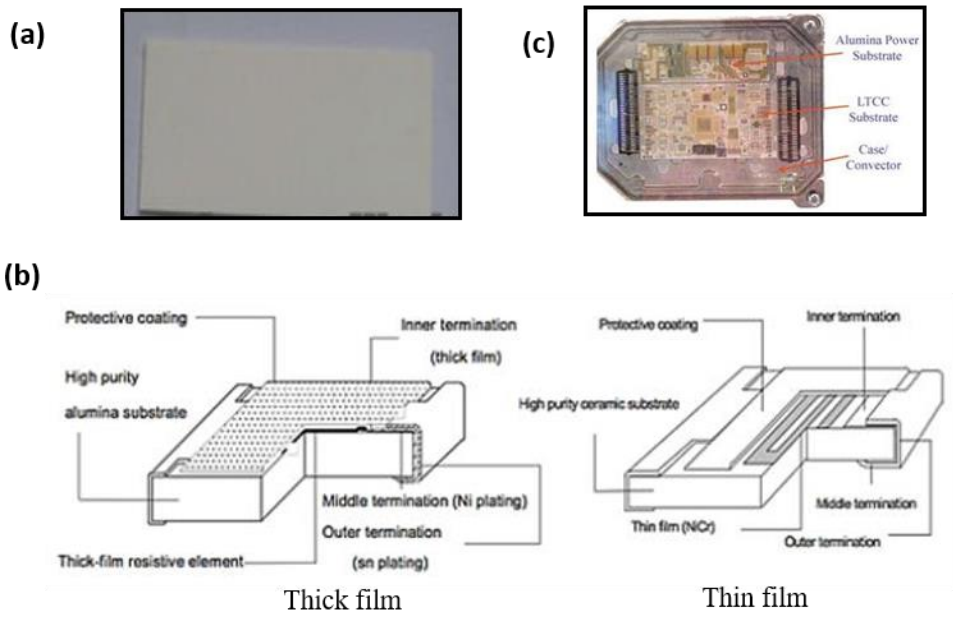

Fig. 2.1 (a) Alumina thick film substrate, (b) Chip resistor, (c) Ceramic -based

Thick and thin alumina films are widely used in large-scale integrated circuits, hybrid IC, semiconductor packages, networks resistors, focusing potentiometers, chip resistors and other related areas of electronic industry (Fig 1.1(a , b)) [21]. In addition, thick alumina films are used as substrates in automotive engine control modules, as components exposed to elevated temperatures, typically from 105 ^{o}C to 125^{o}C (Fig 2.1(c))

H. Dong states that ''*the physical properties of thin films are most strongly related to their morphology. Thermal and electrical conductivity, permeability, colour, toughness, and hardness properties are all very much dependent on morphology and to a lesser extent on the chemistry of the coating.*'' [18]. So that, based on the technique used to produce alumina films it is very important to have a better understanding the effects of processing parameters on the morphology and growth rate of the alumina analysed. This will be taken into account in subsequent analyses.

2.2. Manufacturing methods of thin and thick alumina films

Over the last decade alumina thick- thin film has been actively studied and their fabrication has grown significantly due to their applications in semiconductors, telecommunication, electronic industries, energy storage, and dielectric substrates. Several techniques have been developed to produce aluminium oxide thick -thin substrates. These techniques may produce high-purity alumina substrate. However, these techniques are considered complex and need expensive tools. Moreover the associated manufacturing methods offer insufficient flexibility. These techniques contain many stages to produce alumina films such as grinding, mixing, rolling, trimming, sintering and drying. Therefore the time for processing will be high. In addition ceramic property values changes during the stages of the processing [7]. With a simplified explanation in this introduction, we will present some examples of these techniques.

2.2.1. Roll compaction

Roll compaction Fig 2.2 is a method of fabricating continuous thin sheets of ceramic materials by compacting flowable ceramic powders in a rolling mill. CoorsTek roll compaction substrate technology incorporates three basic steps: spray dried powder preparation, tape fabrication by roll compaction and sintering [6, 22]. Initially, the raw materials (which consist of high purity ceramic powders) are ball-milled with dispersants, organic binders and

plasticizers to achieve proper particle size distribution and slurry rheology. The slurry is then spray dried to form a flowable powder that can be fabricated into a tape when roll compacted [23].

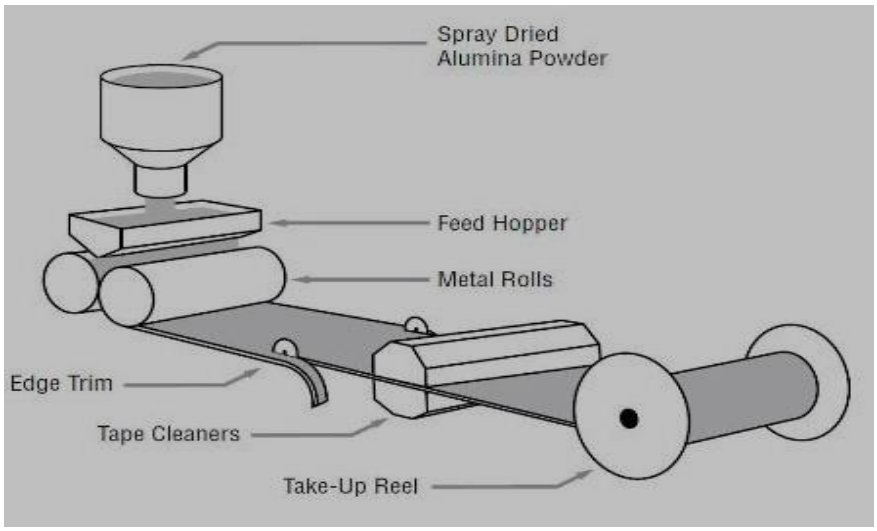

Fig. 2.2. Schematic of the roll Compaction Process

The roll compaction process is related to dry pressing in that it uses spray dried alumina powders as feedstock. However, the process differs in the type and amount of binders and plasticizers used in order to fabricate a flexible, continuous sheet or tape. The process consists of a powder feed system which is controllably presented to roll where it is compacted to sheet of tape. This tape is then trimmed. Tungsten carbide tooling is used to mechanically punch the tape, producing parts of the desired green size and shape. Following the tape punching process, the parts are sintered by passing them through a high-temperature tunnel kiln. The sintering process brings about several significant changes in the ceramic part: total surface area is reduced, bulk volume is reduced and strength increased. [23].

2.2.2. Tape casting

Tape casting is ceramic forming method used in the fabrication of thin sheets of flexible tape. This is the method of choice in manufacturing for a variety of purposes containing the production of electronic elements such as ceramic capacitor, substrate and dielectric, piezoelectric and ferromagnetic materials [24, 25]. Products which are produced by this method are in the range of 100 µm to 1mm thickness [26]. Basically this method produce a flat sheet or layer by spreading the slurry over a surface covered with removable sheet using

controlled blade known as doctor blade Fig 2.3 which can be sintered subsequently into a hard ceramic substrate layer [27-29].

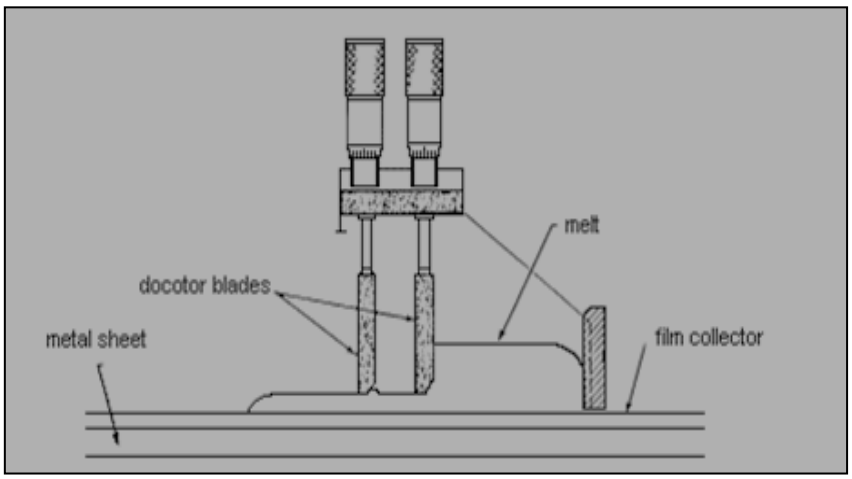

Fig. 2.3. Schematic diagram of the tape casting process

2.3. Plasma electrolytic oxidation

Plasma electrolytic oxidation (PEO) process is derived from conventional anodising, where direct current (DC) is used, usually being controlled at a constant cell voltage. However unlike traditional anodising, PEO treatments are usually performed under high voltage conditions spanned from tens to hundreds of volts [18, 30]. They provide a relatively new electrochemical surface modification method which has gained a lot of interest among researchers in industry and academia due to great potential as an eco-friendly surface engineering solution for those lightweight metals [31]. This treatment is employed to improve the wear, corrosion resistance and creep properties of the materials that are important for automotive, marine, refinery and, oil and gas industry applications.

In 1880s, a discharge phenomenon discovered by Russian scientist, Sluginov [32]. He looked into the behavior of metal electrodes in aqueous electrolytes under high voltages. Fifty years later, a more detailed research in this topic was carried on by Günterschultze and Betz [33]. The mechanism of the deposition on aluminium using an spark discharge also studied by Markov [34]. In 1999, Yerokhin *et al* studied electrochemical treatment processes and categorised the PEO under plasma electrolytic deposition (PED). Since 1980s, a different of PEO processes have been patented in different places. To name a few, Gnedenkov *et al* in Russia [35], Hsing in USA [36], Hishamoto in Germany [37], Jain Sun in Canada [38], Curran in UK [39], A. Yerokhin in UK [40].

In this chapter, the fundamental concepts and characteristics of the PEO process, as well as recent developments in PEO coatings on Al and its alloys are discussed.

2.3.1. PEO processes and associated mechanisms

Several studies have been conducted to better understand the process mechanism and chemical reaction kinetics [9, 11-13, 41-45]. One of the most cited paper in this field of work is prepared by Yerokhin *et al* in 1999 [8]. They introduced the process in depth based on current-voltage (I-V) characteristics of the electrochemical systems involved in the plasma electrolytic oxidation process. Two types of plasma electrolytic deposition methods have been studied. One type is the plasma electrolytic saturation (PES), which employs a high voltage used on the electrolytic cell to result in the metal surface to be saturated with ions, this method is established depending on the mechanisms of heating in electrolytic plasmas, which results in activation of thermal diffusion.

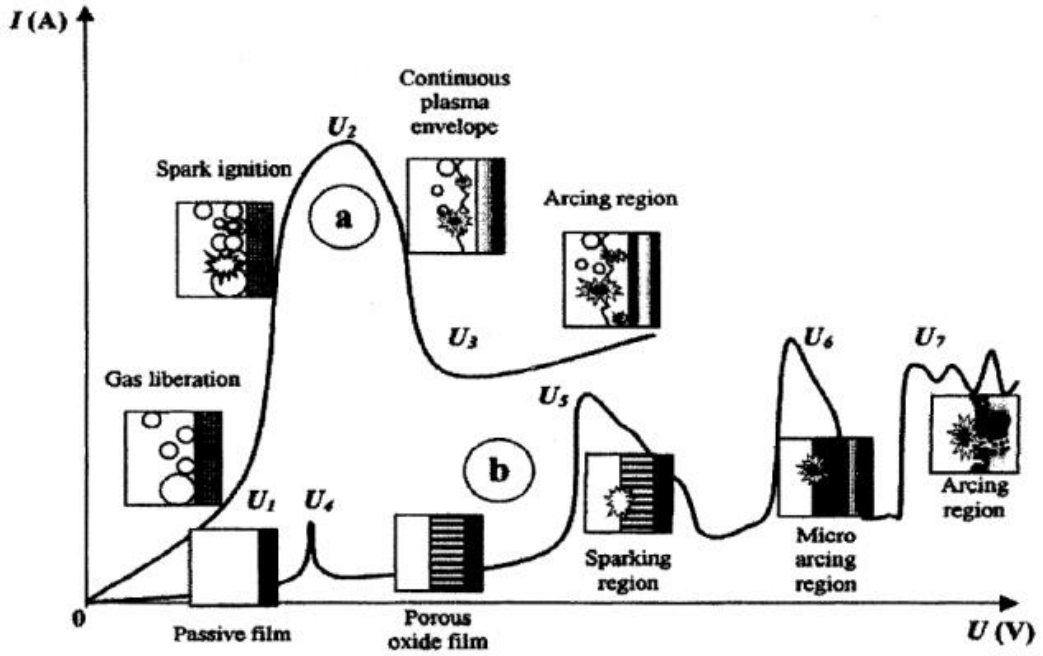

Fig. 2.4 Two types of current-voltage diagram for the processes of plasma electrolysis a) near the electrode area, b) in the dielectric film on the electrode surface [8]

While the other type is the plasma electrolytic oxidation (PEO), which is utilises an elevated potential difference between the working electrode (anode) and counter electrode in the electrolyte to form the oxide film on the surfaces. As the voltage raising, the current density increases leading breakdown voltage and the sparking appear at the surface of the working electrode, which influence the oxide film formation.

Fig. 2.4 show the processes affect the characteristics current-voltage of the electrochemical system. During the initial stages 0-U1 and 0-U4, where the voltage is low, kinetic of the electrode process corresponds Faraday's law. Current oscillation can be observed near the electrode due to the increase in voltage, while the gas products, such as oxygen and hydrogen, partially over the electrode surface, controlling the increasing in current. As increasing in current density, ebullition of the electrolyte around the electrode occurred. Thereafter, the electrode is totally covered by a gas layer with low conductivity. Here, all voltage across the cell is dropped near the electrode area. This produces about 10^6 V/m of electric field strength which generate the ionisation process in the vapour envelop. In U3 (critical voltage) Sparks are then followed by a steady luminosity that is distributed throughout the vapour plasma envelope.

Studying the current – voltage behaviour of systems where dielectric surface oxide layers are formed is more complex than in the vapour layer. Here, as the increasing voltage arrives at the electrochemical breakdown potential, the anodic oxide layer formed prior to U4 begins to dissolve. As a result of repassivation process from U4 to U5 a porous layer was formed. The electric field strength proceeds to raise until it arrives at a critical value of dielectric breakdown of the film at U5. Very small bright sparks surround the surface of the oxide film and enhance the coating growth. In region U6-U7, thermal ionisation is affected by oxide film and micro-arcs form. After that, the elements existing in the electrolyte are combined into the oxide coating and the oxide layer.

Oxygen evolution which requires an appropriate potential can proceed via different pathways, starting from conventional electrochemical water splitting and finishing by the radiolitic and plasma-assisted chemical reactions similar to those shown in Fig 2.5 [8].

$$H_2O_2 + e_{aq}^- \rightarrow OH^- + OH$$
$$O_2 + e_{aq}^- \rightarrow O_2^-$$
$$H^+ + e_{aq}^- \rightarrow H$$
$$2HO_2 \rightarrow H_2O_2 + O_2$$
$$O_2^- + HO_2 \rightarrow O_2 + HO_2^-$$
$$H^+ + OH^- \rightarrow HO_2$$
$$HO_2 \rightarrow H^+ + OH^-$$

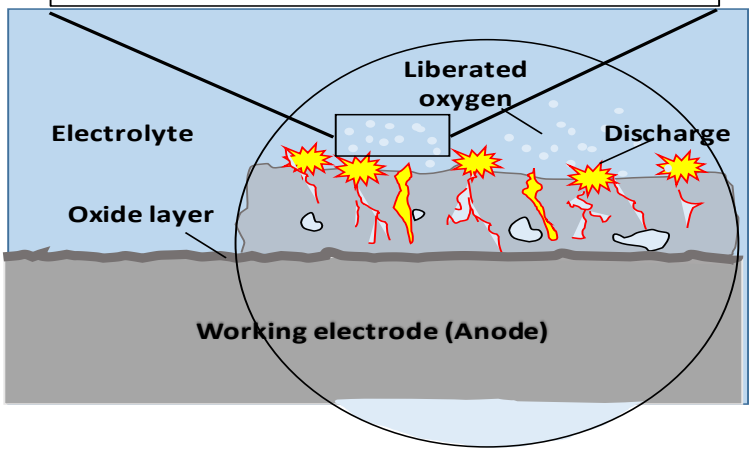

Fig. 2.5 Probable chemical reactions leading to oxygen liberation [4].

Plasma electrolytic oxidation is usually performed on a wide range of treatment time based on the required characteristics of resulting coatings. The overall current efficiency of the oxide layer creation has been estimated to be in the range of 10 to 30 % [46]. If the electrolyte solution is alkaline, such as aqueous solutions of KOH, the film formation, dissolution and oxygen evolution follow the reactions below [47]:

At aluminium-oxide interface: (anodic process)

$$2\mathrm{Al} + 3\mathrm{O}^{2-} \rightarrow \mathrm{Al_2O_3} + 6\mathrm{e}^- \qquad (1)$$

$$\mathrm{Al} \rightarrow \mathrm{AL}^{3+} + 3\mathrm{e}^- \qquad (2)$$

At Oxide–electrolyte interface: a- (anodic process)

$$4\mathrm{OH}^- \rightarrow \mathrm{O_2}\uparrow + 2\mathrm{H_2O} + 4\mathrm{e}^- \qquad (3)$$

In the final stage of the process, Al injected into the electrolyte through discharge channels and then precipitated as a hydroxide on the working electrode surface. A further increase in the coating thickness occurs due to the subsequent plasma discharges which causes dehydration and recrystallisation oxide [46]. In the same context, some researchers categorised the process into four sequential stages [47, 48]; anodising, spark discharge, microarc discharge and arc discharge. At first stage, as the anodic voltage increases across the sample a highly porous coating is formed. While the discharge and intensity shapes is the main difference between the second and third stage. However the mechanism of discharge and thickness growth are same for both stages. In stage four high energy is needed to create larger spark on the surface of the working electrode and also into the electrolyte. Because when the plasma escape into the electrolyte rather than on the as the first and second stage coating surface, this leads to the creation of local microdefects in the coatings which is unacceptable from the point of view of mechanical properties of coatings [47, 48].

2.3.2. PEO coatings on aluminium alloy substrates

As mentioned in introduction, several of studies on production of PEO coatings were performed. Lightweight metals has the most interest in the studies of the formation of the PEO coatings on its surfaces [12, 13, 42, 49-54]. Because this thesis is focused on Al foil, the literature review is mostly focused on PEO coatings on aluminium substrates.

One of the important publications was produced by Snizhko *et al* [46] on anodic process in PEO treatment on an aluminium alloy in KOH electrolyte. In this work, the rates of chemical dissolution of the working electrode and anodic gas liberation were determined. It was assumed that the partial anodic processes of oxide layer growth, dissolution and gas evolution on the working electrode surface follow the Faraday's law. Therefore, the balance equation for current yields of the partial electrode processes on the working electrode surface has the following form:

$$\eta_{Al_2O_3} + \eta_{Al_{sol}} + \eta_{O_2} = 100\ \% \qquad [46]$$

Where; $\eta_{Al_2O_3}, \eta_{Al_{sol}}$ and η_{O_2} are current yields of partial anodic products of alumina, dissolved aluminium and oxygen respectively. The weight loss of Al sample was measured by an analytical balance. Weight of coating grown was calculated from cross-sectional SEM images assuming that the alumina density is around 3.1 gr/cm^3 due to the presence of

porosity. For 1 g/l concentration of KOH, the oxygen evolution was the main the electrochemical process and its current efficiency was 63.9 %. While the current efficiency of the coating growth and aluminium dissolution were 28.9 % and 7.2 % respectively. Increasing the concentration of KOH resulted higher dissolution and less oxidation, however the gas evolution rate remained the same. It is also found that the increase in the current density causes an increase in gas liberation, which means that the amount of gas liberation is independent of electrolyte concentration and dependent on current density.

Parameters of PEO process were studied from many researchers to provide the fundamentals for comprehensive understanding of the PEO technique. Power supply mode is one of the crucial factors effecting the PEO process and playing a key role in the preparation of coatings. Various types of power sources capable of producing different current modes, such as alternating current (AC), direct current (DC) and pulsed DC, and bipolar regime as shown in Fig 2.6, have been used to form oxide layers on lightweight metal alloys. The authors of ref [55] analysed the effects of using pulsed bipolar current regime to produce oxide ceramic coatings on aluminium alloy. It was observed that appropriate combination of the coating growth rate and energy consumption can be obtained in the pulse frequency range between 1 and 3 kHz. The thickness and porosity of produced coatings ranged from 50 to 70 µm and from10 to 15% respectively.

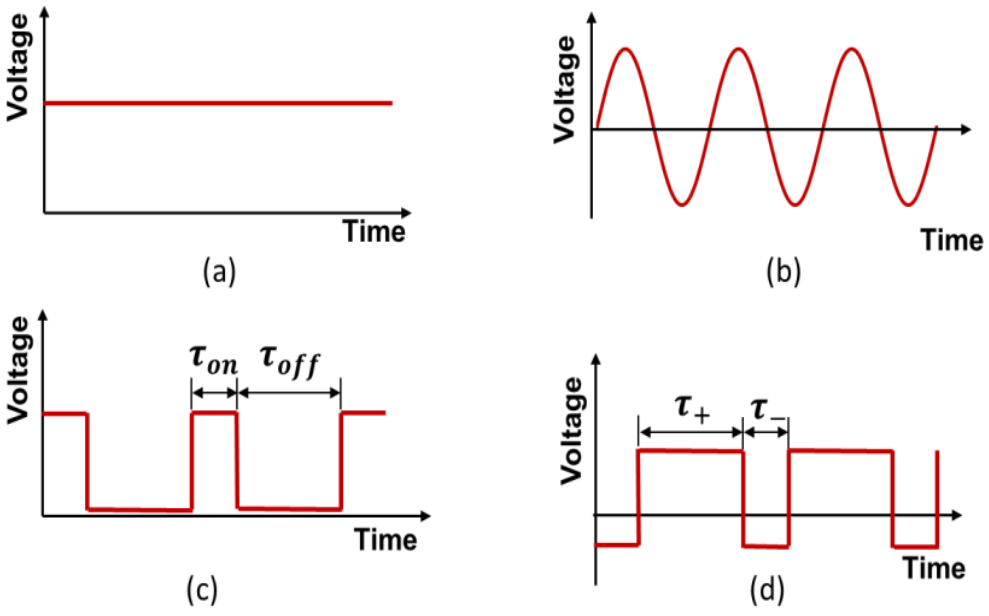

Fig. 2.6 Main electric modes used in the PEO process, (a) DC, (b) AC, (c) pulsed unipolar (PUP), (d) pulsed bipolar (PBP).

Also evidence of δ-Al_2O_3 phase was found compared to the coating produced using a 50 Hz AC process. R.O. Wei Li *et al* [56] also investigated the influence of the anode pule-widths on the microstructure of coatings produced by a PEO treatment of an aluminium alloy. They observed that the hardness and wear resistance of PEO coatings reduced as the anode pulse width increased. The PEO process using pulsed unipolar and bipolar DC current regimes analysed by Hussein *et al* [57]. The influence of current frequency and other current parameters such as period of positive and negative pulses and resting time between the positive and negative pulses on coating formation was studied. It was found that the PEO coating morphology and microstructure were significantly different under different current modes. A unipolar condition is capable of creating a dense coating morphology only if positive to negative ratio of pulse current is determined properly. Appropriate control over these conditions results in elimination of high temperature spikes and strong troublesome plasma discharges. The bipolar current regime might improve the characteristics coating compared with the unipolar current regime, with respect of surface morphology and cross-sectional microstructure. Additionally a thick coating might be obtained by adjusting positive to negative current ratio and their timing to remove or reduce the strongest plasma discharges and thus the high temperature spikes. In general, oxides ceramic layers produced under the bipolar current mode exhibits a significantly more porous morphology with higher surface roughness values (Ra) mostly in longer treatment times [51, 57].

Current density is one of the most important parameters influencing the coatings characteristics and should be applied in an optimum range to achieve the environments required for PEO process. A range from 1 to 30 A/dm^2 have been stated in several publications [8]. Changing the current density can influence the phase composition content, microstructure, growth rate, and physical and chemical properties of coatings produced [8, 58]. Zhenwei Li *et al* [59] investigated the effects of cathode current density using pulsed bipolar current to produce oxide ceramic coatings on 2024–T4 aluminium alloy. They observed that the surface roughness and coating thickness increased as the cathode current density increased. Khan *et al*. [60], in discussion of the residual stresses in PEO coatings on Al alloy formed in the pulsed unipolar current mode stated that the increase in current density leads to a decrease in the residual stresses in the coatings. The reason is that a higher current density means higher plasma micro discharge which promotes stress relaxation by formation

of micro cracks on the surface of the coating. They found that the normal stress ranges from 111 MPa to 818 MPa depending on the PEO current pulse parameter.

Porosity and its size in PEO coatings on 6082 aluminium alloy was studied by Curran and Clyne [61] using SEM. The results show that the coatings are approximately 20 % porous and the porosity is largely surface connected. Also it is noticed from these measurements that the average pore size is around 30 nm and that most of the pores fall in the range of 5 nm to 1 µm. This porosity is expected to influence many properties, such as the low stiffness, the low thermal conductivity and the low friction and good wear resistance under lubricating conditions. Many of these property variations are advantageous. Also, during the PEO oxides formation the porosity may form vacancies in the molten alumina. This may allowing the electrolyte penetrate through the pore network and enhance the coating growing.

Optimisation of the thermal properties of the PEO coatings can make these coatings an excellent choice for thermal barrier layer in electronics applications. Curran and Clyne [62] investigated the thermal conductivity of PEO coatings on aluminium using a steady state thermal method. It was found that the thermal conductivity value was around 1.6 W/mK for the coating thickness of 100 µm. This is significantly lower than the thermal conductivity of the bulk material which is around 30 W/mK°.

In many fields, aluminium and its alloys are progressively more used due to their physical properties such as low density and high specific strength that make them suitable for different applications. However, the low mechanical properties such as hardness and wear resistance of aluminium reduce their application niche to the areas where friction is mainly absent [63]. This drawback can be avoided by surface treatments of Al alloys using a number of processes, with PEO treatment being the most promising [8]. Malayoglu *et al* [63] evaluated the adhesion strength of the coatings using a scratch test method. Results of test indicate that the PEO treated specimens display more desirable mechanical properties compared to hard anodised samples. Due to the presence of α-Al2O3 and γ-Al2O3 crystalline phases in the coating structure, the elastic modulus and hardness of PEO coatings are 2–3 times greater than those of anodic aluminium oxides and subsequently, a higher wear resistance of PEO coatings has been obtained. This is consistent with the results reported by Khan *et al* [9]. As the total thickness of PEO coatings increases with increasing treatment time, the coating

microhardness varies with its thickness. For example X. Nie *et al* [64], who used a PEO process to produce thick oxide ceramic layer on BS Al-6082 aluminium alloy, have found that the position of the maximum hardness (which could reach up to 2400 HV) moves away from the coating-substrate interface with increasing coating thickness.

Most of the studies of PEO processes had been performed on regular shape samples such as rectangular or disk coupons; however, very little attention have been paid to complex shapes such as U, E or L shapes. Chao Gu *et al* [65] focused on PEO processing of long tubes, in order to achieve uniform thickness of ceramic coatings on inner surfaces. The results show that the thickness distribution of PEO coating in the inner surface is non-uniform due to the effect electric field and current density distribution. An auxiliary counter electrode was used inside the tube to eliminate the shielding effect of electric field, which was effective to obtain more uniform coatings on the inner surfaces of the tubes. Shrestha *et al* [66] produced and studied the oxide coating on aluminium AA2219 alloy using the PEO process. The process was capable of depositing a uniform coating at edges and tight corners with a typical coating thickness of about 60-70 µm, see Fig 2.7. The coating seemed well retained over the edge with no noticeable cracking over the tight radius.

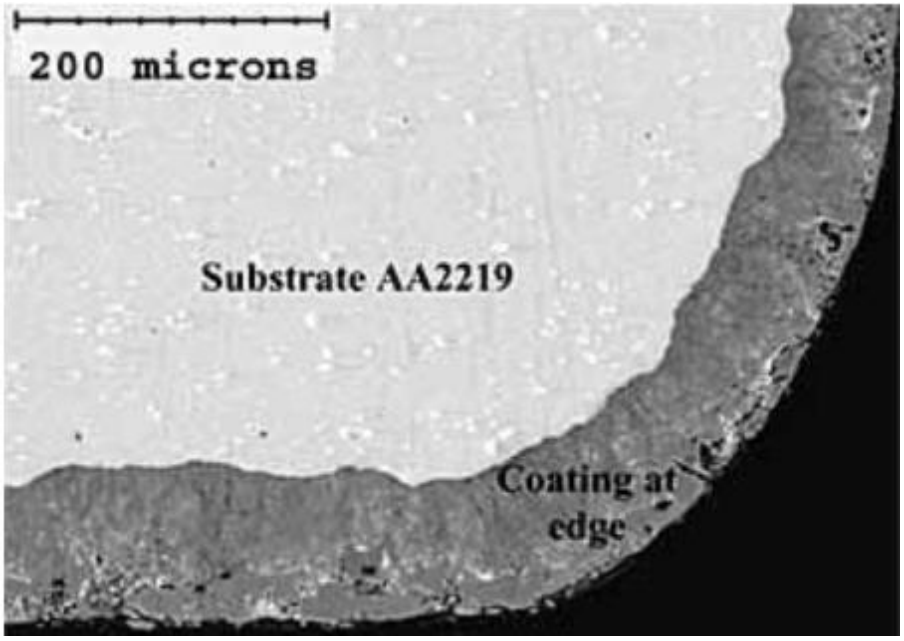

Fig. 2.7 SEM image showing a well-adhered and uniform PEO coating at the edge of Al alloy substrate [66].

The review of PEO process on aluminium and its alloys discussed above provide a significant information on the parameters of PEO process were studied from many researchers. It is also gathers the results and discussions of the effects of different variables on characteristics of the coatings.

2.3.3. Effect of treatment time

Many studies have been carried out on the influence of treatment time on the PEO process, with the times varied from a few minutes up to a few hours. In general, increasing in processing time causes thicker coatings, with more intense and larger micro-discharges occurring, which leaves larger discharge channels in the coating [11, 12, 52, 67-70]. Gun Lee *et al* [70] investigated the effects of time variation on formation of oxide layers on Al 7075 alloy using PEO process. The results showed that the thickness of the coating increases with the increase in treatment time. However, the ceramic coatings formed for 45 min and 60 min have more porous morphology than those formed for 30 min (Fig. 2.8) and the highest value of coating microhardness, 1790 HV was obtained at the process time of 30 min.

In the same context, Sundararajan and L. Rama [11] investigated the properties of oxide coatings produced at different periods of time. The density of discharge channels decreases exponentially with increasing oxidation time while the diameter of the discharge channels increase linearly with the increasing time of oxidation (Fig.2.9). Micro-discharges are created as a result of dielectric breakdown through weak spots in the PEO coating and the number of weak spots is reduced in thicker coatings.

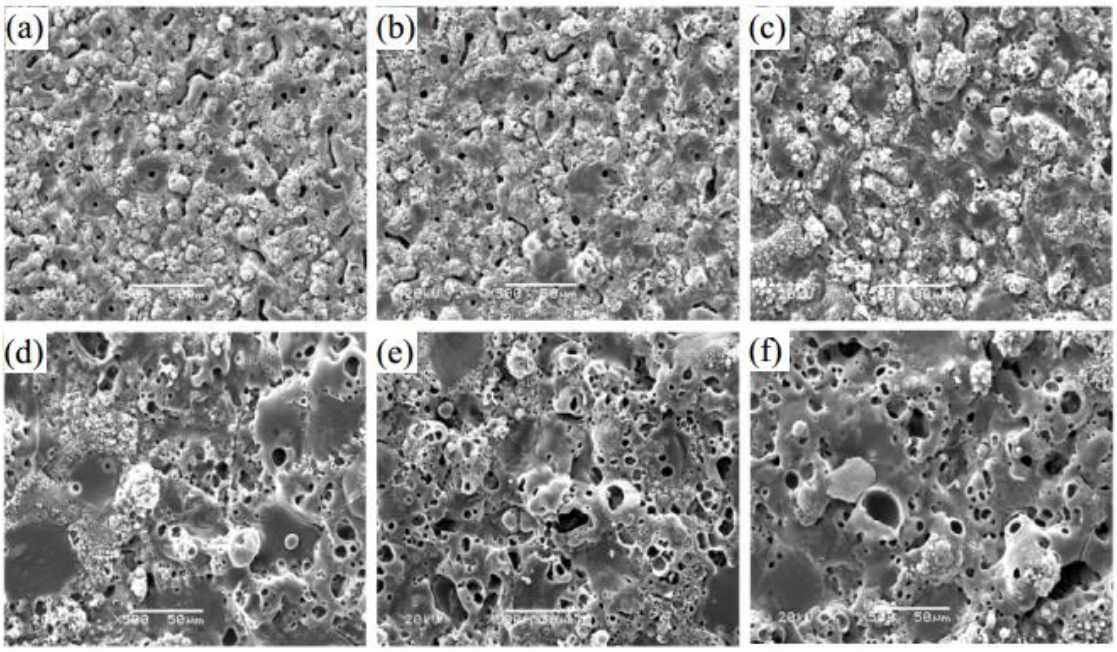

Fig.2.8. SEM image showing surface morphology on Al [70]

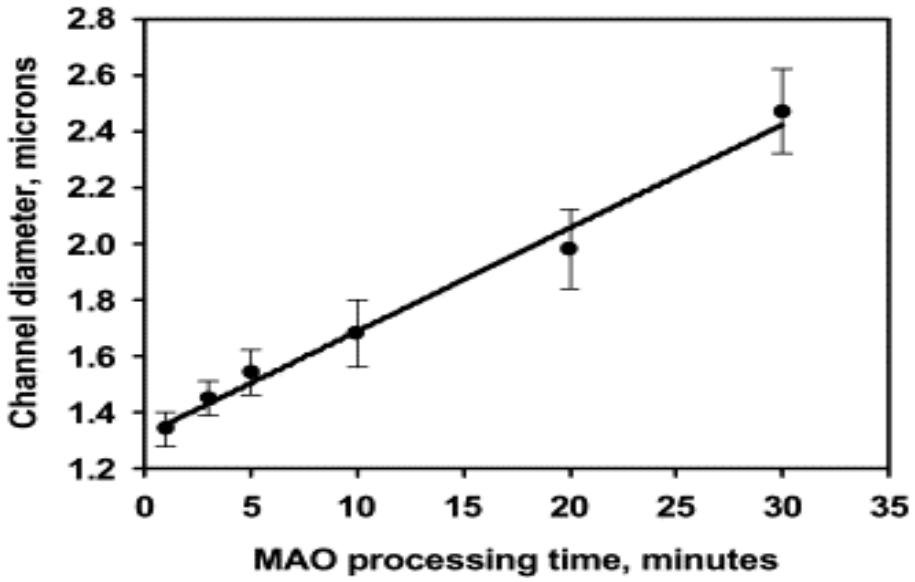

Fig. 2.9 Variation in diameter of the microarc discharge channels vs PEO processing time [11].

Bajat *et al.* [75] evaluated the corrosion performance of PEO coatings on aluminium produced at treatment times varied from 2 min to 1 hr and found that the corrosion behaviour depended on the treatment time. Initially the corrosion resistance increased to a maximum before it decreased for longer treatment times. They found that the coating deposited for 2

min was produced before the breakdown potential was reached, while the 3 min deposition was formed just after reaching the breakdown potential (Fig. 2.10).

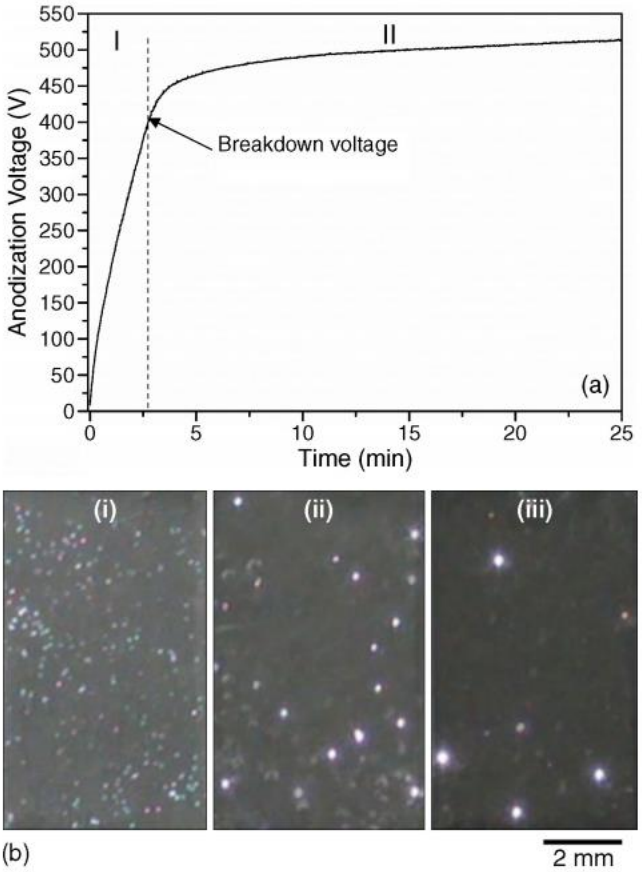

Fig. 2.10 (a) Time variation of voltage during galvanostatic aluminium anodization in 0.01 M $Na_2WO_4 \cdot 2H_2O$ at 15 mA/cm2. (b) Microdischarges appearance at various stages of PEO process: (i) 3 min, (ii) 15 min, (iii) 45 min [71]

So, it can be assumed that coating formed before the breakdown potential point does not have sufficient thickness to provide an efficient barrier to a corrosive agent. On the side, the coating produced for 3 min was neither thick enough nor dense, so the electrolyte easily penetrated through the pores of the coating and even after 1h of exposure to a corrosive agent reached the aluminium substrate.

A brief review of the effect of processing time on the PEO coatings properties explored above provide some ideas for understanding the changes in the coating properties occurred. Analysing the effect of process parameters such as treatment time will be discussed in details in results and discussion chapter.

2.3.4. Effect of electrolyte composition

Electrolyte components play essential role in the PEO treatment and many studies have been focused on optimisation of the electrolyte composition to obtain required coating characteristics [72-74]. A suitable electrolyte not only acts as a medium to conduct current and transmit the energy required to initiate and sustain the PEO process as well as provide oxygen required for the oxide formation process, but also promotes metal passivation and produces an insulating layer, which is essential to trigger the dielectric breakdown responsible for the onset of plasma discharge events. Components of the electrolyte solution influence coating characteristics, including surface morphology, thickness and phase composition and causing to different structure and performance coatings. Yerokhin *et al* [8] classified the electrolyte components which can be used to produce oxide coatings in aluminium alloy in the PEO process as follows:

1. Electrolytes that provide fast dissolution of aluminium such as NaCl, $NaClO_3$, NaOH, and $NaNO_3$.
2. Electrolytes that provide slow metal dissolution as H_2SO_4, Na_2SO_4.
3. Electrolytes that promoting metal passivation in close range of voltage such as H_3PO_4.
4. Electrolytes characterised by complex behaviour such as potassium fluoride and sodium fluoride.
5. Electrolytes promoting weak passivation of the metal.
6. Electrolytes promoting strong metal passivation, e.g. H_3BO_3, H_2CO_3, H_3PO_4

Fig. 2.11 shows typical polarisation curves of Al between the current and voltage in the six groups of electrolytes considered for the PEO treatment [8].

The electrolyte solutions from groups 4-6 make sparking voltage easy to obtain, which is highly helpful for production of ceramic coatings using PEO process.

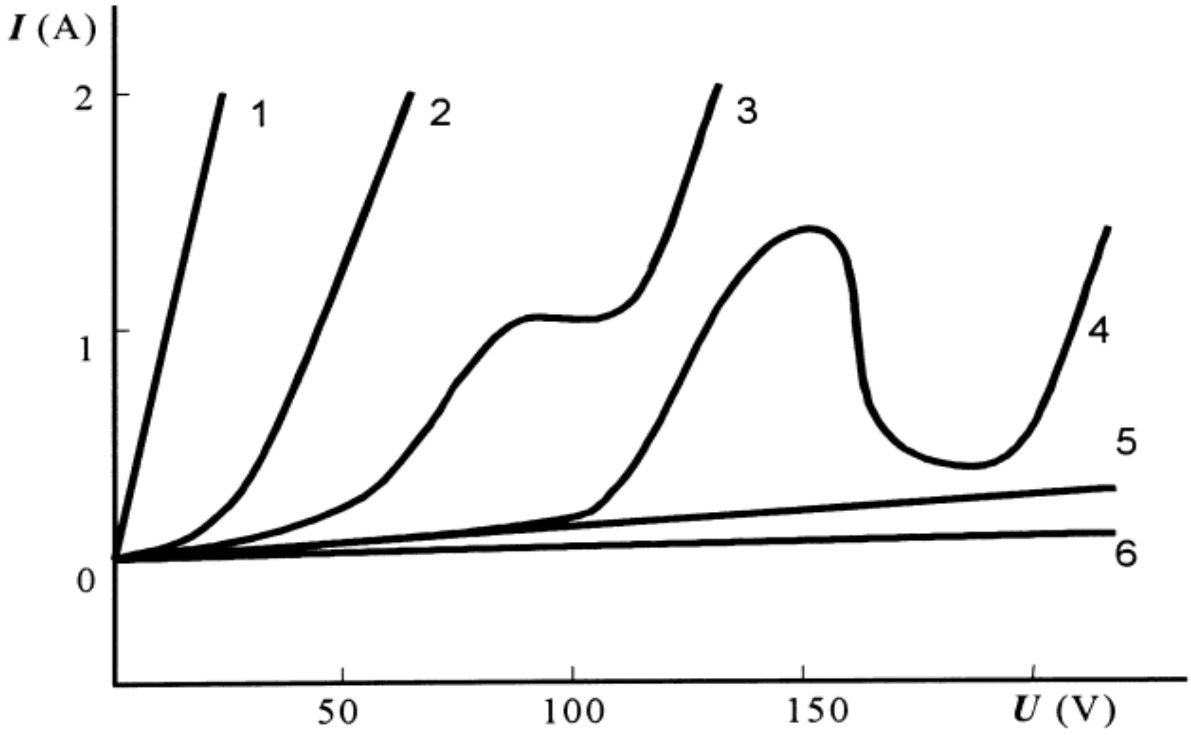

Fig. 2.11 Different electrolytes solutions tested for PEO treatment of aluminium alloy [7].

The last groups of electrolytes were categorised into four sub-groups regarding to their contribution to the coating composition as follows;

i. Electrolytes that include only oxygen into the coatings;
ii. Electrolytes including anionic and cationic components that incorporate other elements into the coating;
iii. Suspensions that provide transportation of particles which contribute to the coating composition

Electrolytes from sub-group (ii) provide possibilities to change the coating properties and enable coating formation by substrate oxidation and electrolyte substances depending on the substrate surface. So, these electrolytes are considered to be the most promising in PEO processing for different applications. Therefore, to assist the conditions required for dielectric breakdown, electrolyte additives such as silicates and phosphates which promote metal passivation are widely used as the basic ingredients of the PEO electrolytes. The solutions may include components which increase the electrolyte conductivity and provide the coating stabilising materials, such as potassium hydroxide (KOH) or sodium hydroxide (NaOH). Several

studies [8, 74-78] have analysed the effects of electrolyte composition, concentration and pH on the PEO treatment of aluminium. Kai Wang et al. [74] produced PEO coatings on Al alloy in silicate and aluminate solutions with and without sodium fluorosilicate, and found that main phases are γ-Al2O3 and α-Al2O3; furthermore, mullite particles were generated around the plasma discharge channels, especially in silicate electrolytes. Also the surface morphologies of PEO layers produced in aluminate electrolytes resulted pancake structures while the volcano structures formed in the layer prepared in silicate electrolytes. Alhosseini *et al* [77] studied PEO treatments of 6061 Al alloy in electrolytes with two concentrations of KOH, 2 and 4 g/l and similarly for Na_2SiO_3. It was observed that the increase in concentration of KOH causes augmentation of the electrolyte electrical conductivity and consequently reduces the sparking voltage, which promotes formation of PEO coatings with finer features. Higher concentrations of Na_2SiO_3 in the PEO electrolyte result in increased Si content in the coating, which causes to increase in the coating thickness and corrosion potential. Guohua *et al*. [79] produced ceramic coatings on aluminium substrate by PEO in two kinds of electrolytes (silicate and phosphate solutions). Alpha, gamma and mullite phases were found in the coatings. Silicon located mainly in the outer region of the coating, while phosphorus distributed homogeneously across the coating.

Investigations into the influences of different processing parameters such as treatment time, electrolyte concentration and current mode on the PEO coating characteristics provide significant amount of detailed information. However, there are specific requirements in the direction with the required applications that give a range to control the process parameters. For instance, many studies reported that the coating porosity and average pore diameter can be increased by either increasing the supplying energy density (high voltage/current density, longer pulse time) or by increasing the electrolyte conductivity or by increasing PEO treatment time.

Appropriate electrolytes not only enhance metal passivation which is necessary to induce discharge events via dielectric breakdown but also affect, as a conductive medium, the current distribution during the PEO process and provide essential oxidising agents to form the coating [47]. Alkaline electrolytes containing phosphate and silicate anions in presence of potassium hydroxide are commonly used in PEO process to produce oxide layers on

aluminium [80-83]. Table 2.4 shows some of electrolyte compositions which used in PEO process.

Table. 2.4 Electrolyte compositions used to create PEO coatings on aluminium alloys and coating phases formed.

Substrate	Electrolyte composition	Phase composition of coating
Al [84]	30 g/l Na_2SiO_3; 10-40 g/l NaOH	α-Al_2O_3, γ- Al_2O_3, mullite, Al_2SiO_5
Al 2024 [85]	2-5 g/l Na_2SiO_3; 3-5 g/l NaOH; 1 g/l organic agent	α-Al_2O_3, γ- Al_2O_3
Al 2017A [86]	0-8 g/l Na_2SiO_3; 2 g/l KOH	α-Al_2O_3, γ- Al_2O_3, mullite
Al 2024 [87]	20 g/ l Na_2SiO_3	γ- Al_2O_3 dominant, α-Al_2O_3, mullite, δ- Al_2O_3
Al 6082 [88]	1 g/l KOH	α-Al_2O_3, γ- Al_2O_3

The electrolyte components and their concentrations change during the treatments, strongly influencing the properties of resulting coatings [89]. For instance, Wang *et al*. [74], in discussion of electrolyte effects on the characteristics of PEO coatings stated that the addition of Na_2SiF_6 may accelerate the growth of the oxide films and substantially increase the hardness by enhancing the density of the coating. Lee *et al*. also reported that the dielectric breakdown voltage of the oxide layer decreases with increasing of sodium silicate and the time to reach dielectric breakdown be shortened on the time-voltage curve. On the other hand, it has been reported that the breakdown voltage was found to be higher in electrolyte containing phosphate than in silicate electrolyte [47]. Also Polat *et al*. in [76] reported that both dense and porous layer of coatings thickness increase with increasing of sodium silicate concentration in the electrolyte, However the increase in the thickness of the dense layer is less than that in the outer layer of the coatings. Due to the incorporation of silicon into the oxide, it has been found that increasing concentration of sodium silicate leads to an extension of the inner dense layer, which is composed mostly of γ and α-Al_2O_3 phases, with some complex Al-Si-O phases [8]. These results also consistent with Jong Kim *et al*. [78] who studied PEO coatings formed on Al alloy in solutions of KOH with different concentrations of Na_2SiO_3, and found that the thickness and roughness of the ceramic oxide was markedly increased by silicate additions. Extensive research of these effects has been performed for to obtain PEO coatings on Al alloys with specific phase compositions [8, 46, 76, 79, 90, 91].

Alumina exists in a number of crystalline phases, with α, γ, and θ polymorphs being most abundant. The α phase of alumina is a thermodynamically stable phase and possesses good mechanical properties. Combined with chemical inertness, this makes it one of the most technologically important ceramic materials [92, 93]. However alumina is normally considered brittle below ~ 1000°C [94, 95].

Earlier literature on PEO of aluminium alloy is summarised in Table 2.5. The scientific studies include characterisation of growth and corrosion behaviour of PEO coatings on aluminium produced in different electrolytes under different current modes. Therefore, from the above it's concluded that the composition of the electrolyte plays a very important role in the PEO process. It can effect a wide range of coating properties such as the morphology and microstructure, growth rate and composition, strength of adhesion to the substrate, micro-hardness, and tribological properties. Although published studies on PEO electrolytes has been on the development of composition and concentration to achieve desirable coating properties, still extensive researches on the effects of the electrolytes compositions nowadays. As treatment time parameter the electrolyte composition effects on the PEO process of AL foil will be discussed in details next chapters.

Table 2.5. Conditions of PEO treatment of aluminium reported in literature.

Ref.	Author	Substrate	Electrolyte	Parameters	Study aim and results of electrolytic characteristics influences
[46]	Snizhko et al	6082 Al alloy	0.5–2.0 g/l solutions of KOH	Current density applied is 46.7-140.7 mA/cm^2	Overall current efficiency of the oxide film growth ranges within the 10–30% and reduces significantly with increasing KOH concentration. Achievement of high voltage. Lower electrolyte concentration promotes oxide film formation and hinders Al dissolution.
[70]	Dong –Gun et al	7075 Al alloy	8 g/l Na_2SiO_3 2 g/l Na_2SiF_6 2 g/l NaOH	AC voltage at 50–Hz frequency (200 V) with constant 260 V DC. Four different treatment time; 5, 30,45 and 60 min.	Increase the pore size with the increase of time. Ceramic coatings mainly consist of mullite, α-Al_2O_3 and γ-Al_2O_3 phase. The thickness of the coating increases with the increase in time. However, the ceramic coatings formed in 45 min 60 min have more porous coatings than coatings formed in 30 min.
[74]	K. Wang et al	6061 Al alloy	0-8 g/l Na_2SiO_3 0-8 g/l Na_2AlO_2 0-0.5 g/l Na_2SiF_6 2 g/l NaOH	Applied voltage; 200 V AC; (60 Hz), 260V DC-treatment time; 5 min-	γ-Al_2O_3, α-Al_2O_3 and mullite the main phase. Addition of Na2SiF6 can accelerate the growth of the oxide layers and increase the microhardness by enhancing the layer density.
[86]	Aytekin Polat et al	2017A Al alloy	- 2 g/l KOH, dis. water - 4 g/l ·Na_2SiO_3·5H_2O, 2 g/l KOH, dis. water - 8 g/l Na_2SiO_3·5H_2O, 2 g/l KOH, dis. Water	Current density 0.150 A/cm^2 Treatment time; 150 min. Conductivity (mS/cm); 7.74, 11.2, 18.1	Increasing the sodium silicate concentration in the electrolyte leads to increase both the thickness of the dense and porous outer layer of the coatings. The coating produced in the electrolyte with low sodium silicate concentration has higher microhardness values and better wear resistance than the one formed in the electrolyte with high sodium silicate concentration and in the electrolyte without sodium silicate.
[42]	A L Yerokhin et al	H30T Al alloy	Na_2SiO_3	Applied voltage -160 to 600V Current density 125 mA/cm^2 Treatment time; 0.5-65 min. Conductivity (mS/cm); 5.2 and PH = 11.3	γ-Al_2O_3 and α-Al_2O_3 are the main phases. Discharge characteristic in PEO of Al, and evolution of phase composition are discussed

[96]	R O Hussein et al	1100 Al alloy	8 g/l Na_2SiO_3, with KOH	Constant DC and unipolar pulsed DC regimes Frequencies varied from 0.2 to 20 kHz Current density 0.15 A/cm^2 Treatment time; 0.5-65 min. Conductivity (mS/cm); 5.2 and PH ;12	The plasma was characterized by OES, and the aluminium oxide coating morphology for different current modes was determined using SEM.
[97]	Wei-Chao Gu et al	Al foil	0.033M Na_2SiO_3 0.008M $Na_6P_6O_{18}$ 0.025-0.5M NaOH	DC power source (600 V, 20 A) Current density 50 A/dm^2 Treatment time; 30-60 min. Temperature ; 303 K	Analyse the influence of electrolyte concentration and composition on PEO coating properties. The high discharge voltage also results in higher content of α-Al_2O_3 phase in the coating prepared in the phosphate electrolyte than that in the coating prepared in the silicate electrolyte.
[98]	Shifeng liu et al	5005 Al alloy	An aqueous alkaline electrolyte, i.e 4 g/l KOH. Red mud as additive.	-150 to 500V, (200Hz) Current density 50 A/dm^2 Treatment time; 60 min.	Possible to produce complex ceramic coating on 5005 Al alloy using PEO with red mud as an electrolyte additive. The coating surface was the colour of red mud. Thickness 80 μm was formed.
[99]	J.A. Curran et al	6082 Al alloy	3-5 Na_2SiO_3 3-5 g/l $Na_4P_2O_7$ 1-2 KOH	AC power was applied with a 50 Hz The voltage was in the 400–600 V in the anodic half-cycle. 150–250 V in the cathodic half-cycle. Current density; 1 KA/m^2	Coatings were produced on Al substrate and characterised using profilometry, scanning electron microscopy, X-ray diffraction and nanoindentation.
[100]	X Nie et al	6082 Al ally	2-10 g/l Na_2SiO_3	Voltage;400-600 V, current density; 100 mA/cm^2, treatment time; 90-150 min, Temp.; 343-353 K	α-Al_2O_3 and γ-Al_2O_3 were formed ; α-Al_2O_3 is the dominant phase in these coatings. PEO coatings appear excellent resistance to abrasive wear and corrosion.
[101]	C.B. Wei et al	2024 Al alloy	Na_2SiO_3 in distilled water with other additives.	Pulsed DC, node voltage was sustained at 260 V during the measurement. Treatment time 25 min.	The current flowing through the anode plate was monitored to investigate the distribution of the anode current and the effects of distance between the cathode and specimen.
[102]	YongJun Guan et al	2024 Al alloy	20 g/L Na_2SiO_3	The ratio of positive current to negative current is set to one with a current density of 0.3 mA/mm^2.	Transient signal gathering system is used to study the current, voltage, and the transient wave during the PEO process. SEM, OM, XRD and EDS are used to study the coatings evolution of morphologies, composition and structure.
[103]	C.S. Dunleavy et al	6082 Al ally	3-5 Na_2SiO_3 3-5 g/l $Na_4P_2O_7$ 1-2 KOH	Current density; 1500 A/m^2 ; treatment time 20 min.	The composition, temperature and electron density of the plasma formed during PEO processing are inferred from characteristics of the emission spectra.
[104]	Hongping et al	6061 Al alloy	10-20 Na_2SiO_3 1-5 KOH	The ratio of positive current to negative current is set to one with a current density of 8 A/dm^2.	Reveal the growth process of PEO coatings on aluminium alloy by analysing conducting behavior and V-I characteristics of an aluminium electrode.

2.3.5. Optical emission spectroscopy of PEO process on aluminium

Understanding the microdischarge phenomena is an important for characterisation of the PEO process. Distribution and types of microdischarges have crucial influence on the formation mechanism, composition, morphology, and various properties of the resultant oxide coatings. Optical emission spectrometry (OES) is the best available technique of chemical analysis that uses the intensity of light emitted from a flame, plasma, spark or arc at a particular wavelength to determine the quantity of an element in a sample [105]. Long years ago, Sluginov [32] was observed the light emission (discharge events) during electrolysis of aqueous solutions. However, the first step of a scientific research of the discharge phenomena was carried out during Al anodising in the 1930s by Gunterschultze and Betz [33], who emphasised to the appearance in the optical emission spectra (OES) of characteristic lines matching both metal electrode and electrolyte species. These results are consistent with earlier observations of optical emission from aluminium in many electrolytes [106].

During PEO treatment, significant amount of sparks moves rapidly on the sample surface. However, the evolution of sparks depends on many parameters such as applied power mode, current density, electrolyte composition and substrate materials [107]. Plasma electron temperature during PEO treatment was evaluated by Kharitonov *et al* [108]. It was found that discharge consists of two microregions, the hot core with temperatures up to 8000 to 10 000 K and a relatively cold (2000 K) bubble separating the core from the electrolyte.

In a discharge model based on optical emission spectroscopy measurements, Hussein *et al.* [109] determined the elements contained in the plasma and evaluated the Plasma electron temperature. They proposed a model in which three different types of discharge, A, B and C occur (Fig. 2.12). The A- and C-type discharges are related to gas discharges occurring in micro-pores of the oxide layer at the oxide/electrolyte interface: type A is in small holes near surface micro-pores, and type C is in relatively deep micro-pores within the coating. While the B-type discharge is related to the dielectric breakdown in a strong electric field at the metal/oxide interface, which propagates throughout the oxide film.

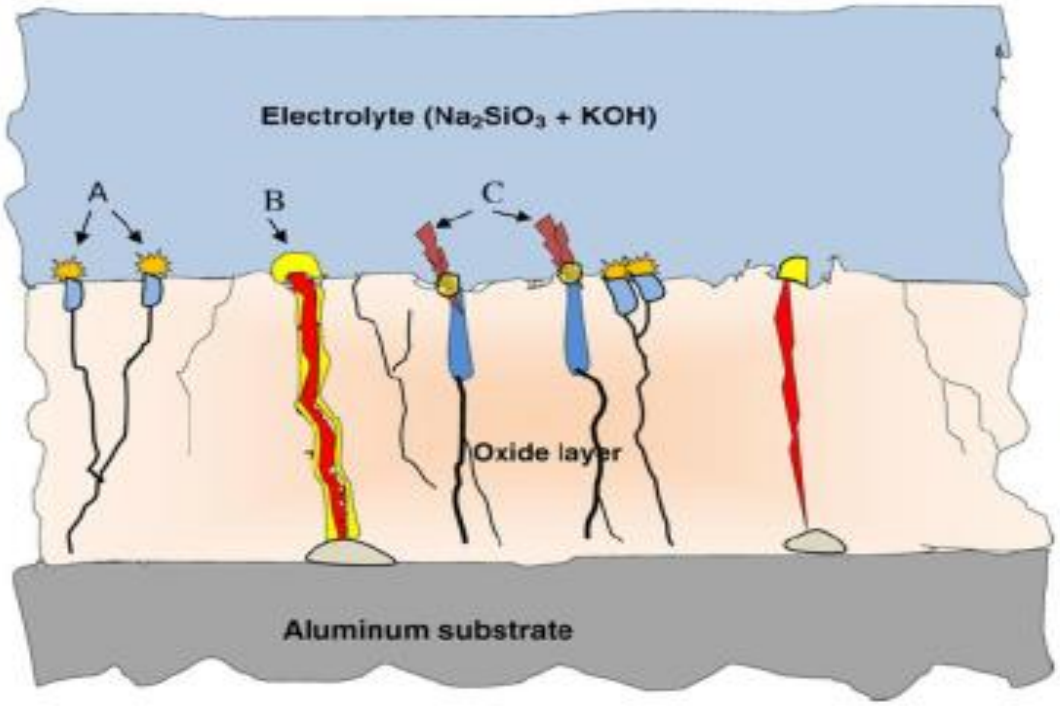

Fig. 2.12 Schematic diagram of the discharge characteristics during the PEO of aluminium substrate. [109]

During these discharges, the Plasma electron temperature raises considerably to an amount enough to excite the aluminium species. It was determined by the line intensity ratio and was found to be in the range of 4500 to 10000 K. Xuan Yang *et al.* [110] analysed the optical emission spectra during PEO process on 7075 Al alloy. They found that the dissolution rate of Al, Zn, Cu, and Mg elements from the working electrode into solution is fast at the initial stage of PEO process. Then the sparks become weak and less populous.

2.3.6. Mechanical properties of PEO coatings

Oxide coatings produced by the PEO process can provide significant strengthening to aluminium substrates, especially for sheet substrates. This effect can increase the effective Young's modulus of the composite to twice value of the metal substrate [8, 111]. The substrate and coatings thicknesses play important roles in this effect. Phase composition is also an important factor affecting the mechanical properties and tribological performance of coatings produced using PEO process [8, 112, 113].

Usual ranges of elastic properties of engineering alumina are summarised in Table 2.6. These properties are frequently needed to provide adequate mechanical or other response of the material to external factors during manufacturing and in service [114].

Table 2.6 Typical values of elastic properties for engineering Al2O3 ceramics [114]

Al_2O_3 / Porosity %	**Young's Modulus GPa**	**Shear Modulus GPa**	**Poisson's Ratio**
≥ 99.6/0-2	410-380	164-158	0.27-0.24
≥ 99.0/1-5	380-340	145-130	0.26-0.24
96.5-99.0/1-5	375-340	140-120	0.25-0.24
86.0-94.5/2-5	330-260	130-100	0.25-0.22
80.0-86.0/3-6	330-260	130-100	0.25-0.22

Earlier studies of PEO treatments of aluminium in alkaline electrolytes [9, 58, 115-117] established that the coatings consist mainly of α-Al_2O_3 and γ-Al_2O_3. For silicate based electrolytes, mullite ($3Al_2O_3.2SiO_2$) can also appear in the PEO coatings. Alpha alumina is a stable phase with a melting point of 2050 °C, while gamma alumina is a metastable cubic phase which can transform into α-Al_2O_3 in the temperature range of 800 to 1200 °C [79, 118]. It has been observed that the contact of electrolyte with molten oxide formed during discharge leads to the formation of γ-Al_2O_3 instead of α-Al_2O_3, which is due to the high cooling rate and lower critical energy for nucleation of γ-Al_2O_3 [11]. Because gamma phase is metastable, by controlling process parameters, such as current density, it would be possible to control transformation of gamma to alpha phase. Curran and Clyne [99] characterised the surface hardness, local stiffness and global elastic constants of the PEO coatings on 6082 Al alloy using nanoindentation, beam bending and curvature measurements. They found that the coating hardness (20 GPa) and stiffness (300 GPa) were both similar to those of dense alumina. This means that the mechanical properties are not in most cases influence by the defects such as porosity an cracks. The effect of structural variations through the PEO coatings on hardness studied by Yerokhin *et al* [8] (Fig. 2.13). It was found that the structural differences tend to cause nonuniform hardness distributions through the oxide coating.

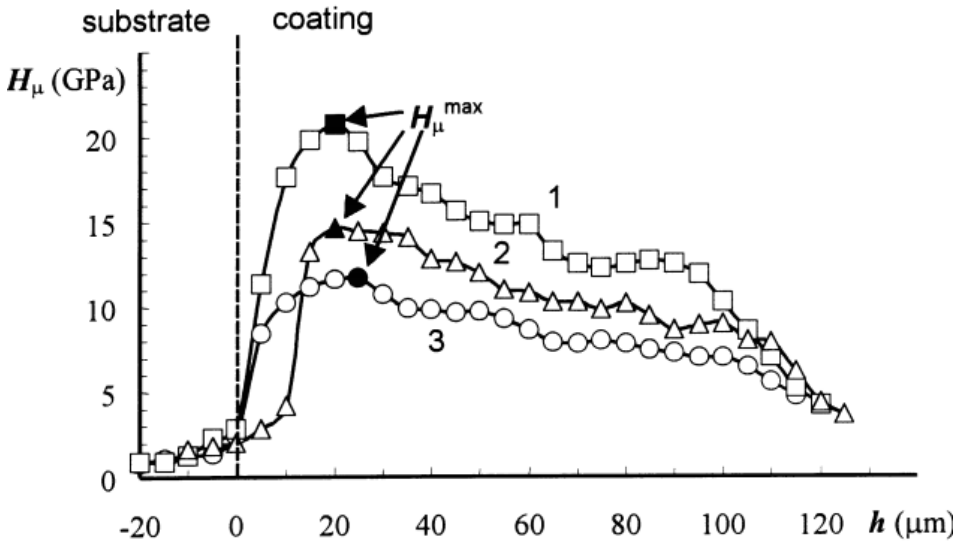

Fig. 2.13 Microhardness profiles through oxide coatings based on (1) α-Al2O3, (2) γ-Al2O3 and (3) mullite. From Yerokhin *et* al [8].

The hardest region exists at around 20 to 30 μm from the coating–substrate interface and relates to the maximum content of high temperature alumina phases in the dense inner coating region. For oxide coatings based on α-Al2O3 phase, the surface hardness was in the range from 17 to 22 GPa. While, it was from 10 to 15 GPa for coatings based on γ-phase and from 4 to 9 GPa for coatings based on mullite.

The subsection above introduced some principles of the mechanical properties of the PEO coatings. It is analyse the effect of the oxide coatings and how strengthening the aluminium substrate. Also mentioned about the properties which may have an effect on increasing or lowering the mechanical properties such as Young's modulus and stiffness.

2.4. Summary

As reviewed above, although alumina films can be produced using a variety of methods, PEO process is an effective technique to produce ceramic films with combination of good mechanical and electrical properties and good price/performance ratio, leading to a wide range of applications. The earliest studies in the area of plasma electrolytic oxidation (PEO) were focussed on evaluating the microstructure, the mechanics, and the thermo-mechanical characterisation of these films. In the following chapters, investigations and analyses for improving the alumina films formed on Al foil using PEO will be discussed and analysed.

Chapter 3
Experimental Procedures

In this work, regular 2D (rectangular) and irregular 3D (L and U) shapes of 50-µm thick aluminium foil samples were used. The studies aimed to convert Al foil to a higher proportion of alumina ceramic by plasma electrolytic oxidation technique, to reveal effects of processing parameters on the degree of conversion and to explore possibilities of obtaining uniform coatings on complex shape substrates that can meet specifications for specific applications. To obtain essential information about the properties of PEO coatings formed on the Al foil samples, it was necessary to study the distribution of the formed oxide layer over the sample surface. For this purpose analyses of the characteristics of PEO coatings such as thickness, porosity, roughness, phase composition, hardness and elastic modulus, as well as composition of plasma discharge, degree of conversion of Al to alumina and evaluation of oxide film growth efficiency during PEO process were carried out on different regions on the sample (edge region, centre region and near the metal part). This chapter contains common details of experiments carried out on the above substrates and outlines materials, experimental procedures, and analytical instruments utilised to achieve the objectives of this research.

3.1. Samples materials

A 50 µm thick foil 1050 aluminium alloy (0.05% Mg; 0.05% Mn; 0.25% Si; 0.07% Zn; 0.4% Fe; 0.05% Ti and Al balance) samples of three different shapes (rectangular, L and U shapes) with surface area (~ 900, 1000, 1500 mm^2) respectively used in most of experiments. The samples cut into the required size (see, Fig. (3.1(a)(b)) were used to convert to a higher proportion of alumina by plasma electrolytic oxidation technique. The samples were cleaned in distilled water and acetone and dried by air before the PEO treatment.

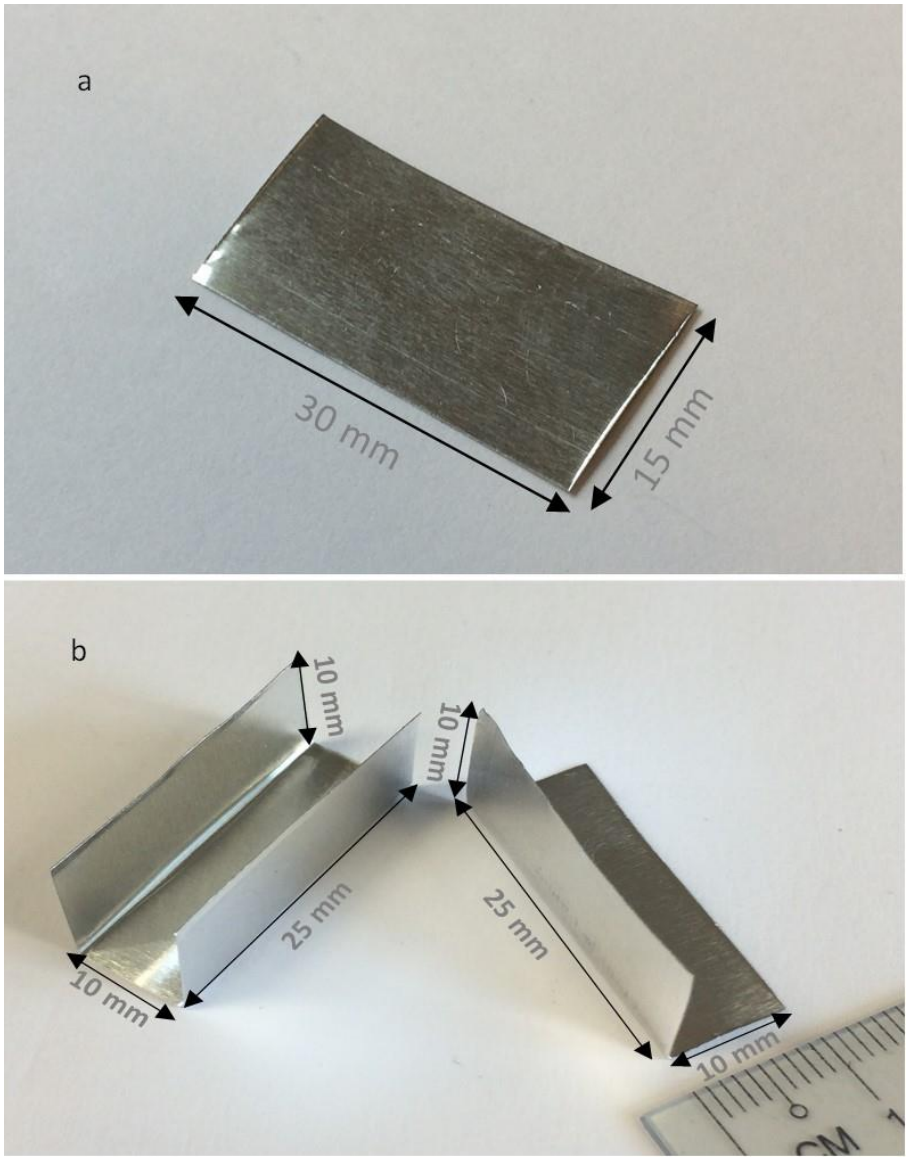

Fig. 3.1. Regular and irregular Al foil (50 µm thickness) samples; (a) Rectangular shape (b) L-shape and U-shape before PEO treatment

3.2. Fixing the samples

Prior to the PEO treatment, due to the very small thickness of the samples during the PEO process, it may move following the movement of the electrolyte solution caused by cooling system and this could cause damage to the samples affected by the uneven electric field and discharges during the process as can be seen in Fig 3.2. Therefore to make it fixed inside the bath during the PEO treatment, it was suggested that rectangular foil samples are fitted using two methods.

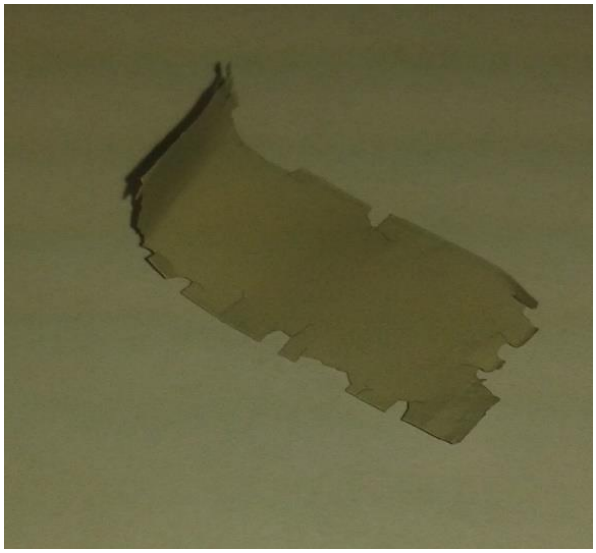

Fig. 3.2 Example of damage incurred due to sample mishandling after the PEO treatment

The first one, it was proposed that foil samples are fixed in a rigid plastic frame holder from four corners as shown in Fig. 3.3 then it is connected from one bolt side by metal holder. However, by using this method still there were some difficulties to connect the samples.

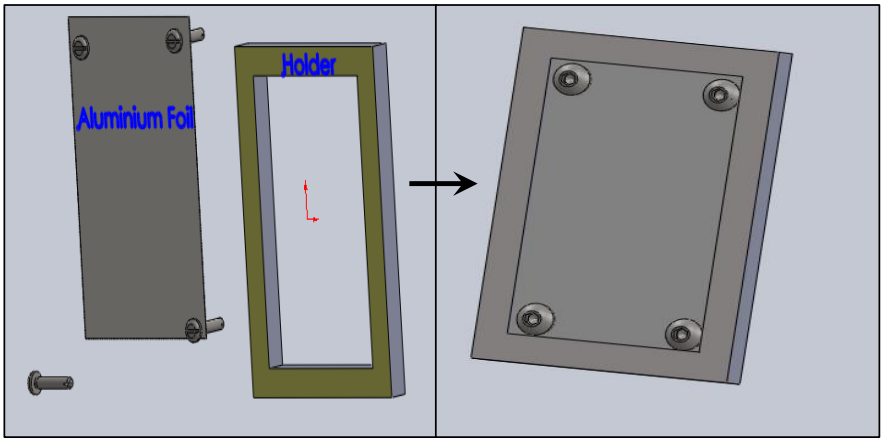

Fig. 3.3 Samples of Al foil fixed in plastic holder.

Another method to fix the specimens during the PEO treatment was proposed and provided better results. This method depends on fixing the Al-foil specimens between two insulated metal holders which are fixed by four jig rods from both sides as shown in Fig. 3.4 and the jig rod was then clamped to the busbar which runs across the electrolyte bath.

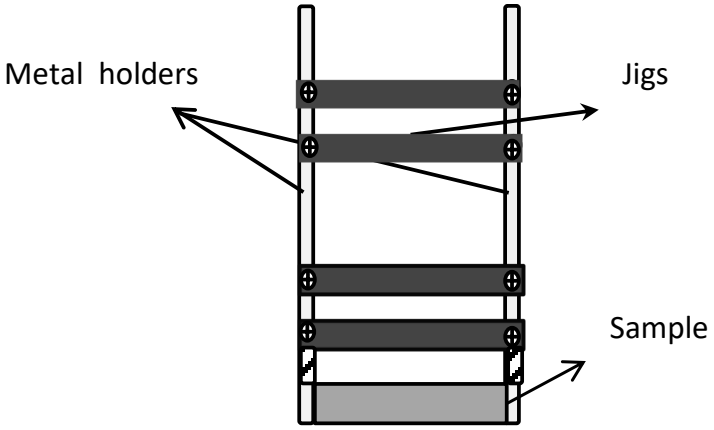

Fig. 3.4 Sample of Al foil stretched between two metal rods.

Furthermore, based on the same idea, irregular samples of L and U shapes were fixed using plastic material from both sides which covered the edges and corners. Then the samples were clamped to the insulated strip of aluminium connected to the power supply. Fig. 3.5 show how the irregular samples are fixed. The samples were fixed by using small rigid plastic pieces and screws.

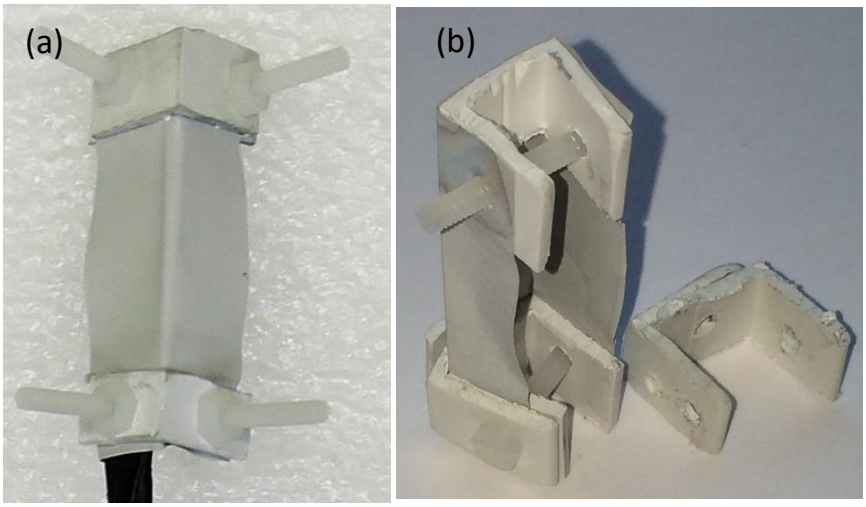

Fig. 3.5 Samples of Al foil fixed in plastic holder (a) L shape (b) U shape.

3.3. Electrolyte solution

The electrolytes were prepared from deionised water and high-purity chemicals. They were prepared by dissolving chemicals, such as potassium hydroxide (KOH), sodium pyrophosphate ($Na_2P_2O_7$), and sodium silicate (Na_2SiO_3), with different concentrations depending on the requirement in 2 litres glass beaker of distilled water and kept stirring by a magnetic stirrer for around 30 min to ensure the complete dissolution for the chemicals. Then

the conductivity and pH of the electrolyte were measured using a conductivity meter (HANNA HI9835) and a pH meter (HANNA-pH211), respectively. The resulting electrolyte pH and conductivity were varied from 11.65 to 12.45 and 3.71 to 7.1 mS/cm respectively also depending on concentration. During the treatment the electrolyte was maintained at room temperature.

3.4. PEO treatment

PEO treatments were performed in a 2 litre steel beaker equipped with electrolyte stirring and cooling system. The plasma electrolytic oxidation processes were carried out in a pulsed bipolar mode (Fig. 3.6) and the process parameters are listed in table 3.1. The treatment time was varied from 2 to 12 min depending on the requirement of a particular experiment. The variations of voltage and current verses treatment time were recorded with a digital oscilloscope linked to a PC. The cooling system maintained the electrolyte temperature below 30℃.

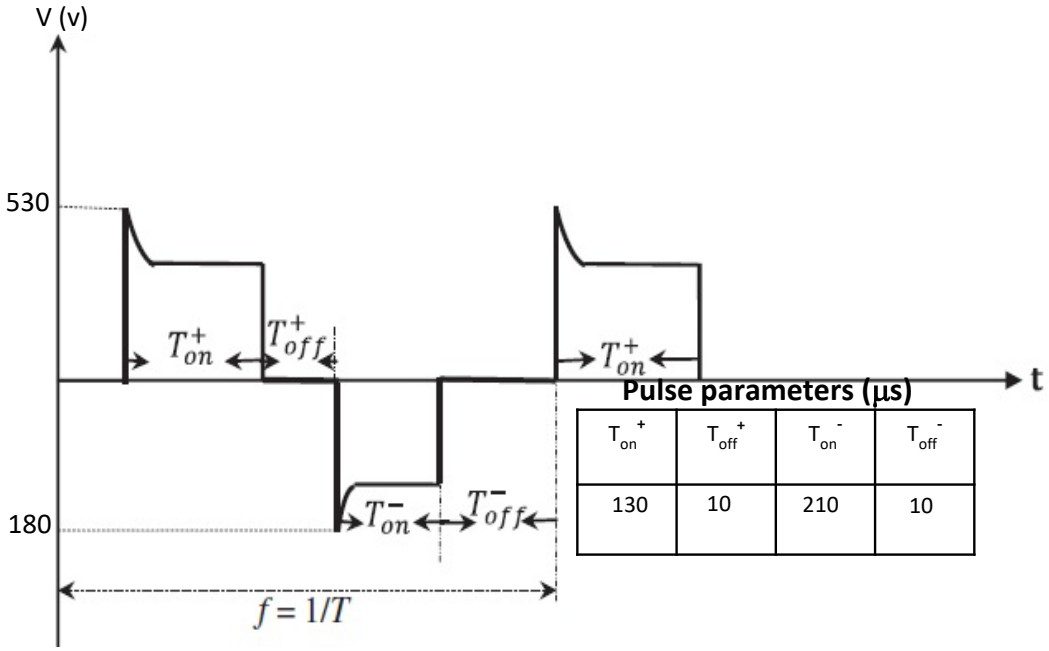

Pulse parameters (μs)

T_{on}^{+}	T_{off}^{+}	T_{on}^{-}	T_{off}^{-}
130	10	210	10

Fig. 3.6. Schematic wave form of the pulse generation.

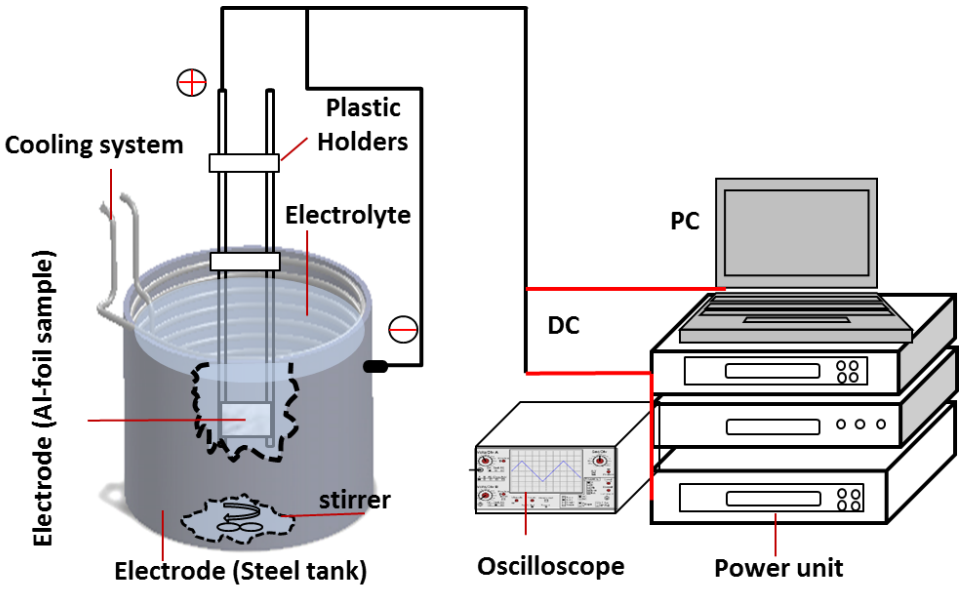

Fig. 3.7 Schematic of PEO process equipment.

Fig. 3.7 shows the overview experimental setup. The process can be briefly described as follows:

I. The working electrode and the counter electrode were connected to the positive and negative outputs of the power supply respectively. Then it was placed at the middle of the steel tank to enhance the equal current distribution during the PEO process.

II. The frequency ($f = 1/(t_{on+}+t_{off+}+t_{on-}+t_{off-})$) applied was set at 2.74 kHz, with 37 % duty cycle ($\delta = t_{on}/(t_{on+}+t_{off+}+t_{on-}+t_{off-})\times 100\%$) for both positive (530 V) and negative (-180 V) voltages.

III. After the PEO treatment, the samples were rinsed thoroughly in water and dried with hot air.

IV. The samples then undergo morphology, thickness, and phase compositions analysis.

3.5. Preparation of mounted samples

For microstructural analysis, the samples were sectioned as appropriate depending on their geometry. Because thin samples, a care should be taken during the cutting process, especially at the edge regions, for which the scissors were used. To prevent the produced oxide layer from damage during handling, copper coating up to 5 µm thickness was applied on the samples by PVD method.

After sectioning, the samples were washed by immersion it in an ultrasonically agitated bath containing acetone and then mounted in resin. The mounting provides convenience in

handling and protection to the edges of the specimen being prepared during polishing operations. In this work, the samples were mounted using a cold moulding method at room temperature. A mixture of epoxy resin with hardener 4:1 by volume was poured over the sample positioned face down in a cold-mounting ring. Then the samples were polished first with a SiC abrasive paper of gradually decreasing grit size from (400-800). Finally, polishing with an alumina suspension was carried out.

For the complex shape samples, the cutting process done when the samples inside the mount with its holder (see Fig. 3.8). This was done to avoid any damage to the coating during handling and analysis.

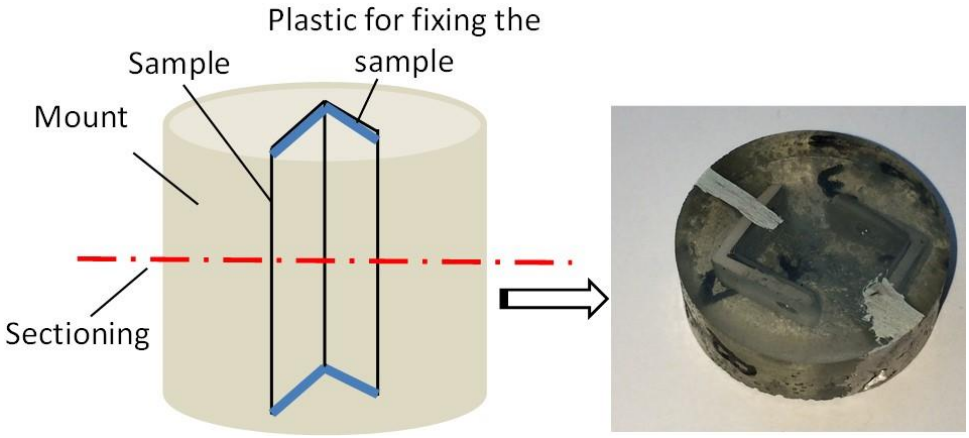

Fig. 3.8. Example of how the L-shape samples were sectioned

Because of the low conductivity of coatings, the samples were also sputter coated with carbon to avoid any surface charging, due of the low conductivity of the ceramics coatings. Additionally, silver paint was used to enhance electrical connection between the Al foil samples and the SEM stage.

3.6. Coating characterisation methods

To develop understanding of correlations between processing parameters, resulting oxide structure, desired properties and performance of composite materials, it was crucial to analyse the coating characteristics. These studies were undertaken utilising different experimental techniques which are described in the following sub-sections.

3.6.1. Scanning electron microscopy

SEM is designed for direct observation of the surfaces of solid objects to study their chemical composition, microstructure and topography. In scanning electron microscope, the electron

beam produced by a biased filament is concentrated by electromagnetic lens towards into sub-micrometre sized spot on the sample and traverses over each point of the specimen. Then the electrons are reflected from each point and collected by a detector which transfers the current into colour intensity [1]. These signals are very sensitive to characteristics of surface morphology such as porosity, roughness (Ra), and cracks.

In this work, the morphology of the alumina layers produced by the PEO method has been studied by a JEOL JSM 6400 and an Inspect F50 scanning electron microscopes (SEM) operated at an acceleration voltage of 10 – 15 kV under vacuum environment. The magnification ranged between 500X to 3000X, in both secondary electron (SE) and back-scattered electron (BSE) modes.

Surface plane and cross-sectional SEM images were analysed using MountainsMap 7.2 software to evaluate the coating porosity, pore size distribution and surface roughness. MountainsMap is a software platform created by Digital Surf Company compatible with most surface imaging, analysis and metrology instruments. It is designed to receive a rich choice of options and provide profile curves and many filtering selections. Coating characteristics such as thickness, porosity, pore size, surface roughness and current efficiency of aluminium dissolution (η_{Al}) in PEO process were analysed by using these programmes.

Surface roughness is extremely important characteristic describing homogeneity of the coating. It has direct effect on mechanical and corrosion behaviour of the coating. A roughness value can be calculated using either a profile (line) or a surface area. Among many different roughness parameters in use, Rz is a universally recognised and the most often used parameter of roughness.

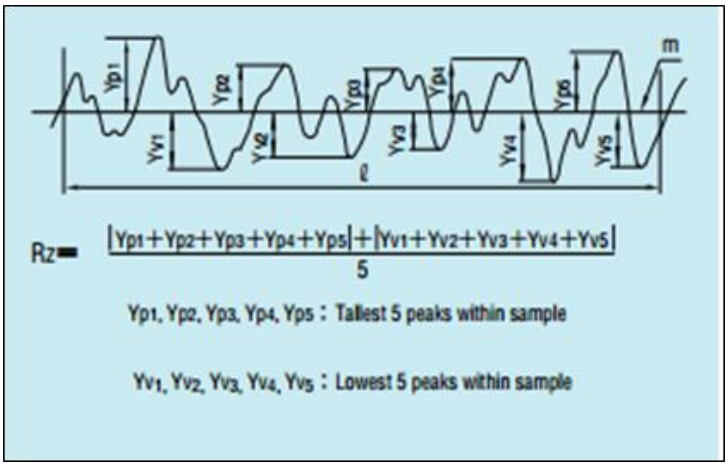

Fig. 3.9 Definition of Rz.

According to JIS B 0031(1994), the surface roughness is defined as the distance between the top profile peak line and the bottom profile valley line of the sampled line measured in the longitudinal magnification direction of roughness curve and the obtained value is expressed in micrometre, (μm) as shown in Figure 3.9.

3.6.2. Coating thickness measurements

Mechanical properties are very important for the applications of the thick and thin films and are influenced by the coating thickness. To determine the thickness of PEO coatings in the SEM images, a MountainsMap 7.4 software was used. Combining SEM with image analysis has been used in many studies. References [1], [2] reported measurement of the oxide layer thickness distribution and its relation to print quality and micro roughness of the base paper. Chinga and Helle [3,4] studied the influence of different coating methods and compositions on the coating characteristics. The density distribution under different conditions was studied by Ratto *et al*. [5]. These analyses and studies provide good examples of evaluation of coating properties based on microscopy and image analysis.

Figure 3.10 shows an example of the cross sectional image of a coated sample, where the coating thickness is denoted as A. To evaluate coating thickness, twenty measurements were taken based on vertical lines in each SEM image. However, in some conditions more than twenty measurements were made to obtain more accurate readings. The results of the measurements were statistically analysed, and the arithmetic average was taken for the coating thickness. The distribution of coating thickness was evaluated to quantify morphology properties of PEO coatings created under different conditions

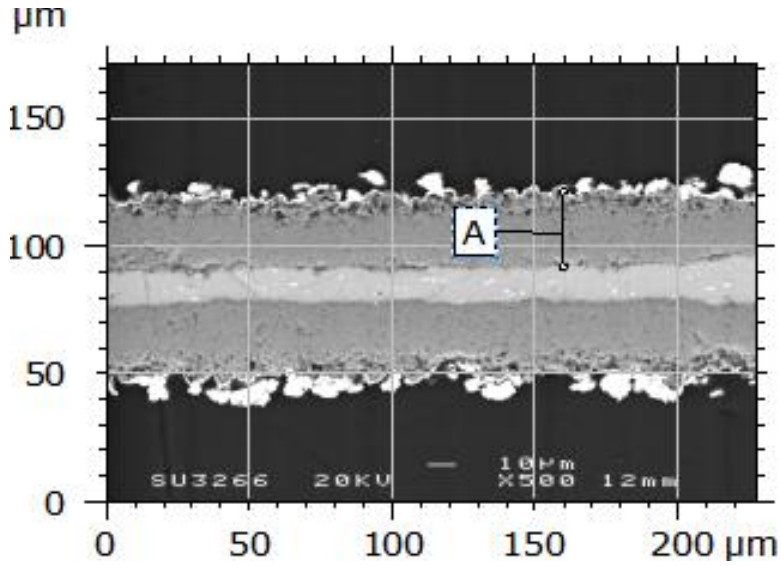

Fig. 3.10 An example of the coating cross section

3.6.3. X-ray diffraction analysis

For further analysis, it was important to detect the alumina phases present and their relative proportions in the produced PEO coatings. X-ray diffraction (XRD) analysis was used to obtain details of phase composition of PEO alumina coatings. This technique is based on constructive interference of monochromatic X-rays and a crystalline sample. The X-rays are generated by a cathode ray tube and filtered to produce monochromatic radiation, then collimated to concentrate, and directed toward the sample. The interaction of the incident rays with the sample produces constructive interference (and a diffracted ray) when conditions satisfy Bragg's Law:

$$2dsin\theta = n\lambda$$

Where $\boldsymbol{d}$ is the crystal lattice plane spacing, $\boldsymbol{\theta}$ is the diffraction angle and $\boldsymbol{\lambda}$ wavelength of electromagnetic radiation. This equation shows the relationship between the diffraction patterns observed when X-ray is diffracted through the crystal lattice and the atomic plane spacing. These diffracted X-rays are then detected, processed and counted. By scanning the sample through a range of 2θangles, all possible diffraction directions of the lattice should be attained due to the random orientation of the powdered material. Conversion of the diffraction peaks to d-spacing allows identification of the mineral because each mineral has a set of unique d-spacing. Typically, this is achieved by comparison of d-spacing with standard reference patterns [119].

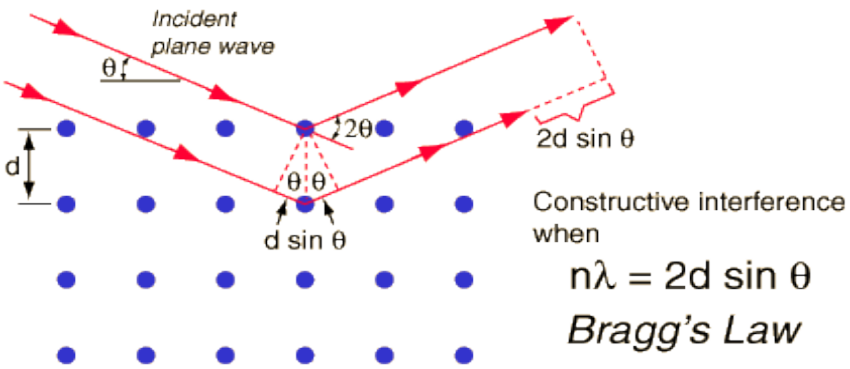

Fig. 3.11 Schematic illustration of XRD principle

In the present study, the XRD experiment was performed using a D2 PHASER X-ray Diffractometer operated at 40 kV and 30 mA with CuKα radiation (wavelength λ=0.15418Å) in the range 35° to 55 ° with 0.2 s per step collection time and the total time was 255.2 s. The obtained diffraction patterns were analysed using OriginLab software.

3.6.4. Nanoindentation tests

Measures of the Young's modulus (E) and hardness (H) of the PEO coatings were obtained by nanoindentation testing using Berkovich indenter with maximum load 10000 μN. AFM Dimension 3100 equipped with Triboscope Nanomechanical test instrument was used. The measurements were taken on cross-sections of PEO coatings. Surface roughness is extremely important in instrumented indentation testing [7], therefore the samples were grinded using 2500 grit sandpaper and subsequently polished using alumina suspension of fine particles 0.3 micron size.

A typical experiment according to the Oliver and Pharr method [120] including controlled loading and unloading of a diamond indenter against the sample surface, at the same time measuring the penetration depth. During unloading, it is assumed that only the elastic displacement is recovered; it is the elastic nature of the unloading curve that facilitates the analysis. For this reason, the method does not apply to the materials in which plasticity reverses during unloading.

The earlier experiments [120] was suggests that, the reduced modulus (E_r) can be determined from unloading data collected through the following equation;

$$\frac{1}{E_r} = \frac{(1-\nu_s^2)}{E_s} + \frac{(1-\nu_i^2)}{E_i} \qquad (2.1)$$

Where v_s and v_i are the Poisson's ratios for the sample and indenter and have values 0.07 and 0.3 respectively, while E_i is the Young's modulus of indenter has value 1141 GPa. A schematic representation of a typical data set obtained with a Berkovich indenter is presented in Fig. 3.12 [120].

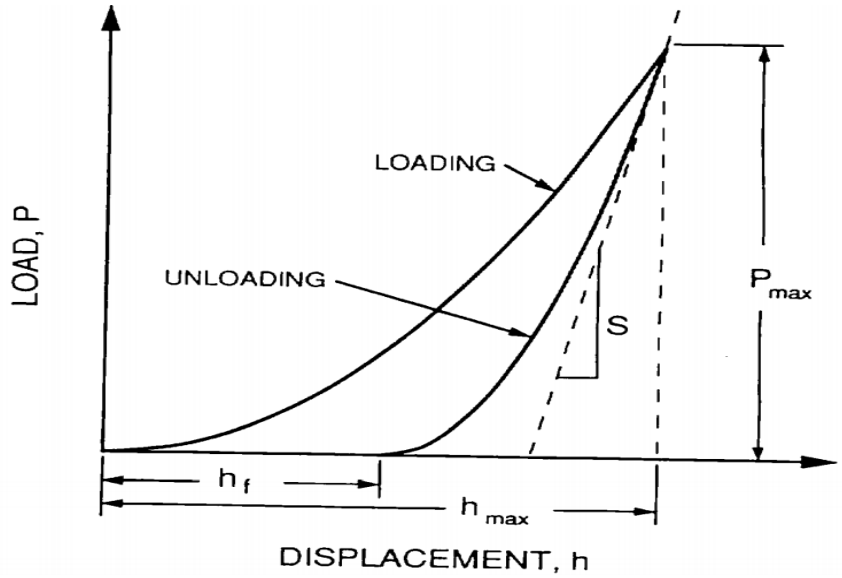

Fig. 3.12 Schematic illustration of indentation load–displacement data showing important measured parameters

This was then analysed according to the equation;

$$S = \frac{dp}{dh} = \frac{2}{\sqrt{\pi}} E_r \sqrt{A}$$

Where S is the experimental measured stiffness of the upper portion of the unloading data, A is the projected area of the elastic contact. Oliver and Pharr's in their analysis stated that the mean contact pressure or (hardness) H, was then determined from the maximum load (P_{max}) and the corresponding projected contact area (A):

$$H = \frac{P_{max}}{A}$$

In the present work, this was indented three areas per specimen by 3x4 grid with an indent spacing of 3 µm.

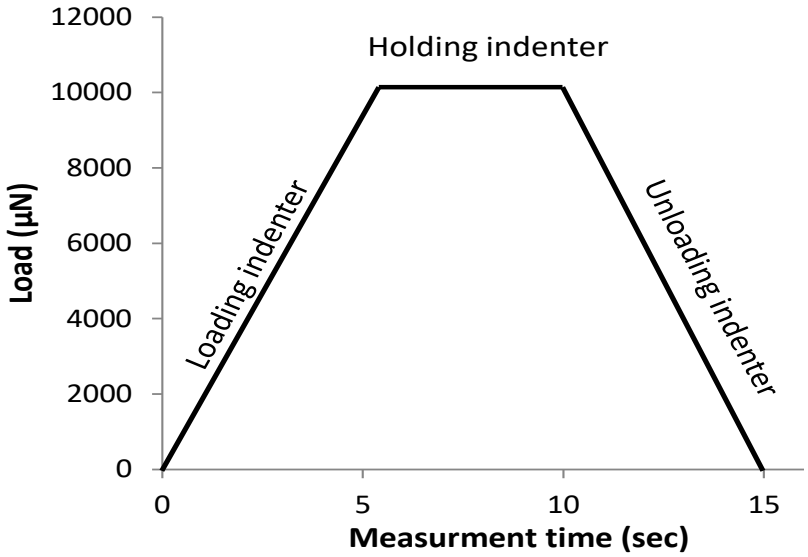

Fig. 3.13. Schematic of load-time curve during each indent; Peak load = 10000µN

All indentation measurements were done on PEO coatings followed a load-time cycle provided in Figure 3.13. As can be seen, a three-step load function was programmed to achieve the nanoindentation loading cycle. The first segment comprises a peak loading in 5 sec, followed by a 5 sec holding at the peak load in the second segment. The third segment retrieved the indenter tip from the sample in 5 sec before reloading for the next cycle. During the measurements, attempts were made to avoid the porosity or large cracks and neglect any indents measured on the coating defects.

3.6.5. Optical emission spectroscopy

Optical emission spectroscopy (OES) study was performed with FloTron XHR spectrometer with effective range of 300 to 900 nm to collect the spectra over duration of 6 min treatment time on L and U shape Al foil samples. To ensure that the maximum light was collected by an optical fibre for both inner and outer surfaces, the lens was placed at around 5 mm in front of the sample. The collected spectra were analysed to identify characteristic plasma species and monitor emission intensity of corresponding spectral lines as a function of processing time.

3.7. COMSOL-Multiphysics modelling

COMSOL Multiphysics software is a powerful finite element (FEM), partial differential equation (PDE) solution engine which is widely used in many fields. It has several modules that enhance the abilities of the basic software into the several application areas such as

AC/DC, chemical engineering, heat transfer and structural mechanics. The COMSOL Multiphysics software also has other supporting software, such as the CAD import module and the material library [8].

To achieve better understanding about the electric field and current density distribution in the electrolyser during the PEO process which strongly influenced the treatment uniformity, a COMSOL MULTIPHYSICS 4.4 [121]modelling software package was used. A simple model was considered to investigate the distributions of the magnitude and direction of the electric field and current density in the electrolyser during the PEO treatment of irregular shape samples. The model description and some considerations for building up the current density and electric potential distribution model in the electrolyser during PEO treatment is introduced in **Section 7-5-1**.

3.8. Summary

This chapter looked at the research methodologies used in this study. The use of these procedures allows understanding of the properties of PEO coatings analysed in the present work to be achieved. Besides it presents useful means to fulfil the aims stated in **Chapter 1**. Detailed information on the using of these methods is given and discussed in the following chapters (**Chapter 4-8**), as particular experimental parameters and analytical methods may differ based on specific conditions, such as different shape of samples, current mode and PEO coating properties.

Chapter 4

Effects of treatment time on formation of PEO coatings on regular shape aluminium foil substrates

4.1. Introduction

One of the important variables needs to be taken into consideration during creation of a PEO coating, is the time of the process. The time affects the morphology and thickness of the PEO coatings which change the coating characteristics [11, 12]. Therefore, the oxidation time for PEO treatment should be investigated and optimized.

Natural brittleness of oxide ceramics become the main obstacle for their extensive use. However, the presence of residual aluminium from the substrate not converted to the oxide may enhance the flexibility of structures based on alumina films [122].

Several parameters have an effect on the PEO process such as current mode, electrolyte and substrate composition as well as electrolyte temperature. Treatment time is one of the main factors influencing the characteristics of PEO coatings [8, 42, 123]. Different treatment times varying from a few minutes to several of hours have been used in research to understand characteristics and properties of the formed coatings [8, 51, 123, 124]. The thickness and morphology of the coatings are affected primarily, which can change the properties. Commonly, increasing the treatment time results in thicker coatings produced under more powerful and larger micro-discharges causing bigger discharge channels in the oxide layer as reported by Sundararajan *et. al*.[11]. However, this increase in thickness may have different effect on coating behaviour. It has been recognized that when using a pulsed bipolar current (PBC) mode for the PEO treatment of aluminium alloys [55], the optimal combination of the coating growth rate and energy consumption can be obtained at a pulse frequency between 1 and 3 kHz. In addition, the PBC PEO process showed improvement in coating morphology, when growing uniform surface layers of 50 to 70 μm in thickness.

Many studies of the PEO coatings formed in alkaline silicate-phosphate electrolytes concluded that the oxide layer thickness initially follows a direct relationship with treatment time, and after reaching the highest point, the film thickness begins to decrease because chemical dissolution starts taking over the coating formation [12]. Dun Lee *et. al* and Hussein *et. al*. [10, 70] reported a linear dependence of the coating thickness on treatment time,

whilst non-linear behaviour was reported by Al Bosta *et. al.* [12]. Treatment time of the PEO process not only influences oxide layer thickness but also surface roughness. The linear increase in coating roughness is directly related to the fact that the mean average diameter of discharge channels also increases linearly with coating time. Crystalline phases such as γ- and α-alumina formed during the PEO process are strongly affected by volcano-like features and the accumulated particles in the coating, which in turn is influenced by the treatment time, and this is consistent with the results reported by Yerokhin *et. al* [8]. The main objectives of this part of the study are: (i) to analyse the effect of PEO processing time on the characteristics and properties of the coatings deposited in different regions of a regular shape aluminium foil substrates; (ii) estimate the coatings growth efficiency during PEO processes (ii) find out the acceptable PEO processing time to get a relatively high degree of conversion of Al into its oxide and the limitations to create uniform coatings on the surface substrates.

4.2. Experiments

Rectangular samples of aluminium foil (0.05% Mg; 0.05% Mn; 0.25% Si; 0.07%Zn; 0.4%Fe; and Al balance) with dimensions of 30 mm × 15 mm × 0.05 mm and surface roughness of Ra ≈ 0.1- 0.2 µm were used. The exposed working area of the samples measured using a vernier calliper was 4.5 cm^2. The experimental setup is shown in Fig. 4.1. The PEO rig consisted of a 30 KW power unit and a 2-L stainless steel tank equipped with magnetic stirring and cooling by continuous pumping via cold water heat exchanger to maintain the temperature between 25 to 35 ^oC.

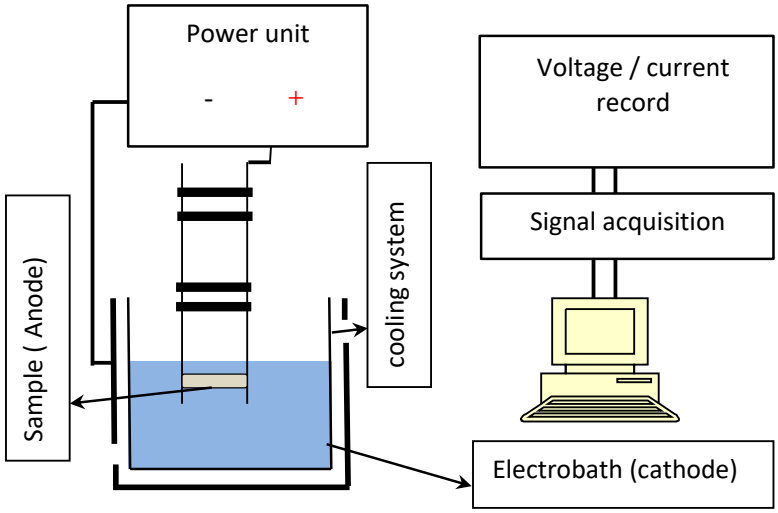

Fig. 4.1. Schematic of PEO processing equipment.

Before the PEO treatment, the samples were cleaned in distilled water and acetone and dried by air. The aqueous electrolyte contained 1.0 g/L KOH, 2.0 g/L $Na_4P_2O_7$, 2.0 g/L Na_2SiO_3 with pH value of 12.05 and conductivity 6.0 mS/cm^{-1}. The electrical parameters of the PEO process are presented in Table 4.1. To keep the same distribution of electric field on the sample surface during the treatment, the working electrodes were suspended and positioned centrally using an isolated metal holder, in the middle of the tank. The treatment was carried out in a PBC PEO mode with frequency 2.74 kHz. The voltage was controlled at +530V and -180V. The variations of voltage and current versus treatment time were recorded with a digital oscilloscope linked to a PC. In order to make comparisons between the samples treated in different experimental conditions, five treatment times were selected (2, 4, 6, 8, 10 min). After the PEO treatment, the samples were rinsed thoroughly in water and dried.

Table 4.1. Electrical parameters of the PEO process.

Mode	**Voltage (V)**		**Pulse parameters (μs)**			
			T_{on}^+	T_{off}^+	T_{on}^-	T_{off}^-
Bipolar	+530	-180	130	10	210	10

4.3. Samples analysis

To understand the properties and characteristics of PEO coatings formed on the Al foil samples, it is an essential to understand the nature of the formed oxide layer. For this purpose, the analysis of PEO coating characteristics such as thickness, porosity, surface roughness, phase composition, degree of Al conversion to alumina, hardness and elastic modulus as well as evaluation of oxide film growth efficiency during PEO process were performed on different regions on the sample (edge region, centre region and near the metal part) (Fig 4.2).

Cross-sectional and surface scanning electron microscopy analyses were performed using ImageJ and MountainsMap 7.2 software to determine the characteristics of PEO coating. Further details of the facilities, equipment used and how the samples were fixed are described in **Chapter 3**.

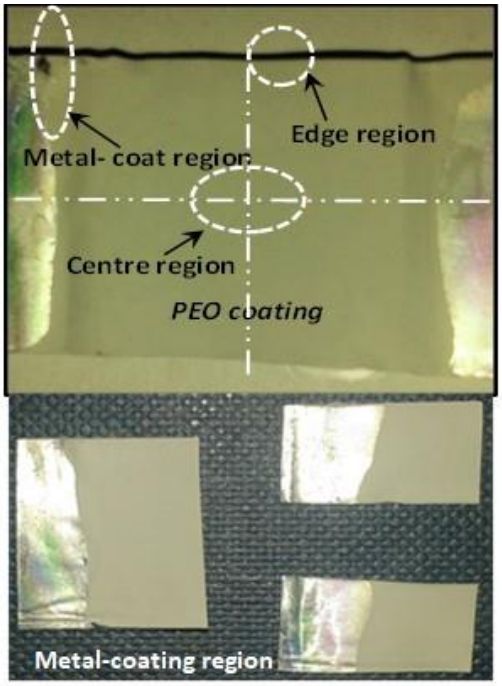

Fig. 4.2 Typical sample appearance after the PEO process showing regions selected for surface and cross-sectional morphology analysis.

4.4. Characterisation of current density during plasma electrolytic process

The current density–time response for the PEO coatings produced for various treatment times are shown in Fig.4.3. At the first stage, an initial linear increase in current density occurred through a short period of time to values from 0.32 A/cm^2 to 0.4 A/cm^2 based on the ramp time setting up for the voltage raise to the pre-set values, which are 530 V and -120 V in our work. Before the required voltage is reached, there were similarities in the shape of curves for all conditions, whatever the current density value is reached. This rising is similar to the creation of the conventional anodic oxidation as well as the thin aluminium oxide film. This appears to be similar to the results in references [12, 52, 55, 125-127]. This stage is controlled by the hydrogen and oxygen reactions products over the working electrode surface, which means the increasing of current is limited by a partial shielding action of hydrogen and oxygen [8].

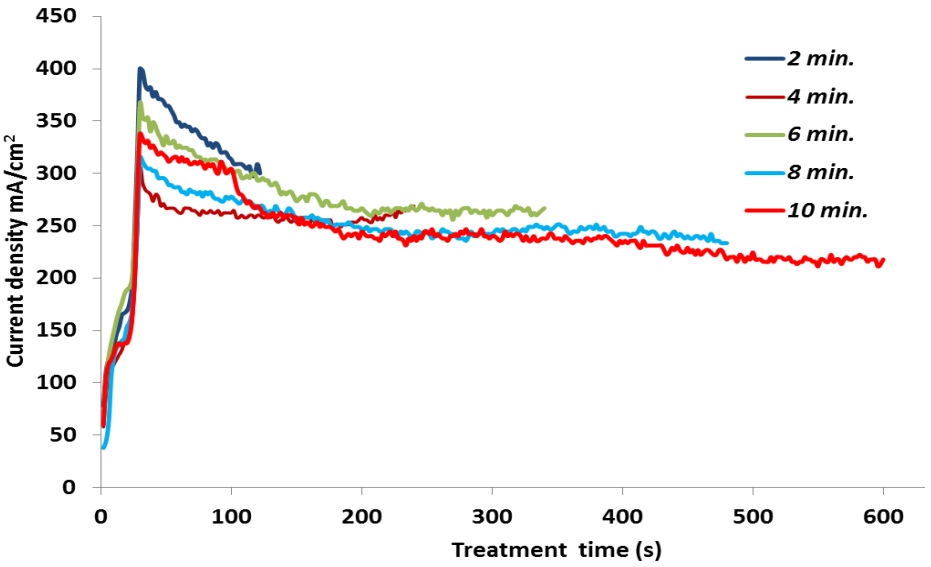

Fig. 4.3. The plot of current density versus PEO treatment time.

A comparison of the curves showed no considerable difference in current density behaviour during the treatments for 6, 8 and 10 min. However, the maximum value achieved in the sample treated for 2 min process time due to the lower electrical resistance gaseous vapour envelope. At this point, the electric field strength on coating reaches the maximum value, which is sufficient to initiate ionisation phenomena at the electrode-electrolyte interface. This corresponds to the breakdown voltage of the oxide film formed on the specimen surface. Then, the current density slowly reduces with time. The major change occurs during the first 160 to 170 s as can be seen in the curves of samples treated for 6, 8 and 10 min. This indicates that the coating thickness changes considerably during this period of time. During the 4-min treatment, it took around 70 sec to reach the steady state, while the sample treated for 2 min did not reach it at all. The duration of this period depends on the critical thickness of oxide film, which in turn depends on the values of current. In our work the treatments were carried out at constant voltages, however the current density varied for different samples. The reason could be related to the fact that the voltage drop in the electrolyte depends on the sample surface area, since during fixing the samples we used insulation tape, so the active surface area during the process maybe differ on each other. Another reason which is related to the changing of the electrical conductivity of the electrolyte during different runs. The time of reaching the steady state wherein the thicknesses of the oxide layers show no insignificant changes was 100, 110, 200, 210 seconds during the treatments carried out for 4, 6, 8 and 10

min respectively. According to visual observations of the PEO process, a disparity in changing the colour and density of the microdischarges occurred during all PEO treatments. The colour of the micro-discharges changed from bluish white to yellow and finally to orange while the discharge intensity increased and density decreased. It is believed [128] that the strong and long-lasting sparks could have a detrimental effect on the coatings.

4.5. Thickness measurements

The thicknesses of coatings formed in side A at different regions on the working electrodes is shown in Fig. 4.4.

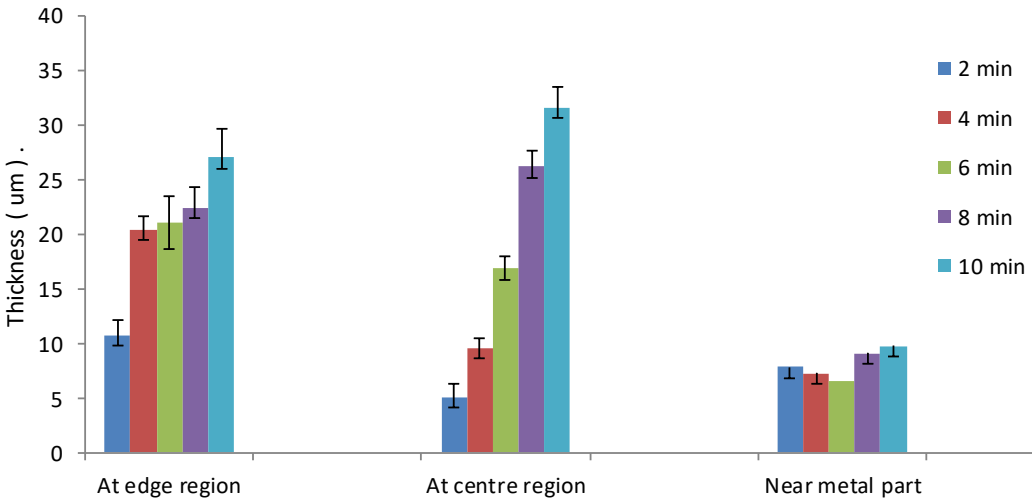

Fig. 4.4 The PEO coating thickness as a function of treatment time in the edge region, at the centre region and near the metal part.

Fig. 4.4 show the thickness of the PEO coatings in the centre and edge regions is often a linear function of the treatment time and the data shows it is possible to obtain coatings with thickness more than 32 µm at one side in the central region. It can be noticed that, as the treatment time of the PEO process increases the coating thickness increases too. This relation between the thickness and treatment time is consistent with the observations by Dunleavy *et. al*.[125], who conducted PEO treatment of an aluminium alloy in a similar electrolyte. To compare the coating thickness between the three regions, the thicker oxide films under all treatment conditions were formed in the edge regions, except samples processed for 8 and 10 min, where the coatings in the central region were slightly thicker than at the edge. This difference may be significant in some application which needs a degree of stiffness in one side. The difference in coating thickness between the edge and centre region for all conditions

ranges from 3 to 5 µm except sample treated for 4 min where the difference reached around 7 µm. This is because the PEO coating formation is strongly dependent on the primary electric field distribution and the sample might not have been in the centre of the tank [129, 130]. From the thickness measurements in various regions of the samples, it appears that the coating thickness is distributed unevenly on both sides, except for the central region of the sample treated for 10 min, which displays difference of up to 9 µm due to the effect of current density at the edges of the working electrode. However in the regions near the metal part, the thickness on both sides along the sample length shows differences varying from 1 to 3 µm from the beginning of the coating formation to around 40 µm as well as high porosity.

Fig 4.5 show the oxide growth rate at different process times. As can be seen in Fig 4.5 the growth rate of the oxide layer formed for 2 min was 0.04 µm/sec and it continues increasing until reaching around 0.06 µm/sec for the coating formed for 8 min. After that the growth rate decreases to 0.05 µm/sec for the coating formed for 10 min. The same logics underlies the decrease in residual aluminium thickness with PEO treatment time. For instance, no significant difference in residual aluminium thickness between samples treated for 8 and 10 min. This means, with an increase in treatment time the dissolution of aluminium becomes very low and the growth of thickness becomes toward the inner direction of the substrate and the removal (ejection) of Al^{3+} ions from the oxide film towards the solution generating the aluminium vacancies in the oxide layer which causes a porous structure [131]. From data of aluminium residual thickness (Fig 4.6), it can be said that the fraction of aluminium foil consumed was around 5 % after 2 min, while it reaches to 80 % for after 10 min of treatment.

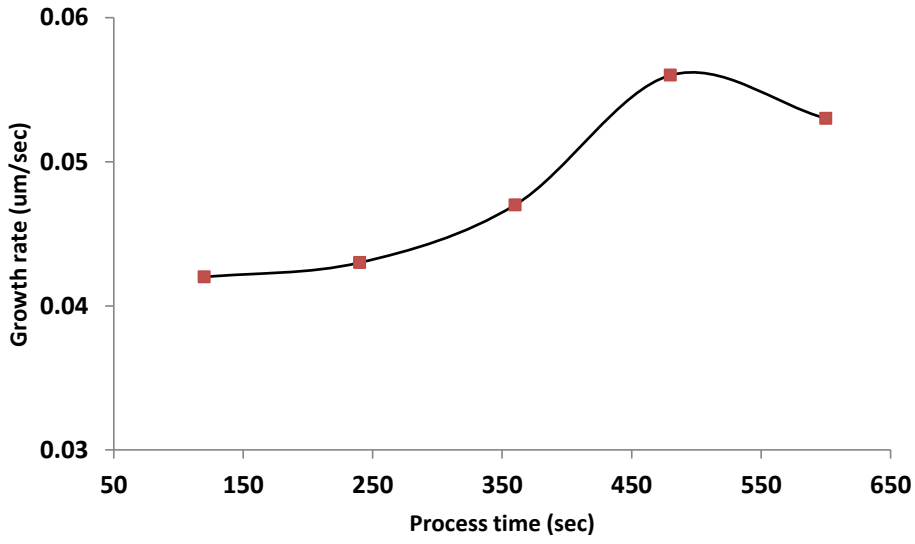

Fig. 4.5 Coating growth rate at different treatment times.

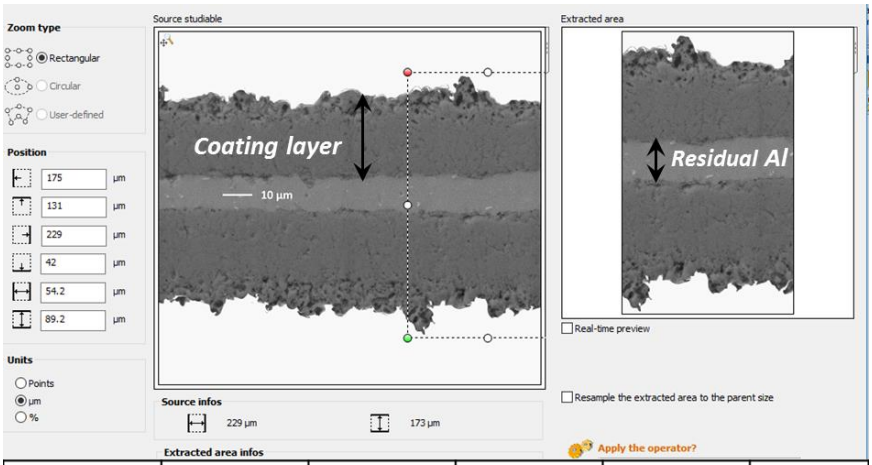

Treatment time (min)	2	4	6	8	10
Residual Al thickness (µm)	47.5	37.5	30	12	10

Fig. 4.6 SEM images of a cross section of PEO coating on Al foil treated for 10 min, showing residual aluminium thickness.

Due to the aluminium dissolution process during formation of PEO coatings, it's difficult to identify the direction of the oxide layer growth, however taking into account a very small difference in the total thickness for whole sample after the PEO process carried out for 8 and 10 min, in the final stages the PEO process, the coating appears to grow mainly toward the aluminium substrate. R.O. Hussein et. al. [10] in discussing the ceramic layer growth mechanism during the PEO treatment stated that the oxide layer grows inwards and outwards concurrently. However during the first stages, the oxide layer grows mainly outwards and after a certain thickness is reached the growth towards the substrate becomes faster. However at the same time, the oxide layer thickness remains increasing on both sides with different degree of growth.

In order to achieve a better understanding about the mechanism of the coating formation and the conversion of Al to alumina, the treatment time was increased to 12 min to achieve the full conversion to alumina. The total thickness of the resulting oxide layer was 75 ± 1.5 µm and the full conversion to alumina occurred except for a small area not exceeding 1.0 % from the total area of bulk material (aluminium foil) distributed in different area along the sample length as shown in Fig 4.7.

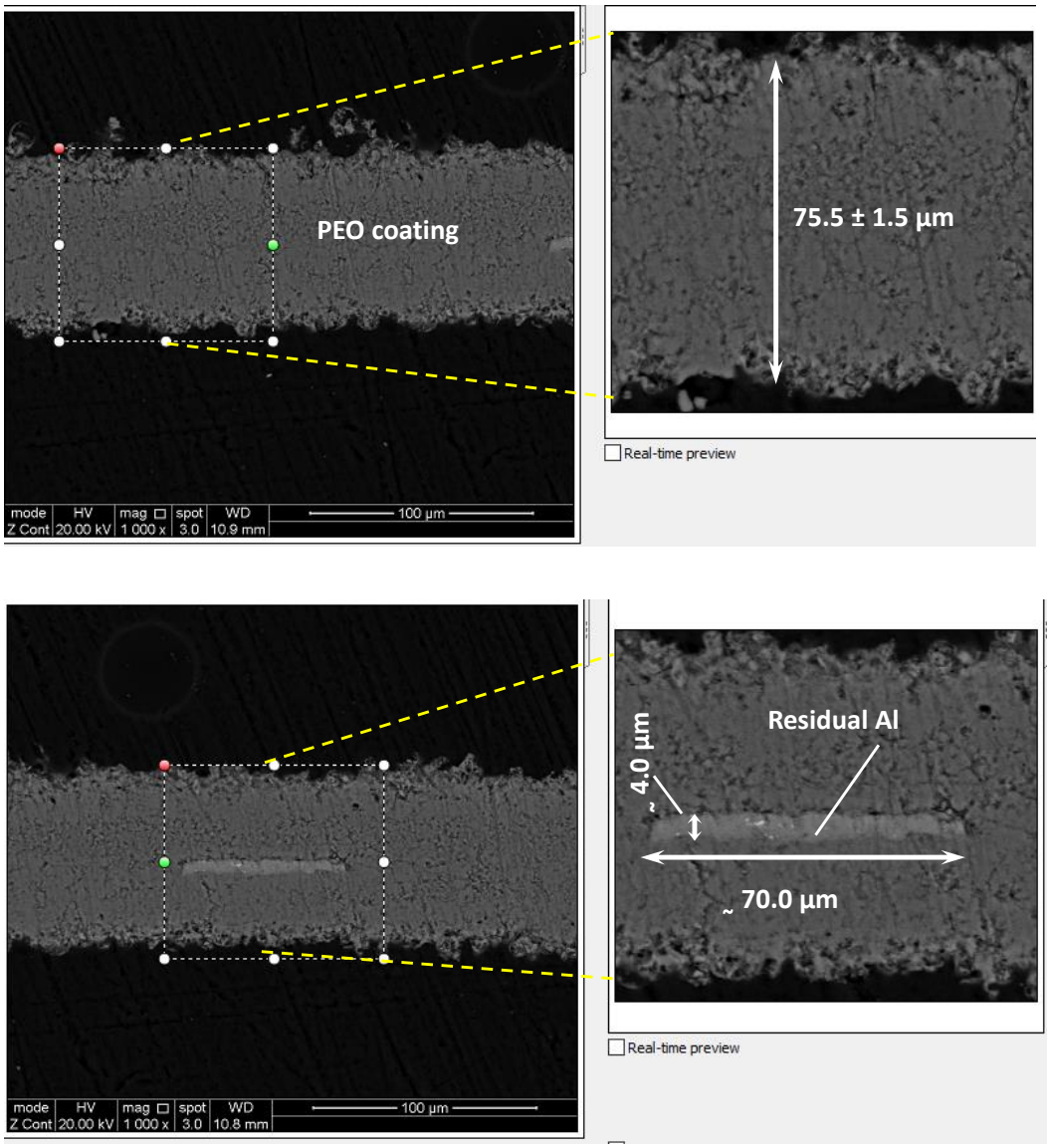

Fig. 4.7 SEM micrographs of cross-sections of PEO coatings on the sample treated for 12 min showing full conversion and a small area of residual aluminium.

4.6. SEM morphologies

Figures 4.8 presents the SEM micrographs of surface morphology of oxide coatings in different regions of Al foil samples treated for different periods of time. All samples showed a number of “pancake” like features, with discharge pores of irregular shape were located on the coating surface, which is a common feature of PEO coatings. In central regions of the samples treated for 6 and 8 min, a centre of each pancake featured a pore formed by the discharge channel through which the molten aluminium surged out, reacted with oxygen and quickly solidified leaving pores and distinct boundaries [12, 74]. In the sample treated for 6 min, the size of the pores in the central region ranged from 3 to 6 µm, with some areas on

the surface occupied by volcano-like structures created by discrete localised micro-discharge events. The volcano-like features indicate the surface temperature during the PEO process was high, which explains the high strength of the microdischarges [11, 99, 115]. Relatively large holes in the centre of the pancake for all samples suggested that there were strong localized discharges and such holes penetrate in the coating thickness. As shown in Fig 4.8, some microcracks exist in the coating at the central region of the sample treated for 8 min, as indicated by the white circle. This is maybe due to the temperature difference between the coating and the electrolyte, which is caused by the rapid cooling. During the PEO treatment the temperature in the discharge channels was very high, reaching thousands degrees Celsius, and the electrolyte temperature ranged from 30 to 40 ^{o}C rate. Therefore, subsequent thermal shocks led to the appearance of cracks in the oxide layer [74, 132]. At the edge regions in the samples treated for 2 and 4 and min, some cracks can also be seen. These cracks could have been caused by handling the thin delicate samples.

SEM micrographs in Fig 4.9 show cross-sectional morphology of the coatings formed in different regions of aluminium foil samples at different processing times. For all samples, the oxide layers appeared to have a significant amount of porosity, holes, and discharge channels within the coating and near the coating substrate interface, in all sample regions. Such defects and porosity were likely to be caused by powerful discharges developed at the sample surface. During the PEO coating growth, the porosity was formed as a result of localized oxygen trapping in molten aluminium in the vicinity of plasma discharges. So it will possible that the pore network helps the creation of relatively high thickness oxide layers by allowing the electrolyte to penetrate deep into the growing layer during the treatment [61].

A comparison of cross-sectional images (Fig 4.10) indicates that the coatings formed for 6, 8 and 10 min comprise two regions, the outer porous and the inner dense region. Most of the pores and defects in the outer region are caused by localised discharges.

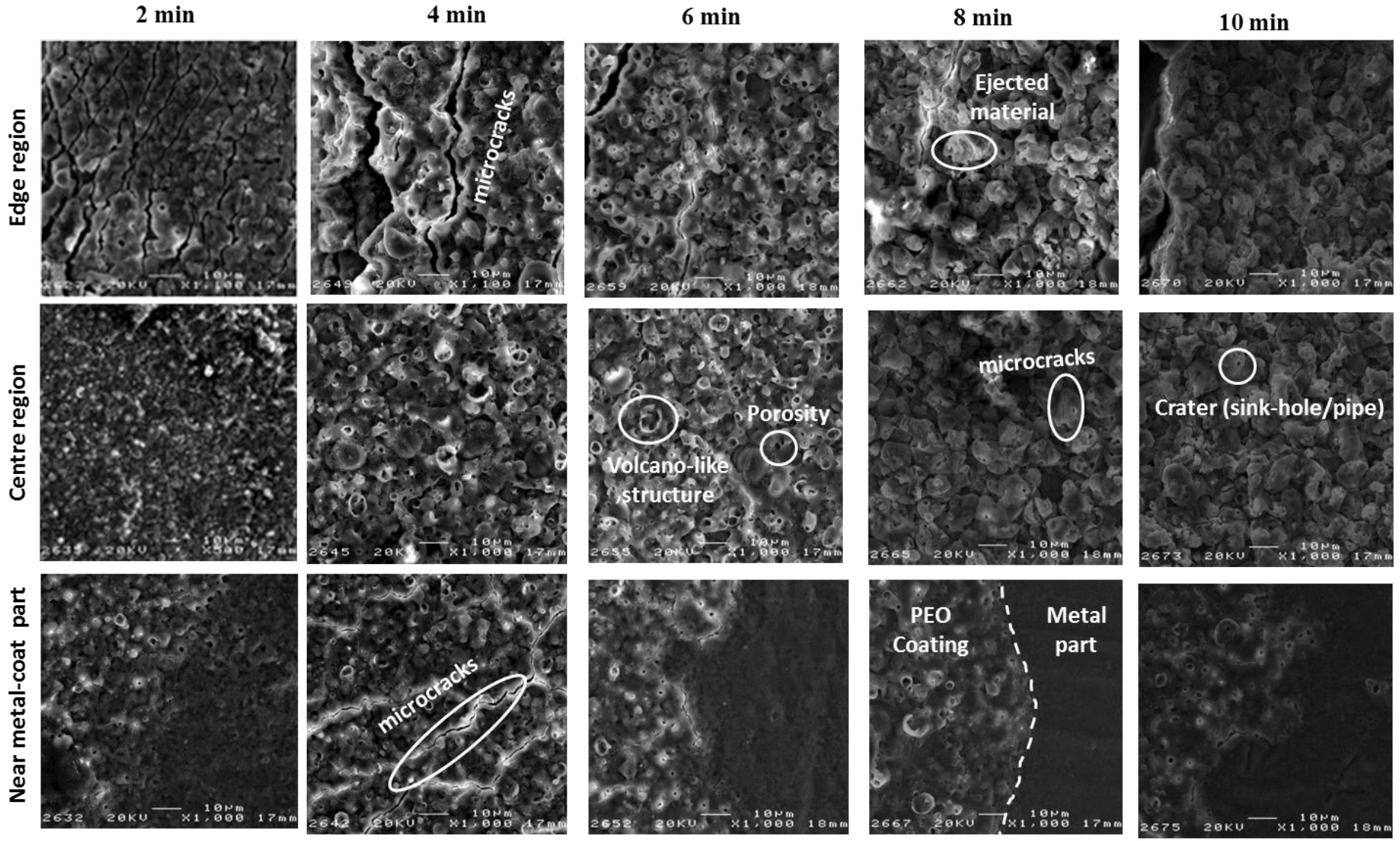

Fig. 4.8. SEM micrographs of surface morphology of oxide films in different regions at different treatment times

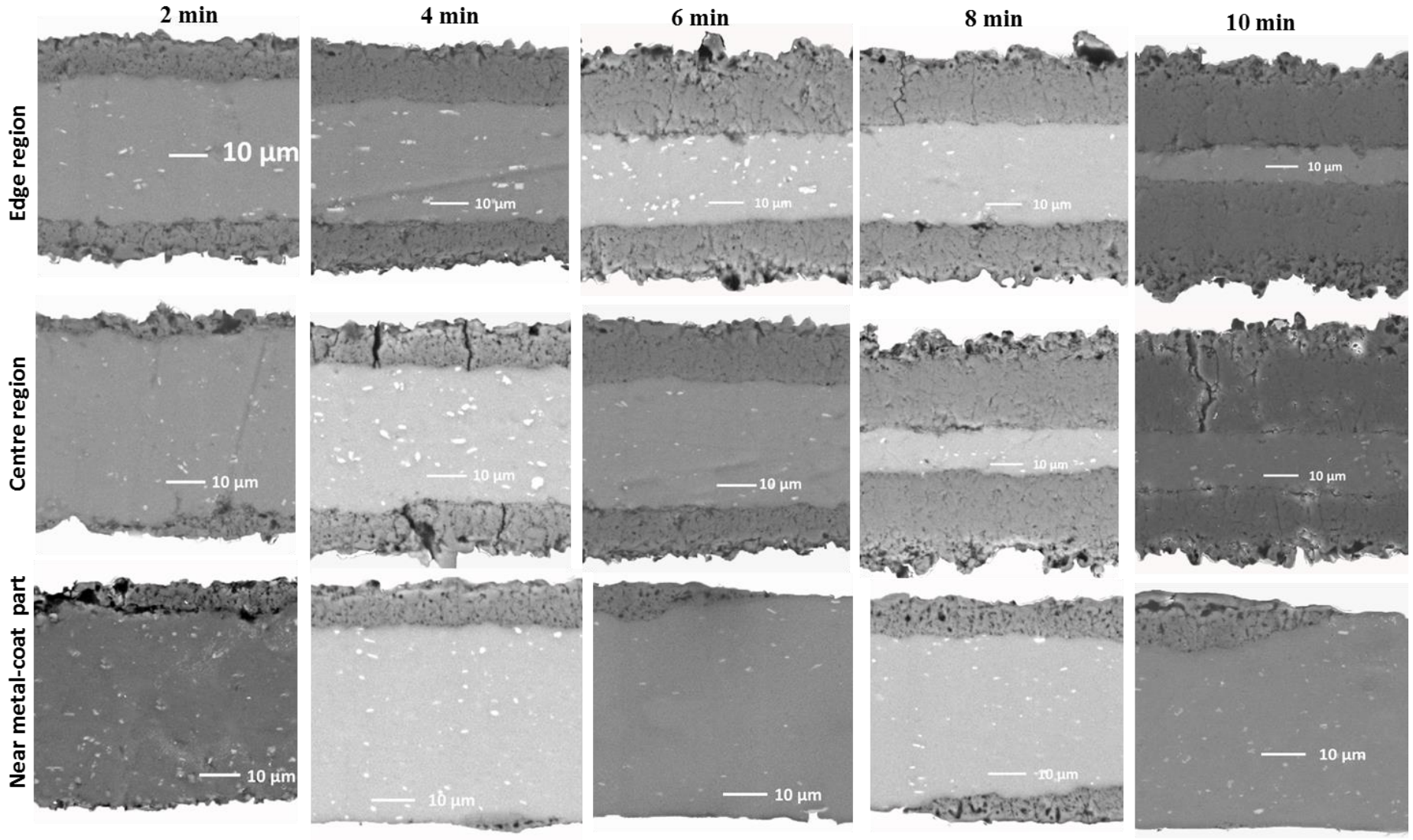

Fig. 4.9 SEM micrographs of cross-sectional morphology of oxide films formed in different regions and for different periods of time.

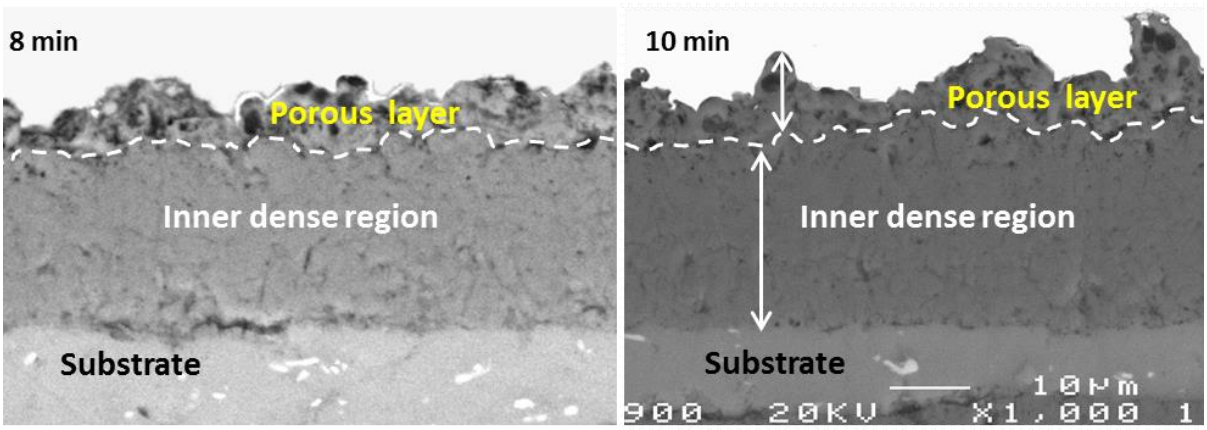

Fig. 4.10 SEM images of PEO coatings on Al foil treated for 8 and 10 min showing the outer and inner regions.

The inner dense region of the coating formed is composed of γ and α alumina phases. It may be subdivided into intermediate dense region and inner barrier layer which is probably the main contributor to the chemical properties of the coating. As mentioned in the methodology chapter, the software MountainsMap 7.2 was used to estimate the coating porosity. Fig 4.11 (a) and (b) show SEM images of surface morphology of the oxide film on the sample treated for 6 min before and after estimation of porosity, depending on the colour variation. As seen in Fig (4.10(a)) the pores in dark are easily distinguishable from other microstructure, which can be identified. Fine pores exist in some regions such as centre region in samples treated in 8 min as seen in Fig 4.9. However, it is unsurprising if not appear, where it could be filled or deformed during the micropreparation of samples. These fine pore network may be cause a limitation of using this method. The highest porosity was present in the edge region in the sample treated for 2 min. While the sample treated for 10 min was characterised by lowest porosity in both regions. Thus porosity decreased steadily with processing time. Also from the cross-sectional images, it can be seen that, for all treatment times, the coatings in the near the metal part regions (Fig 4.12) have higher levels of porosity compared to the other regions. This is because the area close to the metal part displays the beginning of the coating formation which is characterised by lower thickness.

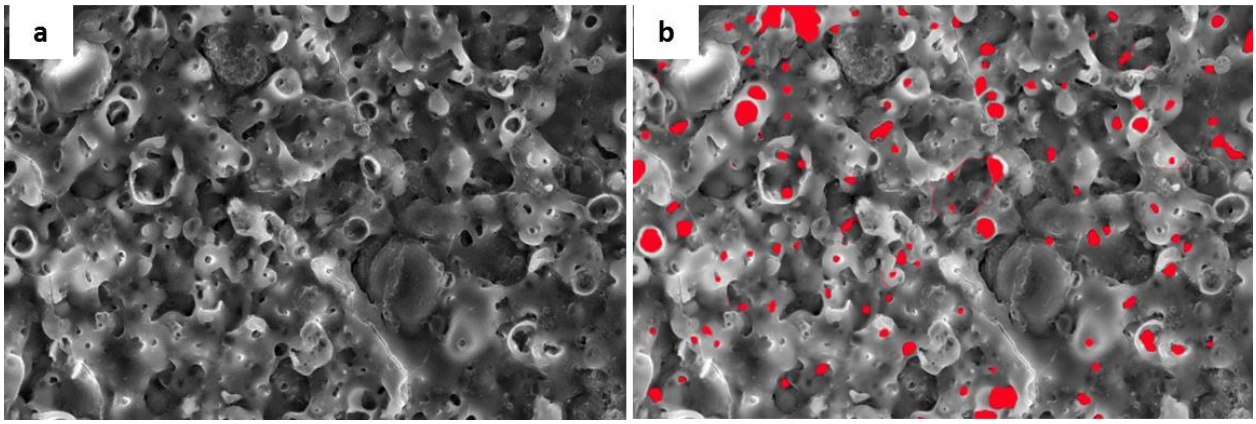

Fig. 4.11 (a) SEM surface morphology micrograph of PEO coating produced for 6 min (b) coating porosity identified using MountainsMap 7.2 software. The required area was determined based on a threshold value.

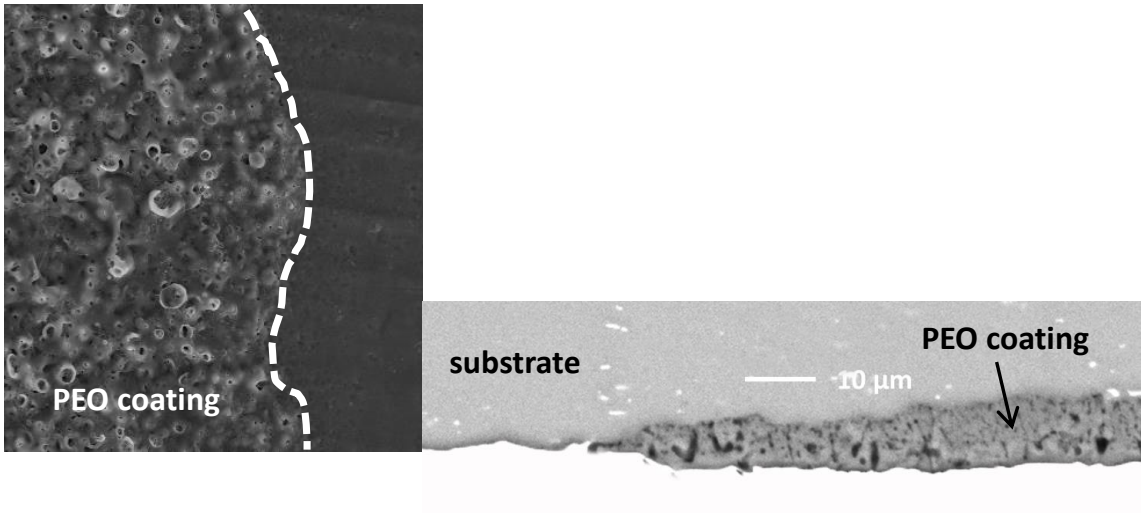

Fig. 4.12. SEM surface and cross section morphology of PEO coatings on the sample treated for 8 min near the metal-coating region.

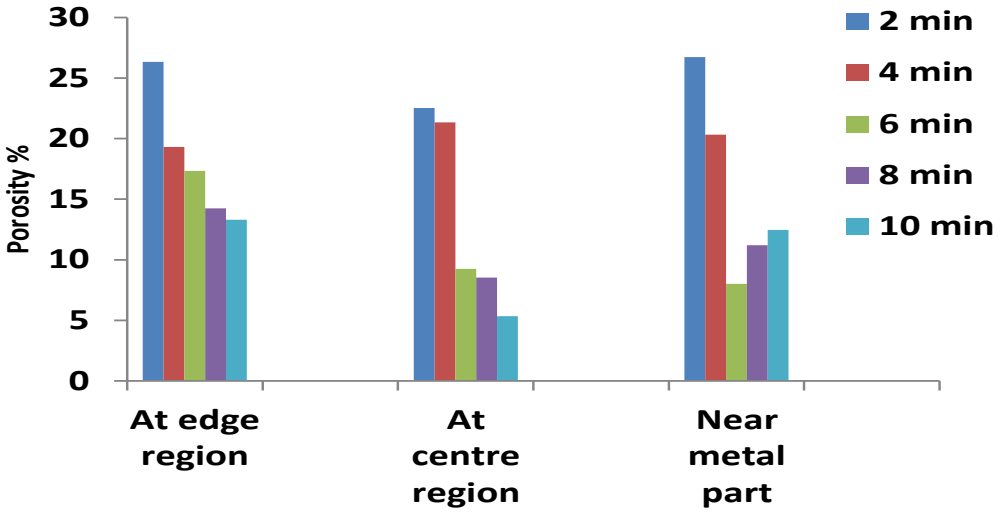

Fig. 4.13 PEO coating porosity in different regions of the sample.

Percentage of surface porosity of PEO coatings in edge, central and near metal part regions of Al foils formed at different treatment times is shown in Fig 4.13. The results obtained indicate that the morphology of oxide films on aluminium foil produced by the PEO process in different regions is significantly different. It can be seen clearly that the porosity at the edges was found to be greater than that at the central region, however in both regions the percentage of porosity on the surface decreases with increase the treatment time. On other side, no relation appear between the treatment time and percentage of porosity in the area near the metal part. Figure 4.14 and 4.15 show the coating thickness and pore size distributions respectively.

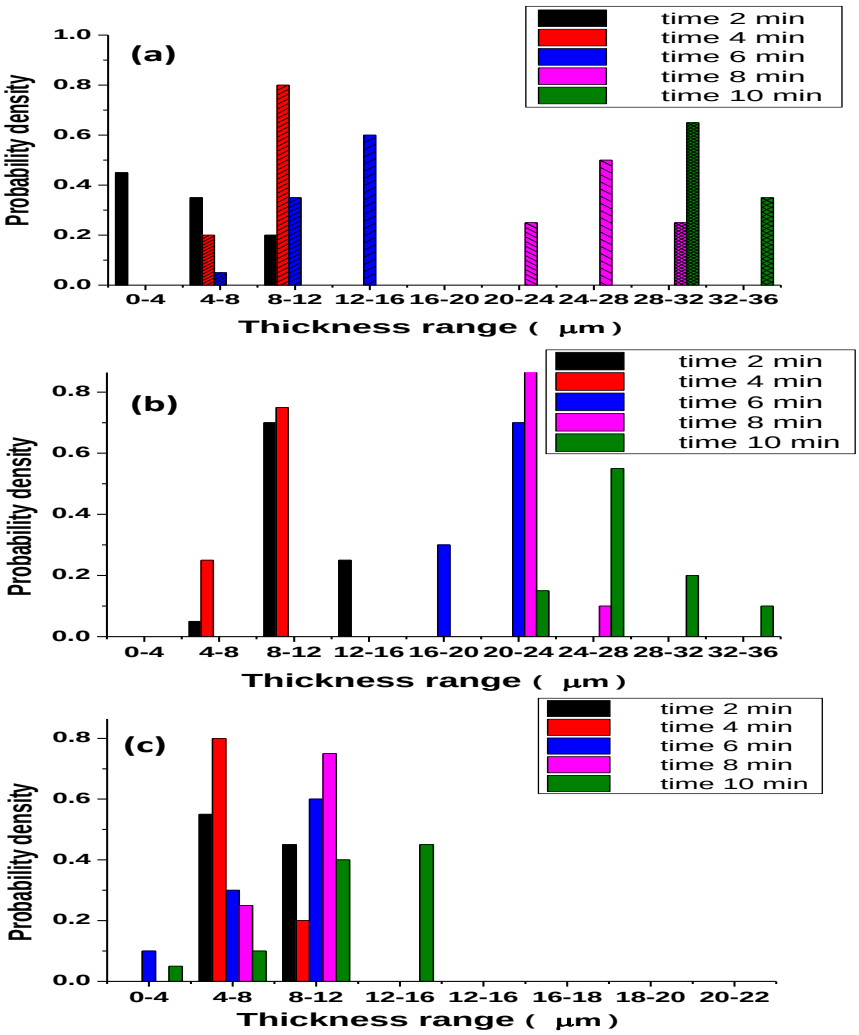

Fig. 4.14 Thickness distribution in different regions of Al foil samples: (a) central region, (b) edge region, (c) near the metal part.

From the coating thicknesses data, it follows that the thickness uniformity in central regions is always greater than at the edge regions, due to a number of factors such as effect of edges on electrolyte concentration gradients and current density distributions during the PEO process. Thus, in the central region of the sample treated for 4 min, the highest probability density of thickness lies in the range of 8-12 μm, while at the edge and near the metal part, it was in the range of 4-8 μm. Fig 4.16 shows a high magnification image of the coating on the sample treated for 10 min in the central region, with the inset illustrating the measurement of the pore size in the top coating layer.

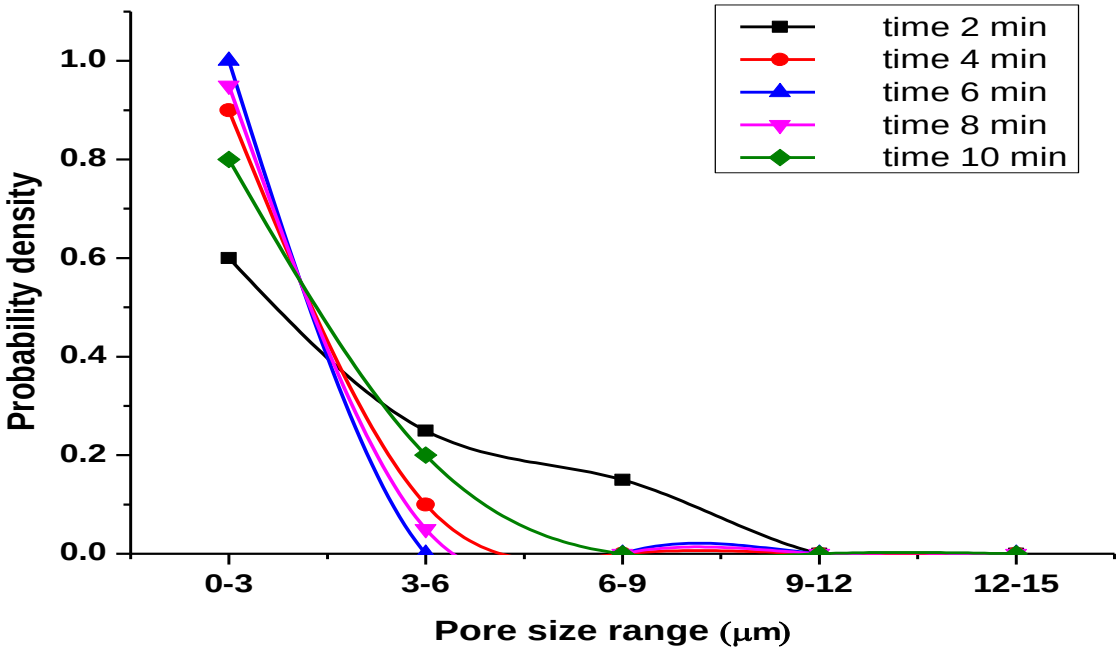

Fig. 4. 15 Effect of treatment time on pore size distribution.

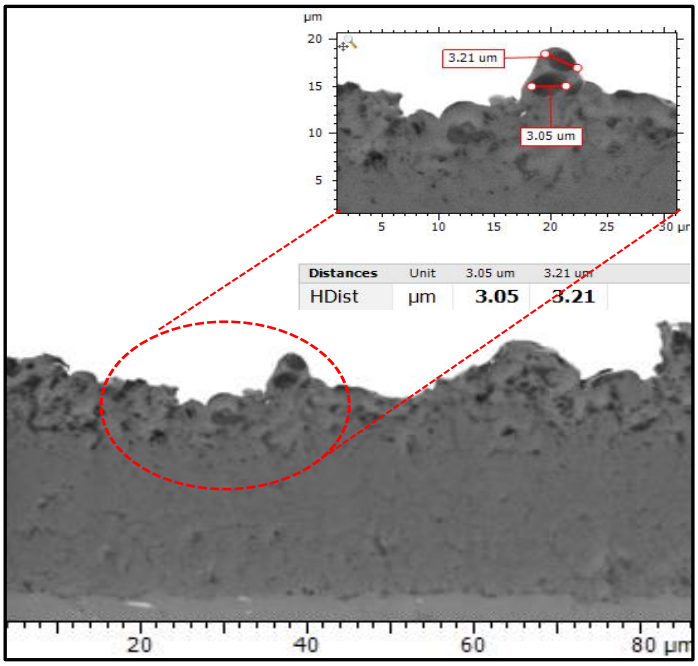

Fig. 4.16 Typical example of a cross-sectional image of the sample treated for 10 min.

The image shows the measurement of pore size using MountainsMap7.2 software. There is strong correlation between the mechanical properties of the PEO coatings and their structure [58, 64]. Porosity can effects on the coating properties, such as hardness, dielectric strength and corrosion resistance. For the lowest porosity, the highest coating hardness, chemical stability and dielectric strength can be expected. However, the combination of good coating adhesion with surface-connected porosity provided by moderated surface roughness confers good tribological performance of PEO coatings in many applications.

Surface roughness is important parameter that may influence the characteristics of morphology. Krishna *et. al.* in his study of the tribological performance of ultra-hard ceramic coatings states that the surface roughness of the PEO coatings is a linear function of the final coating thickness [133]. An increase in processing time provides adequate opportunity for the build-up of the PEO coating, which leads to an increase in the coating thickness. However with an increase in treatment time, the discharges become more energetic and violent, which causes the formation of non-uniform coatings with higher roughness [134]. The results of surface roughness (R_z) analysis are shown in figure 4.17, indicating that the surface roughness increased with the increasing processing time.

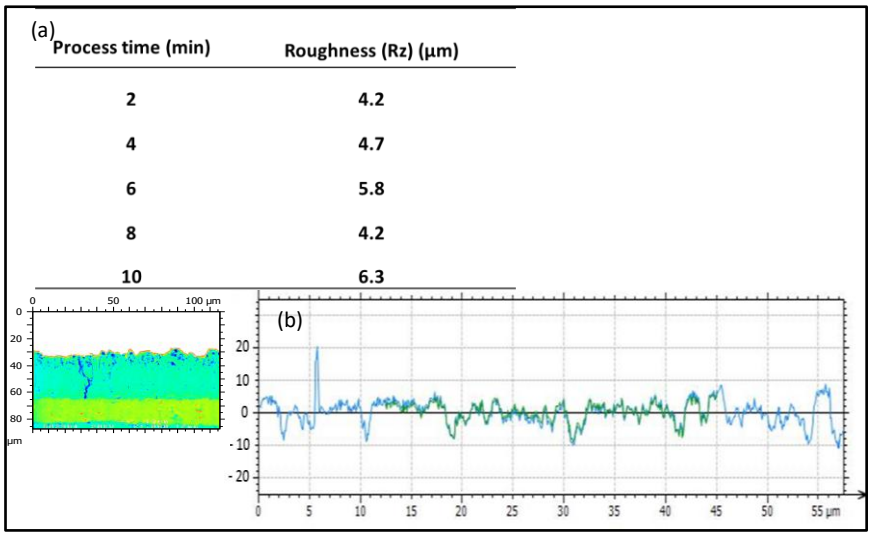

Fig. 4.17. (a) The surface roughness values in the central region of PEO coatings produced at different processing times and (b) an example of corresponding line scan profile of surface roughness on the Al foil sample PEO treated for 10 min.

4.7. Phase composition analysis

Figure 4.18 displays X-ray diffraction patterns of ceramic coatings on the samples treated for 6, 8 and 10 min. From positions of diffraction peaks, the phases were identified by comparison with the reference pattern of γ-Al_2O_3 (PDF# 50-0741), α- Al_2O_3 (PDF# 46-1212) and Al substrate (PDF# 04-0787) [79, 135]. Analysis of the diffraction patterns indicates that all studied PEO coatings are mainly composed of γ-Al_2O_3 and α-Al_2O_3 the ratio of which characterised by the heights of $(400)_\gamma$ and $(113)_\alpha$ peaks located at 46.2° and 43.1° 2θ comprises approximately 6:1, 7:1 and 5:2 for the samples treated for 6, 8 and 10 min respectively. It is found that the intensity of $(200)_{Al}$ peak at 45.10° 2θ decreases as the treatment time increases. However, the highest intensity of $(113)_\alpha$ peak is observed in the sample treated in 10 min. These phase profiles resemble those previously reported by Sundararajan *et al* [11], Xue *et al* [136], and Guangliang *et al* [58]. It is known that the PEO coatings are produced by plasma thermal chemical reactions in the discharge channels. The α-Al_2O_3 phase is thermodynamically stable at high temperatures and posesses very good mechanical properties, whereas γ-Al_2O_3 which hardness is inferior to that of alpha phase is a metastable phase. The content of γ-Al_2O_3 phase is high in the outer porous layer and decreases towards the inner layer of the coating.

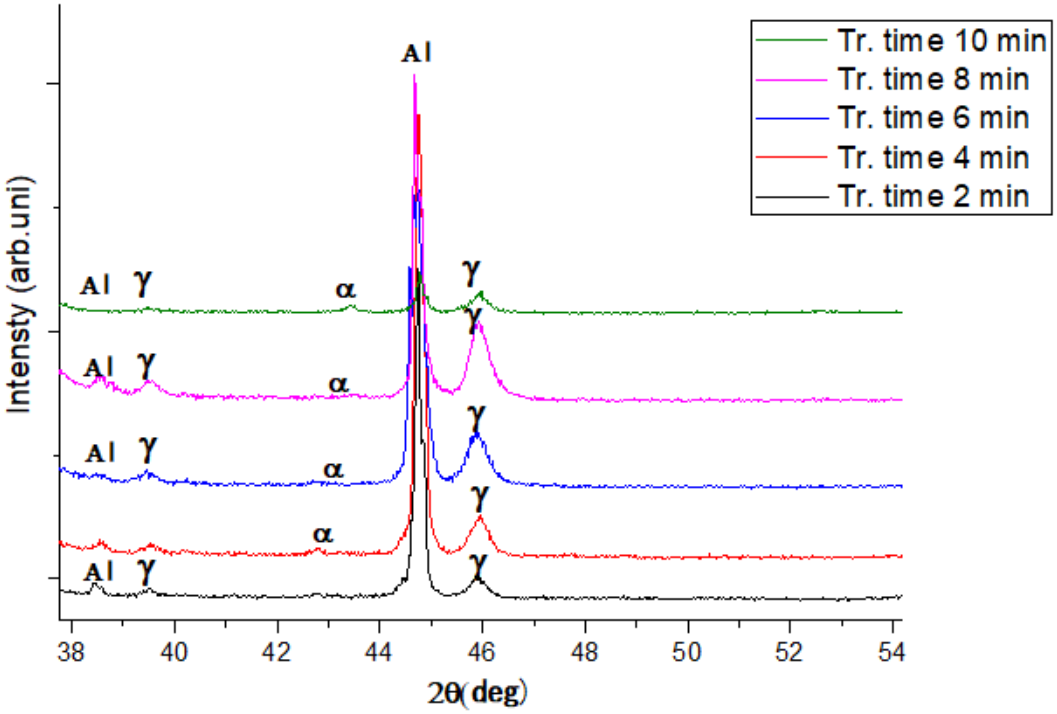

Fig. 4.18 XRD pattern of PEO coatings produced for different process times

Gamma alumina can transform into alpha alumina if heated up to 800-1200 °C [71, 115]. The α-Al_2O_3 content in the PEO coatings rises gradually with increasing coating thicknesses that can be related to the higher thermal energy accumulation in a thicker coating. Therefore it can be inferred that the deposition process of a relatively thinner coating is dominated by the growth of γ-Al_2O_3, while that of a thicker coating is dominated by the growth of α-Al_2O_3.

4.8. Evaluation of oxide film growth efficiency during PEO process

Usually, during anodising the current density (i) passed through the coating layer can be written as the sum of the partial processes of coating layer formation (i_{i}) dissolution (i_{d}) and oxygen evolution (i_{e}) at the anode surface as

$$i = i_{\mathrm{i}} + i_{\mathrm{e}} + i_{\mathrm{d}}$$

where i_{i} is the ionic current of the oxide film growth, i_{d} is the anodic dissolution current and i_{e} is the current caused by oxygen evolution.

PEO process is typically performed from a couple of minutes to 3-4 hours at current density up to 2000 A/m^2 and voltage up to 1000 V [8, 47]. This process is actually associated with high discharge temperature and gas evolution due to the plasma thermochemical reactions in the microdischarges [8, 42, 46]. As a result, the PEO process which combines oxide film formation, dissolution and dielectric breakdown consumes high energy, and under this situation the processes efficiency becomes very important. In research paper published by Bakovets *et. al*. [137] the current efficiency in PEO process of Al in electrolyte solution 40 g/l $Na_2O.3SiO_3$ for treatment time 6 min was 9.1%. Yerokhin *et. al.* [46] evaluated the current efficiency for the partial processes of oxide film formation, dissolution and oxygen evolution in the PEO process of Al in aqueous solutions of KOH with 0.5-2.0 g/l. In this work, the estimations of the PEO process efficiency for the coatings formed in different treatment times are carried out assuming that current yields of the partial processes of oxide layer growth ($\eta_{Al_2O_3}$), dissolution ($\eta_{Al_{sol}}$) and gas evolution (η_{O_2}) on the surface of working electrode are dominated by the Faraday's law. So, on the anode surface the balance equation for the current yields of the partial processes can be written as follows [46]:

$$\eta_{Al_2O_3} + \eta_{Al_{sol}} + \eta_{O_2} = 100\% \quad (1)$$

The equations used in current efficiency calculations for the main reactions of the plasma electrolysis are given in Table 4.3 [46].

Table 4.2 Current efficiency correlations for the main products of the PEO process [34].

Reaction	Electrochemical equivalent (q)	Current yield (η)
Anodic oxidation $2Al + 3O^{2-} \rightarrow Al_2O_3 + 6e^-$	$\frac{M}{6F} = 1.76 \times 10^{-4}$ (g/C^{-1})	$\frac{\delta A \rho}{Q q_{Al_2O_3}}$ (2)
Anodic dissolution $Al \rightarrow Al^{3+}_{soild} + 3e^-$	$\frac{M_{Al}}{3F} = 9.32642 \times 10^{-5}$ (g/C^{-1})	$\frac{m^{sol}_{Al}}{Q q_{Al}}$ (3)
Oxygen evolution $2H_2O + 4e^- \rightarrow O_2 + 4H^+$	$\frac{V^o_{O_2}}{4F}$ = 0.058 (ml C^{-1})	$\frac{V_{O_2}}{Q q_{O_2}}$ (4)

Where the M_{Al} is the molar mass of aluminium, F is Faraday's constant, δ coating thickness, A is the sample area, ρ density, Q is the total charge (I.t), $q_{Al_2O_3}$, q_{Al} and q_{O_2} is the electrochemical equivalents of alumina, aluminium, and oxygen, V_{O_2} gas molar volume.

In our results, the effect of treatment time on the coating thickness is obvious, where the oxide film thickness increases with increasing the treatment time (Fig 4.4), however the growth rate decreases at longer times and the dissolution of aluminium becomes low. To achieve better understanding in oxide film growth and to assist the optimisation of the process efficiency, the current efficiency of the partial electrode processes during the PEO treatment was evaluated. For different treatment times, the mass of lost aluminium m^{sol}_{Al} and the coating thickness were evaluated from the thickness measurements on the samples cross-section using scanning electron microscope techniques (section 3). The thickness of residual aluminium was subtracted from the foil thickness before the PEO treatment and, knowing the aluminium density (2.7 g/cm^3), amount of Al consumed during the process can be estimated.

Table 4.3 Coating thicknesses, dissolved Al and total charge of PEO process in 1 g l-1 KOH, 2 g L-1 Na2SiO3, and 2 g L-1 Na4P2O7 solution for different treatment times.

Treatment time (min)	Charge, Q_{tot} (C)	Coating thickness, (μm)	Al lost, m^{sol}_{Al} (g)
2	425.4	10.0	0.1215×10^{-2}
4	728.5	20.0	8×10^{-3}
6	1036.8	32	0.122×10^{-1}
8	1285.5	52	0.023
10	1291.4	64	0.024

The total charge (C) passed during each treatment was calculated by integrating instantaneous current values over processing time. The calculated values and processing parameters are presented in Table 4.3.

Assuming the alumina density ρ = 3.1 g/cm^3 and based on reference data given in table 4.3 the results of current efficiency for the products of partial anodic processes in PEO of process of aluminium foil in different treatment times presented in fig 4.19

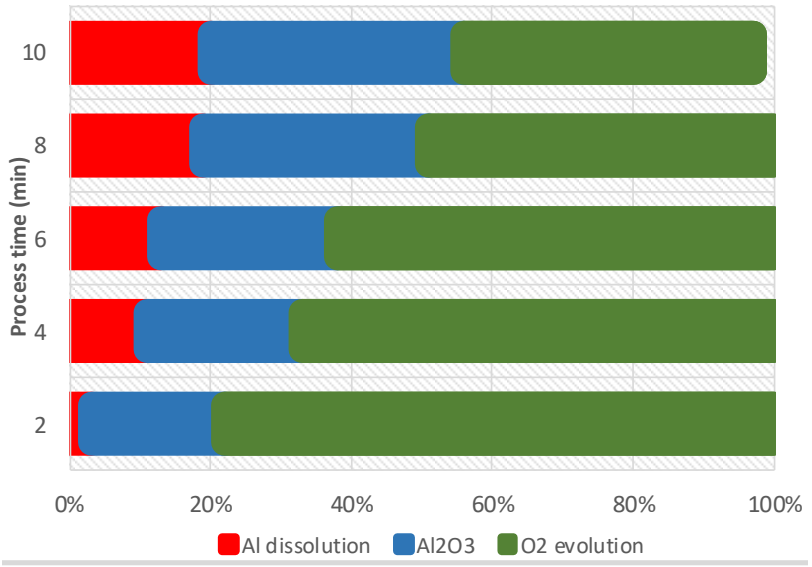

Fig. 4.19. XRD pattern of PEO coatings produced for different process times.

From fig 4.19 it can be seen that the current efficiency of the oxide layer growth ranges from 19-36 %, and increasing with treatment time. Similarly, the aluminium loss increases with treatment time. Although the current efficiency of oxygen evolution decreases with time, the fraction of total current spent on the oxygen evolution is always more than a half of the total current for all conditions, i.e. oxygen evolution remains the dominant electrochemical process.

4.9. Nanoindentation test results

To provide a simple conceptual picture of mechanical properties of produced PEO coatings and associated effects of treatment time, the values of elastic modulus and hardness were estimated. Nanoindentation experiments were performed on mounted cross-sections of PEO coatings produced for 6, 8 and 10 min. Typical load versus displacement curves for the three coatings are shown in Fig. 4.20, with derived values of hardness and elastic modulus presented in Table 4.5.

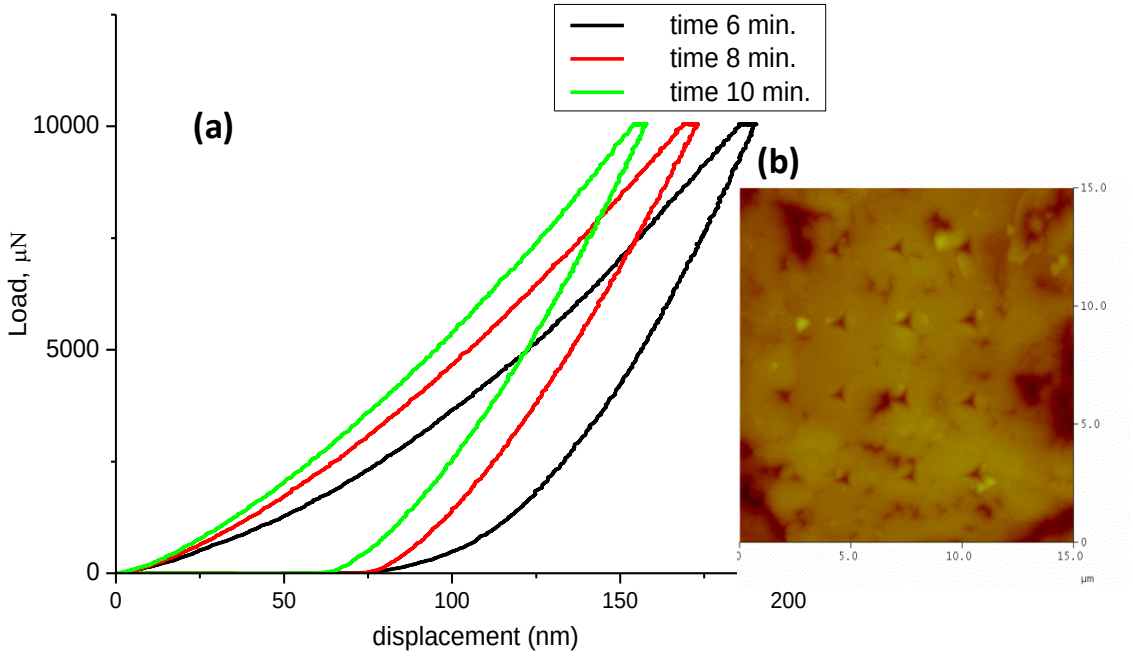

Fig. 4.20 (a), Nanoindentation Load–displacement curves of PEO coatings of samples for different treatment times. (b), Scanning probe Microscopy imaging of the nanoindentation for condition 10 min.

Table 4.3 Coating thicknesses, dissolved Al and total charge of PEO process in 1 g l-1 KOH, 2 g L-1 Na2SiO3, and 2 g L-1 Na4P2O7 solution for different treatment times.

Treatment time (min)	**One side coating thickness (µm)**	**Porosity %**	**No. of indents**	**Av. Young's modulus (GPa)**	**Av. Hardness (GPa)**
Al-foil substrate	-	-	-	69	0.3
6	17	9	29	182 ± 29.0	14.2 ± 3.0
8	27	8.5	22	191 ± 15.0	15.3 ± 2.2
10	32	5	31	211 ± 19	16.6 ± 1.8

From the above results, it has been noticed that the Young's modulus rise to 200% and this is also applies to the hardness measurements. However, the experimental measured stiffness was relatively low, compared with the expected for dense alumina (~370 GPa). This may provide some flexibility to the ceramic-coated structures, which would be advantageous for many engineering applications such as dielectric substrates in semiconductor and electronics instruments.

It can be clearly seen that the maximum hardness observed in the coating on the sample treated for 10 min, which has higher thickness (32 μm). These results are consistent with those reported by Yerokhin *et al*. [8] who stated that the PEO coating can provide a significant strengthening influence to the aluminium substrate. Also it was reported that the hardness of coatings based on gamma phase corresponded to 10-15 GPa, and 17-22 GPa for the coating based on alpha phase. Such observation was also consistent with the results of nanoindentation measurements reported by Curran *et al*. [99]. Although the values of hardness and Young's modulus smaller than those expected for PEO alumina were rejected, some scatter in these data can be observed in Fig 4.21. This is not really surprising when account is taken of the network of micro-cracks and micro-pores present in the coatings. This is clear, if we see adjusted R^2 values provided in Fig 4.21 which mainly has good correlation in sample treated in 8 min, however in sample treated in 10 min showed that the Young's Modulus has relation with around 51 % of the difference in hardness.

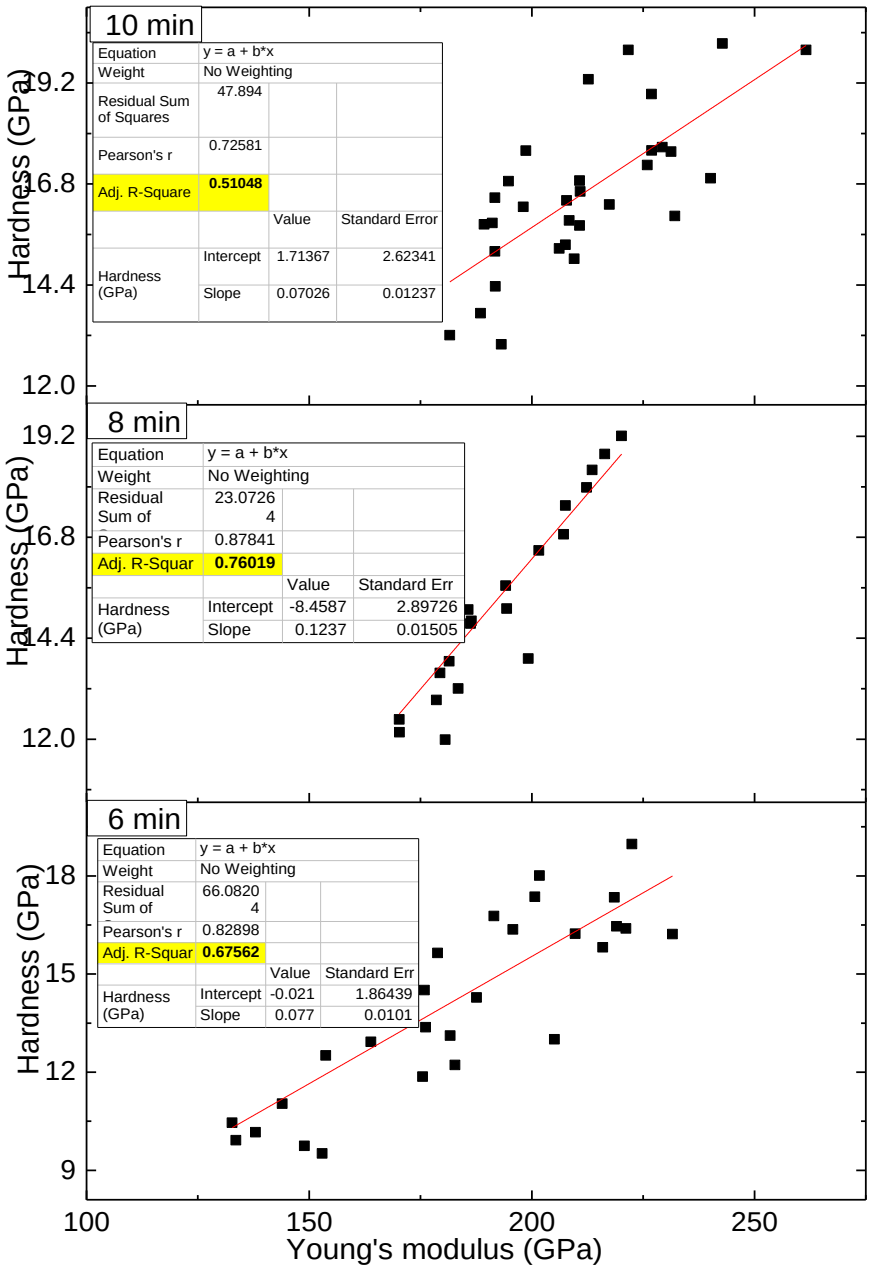

Fig. 4.21 Cross-section tests of coating hardness versus Young's modulus of samples treated for different periods of time.

Some scattered data may be considered for the case when indenter contact with pore which act on the value of hardness. So fine grain size could be enhance the hardness, while porosity can significantly reduce it. Similar observations have been reported in other references [8, 14, 99, 138]. The coatings produced under all studied conditions (treatment time 6, 8 and 10 min) show a fine pore size (0-3 μm) and porosity of 9.5, 8 and 5 % respectively. So the improved hardness is thought to be the result of a reduced porosity and a presence of a considerable proportion of crystalline material, particularly α-phase as described by the Curran *et al*. [61].

Several studies discussed the effects of porosity on the mechanical properties of PEO coatings [61, 139-141]. Curran and Clyne [61] in discussion of the effect of porosity in PEO coatings produced by PEO process stated that the fine porosity can be reduces the stiffness for the coatings. Also Mackenzie in [142] observed that 20% porosity might to be reason for reduce the stiffness of around 30%. In the same context in our study, it was observed that the hardness and Young's modulus increase with decrease the porosity. The correlation between the porosity percentage with the stiffness and hardness can be seen in Fig 4.21.

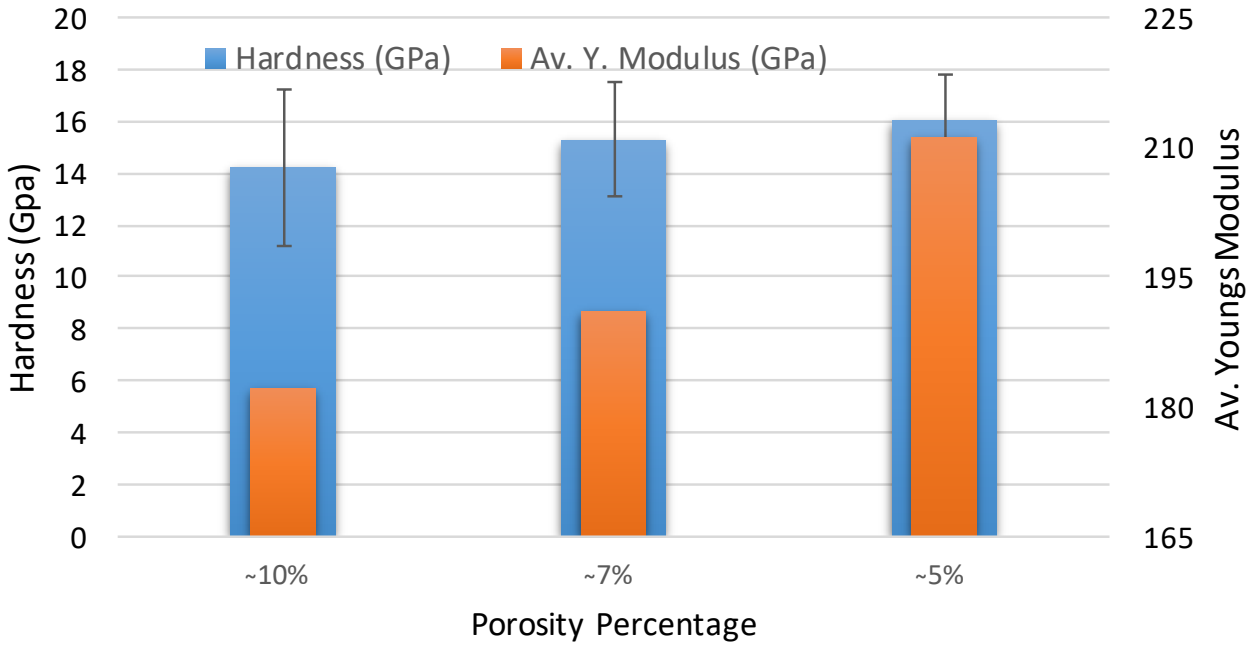

Fig. 4.22 Show the relationship between porosity vs hardness and Young's Modulus.

4.10. Summary

In this chapter, ceramic coatings were prepared on aluminium foil surfaces by PEO treatments at different durations.

No significant differences in values of current density, which ranges from 0.32 to 0.4 A/cm^2 depending on treatment time from 2 to 10 min.

During the PEO process the period of time required for current density to reach a steady state was estimated, and found to be longer for the samples treated for 6, 8 and 10 min compared to those treated for 2 and 4 min.

The results indicated that the oxide layer thickness increases with increasing in treatment time. However in the last stage, the coating growth rate was reduced due to the anodic dissolution and recrystallisation of the coating.

By the treatment for 12 min with resulted in the coating thickness of 75 ± 1.5 µm, complete conversion of aluminium foil into alumina was successfully achieved, except for a very small area that does not exceed 1 % of the sample volume. However such sample showed high brittleness.

According to the results obtained, in the central and at the edge regions, the coating porosity decreased and the surface roughness increased with treatment time. While in the near metal part of the sample, where the PEO coating only started formation, these characteristics showed a non-linear behaviour. The pore size distribution analysis indicated that the pores are mainly smaller than 6 µm under all treatment conditions. However the results in coating of sample treated for 6 min having a more uniformly distributed porosity with smaller pore size.

Treatment time affected the gamma to alpha alumina transformation. Both γ and α - alumina are observed after 6 min varying in relative proportion through the coating thickness. However in coating on the sample treated for 4 min composed almost only of gamma alumina.

The surface mechanical properties of Al foils, such as hardness and stiffness were improved by PEO coatings. However, the substrate flexibility after the treatment should be carefully considered, i.e. when the PEO treatment was applied for a desired period of time, the

produced substrate should exhibit both excellent stiffness and good hardness for practical applications. This could be achieved by controlling the thickness of the residual aluminium. For example, high brittleness of the coatings produced was observed on samples treated for 10 and 12 min.

During the PEO process for all conditions, the oxygen evolution was the main major electrochemical process and it is current efficiency ranged from 78 to 41 % and decreased with increasing treatment time. In the meanwhile, the current efficiency of the coating formation ranged from 19 to 36 % and increases with increase in treatment time.

Chapter 5

Effects of electrolyte composition on the process of conversion of aluminium foil in to alumina ceramics by plasma electrolytic oxidation

5.1. Introduction

To analyse the mechanisms underlying the PEO coating formation, a number of parameters are usually considered, containing treatment time, electrolyte and electric field distribution in the electrolyser. From the results in **Chapter 4**, it follows that although almost full conversion of aluminium foil to alumina can be obtained using a PEO technique, the composite materials shows signs of brittleness. It is also concluded that the coating of sample treated for 6 min in the PEO process having a more uniformly distributed porosity with smaller pore size, and shows a moderate values of stiffness.

On other hand, the importance of the electrolyte in the PEO process and its influences on the coating characteristics has been highlighted in **Chapter 2.** It has been cited that electrolyte composition can influence the coating growth rate, morphology and microstructure, phase composition formation mechanism, adhesion to the substrate. Therefore, the principal objective of the present part of the project is to study the influence of the electrolyte constituents on the coating thickness, morphology and phase composition of the process conversion of aluminium foil in to alumina ceramics to obtain alumina ceramics with a moderate degree of flexibility.

5.2. Experiments setup

Rectangular samples of a 50-µm thick AA1050 aluminium alloy foil with dimensions 30 mm × 15 mm and surface roughness of *R*a ~ 0.1- 0.2 µm were used as substrates. The samples were PEO treated to convert to a higher proportion of alumina. The PEO coatings were produced following the procedures described in **Chapter 3**. The PEO processes were carried out in a bipolar pulsed current (PBC) mode with frequency 2.74 kHz. The voltage was controlled at +530 V and -180 V.

During the treatment, the electrolyte temperature was maintained below 30 ◦C, by cooling the electrolyte in the electrolytic cell. All the samples to be converted to alumina ceramics

were treated for 6 min. Voltage and current transients during the PEO treatment were recorded with a digital oscilloscope linked to a PC.

The electrolytes prepared from different concentrations of potassium hydroxide (KOH), sodium pyrophosphate ($Na_4P_2O_7$), and sodium silicate (Na_2SiO_3) and denoted by E1, E2, E3,…and E9 as shown in Table 5.1. Electrolytes conductivity was determined by HI 9835-conductivity/TDS meter.

Table 5.1. Design table of factor (concentration) varied in the experiments.

Electrolyte code	Factor level			Concentration (g/l)		
				KOH	$Na_4P_2O_7$	Na_2SiO_3
E1	-1	-1	-1	0.75	0	0
E2	-1	-1	+1	0.75	0	2
E3	-1	+1	-1	0.75	2	0
E4	-1	+1	+1	0.75	2	2
E5	1	1	1	1	1	1
E6	+1	-1	-1	1.25	0	0
E7	+1	-1	+1	1.25	0	2
E8	+1	+1	-1	1.25	2	0
E9	+1	+1	+1	1.25	2	2

Nine different electrolyte compositions were formulated according to the design of experiments (Taguchi Method) [143] with full factorial 2^3. The basic factors varied in the design are given in Table 5.2.

Table 5.2. Ranges of factors varied in the experiments.

Factors		Value at encoded Level		
		-1	**0**	**+1**
KOH	g/l	0.75	1	1.25
$Na_4P_2O_7$	g/l	0	1	2
Na_2SiO_3	g/l	0	1	2

After the PEO treatment, the samples were washed in running water and dried. An FEI InspectF scanning electron microscope was used to study coating thickness and morphology. Sixty images were taken at ×2000 magnification on each sample for statistical study. A

MountainsMap 7.1 [144] software was used to evaluate the PEO coating thickness and pores size in the SEM images. Twenty measurements were taken at each SEM image. The probability density of pore size and coating thickness were obtained to quantify morphology characteristics of PEO coatings produced from different electrolytes. The surface roughness (Ra) was measured using a Veeco Dektak 150 profilometer. Three scans for every sample were taken to calculate the average values. Porosity and pore morphology were determined from SEM images by ImagJ and MountainsMap 7.1 software.

From the application point of view, it was deemed important to determine crystallinity, relative proportions of alumina phases present and chemical states of aluminium and phosphorus. Phase analysis of the alumina ceramics samples were carried out using Bruker D2 Phaser X-ray diffractmeter with a Cu Kα radiation and nuclear magnetic resonance (NMR) techniques. The ^{27}Al MAS NMR spectra were recorded at 104.20 MHz using a Varian VNMRS spectrometer and a 4 mm (rotor o. d.) magic-angle spinning probe. They were obtained using direct-excitation with a 1 μs pulse (equivalent to an approximate pulse angle of 20^{o}), a 0.2 s recycle delay, at ambient probe temperature (~25 °C) and at a sample spin-rate of 12 KHz. Between 3000 and 5000 repetitions were accumulated. The solid-state ^{31}P spectra were recorded at 161.87 MHz using a Varian VNMRS spectrometer and a 4 mm (rotor o. d.) magic-angle spinning probe. They were obtained using direct-excitation with a 3.6 μs pulse and a 30 and 300 s recycle delay, at ambient probe temperature (~25 °C) and at a sample spin-rate of 12 s^{-1} Between 40 and 180 repetitions were accumulated. To create the powder, the samples were dissolved in hot (80^{o}C) 2.5M NaOH for 30 min to form sodium tetrahydroxyaluminate ($NaAl(OH)_4$). After cooling, the solution was carefully neutralised with 20 % H_2SO_4 until pH becomes close to 7 to prevent the oxide from re-dissolving. Gelatinous $Al(OH)_3.nH_2O$ was then filtered out from the solution. The filter was washed with distilled water and dried at 150 to 200^{o}C for 10 min [145].

5.3. Current transient behaviour during PEO treatment

Current density–time responses during PEO treatment of Al-foils in electrolytes with different compositions are shown in Fig.5.1. All experiments exhibited a typical current density-time response that can be easily categorised into three stages. Consistent with [4, 8], at the initial stage ranging from 18 to ~ 25 s, a relatively quick anodic reaction proceeds, with the rate linearly increasing to the maximum which varies form 0.23 A/cm^2 to 0.52 A/cm^2 depending on electrolyte composition. Changes in discharge characteristics resulting from the addition of Na_2SiO_3 can be observed similar to [76, 78]. At the second stage, a decrease in the current density with time occurs due to the fast growth of the oxide film and within this process, a transport of Al^{3+} ions and their ejection to the electrolyte result in a slow increase in current density. Thereafter, the current growth rate becomes much slower until an equilibrium is achieved between the oxide layer formation and Al^{3+} ejection, which leads to the achievement of an almost steady-state (stage III). The fast reaction at the first stage may be comparable to conventional anodising process at the beginning of formation of the oxide layer according to the Faraday's law and controlled by the hydrogen and oxygen reactions products over the working electrode surface. The highest value 0.5 A/cm^2 was found for the process carried out in electrolyte E9, while the lowest value 0.23 A/cm^2 was found in electrolyte E2.

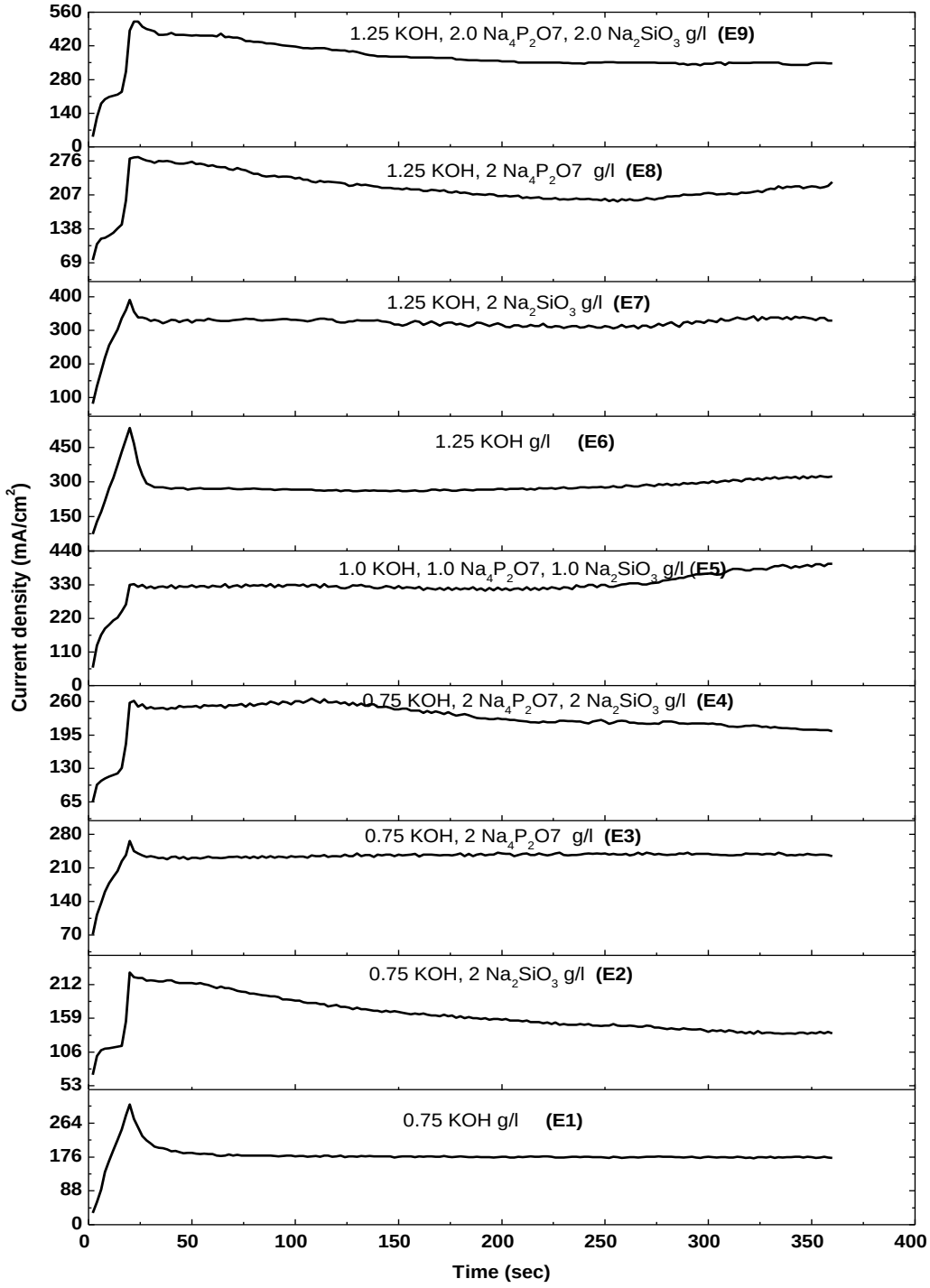

Fig. 5.1. The plots of current density versus PEO treatment time in electrolytes with different compositions

Usually current density ranging between 0.01 A/cm^2 to 0.3 A/cm^2 is required to achieve conditions suitable for PEO process and increasing the current density may enhance the coating growth rate whilst raising the relative content of α-Al_2O_3 [8]. Several researchers [8, 78] declared that when Na_2SiO_3 is added in electrolyte solutions for PEO of Al alloys, it is

possible to achieve improved discharge characteristics, such as high spatial density, frequency and short duration of micro-discharges. It is therefore not surprising that the time required to reach the discharge point was shorter in all electrolytes containing silicate, such as (E2 and E7) compared to those without it.

As shown in Fig. 5.1, the value of current density in the final stage of processing in the silicate containing electrolytes E2 and E7 tends to decrease compared to those without silicate, such as E1 and E6. Also, it is particularly noticeable that higher current densities in the range between 0.32 A/cm^2 to 0.50 A/cm^2 developed in electrolytes with higher KOH content, while this is reduced to 0.2 A/cm^2 to 0.30 A/cm^2 in the electrolytes that contain less KOH. This is due to the effect of potassium hydroxide and sodium silicate on electrolyte conductivity which significantly affects the current density during the PEO process.

5.4. Coating Surface Morphology

Figures (5.2-5.4) show the surface and cross-sectional morphologies of the oxide coatings formed in the studied electrolytes (Table 5.1). All coatings appear to be not very dense in some regions; however, some show less porosity in the inner regions, such as coating produced in electrolytes E1, E6 and E9. As can be seen, the coating surfaces feature randomly distributed pores with various size and shapes, appearing as dark circular spots. Such defects and porosity were likely caused by strong discharges occurring at the electrode – electrolyte interface. The porous features strongly depend on discharge characteristics [8, 76] and may arise from oxygen evolution, which can be generally held responsible for the formation of more obvious macroscopic pores near the PEO coating surface. It is worth mentioning that the substantial temperature and pressure are likely to result in significant concentrations of dissolved oxygen in the molten oxides. Because of the limited duration of discharges which is about 10 μs [61, 146], this evolved oxygen is likely to become trapped in the molten oxide. This could help create electrolyte and escape through very fine interconnected porosity as the melt is fast cooled. It has been verified that the widely interconnected networks is not an issue [147] however the existence of the very fine interconnected porous networks such as created in coating produced in electrolyte E4 (Fig 5.3 d) could be help to explain the stability of the oxide growth which is reflected in increasing the thickness of coating without destructive powerful discharges and prohibitively high dielectric resistance developed [61]. The electrolytes can go

through the thickness of the oxide layer via such networks, and the discharges may occur across the thin layer near the interface with the substrate.

It is also apparent that the PEO coatings formed in the alkaline solutions with no silicate additions such as in electrolytes E1, E3, and E8 (see table 5.1) are much smoother than those formed in presence of silicate, indicating participation of silicate ions in the coating formation during PEO process. Moreover, increasing of silicate concentration in the coatings produced in electrolytes E4, E7 and E9 (see table 3) leads to formation of coarse-grained coating structure, which is consistent with observations of changing discharge characteristics and development of intense sparking in silicate-reach electrolytes. This is based on the fact that the discharging nature involved in phosphate electrolyte is higher than that in silicate electrolyte. There for, coatings produced in electrolytes containing phosphate have more melted materials and cracks and these phenomena are attributed to the higher discharging voltage in the phosphate electrolyte. Higher discharging voltage results in more violent discharge and hence a larger amount of melted materials and sputtered out to form large pores, cracks and pan-like structure. This was consistent with the results of current density vs time (see Fig. 5.1) and can be concluded that the breakdown voltage is higher in phosphate electrolyte than in silicate electrolyte.

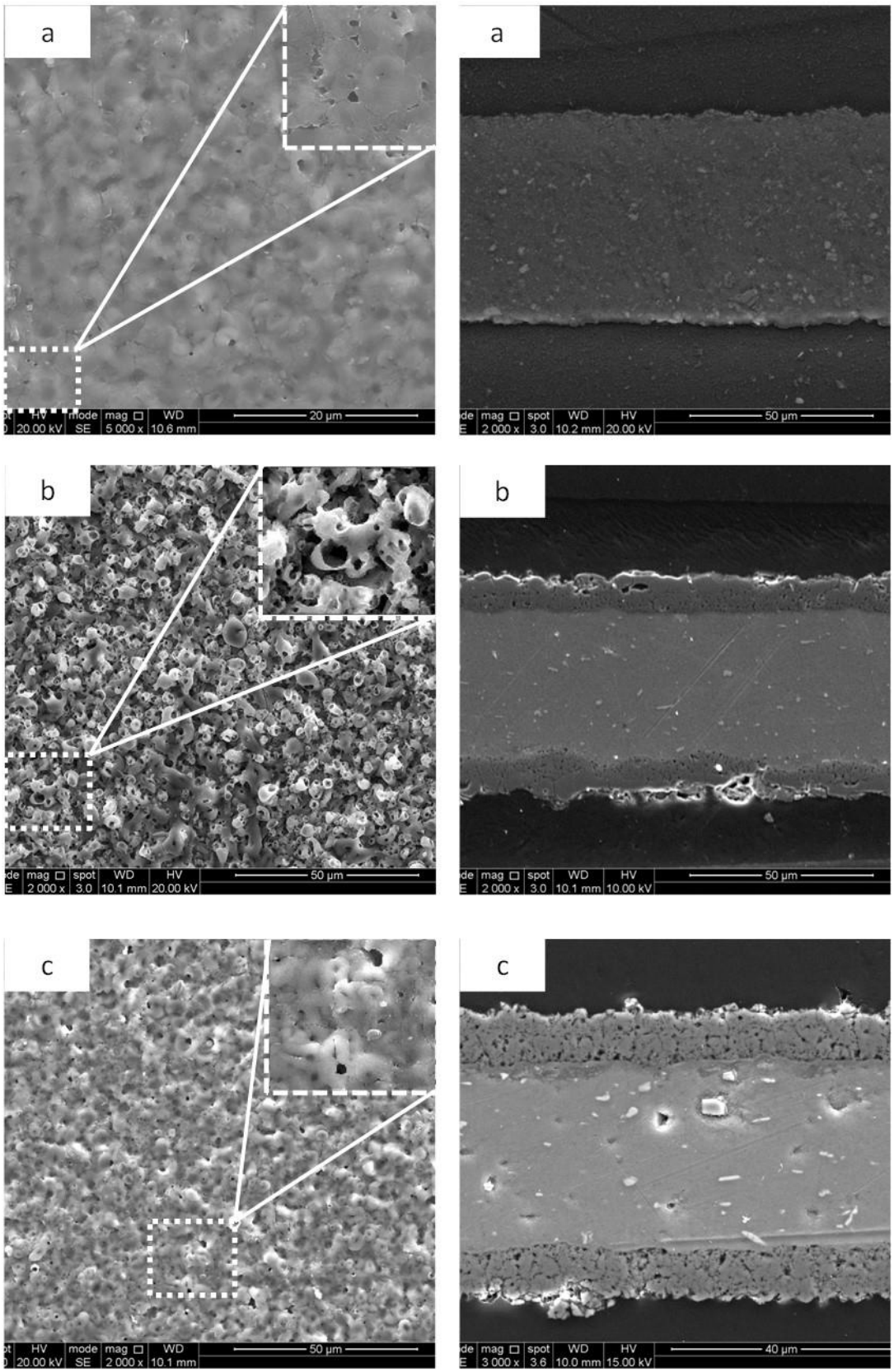

Fig. 5.2 SEM surface and cross-sectional morphologies of PEO coatings on the samples treated in different electrolytes: a; E1; (b) E2; (c) E3

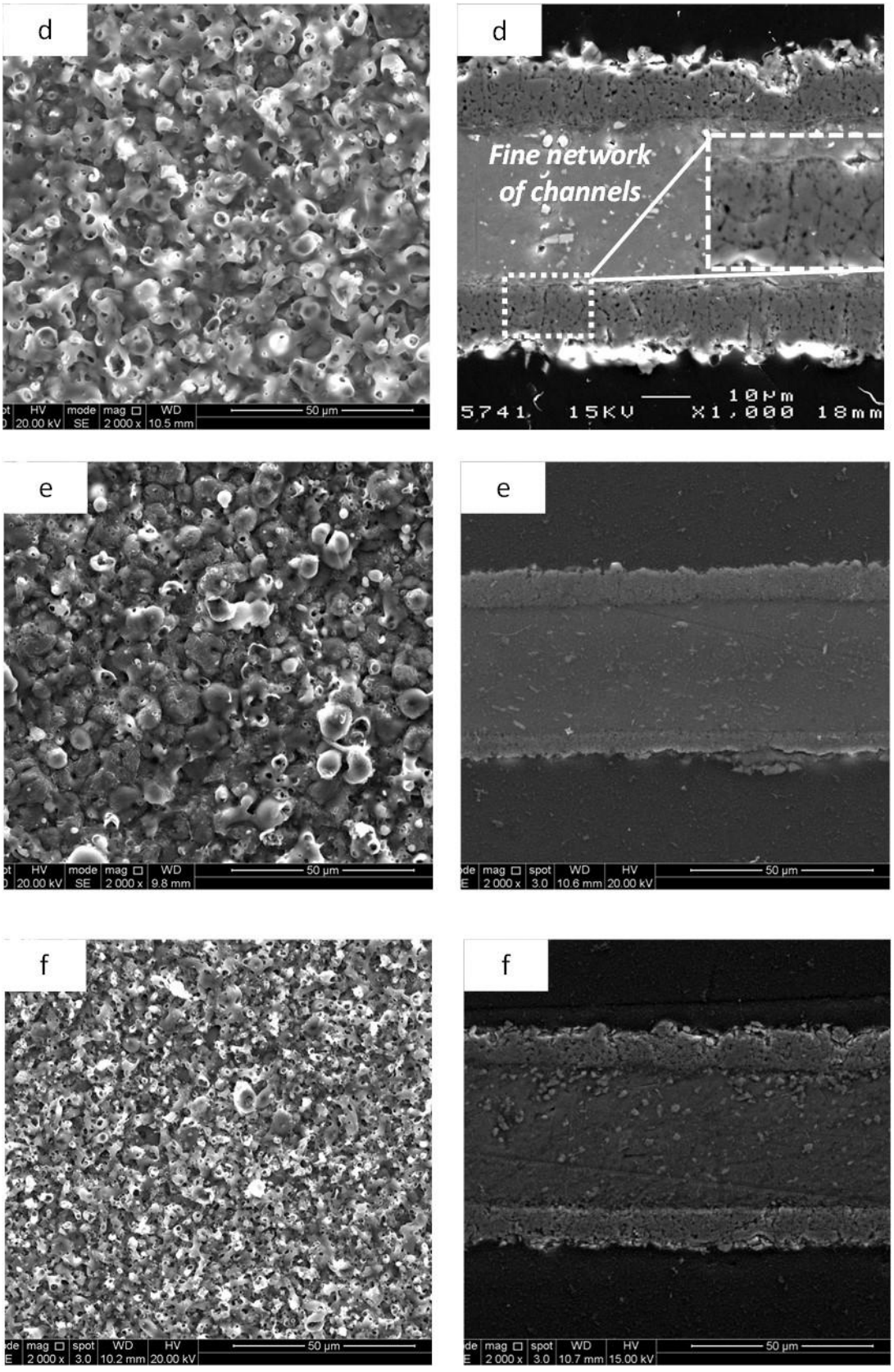

Fig. 5.3. SEM surface and cross-section morphologies of PEO coatings on the samples treated in different electrolytes: (a) E1; (b) E2; (c) E3.

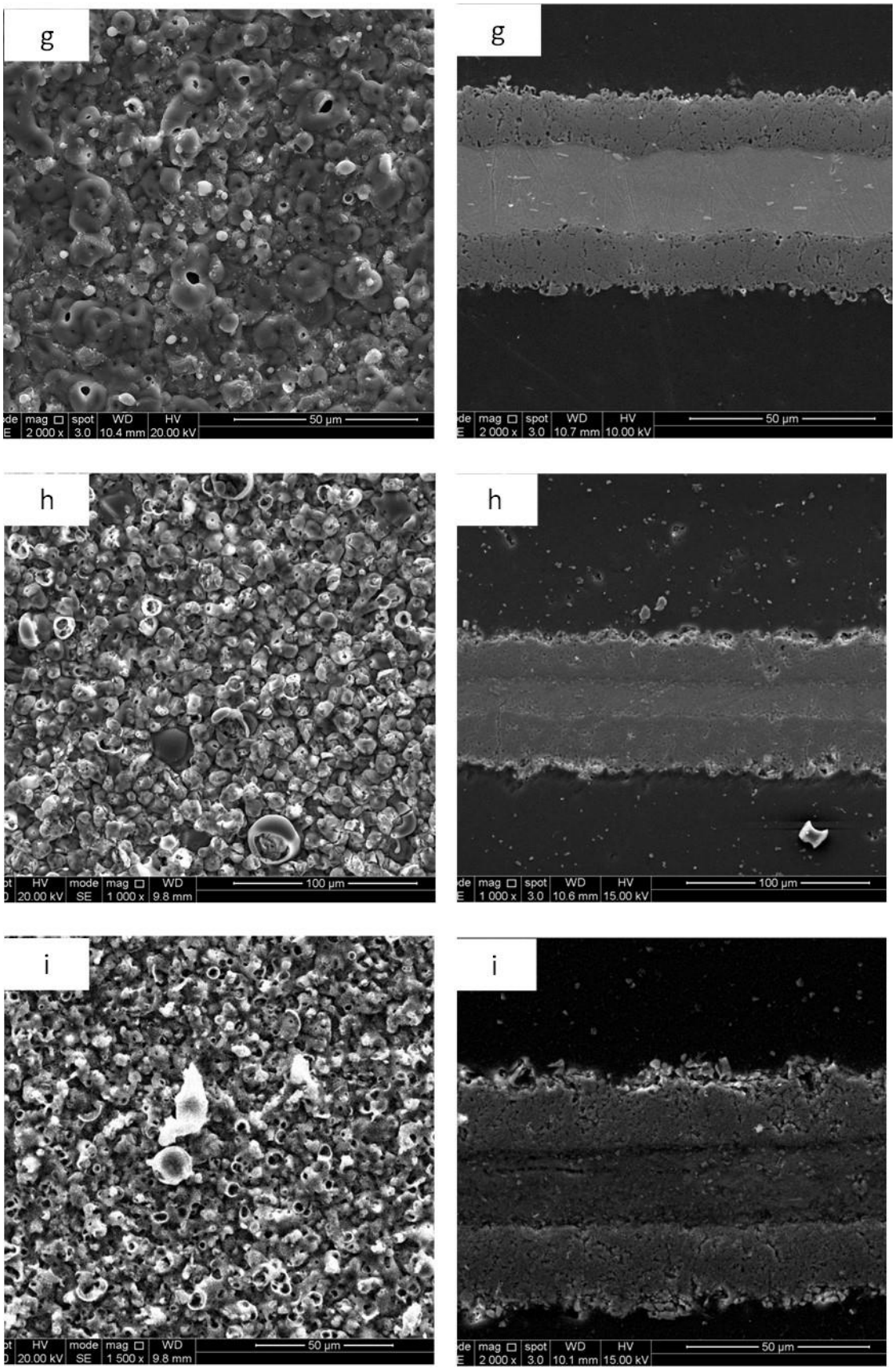

Fig. 5.4 SEM surface and cross-section morphologies of PEO coatings on the samples treated in different electrolytes: (g) E8; (h) E9; (i) E5.

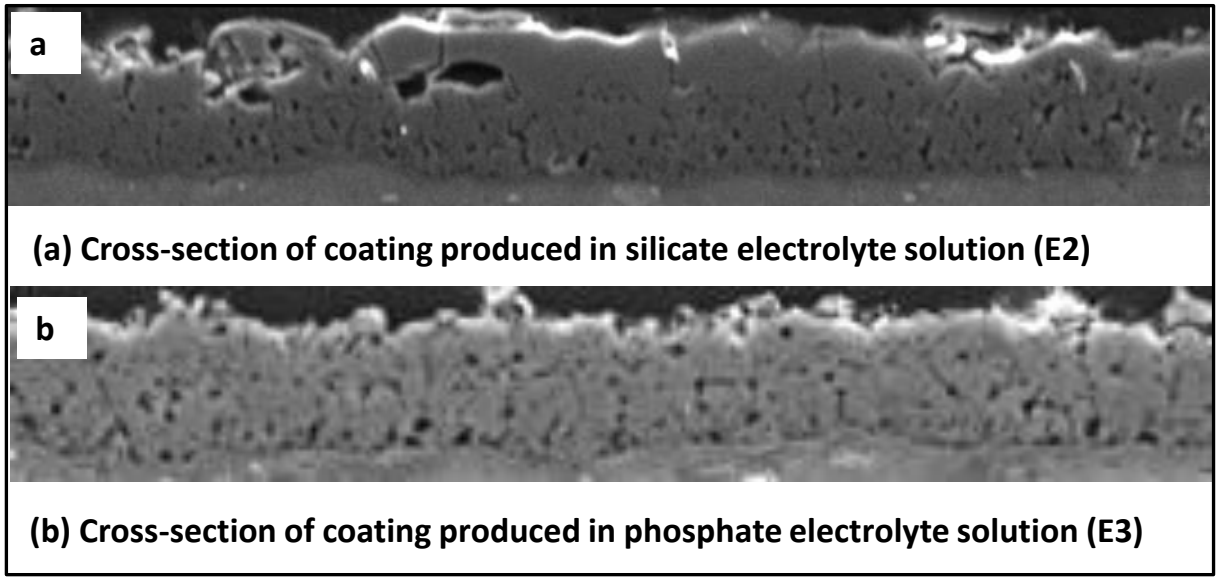

Fig. 5.5 SEM images cross-section of PEO coatings produced in different electrolytes.

Fig. 5.5 (a, b) shows cross-sectional morphologies of oxide coatings formed in silicate and phosphate electrolytes (E2 and E3). As can be seen from Fig 5.5, the coating produced in electrolyte E3 contains many randomly distributed pores, more than coating produced in electrolyte E2, which is also applicable on coatings deposited at electrolytes E7 and E8. This is based on the fact that the discharging nature involved in phosphate electrolyte stronger than that in silicate electrolyte. Therefore, coatings produced in phosphate electrolytes may form large pores, cracks and pancake-like structure. This was consistent with the results of current density vs time (see Fig. 5.1) and can be concluded that the discharging voltage is higher in phosphate electrolyte than in silicate electrolyte.

The cross-sectional micrograph of PEO coating produced in electrolyte E9 is shown in Fig 5.6. It reveals that the coating consists of three layers: a porous outer layer (1), a dense inner layer (2), and a thin interfacial layer (3). However it seems to lose the outer layer of the coating (Fig 5.6). This can depend upon the point where extreme microdischarges arise on the thick coating produced in electrolytes with higher silicate concentration. This may leads to structural defects causing to a loose and coarse-grained structure [8, 61, 76]. Therefore, coating damage occurred in the regions surrounded by the cracks in the loose outer layer. The dense coating layer exhibits better mechanical properties than the porous layer. This is consistent to the results of evaluation of the hardness and Young modulus of coatings in **Chapter 4**.

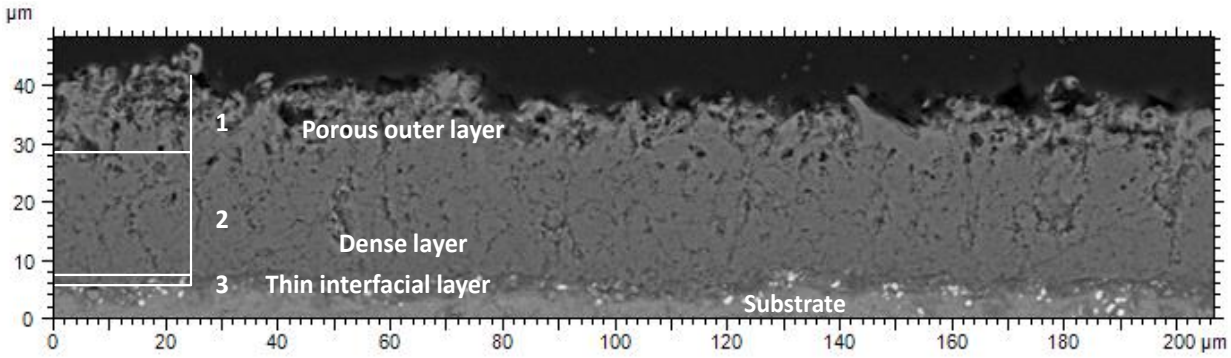

Fig. 5.6 Cross-section of PEO coating produced in electrolyte E9 (1.25KOH,2 Na4P2O7,2Na2SiO3).

The PEO coatings obtained in the alkaline solutions with no sodium pyrophosphate, such as E1, E2 and E6 (see table 3) were thin and uniformly porous due the unstable and discontinuous sparking. The porosity of produced PEO coatings is ranged between 10 to 18.5 %, as shown in Fig. 5.7. The highest porosity was present in the coating produced in the electrolyte E9 (1.25 g/l KOH, 2.0 g/l $Na_4P_2O_7$, 2.0 g/l Na_2SiO_3), while the coatings produced in electrolytes E1 (0.75 g/l KOH) and E6 (1.25 g/l KOH) were characterised by lowest porosity 11% and 10% respectively.

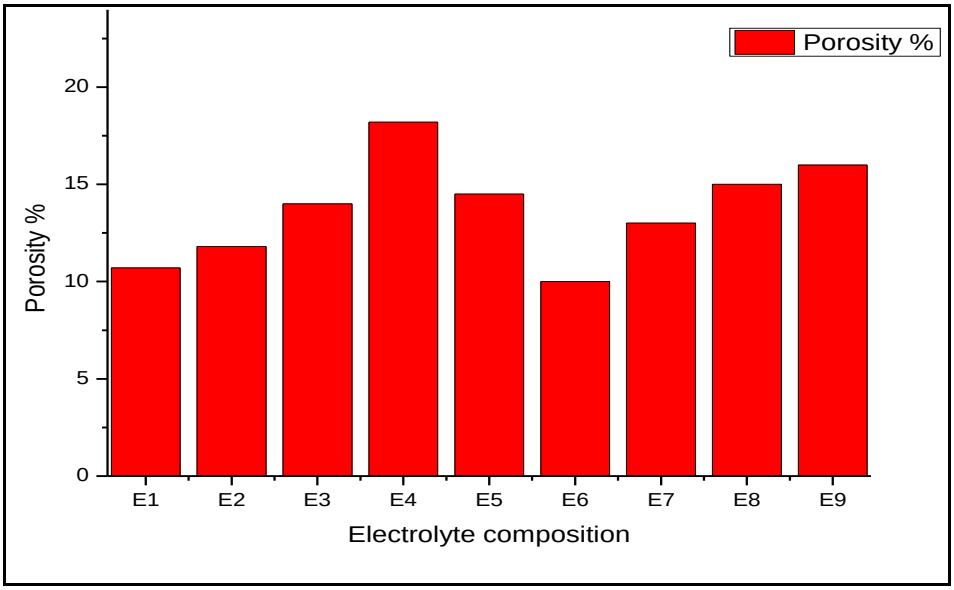

Fig. 5.7 Porosity in the PEO coating in different electrolytes compositions.

It can be seen that the porosity increases with increasing concentrations of sodium silicate and pyrophosphate additions. The reason for this is that increasing in sodium silicate

concentration leads to the appearance of powerful discharges and the sparking voltage can be easily reached in presence of phosphates [8, 79].

Probability density distributions of the coating porosity shown in Fig. 5.8 indicate that the pores with size ranging from (0~3μm) are present in the coatings obtained from all electrolyte solutions E1 to E9. Moreover substantial amounts of pores with size ranging from 1 to 2 μm are present in the coatings produced in electrolytes E8 and E9. While the pores with size ranging from 0 to 1 μm were present in the coatings produced in electrolytes E1 (1.25 g/l KOH) and E3 (1.25 g/l KOH, 2.0 g/l $Na_4P_2O_7$).

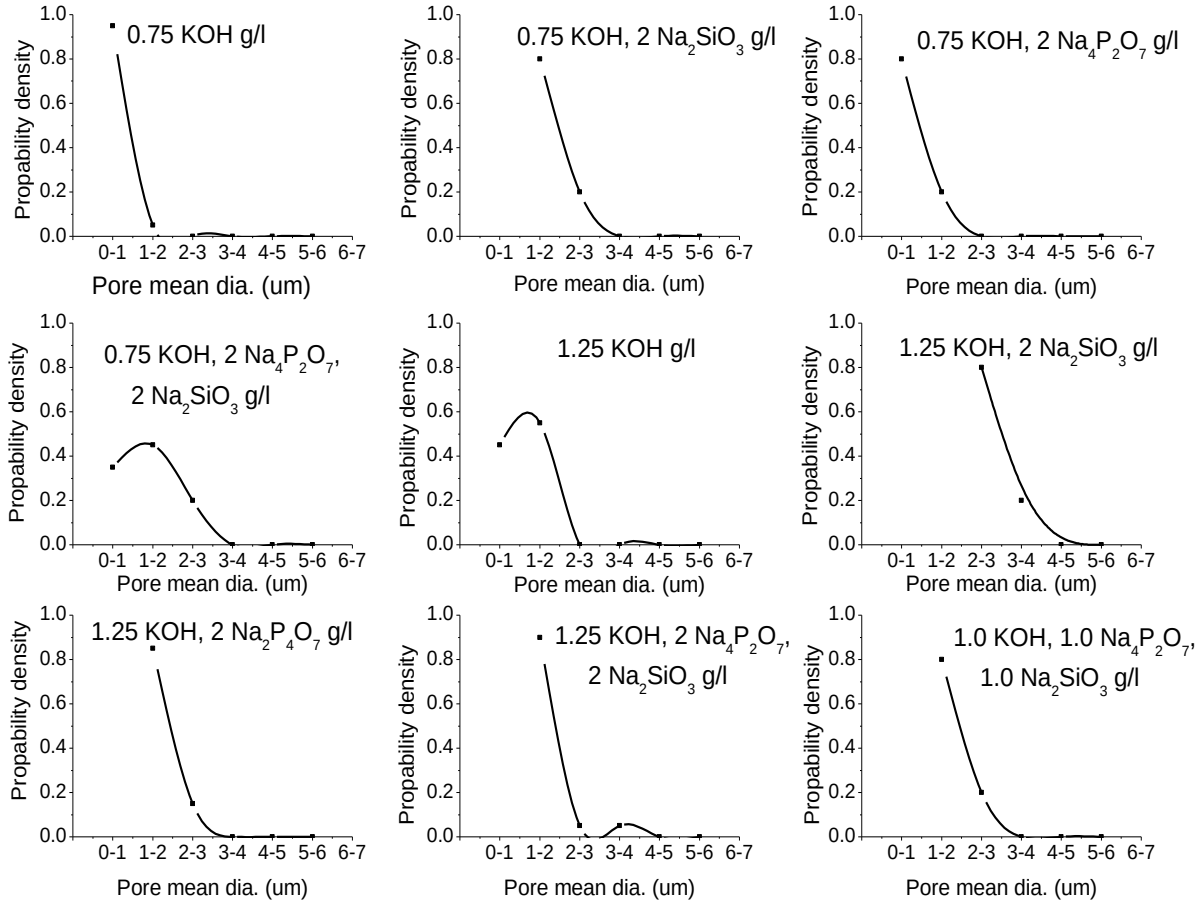

Fig. 5.8 The pore size distribution for coatings produced in different electrolytes.

The pore size distributions in coatings produced in different electrolytes were obtained using image processing software developed by Digital Surf (MountainsMap 7.4). This software allows quite accurate determination of pore size and other statistics by converting the grey scale image to a binary image. Fig 5.9 shows some examples of the estimation of overall pore mean diameter of coatings produced in electrolyte E5 and E4.

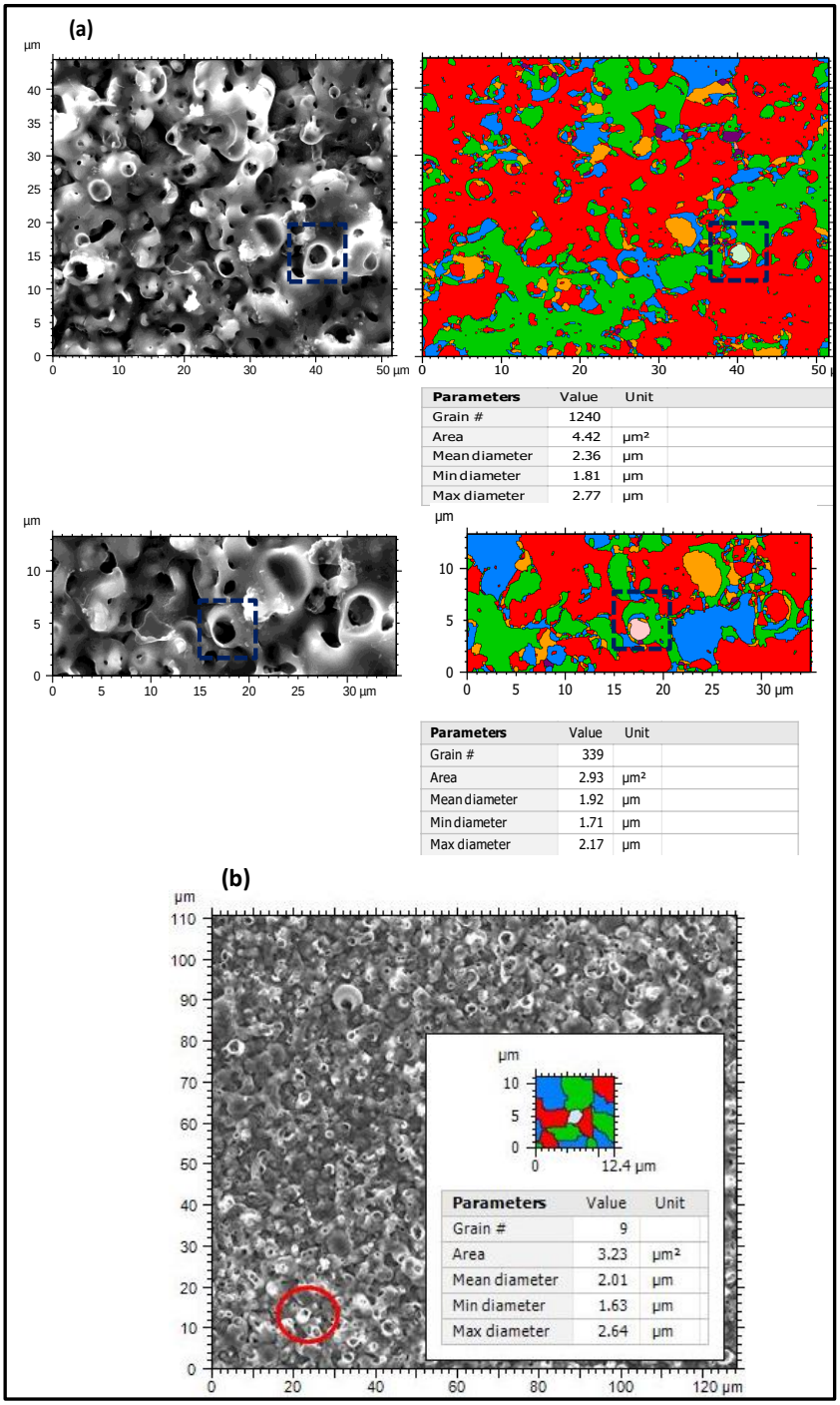

Fig 5.9 Original and binary thresholding SEM images showing the pores identified in coatings produced in (a)1 KOH, 1 Na4P2O7, 1 Na2SiO3 g/l (b)0.75 KOH, 2 Na4P2O7, 2 Na2SiO3

In a detailed study of porosity, Curran and Clyne [61], state that the pores arise from the oxygen evolution during the PEO process. A dense coating, free from pores and defects could be a good candidate for corrosion protection, However in many applications it is considered that the pores of PEO coatings are beneficial [148], for instance dye-sensitized solar cells, large pore size may be also a positive factor, since the formation of pores will cause an

increase in surface roughness and specific surface area that assist light absorption. Typical commercial coatings are commonly reported to have porosity levels of less than 3 %, as estimated by image processing of SEM micrographs [149]. However, the acceptable value may be higher depending on a particular application.

5.5. Coating thickness and roughness

The thickness of PEO coatings produced in electrolytes with compositions from E1 to E9 (table 3) were found to be in the range 1.0 to 27.0 µm Fig. 5.10. The thicknesses of these coatings changes depending on concentrations of sodium silicate and pyrophosphate and presence of potassium hydroxide. Increasing sodium silicate and pyrophosphate concentrations in the solution leads to increase both thickness and roughness of the coatings. The highest coating thickness in one side, 27 µm was achieved in the electrolyte E9 (1.25 g/l KOH, 2.0 g/l $Na_4P_2O_7$, 2.0 g/l Na_2SiO_3) which corresponds of about 80 % of Al foil consumed for whole process of conversion to alumina ceramics. The lowest value, 1.1 µm was found for the coating produced in the electrolyte E1 (0.75 g/l KOH). However the thickness of the coatings produced in electrolytes E3 (0.75 g/l KOH, 2.0 g/l $Na_4P_2O_7$) and E8 (1.25 g/l KOH, 2.0 g/l $Na_4P_2O_7$,) which contain a sole addition of pyrophosphate were higher than those produced in electrolyte solutions E2 (0.75 g/l KOH, 2.0 g/l Na_2SiO_3) and E7 (1.25 g/l KOH, 2.0 g/l Na_2SiO_3) that contain only silicate addition. The influence of silicon is discussed in more details in Ref. [8]. It is found that increasing the silicate concentration in the electrolyte results in accelerated coating growth, because of incorporation of Si into the oxide structure and formation of complex Al-Si-O phases. Beside the silicate, sodium pyrophosphate (Na4P2O7) may also promote oxide layer growth.

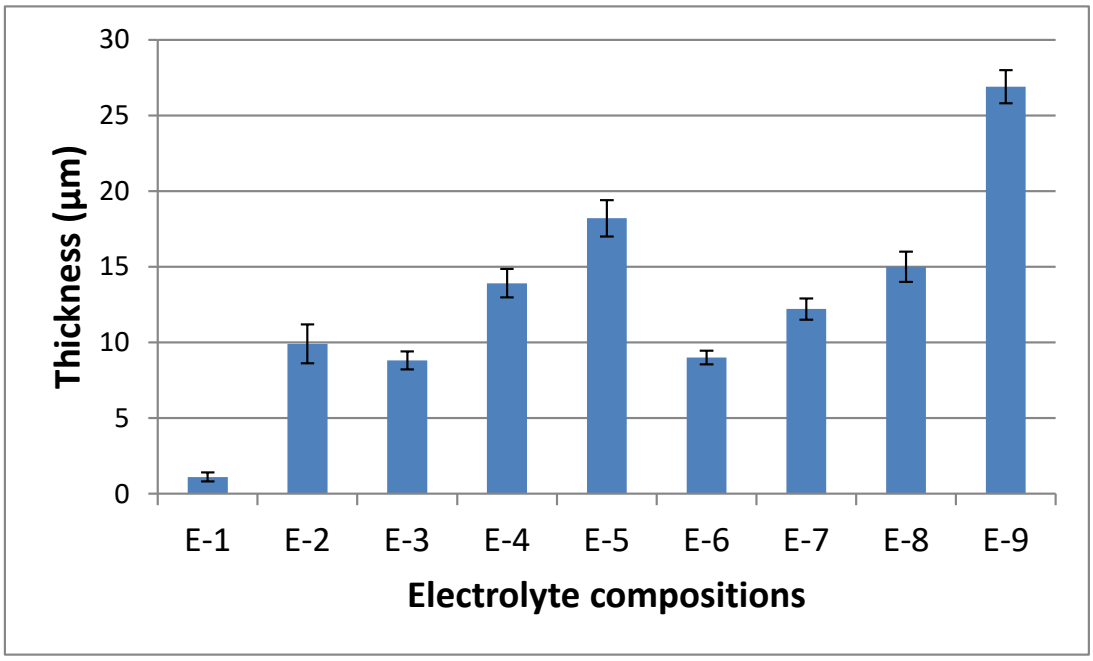

Fig. 5.10. Characteristics of coatings produced from different electrolytes.

Previous studies [9, 150-152] investigated the influence of the current density and electrolyte concentration on oxide film growth on aluminium during PEO treatment in solutions of KOH. They found that the coating thickness increases with increased KOH from 0.5 to 2 g l^{-1}, since the rate of anodic dissolution increases and oxygen evolution is shown to be the main electrochemical process at the potentials corresponding to the plasma stages of the electrolysis. From table 5.10, it can be seen that the PEO coatings prepared at the same parameters in a solution with 0.75 g l^{-1} KOH were thinner than those prepared in a solution with 1.25 g l^{-1} of KOH.

Surface roughness is also another characteristic which may be affected by the coating morphology. Addition of sodium silicate leads to increased discharge intensity which contributes to the accumulation of oxidation products and forms a coarse-grained coating structure with high surface roughness [76]. Table 5.4 shows the results of surface roughness measurements for the oxide layers produced in different electrolytes. As can be seen form table, the surface roughness increased with both sodium silicate and pyrophosphate concentrations.

Table 5.3. Design table of factor (concentration) varied in the experiments.

Electrolyte	KOH g/l	$Na_4P_2O_7$ g/l	Na_2SiO_3 g/l	Thickness (µm)	Porosity %	Roughness Ra (µm)
E1	0.75	0	0	1.1	10.7	0.15
E2	0.75	0	2	8.8	11.8	0.6
E3	0.75	2	0	9.6	14.0	0.65
E4	0.75	2	2	13.9	18.0	0.71
E5	1	1	1	17.2	14.5	1.2
E6	1.25	0	0	9.0	10.0	0.8
E7	1.25	0	2	12.2	13.0	0.91
E8	1.25	2	0	15.0	10.7	0.96
E9	1.25	2	2	27.0	11.8	1.6

Table 5.4 shows the average roughness R_a of PEO coatings formed in the electrolyte E6 is 0.8 µm and E5 is 1.2 µm compared with 1.6 µm for the electrolyte E9. Furthermore, the PEO coatings prepared from phosphate and silicate sodium solutions have a higher total coating thickness and roughness than those prepared from low and without sodium phosphate solutions.

Fig. 5.11. Shows the coefficient of paired correlation measures the strength and direction of the relationships between thickness, roughness and porosity in different electrolytes composition. In comparison, strong correlation was observed between roughness and thickness of PEO coatings produced in different electrolytes. With increasing the thickness, the surface of alumina ceramic coating is gradually roughened as a result of the reducing the pore number as well as the increasing pores size. This observation is in agreement with earlier studies [76, 99, 153]. After increase potassium hydroxide concentration to 1.25 g/l in electrolytes E2 to E9, the trend in the surface roughness and thickness of the coatings increase slightly with increasing the sodium silicate and pyrophosphate concentrations. This may be due to the large discharges occurring on the surface of thick coatings. Because higher power dissipated in larger discharges larger molten pools can be formed resulting a coarser morphology of solidified products and leading to a higher surface roughness.

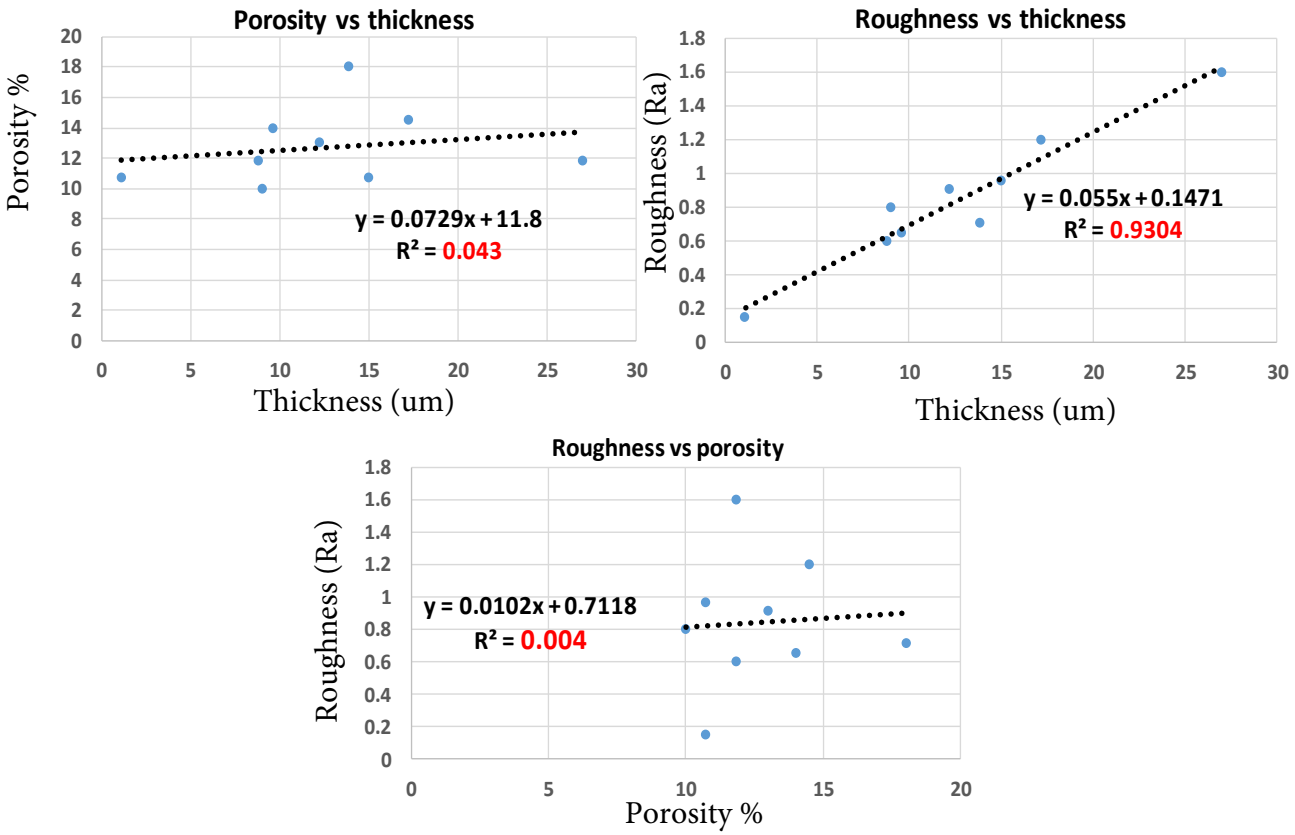

Fig. 5.11. Shows the coefficient of paired correlation evaluated in different electrolytes composition.

5.6. Phase Composition

Fig. 5.12 show the XRD patterns of produced PEO coatings. Strong diffraction peaks of Al are detected in all coatings because the oxide layers are thin and the X-rays can penetrate them easily. It is seen also that both γ and α alumina are present in the coatings. However characteristic diffraction peaks of γ-Al_2O_3 phase in the coating produced in electrolytes which contain sodium pyrophosphate (E3 and E8) are stronger than those in electrolytes containing sodium silicate (E2 and E7). While the intensity peaks of α-Al_2O_3 phase in the coating produced in E9 solution is stronger than those produced in other solutions. This appears to be consistent with the results of Polat *et al*. [76].

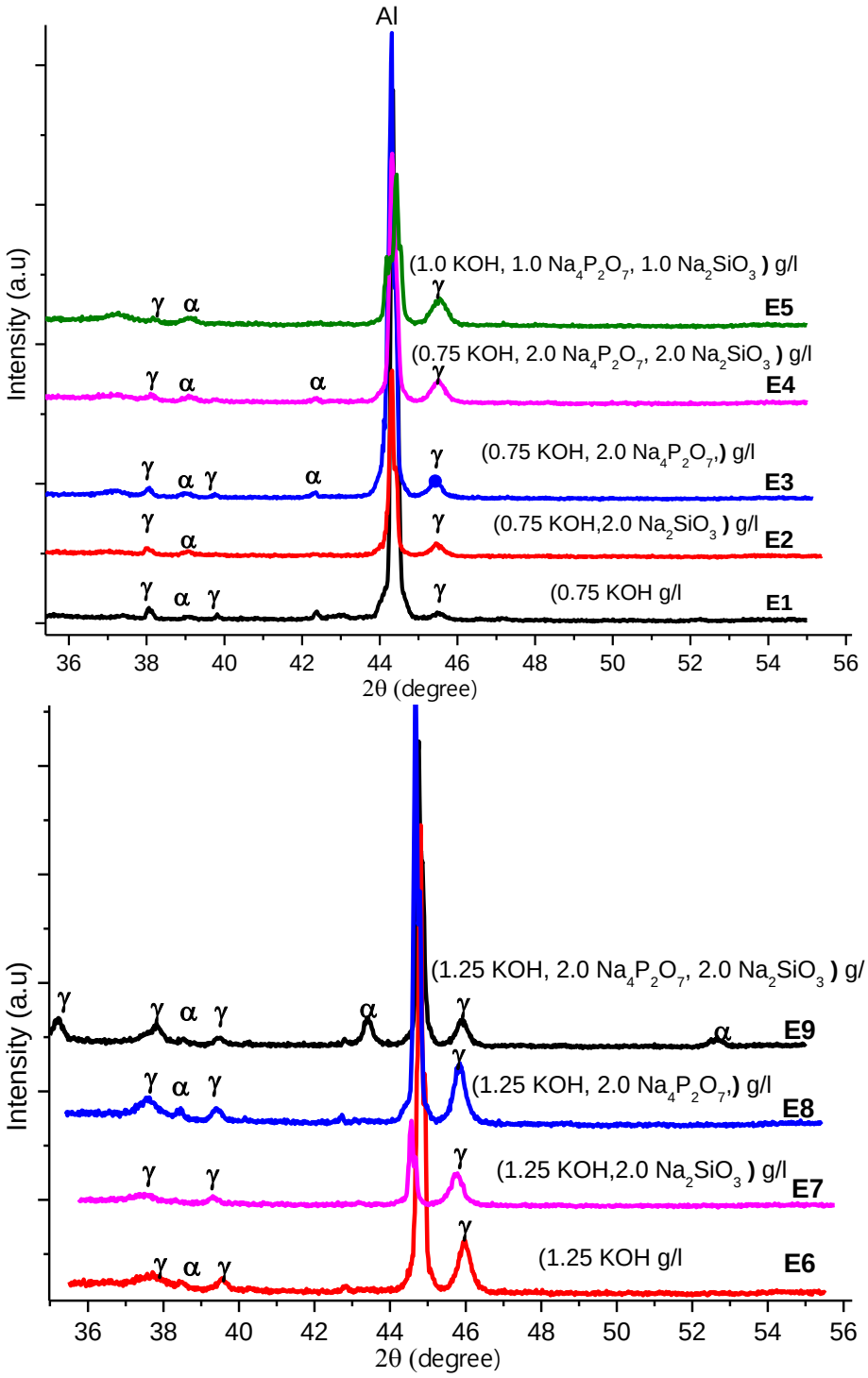

Fig. 5.12. XRD patterns of the oxide coatings deposited on Al foil in the different solutions; E1 to E9.

They suggested as Na_2SiO_3 concentration in the electrolyte increases, the intensity of diffraction peaks of alpha and gamma alumina decreases. This is due to the incorporation of silicate into the oxide layer. From the XRD results it can be seen that for electrolytes E1, E2 and E7 the coatings are mainly composed of γ-Al_2O_3. While the coatings produced in

electrolytes containing pyrophosphate, such as E4, E6, E8 and E9, have undergone γ to α alumina transformation and therefore contain increased amounts of α -Al_2O_3. Due to the high cooling rate during the contact of the oxide ejected out of discharge channels with the electrolyte, γ-Al_2O_3 is mainly formed. However, as a result to the low thermal conductivity of alumina the temperatures and pressures in the channels of plasma micro-discharges rise as the process continues, which leads to transformation of γ-Al_2O_3 to α-Al_2O_3. Thus, the fabrication of γ- and α- alumina and several other compounds on Al have previously been reported [8, 11, 132, 154].

The phase composition of PEO coatings depends on coating thickness and changes from surface to the coating substrate barrier [76]. As can be seen from Fig 5.12, this the case for PEO coatings formed in electrolytes E8 and E9 which have thickness 15.4 and 27 µm respectively where the intensity peaks of alpha alumina phase increases from the surface to the coating/substrate interface.

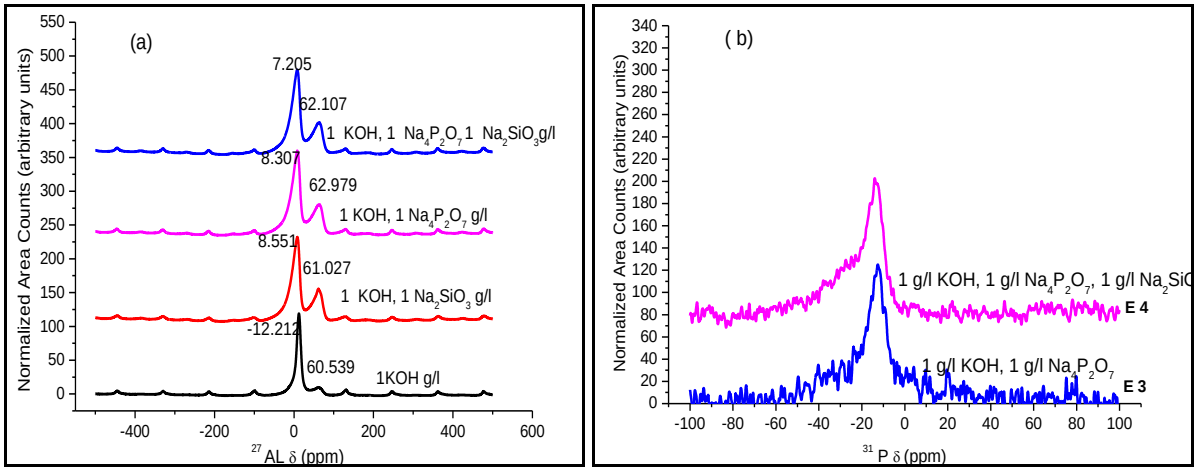

Fig. 5.13 NMR spectra of alumina ceramics in different electrolytes composition for (a) 27Al and (b) 31P.

Fig. 5.13 shows the ^{27}Al MAS NMR and ^{31}P MAS NMR spectra obtained from the powder samples produced from the coatings formed in different electrolyte solutions. From Fig. 5.13 (a) it can be seen that the aluminium spectra show two resonances, near 0 ppm from octahedrally coordinated aluminium and near 60 ppm from tetrahedral coordination [155]. For PEO coatings produced in E2, E3 and E4 electrolytes the octahedral peak has a similar shape and position, while for the coating produced in E1 electrolyte the peak is narrower and has less asymmetry, so this coating appears to be more ordered. Similarly, it can be seen that the phosphorus spectra show relatively week signals [155]. The signal appears have two

components, one peaking at ~ -13 ppm in coating produced in electrolyte E3 (0.75 g/l KOH, 2.0 g/l $Na_4P_2O_7$) and a broad and less frequency of the first in coating produced in electrolyte E4 (0.75 g/l KOH, 2.0 g/l $Na_4P_2O_7$, 2.0 g/l Na_2SiO_3). While no phosphorus signals in coating produced in electrolyte E1 (0.75 g/l KOH) and electrolyte E2 (0.75 g/l, 2.0 g/l Na_2SiO_3).

5.7. Correlations between processing parameters and coating characteristics

To understand how the electrolyte composition affects thickness, surface roughness and porosity of produced PEO coatings, a multiple linear regression (MLR) analysis was applied to the data obtained in the experiments discussed. MLR builds up models by fitting to linear equations the relationship between concentrations of electrolyte components, as independent variables, and the observed coating characteristics (thickness, roughness and porosity), as response functions. These models reveal how the independent variables influence its response and predict at what extent the value of one variable could influence the response when the other variables are known. Previous studies have used the MLR method to analyse the influence of some parameters such as electrolyte temperature and treatment time of PEO ceramic coating on Al-alloy [12, 81, 141, 156, 157]. The general form of a linear equation with three independent variables takes the following form [141, 158-160]:

$$\mathbf{Y = a_o + a_1X_1 + a_2X_2 + a_3X_3 + \ldots + a_i\,X_n}$$

where Y; is a target property (thickness, roughness and porosity); X_1, X_2, X_3 … X_n are concentrations of electrolyte components (C_{KOH}, $C_{Na4P2O7}$ and $C_{Na2SiO3}$) varied as basic factors of the experiments (table 5.2); a_o is the constant where the regression line intercepts the Y axis, representing the amount the dependent Y will be when all the explanatory variables are at level; a_i is the standard partial regression coefficient, representing the extent the response variable Y; (i.e. the thickness, roughness or porosity) changes when the explanatory variable changes at level (table 5.2). So, the thickness can be expressed in the form of PEO parameters as given below:

$$\mathbf{Thickness}\ (ħ) = \mathbf{a_o + a_1C_{KOH} + a_2C_{Na_4P_2O_7} + a_3C_{Na_2SiO_3}} \qquad (2)$$

Similar equations can be provided for roughness and porosity. The Analysis of Variance (ANOVA) test was conducted for the three responses and the results are shown in Table (5.4 (a, b and c)).

Table 5.4. The output multiple linear regression analysis (ANOVA results) for (a) thickness, (b) roughness and (c) porosity data.

(a)

SUMMARY OUTPUT									
Regression Statistics									
Multiple R	0.92951								
R Square	0.86399								
Adjusted R Square	0.78238								
Standard Error	3.25484								
Observations	9								
ANOVA									
	df	*SS*	*MS*	*F*	*gnificance F*				
Regression	3	336.49	112.16245	10.5873	0.0132				
Residual	5	52.97	10.594014						
Total	8	389.46							
	Coefficients	ndard Er	t Stat	P-value	.ower 95%	Upper 95%	Lower 95.0%	Upper 95.0%	
Intercept	-9.52056	5.0014	-1.903592	0.11533	-22.377	3.335861	-22.3769719	3.3358608	
X Variable 1	14.57	4.603	3.1652956	0.02495	2.73749	26.40251	2.737494566	26.402505	
X Variable 2	4.2175	1.1508	3.6649648	0.01452	1.25937	7.175626	1.259373642	7.1756264	
X Variable 3	3.3175	1.1508	2.8828739	0.03447	0.35937	6.275626	0.359373642	6.2756264	

(b)

SUMMARY OUTPUT									
Regression Statistics									
Multiple R	0.8401								
R Square	0.7058								
Adjusted R Square	0.5293								
Standard Error	0.2341								
Observations	9								
ANOVA									
	df	*SS*	*MS*	*F*	*nificance F*				
Regression	3	0.6575	0.2192	3.9986	0.0849				
Residual	5	0.2741	0.0548						
Total	8	0.9316							
	Coefficient	*ndard Er*	*t Stat*	*P-value*	*ower 95%*	*pper 95%*	*wer 95.0*	*per 95.0*	
Intercept	-0.268	0.3597	-0.744	0.4901	-1.193	0.657	-1.193	0.657	
X Variable 1	0.9	0.3311	2.7183	0.0419	0.0489	1.7511	0.0489	1.7511	
X Variable 2	0.1375	0.0828	1.6612	0.1576	-0.075	0.3503	-0.075	0.3503	
X Variable 3	0.1125	0.0828	1.3591	0.2322	-0.1	0.3253	-0.1	0.3253	

(c)

SUMMARY OUTPUT									
egression Statistics									
Multiple	0.9735								
R Square	0.9477								
Adjusted	0.9163								
Standarc	0.0084								
Observat	9								
ANOVA									
	df	*SS*	*MS*	*F*	*nificance F*				
Regressi	3	0.0063	0.0021	30.201	0.0013				
Residual	5	0.0003	7E-05						
Total	8	0.0067							
	Coefficient	*ndard Er*	*t Stat*	*P-value*	*ower 95%*	*pper 95%*	*wer 95.0*	*per 95.0*	
Intercept	0.0937	0.0128	7.3	0.0008	0.0607	0.1267	0.0607	0.1267	
X Variabl	0.0075	0.0118	0.6349	0.5534	-0.023	0.0379	-0.023	0.0379	
X Variabl	0.0244	0.003	8.2539	0.0004	0.0168	0.032	0.0168	0.032	
X Variabl	0.0139	0.003	4.6983	0.0053	0.0063	0.0215	0.0063	0.0215	

Obtained MLR equations that optimise, on the basis of the results presented in Table 5.4, the models for the relationships between thickness, roughness and porosity and electrolyte composition, in terms of encoded levels, and corresponding statistics calculated are shown below:

$$\text{Thickness } (\mu m) = -9.52 + 14.57\ C_{KOH} + 4.2175\ C_{Na4P2O7} + 3.3\ C_{Na2SiO3}$$

$$\text{Adjusted } R^2 = 0.78; \quad N = 9$$

$$F = 0.013; \quad P < 0.03$$

$$\text{Roughness } (\mu m) = -0.268 + 0.9\ C_{KOH} + 0.14\ C_{Na4P2O7} + 0.112\ C_{Na2SiO3}$$

$$\text{Adj. } R^2 = 0.52; \quad N = 9$$

$$F = 0.08; \quad P < 0.04$$

$$\text{Porosity (\%)} = 0.09 + 0.0075\ C_{KOH} + 0.0244\ C_{Na4P2O7} + 0.014\ C_{Na2SiO3}$$

$$\text{Adj. } R^2 = 0.91; \quad N = 9$$

$$F = 0.001; \quad P < 0.0004$$

From the above results, it is clear that the adjusted R^2 for the thickness, roughness and porosity are 0.78, 0.52 and 0.91 respectively. Also the F-value for the models is 0.013, 0.08 and 0.001. This suggests that the models are significant, however roughness model can explain just 52 % variability of the response data.

Polycondensation of SiO_4^- is an important process of the oxide growth diffusion during the PEO process [161], and an increase in sodium silicate helps polycondensation of silica at sample edges. In addition, an increase in concentration of KOH may leads to local dissolution of the oxide layer. This means when alkali and silicate are in balance, the polycondensation process stops oxide dissolution, which is reflected in the coating thickness distribution which becomes more uniform. According to the MLR models, a strong correlation was observed between thickness and porosity with electrolyte concentration. It follows that the concentration of potassium hydroxide C_{kOH} has the most significant effect on the oxide ceramic layer growth which is the main component which provides electrolyte conductivity. Therefore the higher coating growth rate explained by the increase in coating thickness results in increase in electrolyte conductivity. Taking into account the other studied factors, the MLR analysis shows that the sodium pyrophosphate has the strongest effect on the coating porosity.

5.8. Summary

- Addition of potassium hydroxide (KOH) into the electrolyte provides the electrolyte conductivity and increase the rate of anodic dissolution and oxygen evolution which leads to the increase in the current density during the PEO process and resulting coating thickness. Multiple linear regression modelling confirms the strongest effect of KOH on the coating thickness and roughness, whilst porosity is most strongly affected by $Na_4P_2O_7$.
- The PEO coatings prepared from sodium pyrophosphate- and silicate-containing solutions have higher total thickness and surface roughness than those prepared from solutions with low concentrations of these additions and without sodium phosphate.
- The thickest coating corresponding to conversion of about 70% of Al foil to alumina ceramics, with residual aluminium foil thickness of around 20 µm, has been achieved in electrolyte E9 (1.25 g/l KOH, 2.0 g/l $Na_4P_2O_7$, 2.0 g/l Na_2SiO_3). The presence of some residual Al may enhance the flexibility of the ceramic-metal composite as explained in **Chapter 4**.
- The introduction of sodium silicate into the electrolyte significantly affects the characteristics of plasma discharge during the treatment. This contributes to the accumulation on the surface of oxidised products and promotes formation of coarse-grained coatings structure with high surface roughness.
- The coatings comprise mainly γ-Al_2O_3 and an amorphous component. Octahedral and tetrahedral coordination of Al in alumina are affected by additions of silicate and pyrophosphate to the electrolyte. Whereas the coatings produced in presence of sodium silicate and pyrophosphate, the octahedral peak has a similar shape and position, for the coating produced in electrolyte E1 (1.25 g/l KOH), the peak is narrower and has less asymmetry, so this coating appears to be more ordered.
- Among the three electrolyte constituents investigated, potassium hydroxide is found to be the predominant factor affecting coating thickness and surface roughness; this is followed by sodium pyrophosphate and sodium silicate.

Chapter 6

Cyclic voltammetry studies of PEO processes in alkaline and silicate/phosphate electrolytes and resulting coatings

6.1. Introduction

Plasma electrolytic oxidation is electrochemical conversion of a metal surface to produce an oxide ceramic layer [150, 162]. The PEO process is a complex process including concurrent partial processes of oxide layer formation, dissolution and dielectric breakdown. For example several researchers used a number of considerations to define the breakdown voltage. They found, in addition of type of working electrode the sparking voltage depends on concentration, composition and temperature of electrolyte and current density.

The CV method was used to understand and identify the potential variations corresponding to differential behaviour of Al foil electrodes during the process which is very helpful in clarifying the mechanisms of the coatings formation.

Although, there are several factors that affect coating thickness uniformity, such as current mode and density, electrolyte pH, composition and concentration as well as chemical composition of the substrate, the of electrolyte plays a very important role in the PEO process. Electrolytes used usually promote metal passivation by forming a thin insulating surface layer which provides a prerequisite for the dielectric breakdown to induce spark discharge [8, 74, 80, 86].

Some additives such as silicates, phosphates and aluminates are widely used as basic ingredients of the electrolytes to enhance metal passivation and facilitate sparking. These additives may increase either electrolyte conductivity, thus reducing the breakdown voltage, or the quality of the ceramic coating. This is reflected in current and voltage transients which have been widely studied to reveal the electrode surface state and underpinning electrochemical processes, such as anodic dissolution and film growth [8, 150]. For instance, an increase in alkaline electrolyte solution concentration of KOH from 0.5 to 2 g/L was found to lead to decreases the film growth rate and increases in the rate of anodic dissolution due to the chemical attack by hydroxide ions OH^- [82, 150].

Often in the literature, the PEO process has been subdivided into two to four different stages [150, 163-165]. However, the explanations are not always consistent and not all of

these stages are always clearly identifiable in the electrical transients. In the presence of oxide film on aluminium surface, the anodic dissolution of aluminium may be categorised into two types. The first one is a direct metal dissolution reaction by movement of aluminium ions through the oxide layer, while the second is an indirect metal dissolution reaction by consecutive electrochemical film formation at the metal/oxide interface, owing to the movement of OH^- through the film towards aluminium, and chemical film dissolution due to OH^- attack at the film/solution interface [164, 166]. It is also often assumed that OH- could also get deprotonated at the oxide-electrolyte interface and O_2- ions would then provide a much greater fraction of the anionic flow. Discussing the mechanism of anodic dissolution of aluminium in alkaline media, Moon and Prabhu stated that the direct metal dissolution, which involves direct ejection of aluminium ions from the film into the solution definitely does not occur in alkaline solutions, due to the instability of aluminium ions because aluminium ions are not stable thermodynamically in alkaline solution [164, 166]. Therefore, for analyse the dissolution mechanism of pure aluminium in alkaline solution, it will be sufficient to consider indirect working electrode dissolution by consecutive oxide layer formation.

Thickness variations of PEO coating on Al are often observed. Although the chemical composition and microstructure including (crystal structure, crystalline size, orientation, defects and density) are the factors affecting mechanical properties of the coatings, these are also strongly influenced by the coating thickness. Several authors discussing the importance of the coating thickness in the mechanical properties of PEO coatings stated that thicker coatings usually show better mechanical properties [167, 168], however this is not always true as the defects such as porosity may play crucial rule in the mechanical performance of thick PEO coatings [168]. Design engineers specify thickness for various reasons, including some applications which need specific aim, such as the need of a degree of flexibility which influence by the residual metal in the component [169]. The primary objective of this part of the study is to provide better understanding of the electrochemical behaviour of Al in an alkaline electrolyte with and without silicate and pyrophosphate additives under the potentials corresponding to those applied in PEO treatments, using cyclic voltammetry (CV) technique. This is also used to understand the coating formation process during the PEO treatment such as the underlying metal-electrolyte interactions. Cyclic voltammetry is commonly utilised to investigate mechanisms and kinetics of electrochemical processes [170-

172]. In our work, CV method is adapted to understand the complexity of the coating formation mechanism involved during the PEO process.

6.2. Experiments

Rectangular shape samples of 50 μm thick aluminium foil with dimensions 30 mm × 18 mm × 0.05 mm and surface roughness of *R*a ~ 0.1 to 0.2 μm were used as substrates. Prior to the treatment, the samples were cleaned in distilled water and acetone and dried by air. The cleaned samples were suspended in the electrolyte using an insulated metal holder. The process was carried out in two different electrolytes (1.25 g/l KOH) and (1.25 g/L KOH, 2.0 g/L $Na_4P_2O_7$, 2.0 g/L Na_2SiO_3) with conductivities of 0.55 and 0.70 S/m and pH values of 11.88 and 12.10 respectively, denoted as K and KSi2P2 electrolytes. The voltage was ramped with a scan rate of 2.44 V sec^{-1} over the range of 0-550 V, corresponding to the conditions of PEO treatment. Fig. 6.1 shows the geometry of the electrolytic cell used in the experiment. It consists of a working electrode sample connected to the positive output a 30 kW DC power supply and a 2-L cylindrical stainless steel tank with inside diameter of 130 mm and height of 145 mm, which served as a cathode with surface area of 8.57×10^{-2} m^2, equipped with a stirring and cooling system. The electrolyte temperature was kept within the range of 30 to 35 ^oC. In order to correlate optical emission and physicochemical processes on the sample surface during the PEO treatment, optical emission spectroscopy (OES) study was carried out using a FloTron XHR spectrometer operated in the range from 300 to 900 nm wavelength range with a resolution of 1.8 nm.

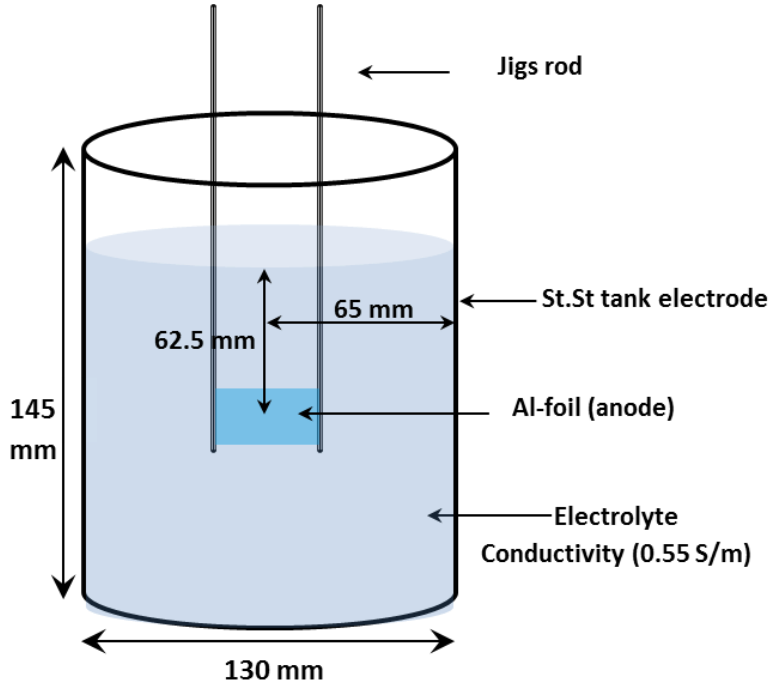

Fig. 6.1 The electrolytic cell used in the studies of the PEO process.

To evaluate the distribution and thickness of the PEO coating on the Al foil, SEM images were taken along the length of the whole sample. The Images were obtained at 2000× and 5000x magnification using an Inspect F50 SEM operated at a 15 kV accelerating voltage and 10.8 mm working distance. The size of the images was 1024×943 pixel. A MountainsMap 7.1 and ImagJ software were used to analyse the SEM images.

Results and discussion

6.3. Formation mechanism of PEO coatings

Fig. 6.2 shows the current density-voltage responses obtained from CV experiments corresponding to the conditions of PEO treatment in the K and KSi2P2 electrolyte.

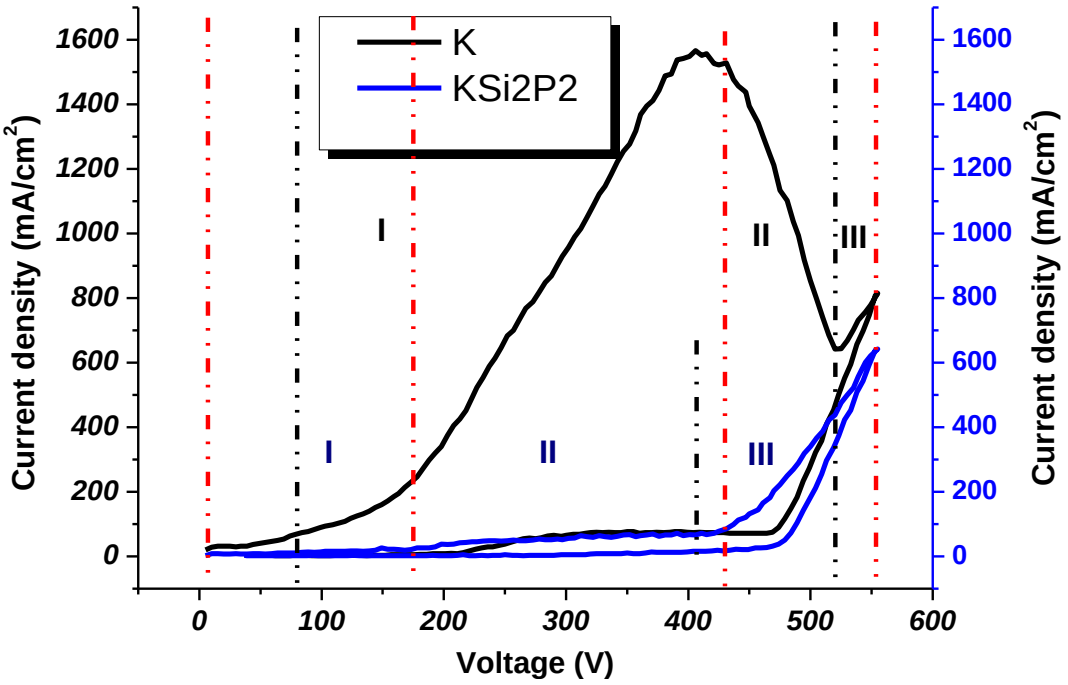

Fig. 6.2 Current density-voltage characteristics of PEO process of aluminium foil in K and KSi2P2 electrolytes.

Often in the literature, the PEO process has been subdivided into two to four different stages [150, 163-165]. However, the explanation of the different stages is not always the same and not always clearly identifiable in the voltage-time response diagrams. The anodic reaction on the surface of aluminium foil sample treated in K electrolyte is considered as indirect metal dissolution and the hydroxide film formation starts electrochemically on the surface of aluminium by migration of hydroxide ions through the aluminium/film interface. The following reactions are suggested to explain the mechanism of dissolution and formation of the PEO coating:

$$Al + 3OH^- = Al(OH)_3 + 3e^- \quad (1)$$

The aluminium hydroxide film which formed electrochemically will be dissolved chemically by an attack of OH^- ions at the film/solution interface and form aluminate ions $Al(OH)_4^-$ as:

$$Al(OH)_3 + OH^- \rightarrow Al(OH)_4^- \quad (2)$$

Additionally, as a result of aluminium anodic dissolution, hydrogen evolution takes place as (Eq 3):

$$Al + 3H_2O + OH^- \rightarrow \frac{3}{2} H_2 + Al(OH)_4^- \quad (3)$$

The curve K in Fig.6.2 appears to be composed of three stages. The first stage I (0-380V) corresponds the steep climb of current density to the peak of about 1550 mA/cm^2. Certainly, that the increase of the current density in the first stage is due to the anodic dissolution occurred on the surface of aluminium (Eqs. 1&2). Pyun and Moon [164] stated in that the increasing rotation rate of the sample causes fast supply of OH^- ions to the film/solution interface and rapid removal of aluminate ions $\mathrm{Al(OH)}_4^-$ away from the film solution interface. At the oxide/electrolyte interface, the oxygen evolution is quite common for aluminium anodising in alkaline solution. Also the potential is very high and the water splitting potential is already passed. Therefore, it may either have another reactions due to the water splitting which is caused by high voltage where the OH^- anions are absorbed on the surface, (Eqs. 1) and direct combination of Al and O atoms in plasma state under the effect of spark discharge, (Eqs. 4-6) [173, 174].

$$4OH^- \rightarrow O_2 \uparrow + 2H_2O + 4e^- \quad (4)$$

$$2Al_{ejected} + 6\,OH^- \rightarrow Al_2O_3 + 3\,H_2O + 6e^- \quad (5)$$

In reaction Eq. 6 a multistep process will happened, where Al hydroxide would have formed first and then either progressively dehydrated to form alumina or transformed into alumiate ion which would dissolve in the solution. This would then precipitate back on the surface if the solubility limit of aluminate is reached locally

The stage II Fig.6.4 shows a more complex behaviour, where reaction rates may be affected by mass transport, in particular, how fast the species can depart from the surface of the sample. That means, if the species depart slowly this will hold the reactions and dissolution is offset by transport limitations, not by the barrier-type anodic film formed. So the current eventually becomes reduced as seen in Fig. 6.2, and even independent of potential. When the electric field strength was strong enough, the breakdown voltage and dielectric breakdown take place across the oxide film at around ~535V, accompanied with numerous of spark discharges. Hereafter, the current density climbed steadily as seen in stage III (535-560V). During this stage, the main reactions that occur on the aluminium electrode are associated with transformation of the hydrated anodic oxide to ceramic alumina and combination of aluminium and oxygen atoms in plasma state under the influence of spark discharge, also to form alumina [8, 46] .

According to Fig. 6.2, addition of 2 g/l for both Na_2SiO_3 and $Na_4P_2O_7$ to 1.25g/l KOH electrolyte shows completely different current-voltage behaviour. Adding silicates and pyrophosphates to alkaline electrolytes is commonly used to promote metal surface passivation due to the formation of insoluble compounds and allow the sparking voltage to be easily reached which is the most beneficial for the coating production by the PEO process. The cyclic voltammetry curve for KSi2P2 electrolyte in Fig.6.2 does not actually show evidence of anodic dissolution, although it also displays three distinguished stages according to the applied voltage. Stage I (0-150V), indicating no significant current density change due to the fact that the formation rate of the passive oxide layer takes control over the metal dissolution rate on the surface. The second stage II (150-425V) corresponds the slight increase in current density with applied voltage to peak at about 100 mA/cm^2. At around ~425V, the current increases and the electric field strength in the oxide film reaches a critical value which causes dielectric breakdown of the oxide film. In the stage III (425-550V), the current density increases sharply with increasing voltage. As shown in Fig. 6.2, addition of sodium silicate leads to production of SiO_2 due to the transport of SiO_3^{2-} anions towards the coating/electrolyte interface during the PEO process. The silica produced may inhibit the release of Al^{3+} cations, leading to a decrease in breakdown voltage. In other side, the electrolyte may include substances which enhance to decrease the electrolyte resistivity such as sodium hydroxide or potassium hydroxide (1-50 g/l) [8]. This according to Ikonopisov equation [175] could be cause the decreasing of breakdown voltage. The following reactions are suggested for the formation of such silica.

$$SiO_3^{2-} + 2H^+ \rightarrow SiO_2 + H_2O \qquad (6)$$

$$SiO_3^{2-} + 2H^+ + (n-1)\ H_2O \rightarrow SiO_2nH_2O \qquad (7)$$

6.4. Relationships between OES and current-voltage behaviour

Figure 6.3 displays the recorded spectrum of optical emission from the exposed area of the plasma discharge during the PEO process in K and KSi2P2 electrolytes which contain aluminium (Al 309 and Al 396 nm) from substrate and potassium, soduim, and hydrogen α and β (K-765, Na-589, H_α-656 nm and H_β) lines from electrolytes.

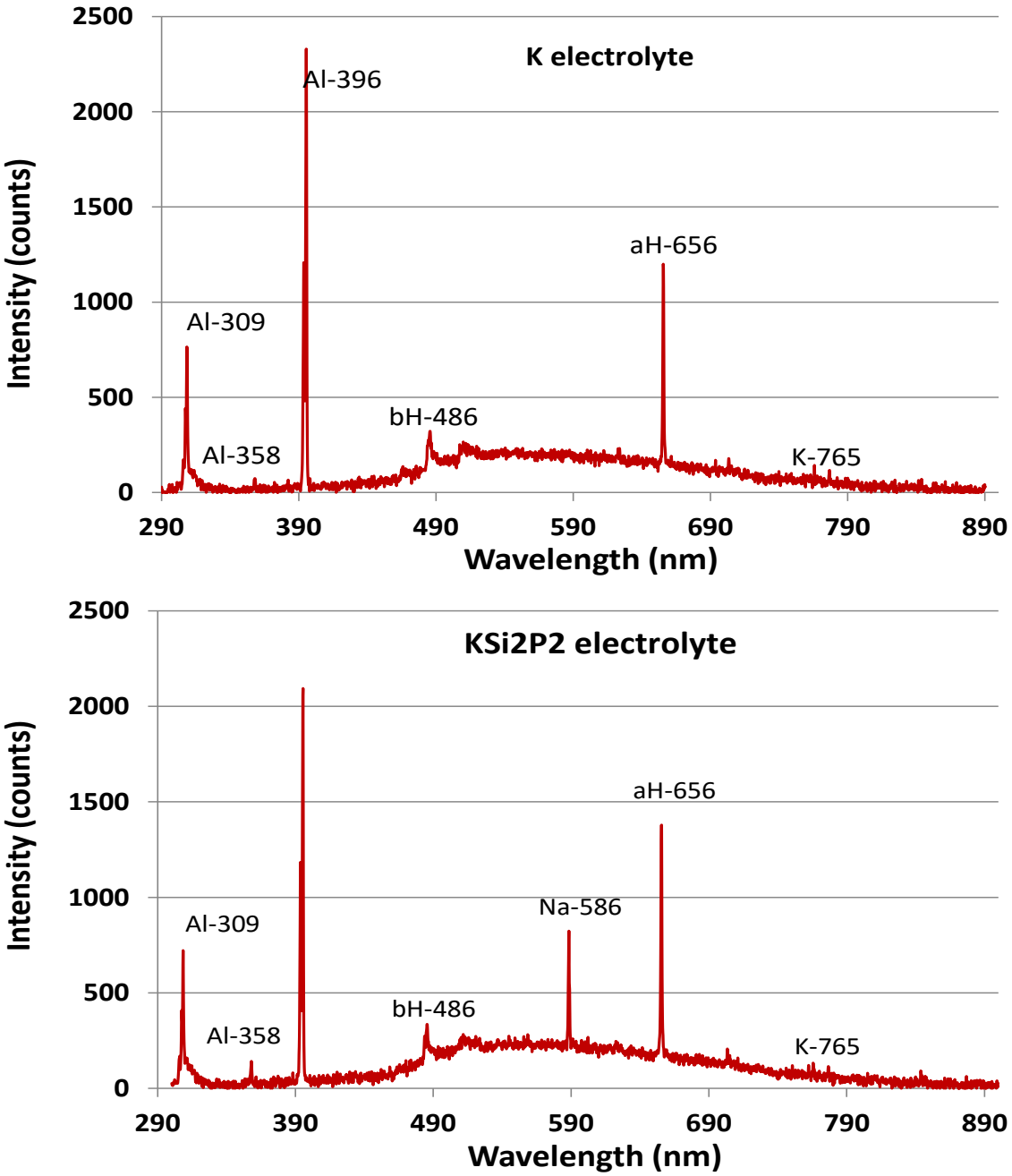

Fig. 6.3 Optical emission spectrum during the PEO process on Al foil in K and KSi2P2 electrolytes.

In this experiment, OES signal with the wavelength shorter than 300 nm cannot be registered, because it is absorbed by the electrolyte. As seen in Fig.6.3, for samples treated in both electrolytes, the strongest observed lines correspond to aluminum (Al-396 nm) and (H_α-656 nm). While the relatively low intensities were recorded from potassium (K-765 nm) and (Hβ- 486 nm). In addition, sodium line (Na-589 nm) arises in the spectra of microdischarges on the sample treated in the KSi2P2 electrolyte.

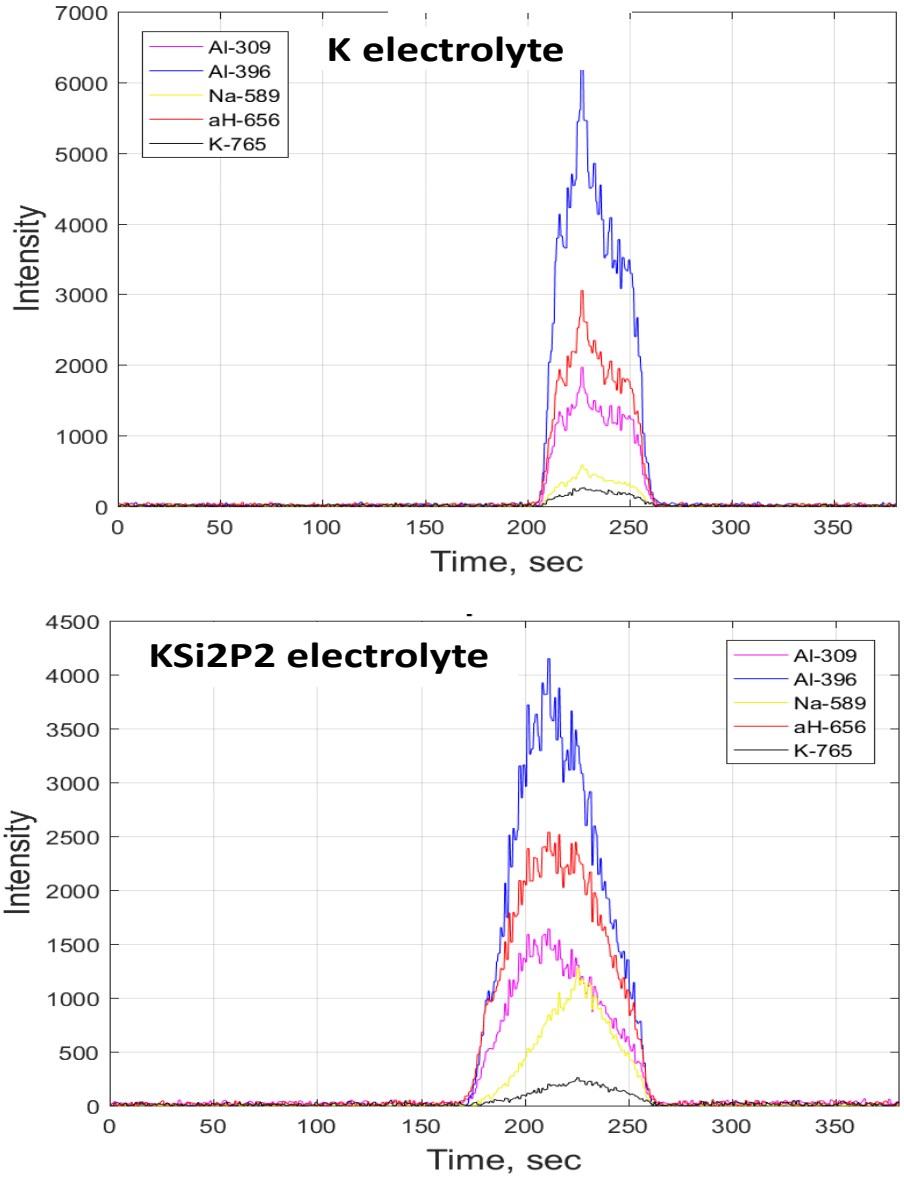

Fig 6.4 Typical time variation of the emission line intensity during CV studies of the PEO processes in (a) K and (b) KSi2P2 electrolytes.

Evolution of emission line intensities with the treatment time in CV mode is presented in Fig 6.4-6.5. Differences OES signal during treatments in K and KSi2P2 electrolytes are attributed to the additions of silicate and phosphate to the electrolyte. The OES signals of samples treated in K electrolyte become visible after about 205 sec to reach voltage 525 V for 0.8 A/cm^2 and ended after around 255 sec to reach voltage around 460 V for 0.1 A/cm^2. While signals of samples treated in KSi2P2 electrolyte started after 175 sec with voltage 425 V for 0.1 A/cm2 and ended at the same time as for the sample treated in K electrolyte with voltage 480 V for 0.01 A/cm^2. The time to reach the breakdown voltage was significantly shorter in

the electrolyte solution containing silicate compared with that without, which is consistent with the analysis of the electrical breakdown phenomenon reported by R.K. Nigam *et al* [176]. Results Figure 6.5 shows the atomic line intensity - voltage diagrams plotted in the same scale as the current density - voltage diagrams of Al foil in (a) K and (b) KSi2P2 electrolytes.

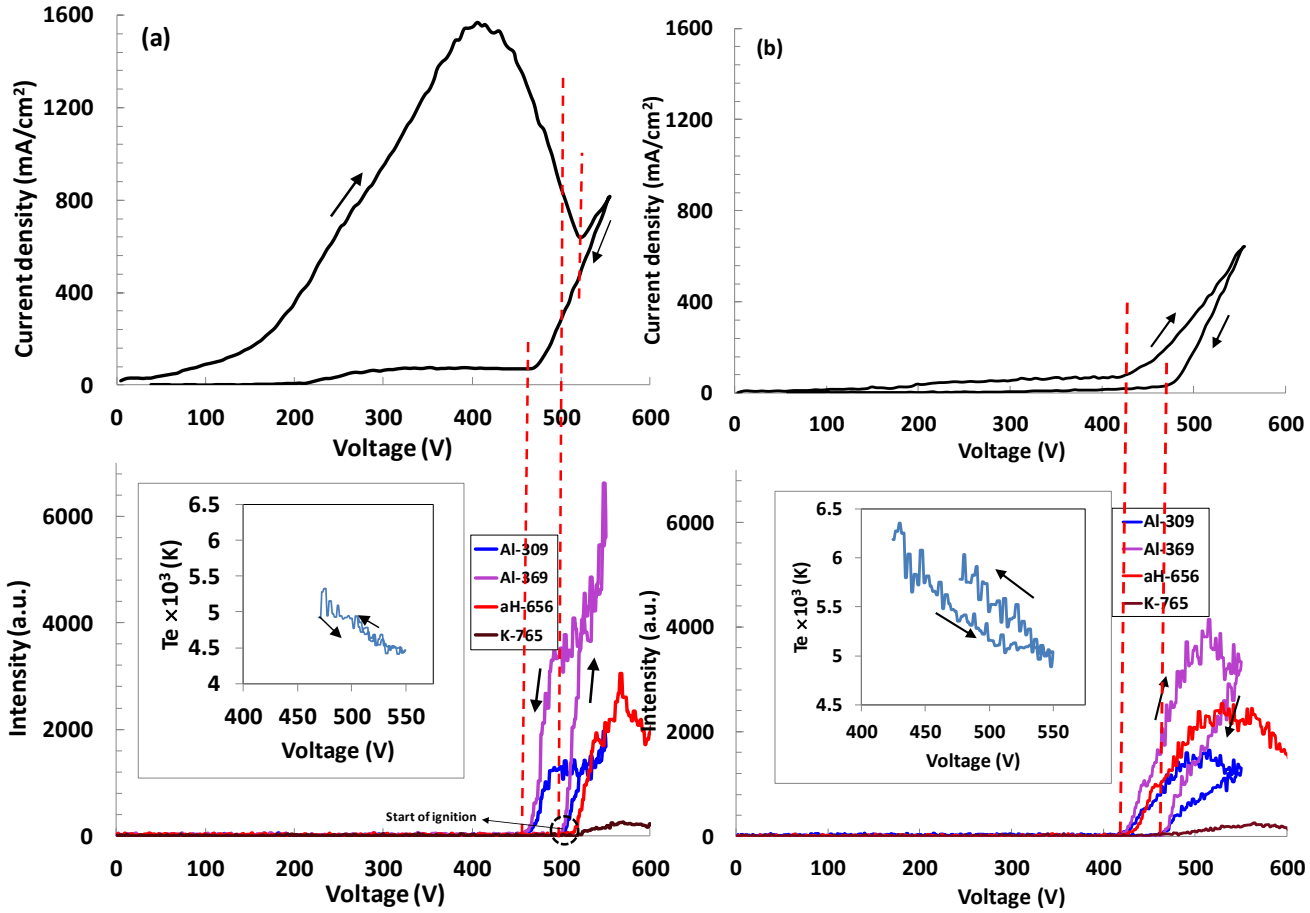

Fig.6.5. Plots of intensity versus voltage during the PEO process at same scale with current density versus voltage of Al foil in (a) K and (b) KSi2P2 electrolytes.

A comparison of the curves in Fig. 6.5 (a&b) showed dissimilar behaviour of emission intensity lines and a considerable difference in values of current densities at the discharge ignition during the two PEO treatments at the same voltages. Generally the discharge in PEO process takes place when the applied voltage reaches a specific value corresponding to the breakdown of the oxide layer formed on the sample surface, which causes a generation of intense light emission at the microdischarge sites [109]. However as seen in Fig. 6.5 (a) the OES signals of the species generated from the sample treated in K electrolyte recorded in the period before the breakdown voltage (535 V) occurs. It is noticed that after the current is fallen and dissolution is offset by transport limitation (not by barrier type), the optical

emission observed started prior to the current starts increasing. The ignition and extinction voltages were around 500 V voltage and 460 V respectively, while in K2P2Si2 electrolyte, the OES signal originated at the breakdown voltage (around 425 V) and the extinction voltage is higher (470 V). From Fig. 6.5, it can also be seen that the breakdown voltage of the sample treated in KSi2P2 is shifted about 110V towards lower values in respect to that of the sample treated in K electrolyte, however corresponding values of current densities show opposite trend, $0.8\ A\ cm^{-2}$ versus $0.085\ A\ cm^{-2}$ for the samples treated in K and KSi2P2 electrolyte respectively.

In K-electrolyte condition at voltage 425 V there was a fluctuation in the electron plasma temperature (4800 to 5200 K) which is corresponding to the early period of discharges as seen in Fig. 6.5 (a&b). While in K2P2Si2 electrolyte at the same voltage the fluctuation was less at the early stage of sparking (6100-6300). The previous difference could be related to the different in electrolyte conductivity, where the voltage drop at higher electrolyte resistance would means less driving force for the coating to grow, so it means less sparks, less energetic discharge and less plasma temperature. This analysis reflects with what we have from our results in Fig. 6.5 (a&b).

Fig. 6.5 (a&b), also displays the hysteresis of plasma temperature (K) versus voltage (V) in both conditions. Despite a lot of PEO research, how the plasma temperature hysteresis remains not have a good size of analysis and discussion. As can be seen in Fig. 6.5 (a&b) sample treated in K- electrolyte shows a smaller width of T_e - V hysteresis than sample treated in KSi2P2 which is not easy to observe. The reason could be related to the substances added to electrolyte K2P2Si2, where the presence of silicate causes substrate passivation by inhibition anodic dissolution of the Al. So the above results provided a connection between the electrolyte concentration, plasma temperature and the plasma discharge behaviour.

6.5. Thickness and uniformity of the coating layer

The thickness distribution of the PEO coating layer along the Al foil was calculated based on the area comprised by the coating layer in the cross-section and the length of the image. However, the same region (cross sectional coating area) can be approximated by scanning vertical lines for thickness evaluation. These lines should scan across the oxide film randomly in order to obtain a representative value of the full sample length. Figure 6.6 (a)-(b)), displays

a sketch diagram of the coating thickness measurement. Further details of the methods used to identify the thickness and distribution of the coating layer based on the scanning electron microscopy images are discussed in References [177-179].

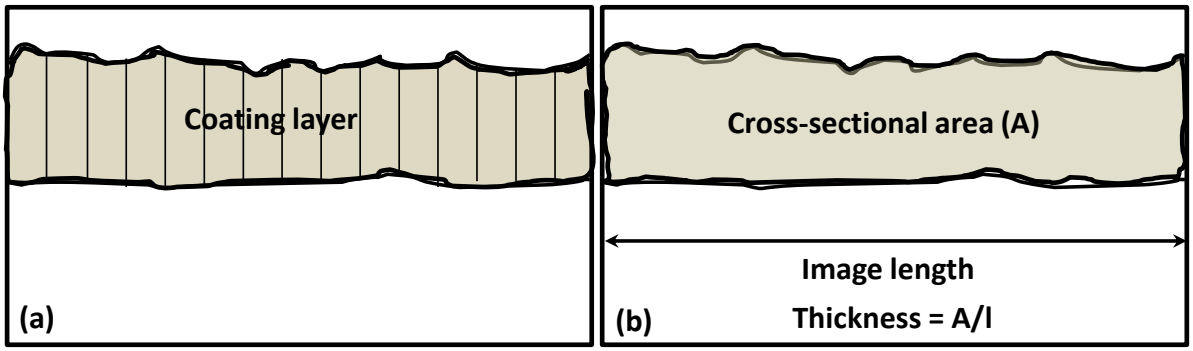

Fig. 6.6 (a)-(b)) Schematic representation of thickness measurements of the coating layer (a) with scanning vertical lines (b) based on the PEO coating cross-sectional area and image length.

Cross-sectional SEM images of the PEO coatings and residual aluminium layer on the samples treated in K and KSi2P2 electrolytes are shown in figure 6.7 (a)-(b)), respectively. Results show that the PEO coating layer thickness grown in K electrolyte varies from 1.2 ±0.2 µm at edges to 0.6 ±0.2 µm at the middle region of sample. While it ranges from 2±0.2 µm at edges to 1.7±0.2 µm in the middle of the sample treated in KSi2P2 electrolyte.

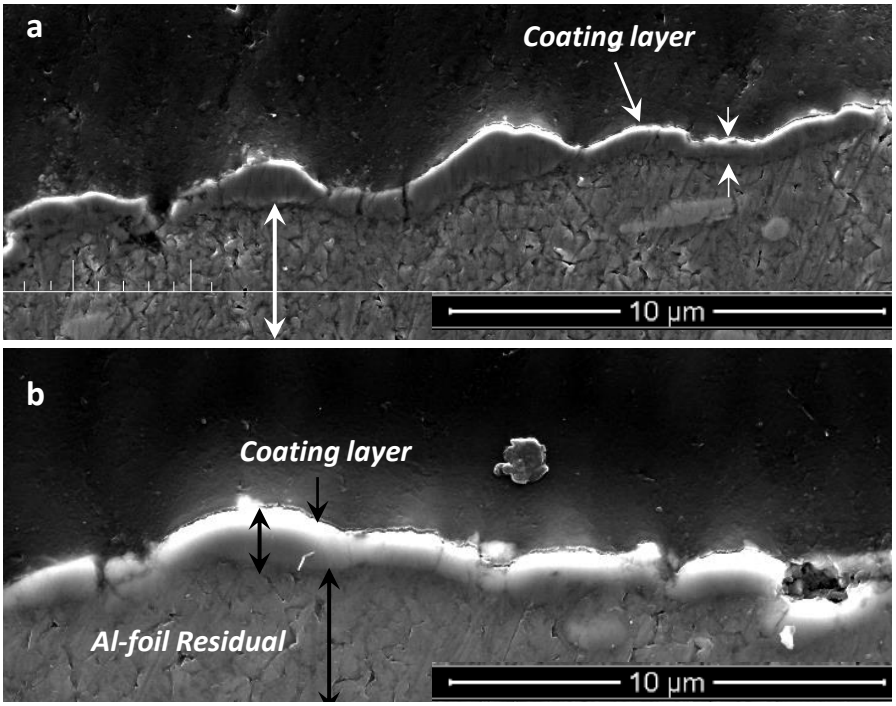

Fig. 6.7 (a)-(b)). SEM cross-sectional micrographs of the PEO surface layer on the samples treated in (a) K and (b) KSi2P2 electrolytes

The results show variation in thickness over all surfaces of both samples. However, the coating layer on the sample treated in KSi2P2 electrolyte shows a more uniform coating thickness distribution than that produced in K electrolyte (Fig. 6.8 and 6.9).

The thicknesses of the PEO coating and residual aluminium were determined at each millimetre (mm) along the specimen length. Then, in respect to the sample length, it becomes possible to determine the aluminium lost for anodic dissolution and ejection in electrolyte as well as Al consumed for the coating during whole the PEO process by formula;

$$ħ = \frac{m}{A \times \rho} \quad (1)$$

Where;

ħ = thickness (μm)

m = mass (g)

A = total area, (cm^2)

ρ = density, (g/cm^3)

$\rho_{(Alumina)} \approx 3.1\ g/cm^3$

So, for the sample treated in K electrolyte, at each mm of length, the residual aluminium thickness of 34 μm has been subtracted from the 50 μm of foil thickness before PEO treatment to obtain 16 μm of the thickness of aluminium lost during the PEO process. This value corresponds to around 8×10^{-4} g (obtained by sample volume multiplication by Al density of 2.7 (g/cm^3). The difference between the mass of Al lost during the whole process and Al consumed for the coating is the mass of Al lost for anodic dissolution and ejection in electrolyte, which is equal around 6.0×10^{-4} g per mm length and 0.02 g along whole sample. According to Eq [1], this is equal to 0.21 μm of sample thickness.

Residual thicknesses of coating and aluminium, as well as mass of aluminium consumed for dissolution and ejection, all are presented in Table 6.1. In spite of previous calculated values seem to agree well with the logic impression one get from the SEM, it has to be considered only as an approximation, due to possible errors, such as the true density of the oxide layer forming phase due to present of porosity that can differ significantly from aluminium or its oxide.

Table 6.1 Results of thicknesses over the length of sample.

sample length point (mm)	Samples treated in K electrolyte				Samples treated in KSi2P2 electrolyte		
	Total coating thickness (μm)	Al residual thickness (μm)	Al consumed for whole process (g)	Al consumed for dissolution and ejection (g)	Total coating thickness (μm)	Al residual thickness (μm)	Al consumed for whole process (g)
1	2.4	34.0	8.0×10^{-4}	6.0×10^{-4}	4.0	41	4.0×10^{-4}
3	2.0	35.0	8.0×10^{-4}	7.0×10^{-4}	4.0	43	3.0×10^{-4}
6	1.6	37.0	6.0×10^{-4}	5.4×10^{-4}	3.5	45	3.0×10^{-4}
9	1.4	37.0	6.0×10^{-4}	5.1×10^{-4}	3.5	47	2.0×10^{-4}
12	1.4	39.0	4.0×10^{-4}	4.1×10^{-4}	2.0	47	2.0×10^{-4}
15	1.4	37.0	4.0×10^{-4}	6.0×10^{-4}	2.0	46	2.0×10^{-4}

As can be seen from Fig. 6.8, the thicknesses of oxide layer showed a sharp fall until reaching around 0.6 μm at 7 mm distance from the edge of the sample and before moving steady between 10 and 15 mm, with almost no thickness increase. Then the thickness grows linearly between around 20 mm to 30 mm distance of the sample length. This fluctuation in oxide film thickness also appeared in the thicknesses of residual aluminium and that lost for dissolution during the process along the whole sample, as shown in Fig. 6.8 and 6.9.

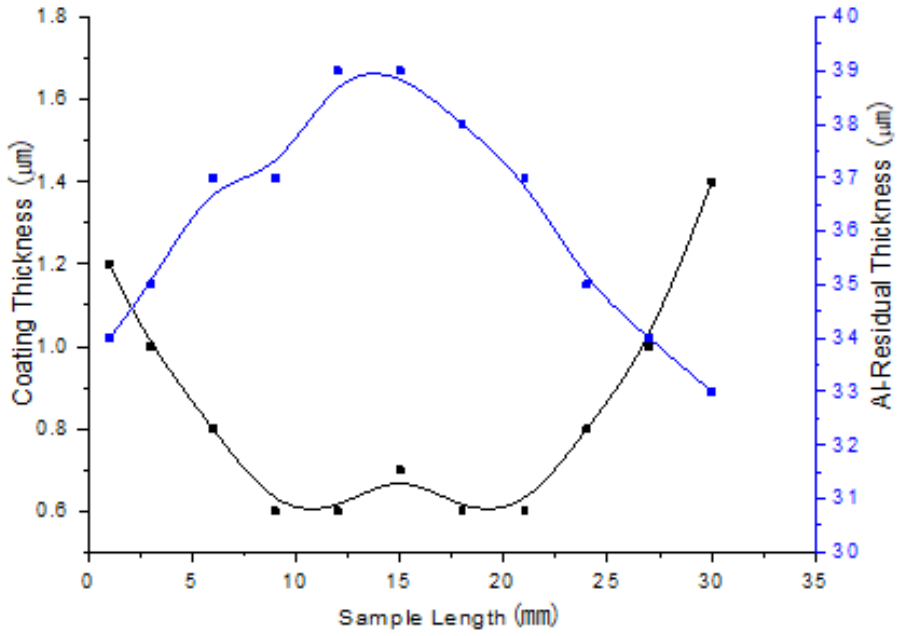

Fig. 6.8 Thickness distributions of PEO coating and residual Al along the length of the sample treated in K electrolyte.

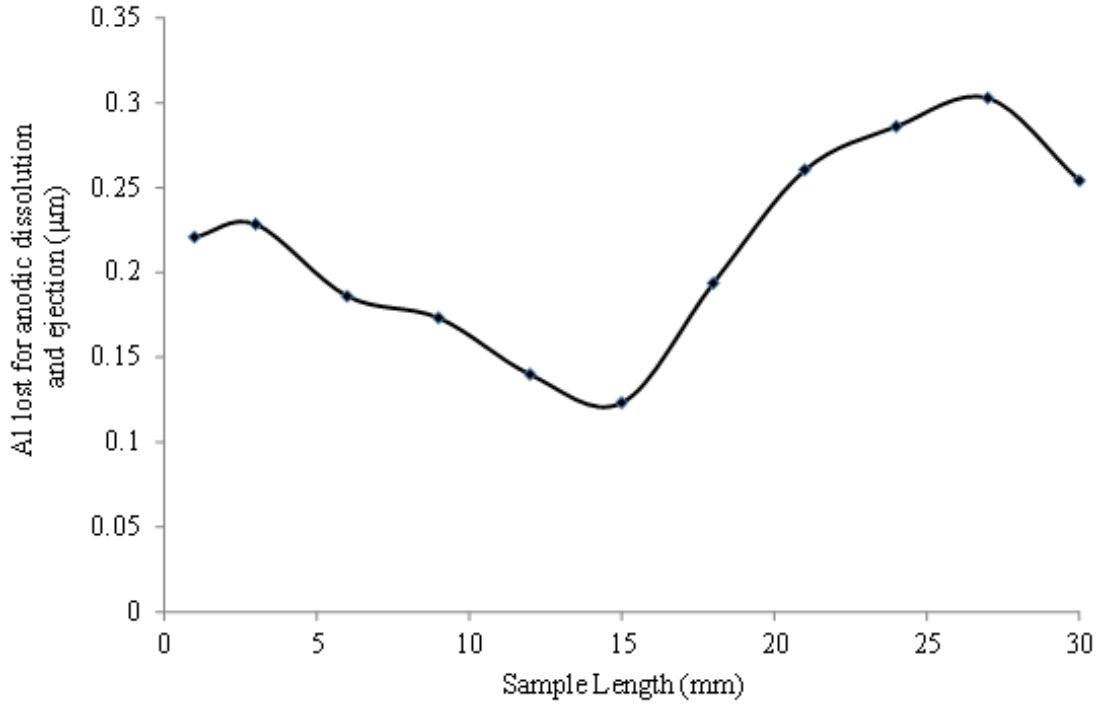

Fig. 6.9. Thickness of Al lost for anodic dissolution and ejection for the sample treated in K electrolyte.

In general, the relationship between the PEO coating layer thickness and the charge density passed through the sample surface is direct [150], however, in our results the character of this trend differs for the thickness of oxide film and residual aluminium along the sample length. The non-linear rate distribution of anodic dissolution reaction obtained from such analysis of the sample treated in K-electrolyte (Fig.7) could be of great help in investigation why the variations in residual thicknesses of coating and aluminium occurred. In particular, when the current falls sharply from 1550 to 650 mA/cm^2 at the breakdown voltage, before it starts gradually increasing and following this trend. Also it should be noted that the OES signal commenced before the minimum current is achieved (Fig.6.5). This changing behaviour may influence the distribution of the rates of dissolution and precipitation processes over the sample length, which would affect the thickness distribution of the oxide film.

In the other hand, the sample treated in KSi2P2 electrolyte showed less variation in coating thickness than that treated in K electrolyte. The decline in the coating thickness from the sample edge to the middle was around 25% while of sample treated in K electrolyte was 50% (Fig. 6.10 and 6.11). As stressed previously the cyclic voltammetry curve in this case does not show evidence of anodic dissolution. This indicates surface passivation dominates over dissolution due to the presence of silicate and phosphate. It has been reported that the

addition of sodium silicate into KOH solution can promote formation coating layer and increase both the thickness of coating and adhesion strength [77, 78].

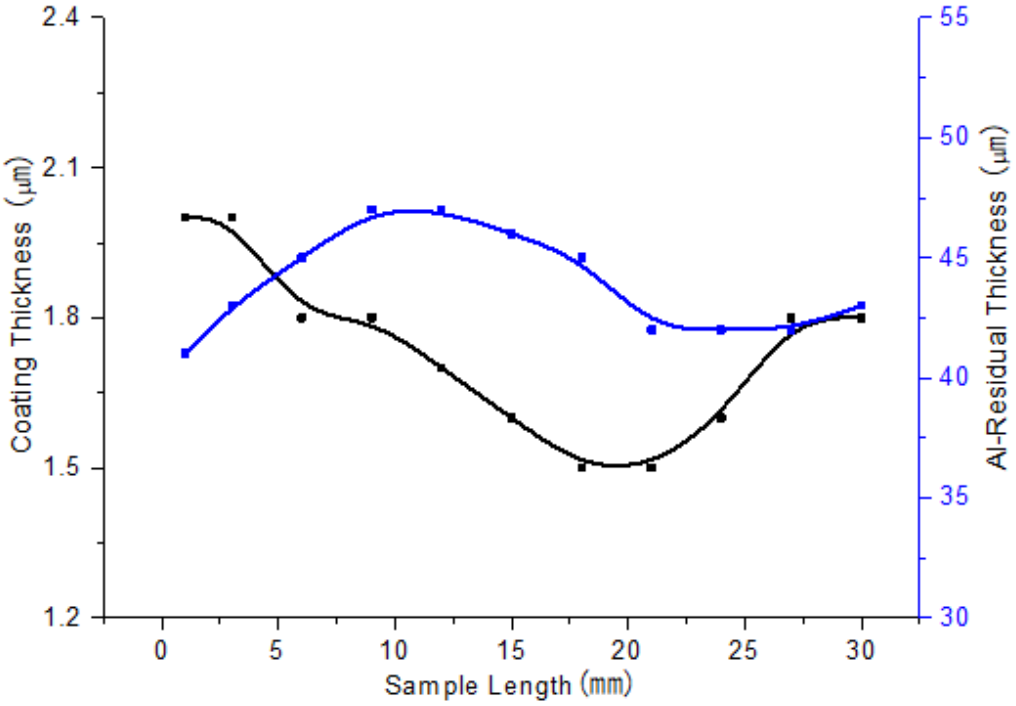

Fig. 6.10. Distribution of PEO coating and residual Al thicknesses along the length of the sample treated in KSi2P2 electrolyte.

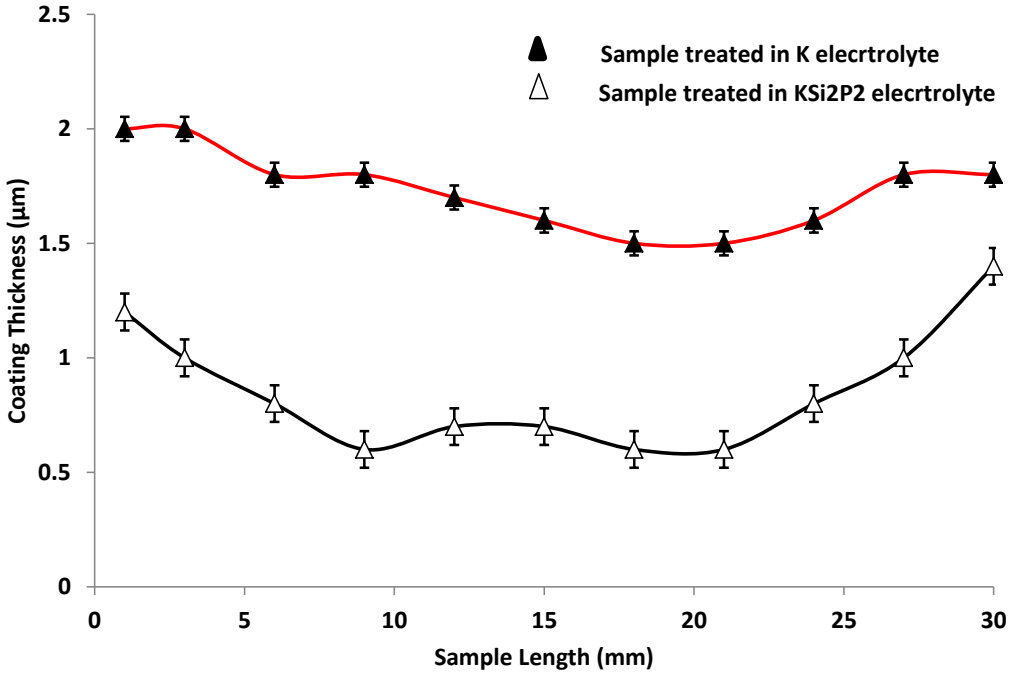

Fig. 6.11. Oxide layer thickness produced in K and KSi2P2 electrolytes.

6.6. Summary

A cyclic voltammetry (CV) method was employed to clarify the electrochemical behaviour of Al in alkaline silicate/phosphate electrolytes over a voltage range of 0 to 550V and study the growth process of PEO coatings on rectangular shape Al foil samples.

The non-linear behaviour of the current – voltage curve reflects a combination of three processes, including dissolution, passivation and formation of PEO coating under discharge conditions.

Different thickness distributions of oxide layer and residual aluminium along the sample length were observed. Similarly, the total Al consumed for the coating process at the edge of sample was more than in the middle.

Silicate addition obstruct anodic dissolution of Al, which enhanced the oxide growth. While phosphate, in addition of promoting α-Al2O3 phase formation it is also enhancing strong metal passivation and allow the breakdown voltage to be easily obtained.

Breakdown voltage depends on the concentration and electrolyte composition. Under the studied conditions, we can also conclude that the sparking voltage decreases when electrolyte resistivity decrease which is consistent with Ikonopisov equation [175]. However which's more surprising and unexpected in K electrolyte, is the earlier emission starting prior to the current starts increasing.

There are a number of considerations used to determine the breakdown voltage such as reaching of maximum voltage, rapid voltage fluctuation. However, the appearance of visible sparking is not a criteria for detecting the dielectric breakdown as concluded in our study although many literatures considered this as criteria.

Chapter 7

Electric Field Modelling during Plasma Electrolytic Oxidation of Al foil substrate

7.1. Introduction

For complex shape components made from advanced materials, it is a vital to model a treatment process before full scale prototyping. Neglecting this important step could lead to a waste of expensive materials, deterioration of equipment and excessive labour costs.

To predict thickness distribution of electrodeposited coatings over a complex shape component, electromagnetic field simulation can be applied. For the PEO process, such modelling is partially hindered due to the lack of appropriate methodology that would allow the coating uniformity on the complex shape parts to be estimated. In conventional electrochemistry this methodology is well- established and has been successfully applied to simulate processes and optimise electrolysers before physical tests [8]; it supports simulation and structural optimisation of electrolysers before physical tests. Modern software offers electrochemical modules which allow introducing electrochemical reactions, kinetic, thermodynamic or mass transport equations. However, this software has limited capability to simulate systems, such as PEO, wherein significant voltage drop occurs over a very thin layer near the working electrode. The modelling of PEO processes is also affected by complex behaviour of current-voltage diagram, reflecting characteristics of plasma discharge and electrolytic gas evolution. Another complication is the coating growth which proceeds both inwards and outwards of the original surface. Therefore, it is vital to develop a methodology for accurate estimation of PEO coating thickness distribution over complex geometry components.

A very limited number of publication discuss PEO process modelling in terms of current density distribution (CDD) and resulting oxide layer thickness; however, this is a topical area for advanced research [180]. The surface oxide layer formed on the part subjected to the PEO treatment is usually considered as a component of the system with the highest electrical resistance in the circuit [8] and the voltage drop over the electrolyte is often neglected. Consequently, the current density at the oxide-electrolyte interface is averaged and considered constant [180, 181]. Such level of approximation is applicable only when using the

simplest electrode shapes and layouts, e.g. coaxial cylindrical cells. Any deviation in the electrode shape or position can lead to the uneven coating growth, which must be taken into account in modern technological processes [6].

Therefore, the objective of this part of research is to develop a modelling methodology which considers nonlinear current-voltage diagrams and becomes applicable for relatively complex cell layouts. A plate in a conductive cylinder configuration was chosen as an example for theoretical calculations. A thin aluminium foil was selected as a working electrode for experimental assessment, since it has stable and known thickness that allows calculation of both coating thickness distribution and metal losses following the treatment [182].

7.2. Electric field modelling

7.2.1. General approach

This part of the research attempts to join the results of theoretical and experimental studies of PEO treatment of aluminium. A closely related 2D electric field modelling problem has been successfully solved using mesh method for electrolytic plasma polishing process [182] where a vapour gaseous envelope was described as a lumped nonlinear element. A similar general approach, boundary conditions and assumptions are used here. A specific interest was paid to the mesh surrounding the anode in order to represent the oxide layer and the discharges along the sample surface. The method also employs three adjustment parameters that allow to bring the 3D problem to be reduced to the 2D model due to symmetry along the axis and provide an estimation of uneven coating growth over the sample perimeter.

7.2.2. Assumptions

The following assumptions have been made before modelling:

1. The problem is solved for the case of the PEO treatment during anodic regime under potentiostatic conditions.
2. The electrolyte is stirred and its temperature T is constant.
3. The electrolyte is considered as a linear homogeneous conductive medium with constant specific conductivity γ.
4. The system nonlinearity is introduced by the resistance of the oxide layer through the current-voltage diagram.

5. The CDD is obtained for longitudinally invariant field in 2D model and then adapted to 3D model by using effective length z_3.

7.2.3. Boundary conditions

The boundary problem concerns 3D current density distribution in the electrolyte. This corresponds to a rectangular sample placed in a conductive cylinder (Fig. 7.1). This setup is commonly used in both research and industrial applications but should be simplified for further calculations.

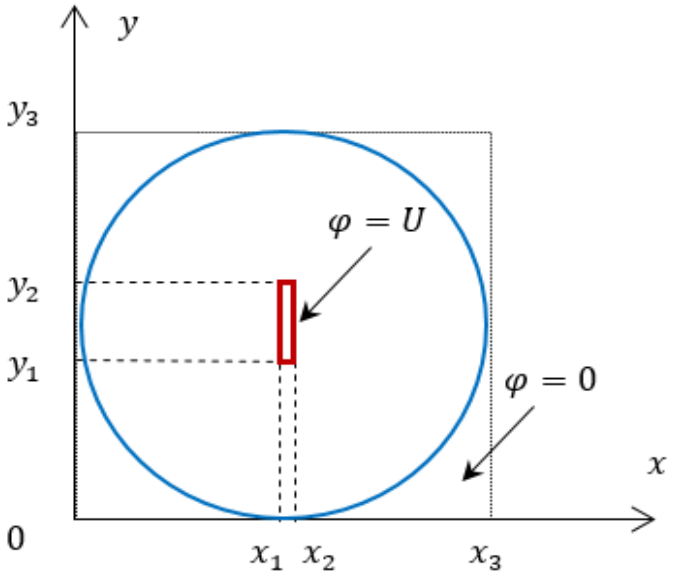

Fig. 7.1 Electrode layout for the electric field analysis

The 2D field distribution in the conductive medium is obtained by numerically solving the Laplace equation

$$\nabla^2\varphi = 0 \qquad (1)$$

in Castesian coordinates (x, y, z) with respect to the electric potential φ [183]. Based on assumption (5), the 2D problem (Fig. 7.1) isolved for the longitudinally invariant field $\varphi = \varphi(x, y)$. A thin rectangular anode is placed in the centre of the system at a position $(x_1; y_1)$ and the cathode with diameter $x_3 = y_3$ forms the perimeter of the system. Dirichlet boundary conditions

$$\varphi = 0 \; and \; \varphi = U \qquad (2)$$

are adapted at the cathode and anode respectively. In order to create a round cathode in Cartesian rectangular matrix field, the potentials of all points placed outside this diameter

were taken as $\varphi = 0$. As result, the distribution of the current density can be assessed along the perimeter of the anode cross-section parallel to the xOy plane.

The Laplace equation adapted to this case is:

$$\frac{\partial^2 \varphi}{\partial x^2} + \frac{\partial^2 \varphi}{\partial y^2} = 0 \qquad (3)$$

This can be solved using a finite difference or finite element method for a mesh covering the area of interest, so that for each node with coordinates (i, j) of the mesh, the potential $\varphi_{i,j}$ is calculated. This solution can be achieved using any electric field modelling software, e.g. COMSOL, ElCut and other.

7.2.4. Equivalent circuit of the electrolyser

A simplified equivalent circuit of the PEO process is presented in Fig. 7.2. There are the linear electrolyte resistance *R1* and the nonlinear oxide layer resistance *R2*. When the voltage *U* is applied to the system, the current I produces voltage drops *U1* and *U2* across these two resistances respectively.

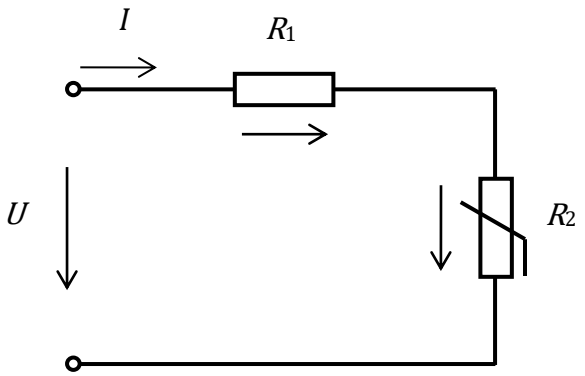

Fig. 7.2 DC equivalent circuit of the electrolyser:

Kirchhoff's voltage law: $U = U_1 + U_2$

Electrolyte voltage drop: $U_1 = R_1 \times I$

7.2.5. Current density distribution along the sample perimeter

A Laplace problem for the primary electric field distribution in the electrolyser with *U* = 1 V for boundary conditions (2) is solved. The result is a $m \times n$ matrix of potentials $\varphi_{i,j}$. This solution corresponds to a given voltage *U* without taking into account the voltage drop over the oxide layer. Since the electrolyte is assumed to be a linear conductive medium, this

voltage can be adjusted according to the experimental measurements of the potential in certain points within the electrolyte. The adjustment is made by multiplying the matrix of potentials by K_1. This scaled value is the voltage drop over the electrolyte $U_1 = K_1 \cdot (1\ V)$ which represents linear resistance R_1.

Then, the adjusted matrix of potentials is used for calculation of cell current I_{calc1} by the line contour integral along the anode perimeter. The resulting potential distribution is used for obtaining the electric field $\vec{E}$ using a gradient operator:

$$\vec{E} = -\nabla\varphi \tag{4}$$

and further the current density $\vec{\delta}$ via Ohm's law:

$$\vec{\delta} = \gamma\vec{E} \tag{5}$$

where γ is the specific conductivity of the electrolyte.

Both $\vec{E}$ and $\vec{\delta}$ are obtained as numerical derivatives and stored as paired matrixes $m \times n$ of their projections (e.g. $\delta_{(x)i,j}$ and $\delta_{(y)i,j}$) to x and y axes.

The integration of the current density over the anode surface S_a provides current through the electrolyte:

$$I_{calc1} = \oint_{S_a} \vec{\delta}\,\overrightarrow{ds} \tag{6}$$

which, for the chosen mesh and four sides of the anode, becomes

$$I_{calc1} = \left(\sum_{j=1}^{n} \left|\delta_{(x)m_1,j}\right| \Delta y + \sum_{j=1}^{n} \left|\delta_{(x)m_2,j}\right| \Delta y + \sum_{i=1}^{m} \left|\delta_{(y)i,n_1}\right| \Delta x + \sum_{i=1}^{m} \left|\delta_{(y)i,n_2}\right| \Delta x \right) \cdot z_3 \tag{7}$$

where z_3 is the longitudinal size of the system along axis z, $m_1 = \frac{m}{x_3} x_1$, $m_2 = \frac{m}{x_3} x_2$, $n_1 = \frac{n}{y_3} y_1$, $n_2 = \frac{n}{y_3} y_1$. This value is different from I_{exp} and represent the longitudinally invariant cell current with only conductive cylinder's wall around the sample. To meet the 3D requirements effective system depth must be changed in order to take into account conductive bottom as well as the upper and lower parts of the wall in the steel tank for a real experiment. The correction is made via multiplication of the matrix of potentials by coefficient $K_1 > 1$ so that the cell current I_{calc1} is equal to the experimental cell current I_{exp}, measured by an ammeter.

After the potential adjustment, a primary CDD over the anode surface can be calculated via equation (5) by using electric field at the last mesh step around the anode.

7.2.6. Nonlinearity. Oxide layer

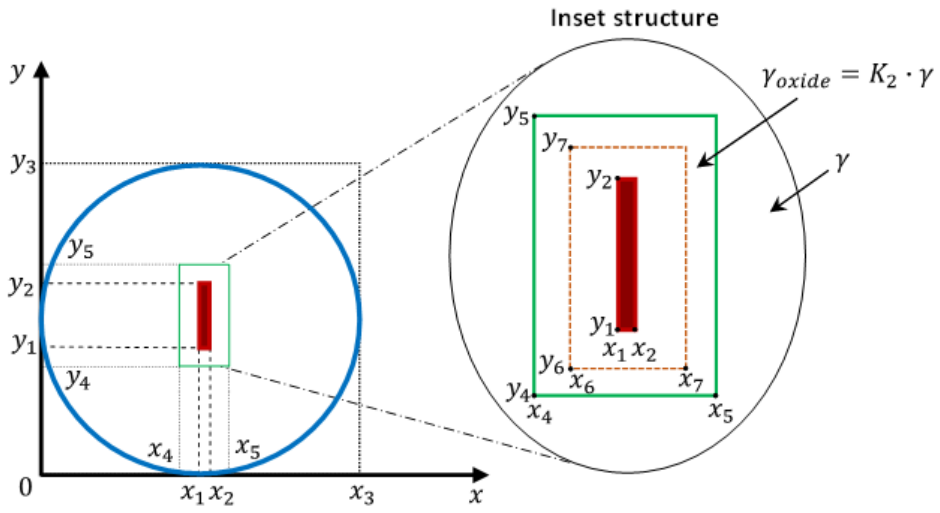

Fig.7.3. Electrode layout for the electric field analysis with anodic inset structure

In order to describe the nonlinear resistance R_2, an inset around the anode was introduced (Fig. 7.3). The inset encloses the anode which potential is set equal to the cell voltage (having cathode potential equal to zero) and a small surrounding rectangle S_{inset} (bounded by x_4, x_5, y_4, y_5) in order to account for the input of vapour-gaseous media, microdischarges and the oxide layer input into the electric field distribution. The boundary conditions are selected as U_a = 550 V and U_c = $U_{electrolyte}$, where $U_{electrolyte}$ is the electrolyte potentials at the boundary between the potential matrix and the inset. To comply with the boundary conditions imposed on the Laplace equation (3), the potentials within the inset must be recalculated.

Before calculation of the secondary CDD, the following two adjustment steps need to be made. Firstly, the integral cell current I_{calc2} along the undercut loop selected inside the anodic inset must be calculated by using equation (6). The perimeter S_{a1} is defined by the points $m_{ins1} = \frac{m}{x_3}\frac{x_5-x_2}{\Delta x_5}K_2$, $m_{ins2} = \frac{m}{x_3}\frac{x_1-x_4}{\Delta x_4}K_2$, $n_{ins1} = \frac{n}{y_3}\frac{y_5-y_2}{\Delta y_5}K_2$, $n_{ins2} = \frac{n}{y_3}\frac{y_1-y_4}{\Delta y_4}K_2$ where $0 < K_2 < 1$ is position of the loop. The coefficient K_2 represents a percentage of anodic inset enclosed by S_{a1} loop and used for current calculation. Secondly,

the resulting current is usually overestimated and must be brought in agreement with the experimental current $I_{calc2} = I_{exp}$ by adjusting the effective inset conductivity $\gamma_{oxide} = K_3 \cdot \gamma$, where $K_3 < 1$.

7.2.7. Nonlinearity. Connection to the current-voltage diagram

The next stage in description of the system nonlinearity is the introduction of an experimental current-voltage curve. Polarisation curves for the PEO process can vary depending on electrolyte, substrate material and electrical mode. For instance, a typical current-voltage diagram of PEO of aluminum in an alkaline electrolytes is presented in Fig. 7.4 (a). Three regions can be easily distinguished, the first showing showing surface, the second – intensive anodic dissolution followed by a region of negative differential resistance due to deposition of reaction products and the third – dielectric breakdown of the passive film resulted in current rise with voltage. A typical current-voltage diagram of Al in the alkaline electrolyte with addition of sodium silicate is presented in Fig. 7.4 (b). It has only two different regions where the first one shows a strong surface passivation and the second one shows dielectric breakdown at relatively high voltages, with sharp increase in current.

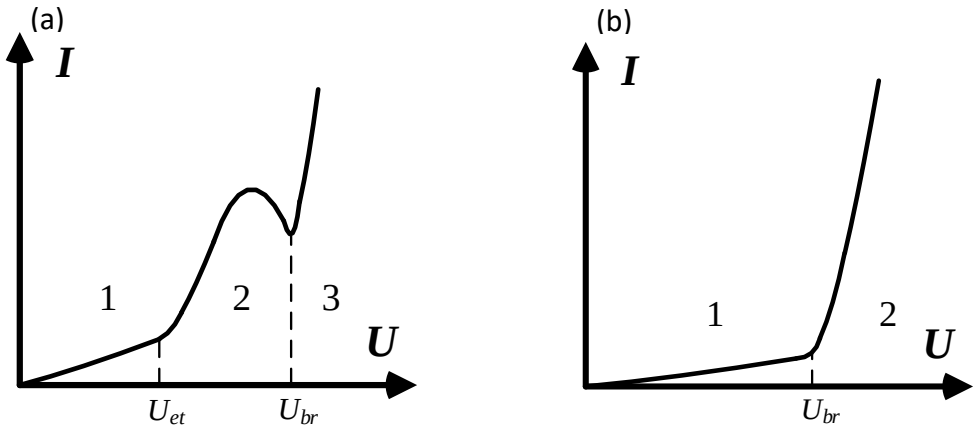

Fig. 7.4 Current voltage diagrams for PEO of Al simple in (a) alkaline and (b) alkaline-silicate electrolytes

The aforementioned nonlinearities and differences in current-voltage behaviour can significantly influence the final coating thickness distribution because the voltage drop at the electrode-electrolyte interface and corresponding secondary CCD over the sample surface would vary differently.

Oxide voltage drops calculation:

Further, a voltage drop in the oxide layer is calculated from the matrix of potentials obtained in section 7.2.5. Potentials along the sample are subtracted from the cell voltage and shifted down to its mean value to keep the average current equal to I_{exp}. Then the resulting voltage distribution is applied to the selected current-voltage diagram. Finally, this distribution is used for obtaining the secondary CDD via equation (5).

The secondary CDD can be used for qualitative estimation of the coating thickness distribution through the Faraday's law:

$$m = \frac{1}{F} \cdot \frac{M}{z} \cdot \delta \cdot s \cdot t \cdot \eta$$

where F=96484 C·mol^{-1} is Faraday constant; z is the number of electrons in the electrochemical reaction; M is the molar mass of oxide; δ is the anode current density; t is treatment time, η is current efficiency.

To adjust the secondary CDD in order to tune the model to meet the experimental data, three inset parameters can be used; cell voltage *Ua*, area of the inset *La* and position of the loop K_3 for the current integration according to p. 7.2.6.

7.2.8. Nonlinearity. Connection to the current-voltage diagram

The order of calculation is presented in the block diagram (Fig. 7.5).

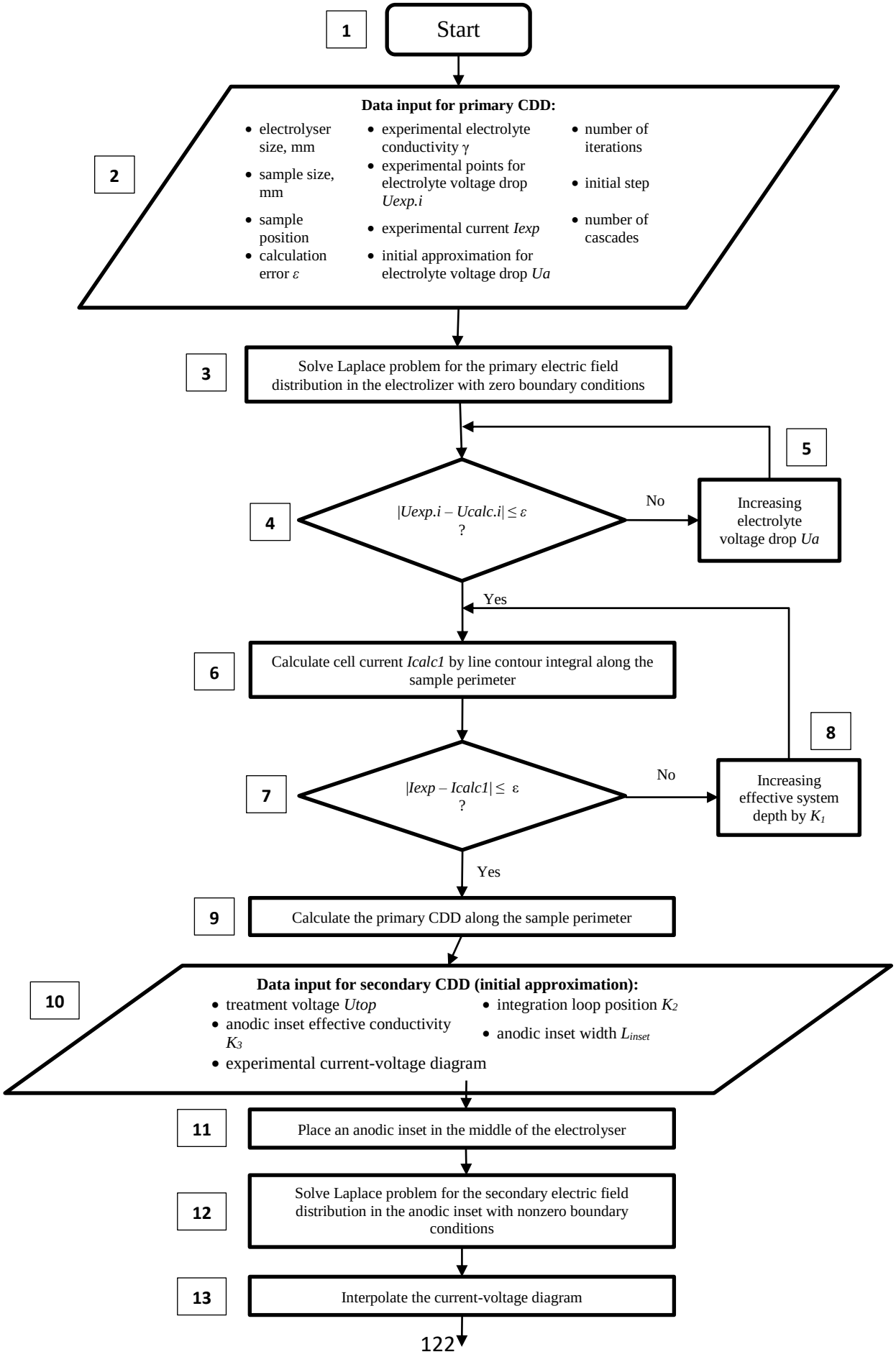
1
Start
2
Data input for primary CDD:
electrolyser size, mm
sample size, mm
sample position
calculation error ε
experimental electrolyte conductivity γ
experimental points for electrolyte voltage drop Uexp.i
experimental current Iexp
initial approximation for electrolyte voltage drop Ua
number of iterations
initial step
number of cascades
3
Solve Laplace problem for the primary electric field distribution in the electrolizer with zero boundary conditions
4
|Uexp.i – Ucalc.i| ≤ ε ?
No
5
Increasing electrolyte voltage drop Ua
Yes
6
Calculate cell current Icalc1 by line contour integral along the sample perimeter
7
|Iexp – Icalc1| ≤ ε ?
No
8
Increasing effective system depth by K1
Yes
9
Calculate the primary CDD along the sample perimeter
10
Data input for secondary CDD (initial approximation):
treatment voltage Utop
anodic inset effective conductivity K3
experimental current-voltage diagram
integration loop position K2
anodic inset width Linset
11
Place an anodic inset in the middle of the electrolyser
12
Solve Laplace problem for the secondary electric field distribution in the anodic inset with nonzero boundary conditions
13
Interpolate the current-voltage diagram

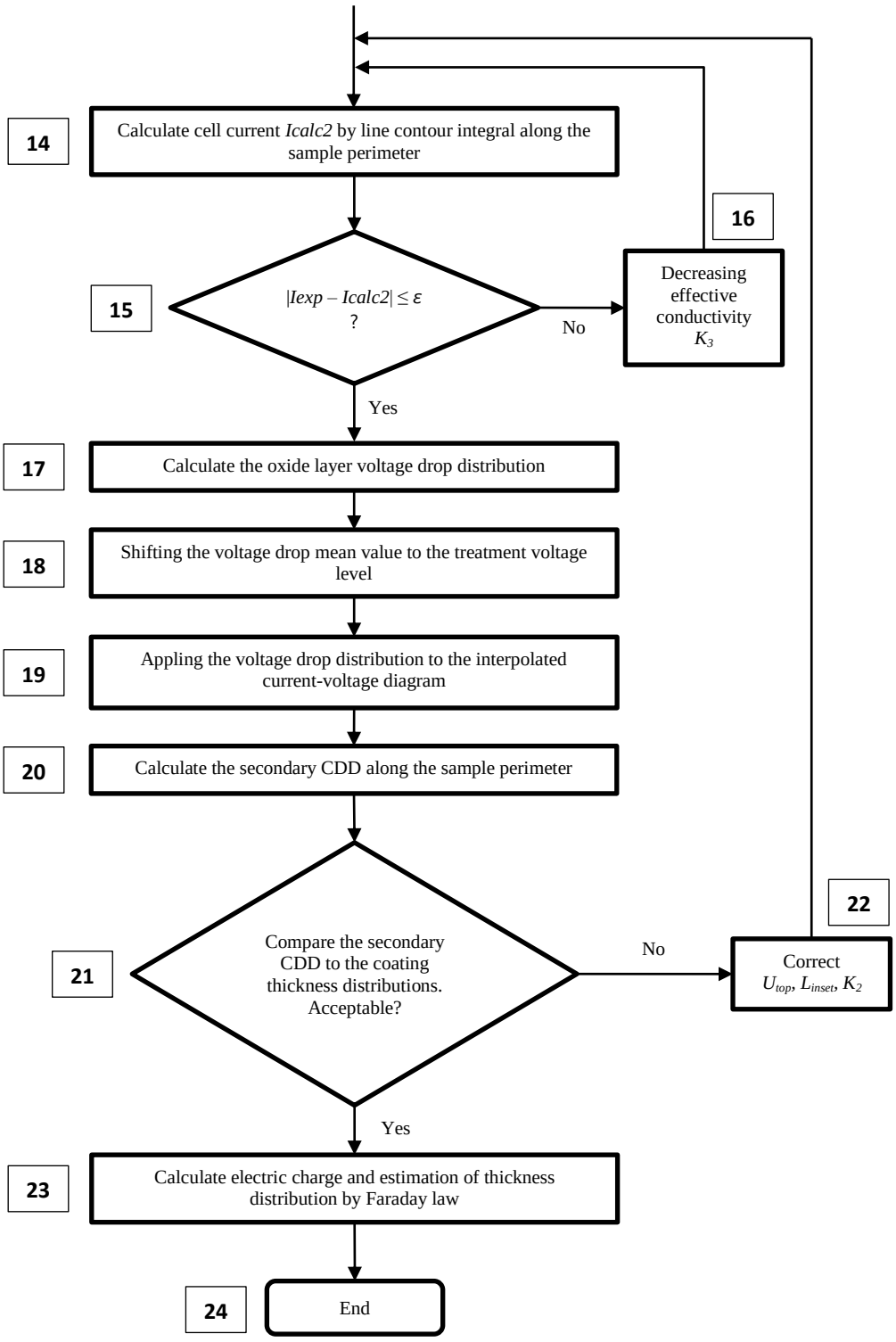

Fig. 7.5. Block diagram for the current density calculation

7.3. Experimental

7.3.1. PEO treatment

The PEO coatings were produced on Al foil as the base layer following the procedures described in **Chapter 6**. The PEO rig consisted of a 30 kW DC power supply and a cylindrical stainless steel tank (130 mm inside diameter, 130 mm liquid height), equipped with a water cooling system and a magnetic stirrer and served as the cathode. The working electrode was positioned in the middle of the steel tank. The distance from the centre of working electrode to the inner face of the tank was 65 mm, and the depth distance from the electrolyte surface was 65.0 mm (see Fig.7.6). The temperature of the electrolyte was kept within the range from 25 to 35 C°

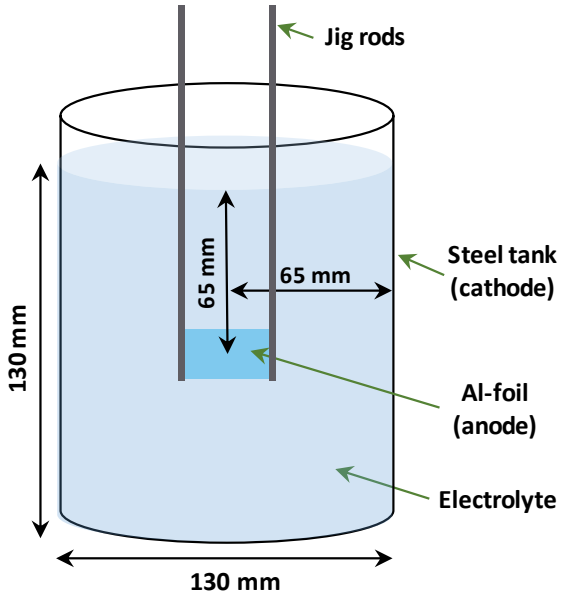

Fig. 7.6. The electrolytic cell used in the PEO process

7.3.2. Electric field measurements

To evaluate distribution of the voltage drop in the electrolyte, voltage probe measurements were carried in the same setup. Firstly, a voltage probe represented by an insulated metal wire with the open end was immersed in the electrolyte at the same depth as the middle of the sample. The top view of voltage probe positions and their values are shown in Fig.7.7 and Table 7.1 respectively. The dry end of the probe was connected to the positive terminal of Fluke 15B digital voltmeter. A negative terminal of the voltmeter was connected to the steel tank. Further, the aluminium foil sample was treated in DC mode at

550 V for 3 minutes. Once the steady state conditions were achieved, the voltage probe was consequently moved from position 1 to 6. After each shift the power supply was shortly switched on for 3 seconds and the voltage reading was recorded.

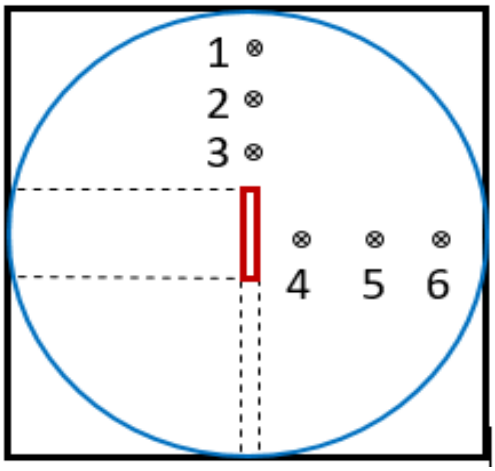

Fig. 7.7. Voltage probe positions in the electrolyser for voltage distribution measurements

Table 7.1. The values of voltage drop in the electrolyte

Number of voltage probe position	Distance from the tank wall, mm
1	12.5
2	25
3	37.5
4	48.8
5	32.5
6	16.3

7.3.3. Surface characterisation

To evaluate the thickness distribution of the PEO coating across the Al foil samples, cross-sectional images were taken along the length of the whole sample using an Inspect F50 SEM. The images were generated using a 15kV accelerating voltage, 10.8 mm working distance and 2000x and 5000x magnification. The size of the images was 1024×943 pixel. A MountainsMap 7.2 and an ImageJ software were used to analyse the SEM images.

The thickness distribution of the PEO coating on the Al foil was calculated based on the area comprised by the coating layer in the cross-section and the length of the image. These lines should scan the oxide film randomly in order to obtain a value representative of the full sample length. A diagram sketch of thickness measurements of the coating layer was presented in Fig. 6.6 **section 6-5**.

7.3.4. Calculation details

To meet the experimental conditions, the system parameters for calculations were introduced with electrolyser diameter 130 mm, anode size 30 x 0.05 x 18 mm. The solution of the Laplace equation was obtained by finite differences method using originally developed program in MATLAB environment. The program solves the Laplace equation for a uniform mesh with boundary conditions *Uc* = 0 V and *Ua* = 1 V (step 2 in Fig. 7.5). The mesh step was $\Delta x_5 = \Delta y_5 = 0.0625$ cm. The voltage drop in the electrolyte was found by increasing *Ua* until potentials in the six specific points of the electrolyser coincided with the experimental values within 5% tolerance. For the E1 electrolyte that value was Ua=40 V (steps 3-5 in Fig. 7.5).

The cell current I_{calc1} was calculated and brought into correspondence with the experimental current I_{exp} =3.45 A by increasing the effective system depth $z_3 = z_{anode} \cdot K_1 = 18\,mm \cdot 3.753 = 67.55$ mm (steps 6-9 in Fig. 7.5).

Due to the complexity of the mathematical model, a computational experiment was conducted in order to determine optimal values of the most significant parameters so that an accordance with the measurements was achieved. The computational experiment was performed by varying 3 parameters (Table 7.2) - inset area width $L_{inset,}$ cell voltage *Ua,* current integration loop position coefficient K_2 (steps 14-22 in Fig. 7.5). The first parameter stands for a shift from the anode side towards the medium of the surrounding rectangular inset S_{inset} in section 6.2.6, and it was varied within 3 to 9% range of the electrolyser diameter. The value of *Ua* was selected within the range of voltages from 510 to 550 V commonly used for PEO treatment of aluminium and the value of K_2 was varied from 0.05 to 0.955. At each iteration of the experiment, the cell current I_{calc2} was brought into correspondence with the experimental current Iexp=3.45 A by adjusting the effective conductivity of oxide and surrounding medium $\gamma_{oxide} = \gamma \cdot K_3$ (steps 14-16 in Fig. 7.5).

To obtain the secondary CDD steps 17-23 of the algorithm were performed (Fig. 7.5).

Table 7.2. Design of the computational experiment

Factor	***Ua (V)***	***L_{inset}, %***	***K_2***
Higher level	550	9	0.95
Lower level	510	3	0.05
Step size	20	3	0.05

7.4. Coating thickness distribution

Typical cross-sectional SEM images of the PEO coatings for samples treated in E1 and E4 electrolytes are shown in **section 6-5 (**Fig. 6.7 (a)-(b)), whereas Fig. 7.8 shows corresponding coating thickness distributions over the sample length. It can be seen that for electrolyte E4, the coating thickness has one minimum in the middle of the sample.

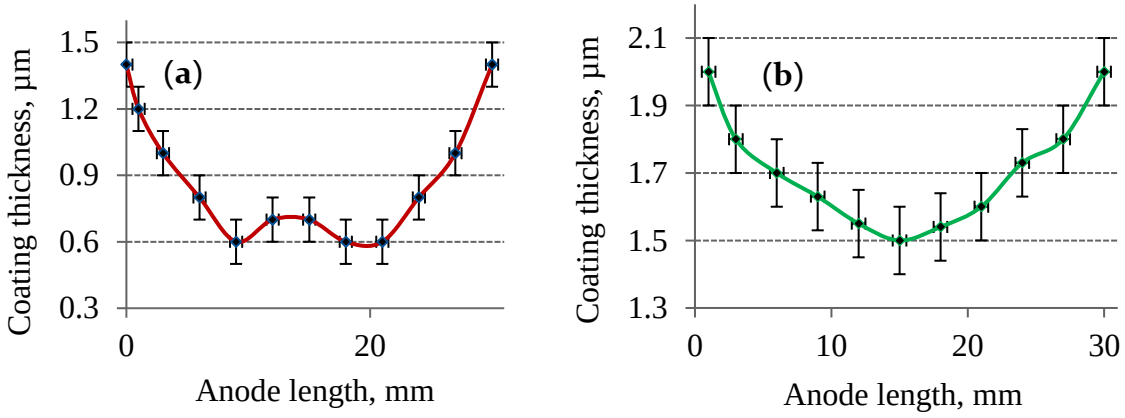

Fig. 7.8 Oxide layer thickness produced in electrolytes E1 (a) and E4 (b).

Such thickness distribution is typical for most coatings electrodeposited on flat electrodes in electrolysers without auxiliary counter-electrodes, which is due to similar primary current density distributions. In contrast, for the coating formed in electrolyte E1, a peak in the middle of the sample can be observed. Although this appears to be a rather unusual feature, the significance of this peak has been verified by repeated experiments. If the thickness of the coating formed in electrolyte E1 varied from 1.2±0.1 µm at the edges to 0.6 ±0.1 µm in the middle region of the sample, for the sample treated in electrolyte E4, it ranged from 2.0 ±0.1 µm at the edges to 1.7 ±0.1 µm in the middle of the sample.

7.5. Current density evolution during PEO process

Experimental current-voltage diagrams (CVD) for PEO treatments of Al in in electrolytes E1 and E4 electrolytes are presented in Fig.7.9.

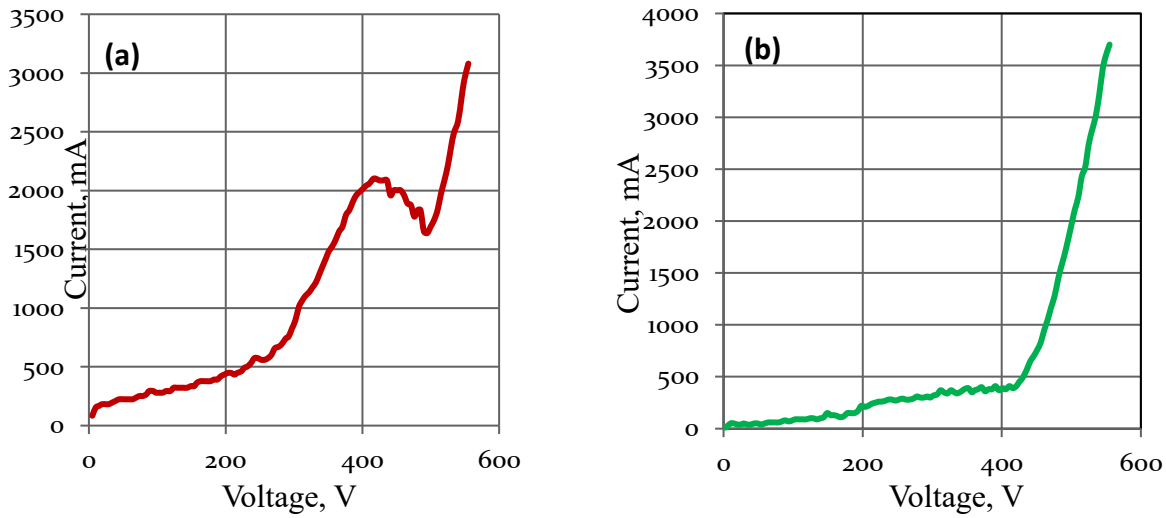

Fig. 7.9 Current voltage diagrams: a- for alkaline electrolyte, b - for alkaline silicate electrolyte.

The main feature of the diagram (a) is the region of a negative differential resistance between 410 and 500 V and electric breakdown at approximately 500 V. In the diagram (b), there is a wide passivity region lasting up to 400 V followed by a breakdown at approximately 410 V and sharp current increase afterwards.

7.6. Current density distribution

The results of computational experiments on evaluation of electric field and corresponding CDD for E1 and E4 electrolytes are presented in Fig.7.10 - 7.15. The 2D field distribution in electrolyte E1 (see section. 7.2.8, steps 3-5 in Fig.7.5) is presented in Fig.7.10. It shows a max imum value of 40 V; red dots indicate voltage probe positions in the electrolyser (see section. 7.3.2). The rectangle in the centre indicates the loop used for the anodic inset (see section. 7.2.8). In Fig. 7.11, the resulting potential distribution bounde by the loop is presented for experimental conditions Ua = 550 V, L_{inset} = 6 %. These two plots show rapid potential decrease from anode to cathode; the most part of the voltage (510 V) drops across a relatively thin oxide layer and surrounding vapour-gaseous medium with microdischarges.

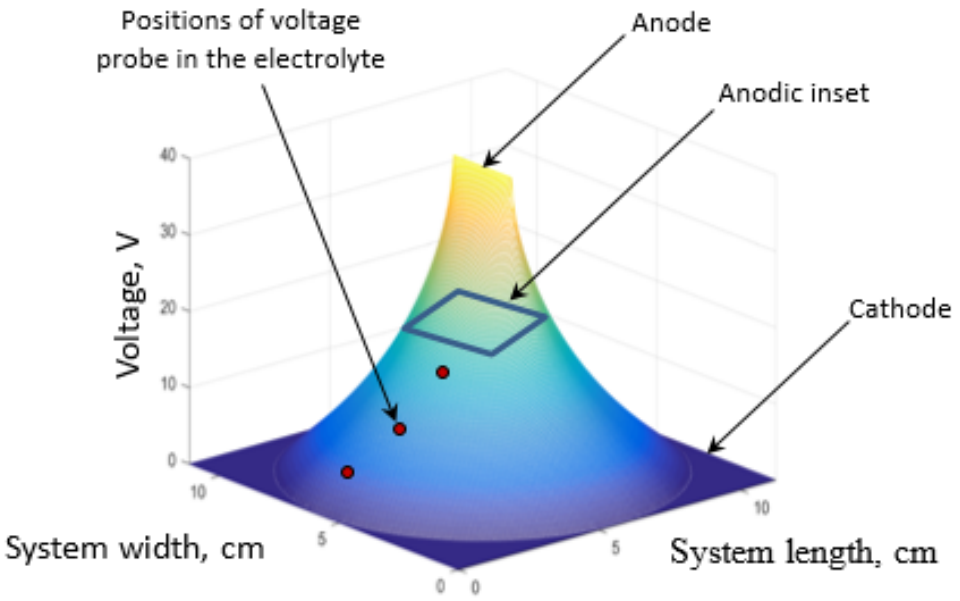

Fig. 7.10. Potential distribution in electrolyte E1

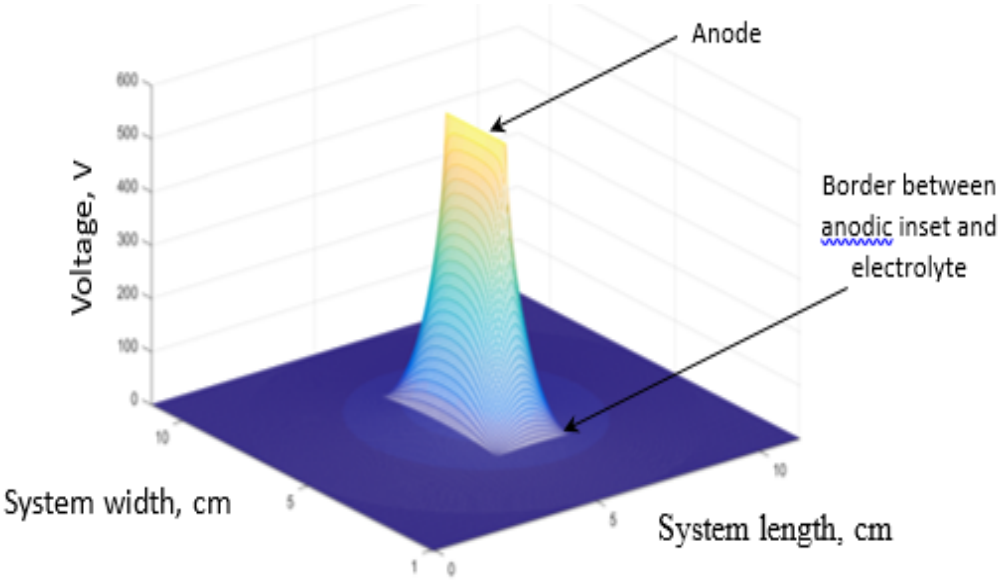

Fig. 7.11. Potential distribution within the anodic inset in electrolyte E1. (*Ua* = 550 V, L_{inset}= 6%)

Following the experimental design (Table 7.2), optimal conditions providing the closest similarity of the secondary CDD and the experimental coating thickness distribution (Fig.7.8 were selected as follows. The integration loop position was determined to be K_2 = 0.5 corresponding to the middle of the anodic inset for all cases. Then, an optimal anodic inset surface area L_{inset} was selected at maximum cell voltage 550 V. Corresponding plots for

electrolyte E1 are shown in Fig.7.12. Fig.7.12a shows the voltage drop within the inset; Fig.7.12b shows the primary CDD in the electrolyte; Fig.7.12c shows the mean voltage drop within the inset on the current-voltage diagram (points (1), (2) and (3), Fig.7.12d shows secondary CDD within the inset. The secondary CDD curve (2) in Fig.7.12d with L_{inset} = 6% was selected for further calculations as providing the closest shape approximation to the coating thickness distribution is presented in Fig.7.8a.

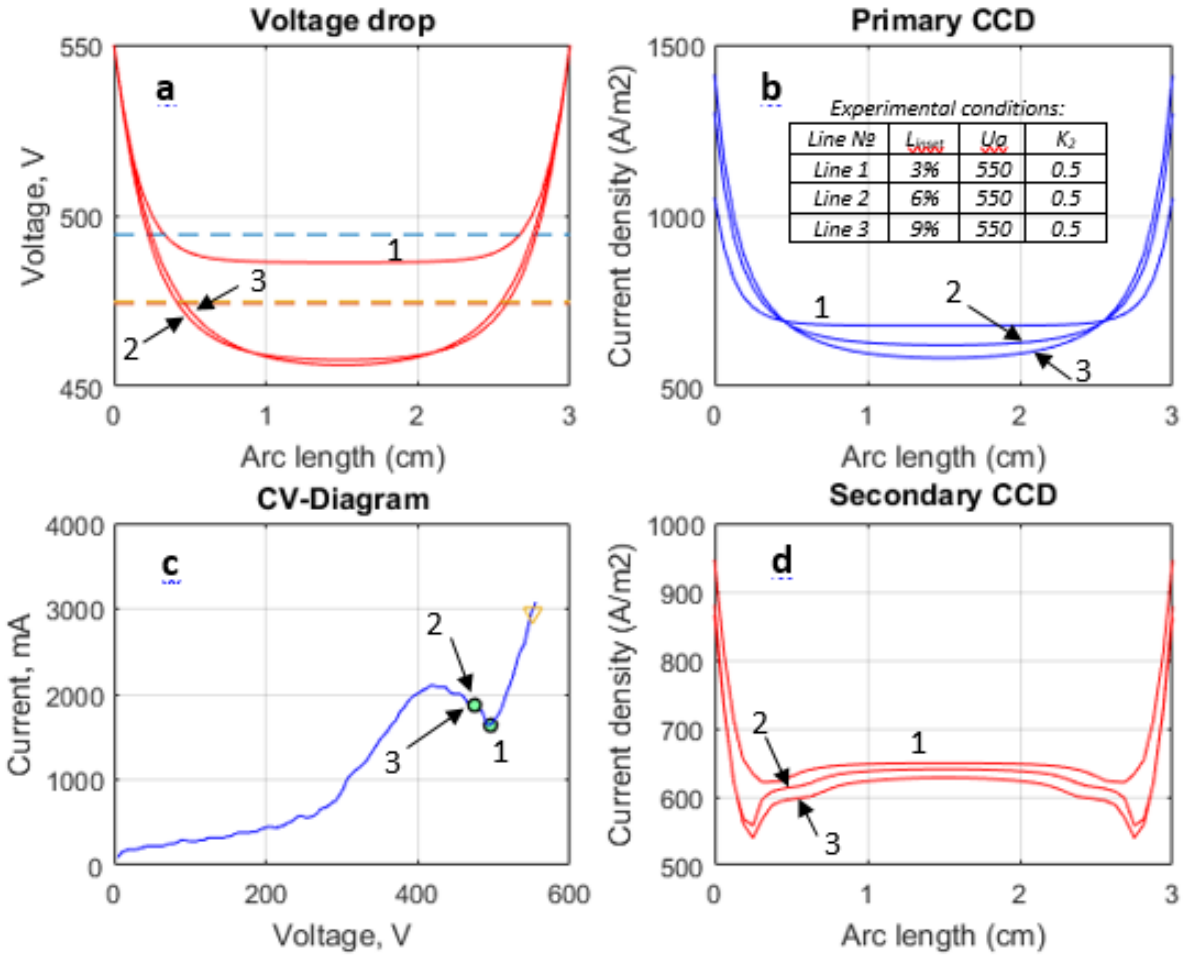

Fig. 7.12. Modelling plots for electrolyte E1 with different anodic inset area width

Next, the inset area width L_{inset} = 6%, K_2 = 0.5 were fixed and cell voltage *Ua* was varied. In this case, the secondary CDD curve (1) with *Ua* = 510 V was selected as optimal because it has the highest current density on the edges and moderately increases in the middle of the sample.

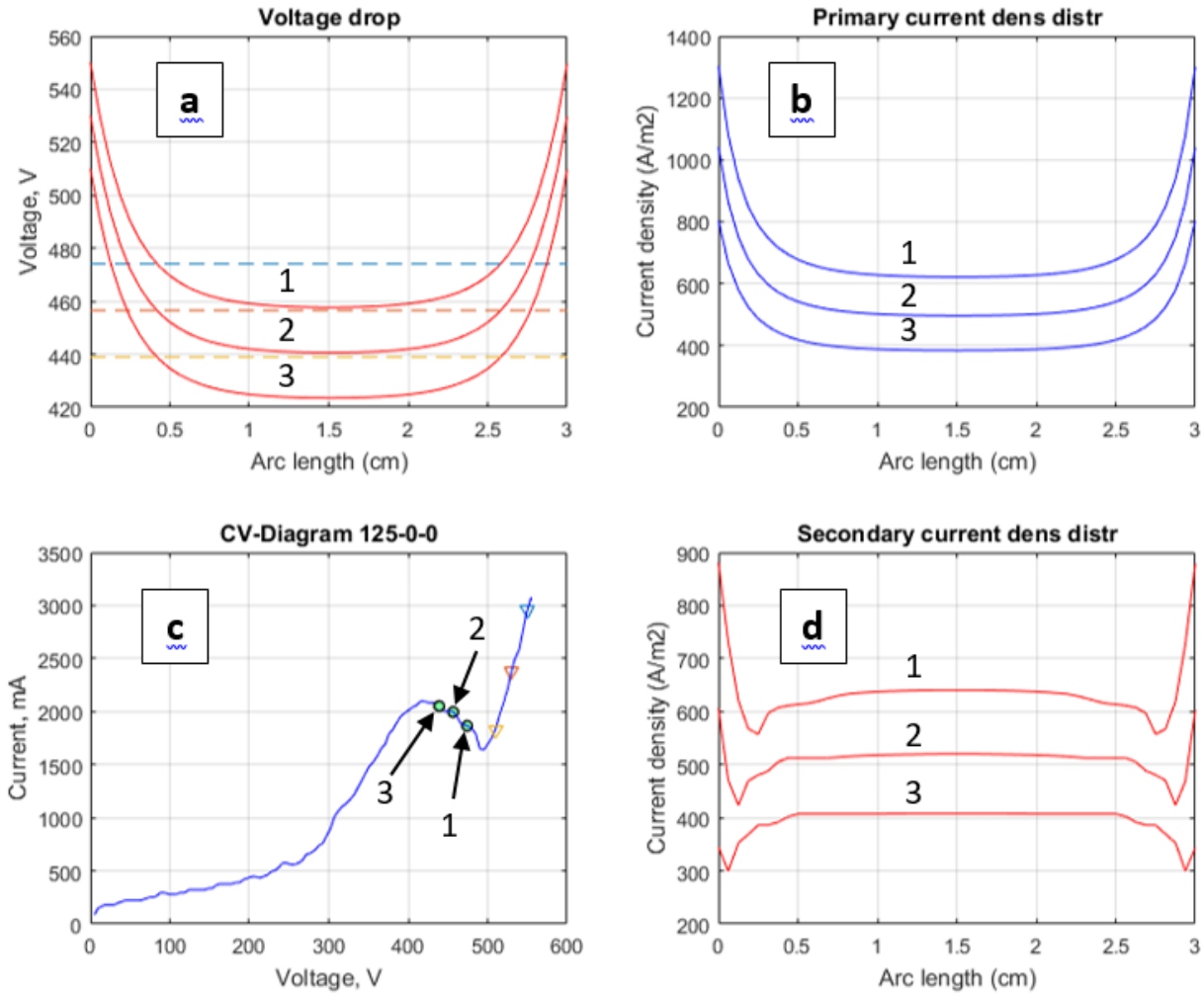

Fig. 7.13. Modelling plots for E1 electrolyte with different treatment voltages

Fig. 7.13 shows the secondary CDD around the anode in electrolyte E1 with the optimal parameters *Ua* = 510 V, *La* = 6% and K_2 = 0.5. This distribution has the closest correlation with the coating thickness distribution, and it can be used for estimation of the coating thickness distribution over the surface of complex shape substrates treated in electrolyte E1.

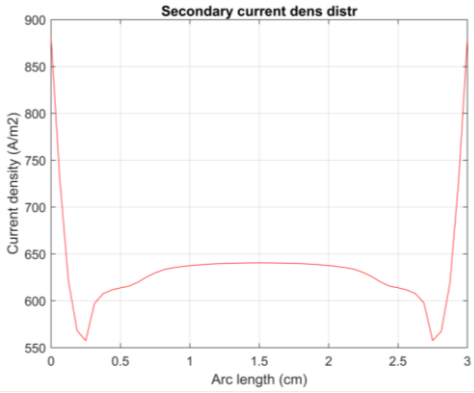

Fig. 7.14. Secondary CDD for E1 electrolyte calculated for optimal computational parameters: Ua = 550 V, La = 6%, K2 = 0.5

Compared to E1, in electrolyte E4 with relatively smooth current-voltage diagram, the calculation process is much simpler. Plots in Fig. 7.15 show the CDDs for various voltages *Ua* in electrolyte E4. For E4 electrolyte show the CDDs for various voltage *Ua*. Curve (*2*) was chosen as the optimal due to moderate differences between the current density on the edges and in the middle of the sample.

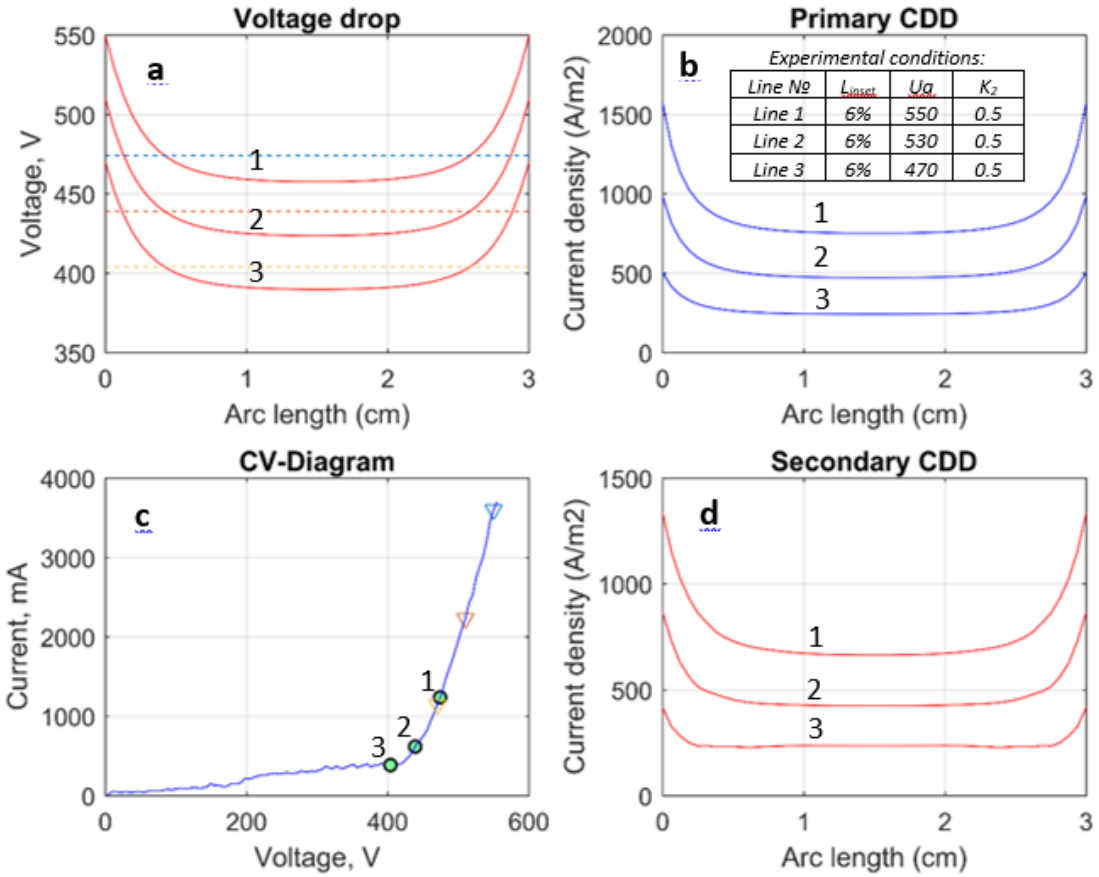

Fig. 7.15. Modelling plots for electrolyte E4 with different cell voltage

Comparison of modelling results for electrolytes for E1 and E4 provides a clear evidence of significant nonuniformity introduced in the secondary CDD by the shape of the current-voltage diagram

7.7. Summary

A calculation methodology of nonlinear current-voltage diagrams was developed. It provides secondary current distribution that qualitatively differs from primary current distribution. The results was confirmed by experimental data and can be suggested as description of a new physical phenomenon.

Chapter 8
Studies of PEO processes for fabrication of 3D thin-walled ceramic structures

8.1. Introduction

As shown in **Chapter 4**, PEO coatings were formed under bipolar current mode in 1 g/l KOH, 2 g/l $Na_4P_2O_7$, 2 g/l Na_2SiO_3 electrolyte with various treatment times. It was concluded that the coatings produced for 6 min presented the best degree of flexibility compared with the coatings produced at other treatment times. Also, as discussed in **Chapter 6**, the electric field and current density may influence the thickness distribution of the PEO coatings. The thickness uniformity is one of the important factors influencing the performance of PEO coatings on complex shape substrates. It affects the overall performance of the engineered coating which's not only helps make that good first impression but the overall evaluation of the product throughout its life cycle. However, difficulties are generally encountered in producing uniform coatings on substrates having irregular shapes. Edges, corners and holes are particularly troublesome [184].

Electrochemical cells are known to be characterised by the relation of the current the cell passes to the voltage across it, and the current density may not be uniformly distributed on the working electrode surface during PEO process which leads to poor performance due to uneven coating thickness and low degree of coatings uniformity [185]. In addition, complex physical and chemical process occur during the PEO process. Therefore, monitoring the evolution of spectral signal could be helpful in understanding the mechanism underlying PEO process of irregular shapes and provide a correlation between the oxide formation and growth rate and thickness with diffusion of oxygen and its effect on the coating formation [186].

To produce PEO coatings with uniform thickness on complex shapes it is necessary to analyse the effect of edges and corners existing in such substrates. In this chapter two irregular shapes, L and U, were produced using a pulsed bipolar current PEO mode with the process time of 6 min in different electrolytes. The characterisation of the PEO coatings, including coating morphology was performed by the methods discussed in **Chapter 3.** The coating thickness variations on the inner/outer surfaces and at edges were determined and

compared. The plasma discharge behaviour during the PEO treatment of complex shapes was investigated. The plasma electron temperature was evaluated by analysing characteristic lines of Al in the optical emission spectra. Before all these analyses, to achieve better understanding of the current distribution in the electrolyser during the PEO process of irregular shapes, numerical modelling was used.

8.2. Problem statement

Most research studies focused on the plasma electrolytic oxidation (PEO) processes for workpieces of regular shapes such as rectangular and circular samples, and little paid attention is paid to more complex samples such as E, U, L and star shapes.

It is common that the PEO coatings may have varied thickness and morphologies at the surfaces of the electrodes [8, 167]. This indicates the current density during the process changes from place to place along the electrode surface. Also, the potential difference at the electrode- electrolyte interface can be site dependent. The thickness and morphology of the coatings would be non-uniform at various points across the sample if the current density is not uniformly distributed when the working electrode is irregular [187]. The reaction rate is directly proportional to the current density and its surface distribution significantly affects the electrochemical process [58, 188]. The current density during the electrochemical process depends on several factors such as electrolyte conductivity, electrode surface area, and geometry as well as cell layout.

Many studies addressed the current density distribution using empirical and analytical methods, however there is a growing use of numerical and computational methods. COMSOL package is the one of the most popular software used to model and represent the current distribution in the cells. The basics of numerical modelling using COMSOL software are provided in (**Chapter 3**).

Morphology and thickness of PEO coatings are important in all applications of protective finish to ensure optimum performance is obtained [189]. Recently, studies have analysed the formation mechanisms [70, 83, 190-192], and tribological properties [63, 86, 133, 193, 194] of PEO coatings formed on different Al alloy substrates of regular shape. However, very rare studies paid attention to the growth process, characteristics and properties PEO coatings on irregular shape substrates. Essential work is therefore required to achieve better

understanding regarding the characteristics of discharge phenomena and their effect on the mechanisms of the coating formation at the edges and on the inner surfaces of complex shape substrates. Therefore, the specific objectives of this part of the project have been defined as follows:

- Fabrications of 3D thin-walled ceramic structures (L and U shapes) by achieving a uniform thickness of ceramic coatings on edges and inner surfaces of samples.
- To attain a better understanding of the PEO coating formation on Al foil samples of irregular shape by comparing characteristics of PEO coatings produced on inner and outer surfaces of irregular shape samples.
- Investigate effects of the shape of working electrode on characteristics of plasma discharge during the PEO process and resulting coatings.
- Study effects of primary current density distribution in the cell on the characteristics of the PEO process and coating growth behaviour.

8.3. Experiments set-up

8.3.1. Materials and PEO process

A 50-µm thick irregular-shape aluminium foil samples (L and U shapes) of dimensions (25 × 10 × 0.05 mm) as can be seen in Fig. 8.1, and surface roughness of *R*a ~ 0.1- 0.15 µm were used as substrates for conversion to alumina using PEO process.

Table. 8.1. Different solutions of electrolytes used for PEO coating process of irregular Al foil samples.

Electrolyte code	Concentration (g/l)		
	KOH	$Na_4P_2O_7$	Na_2SiO_3
E1	0.75	0	0
E2	0.75	0	2
E3	0.75	2	0
E4	0.75	2	2
E5	1	1	1
E6	1.25	0	0
E7	1.25	0	2
E8	1.25	2	0
E9	1.25	2	2

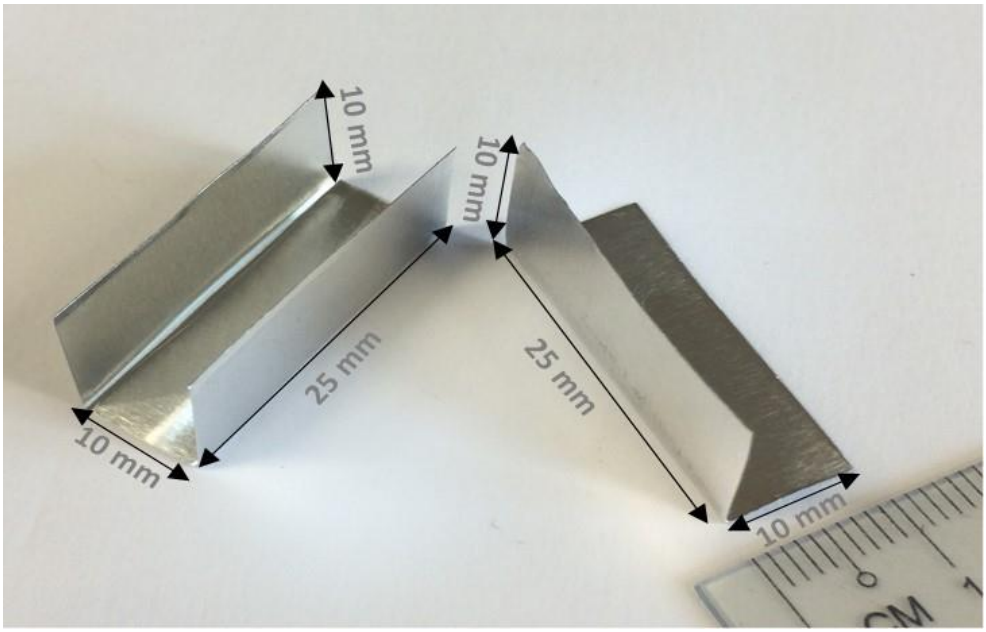

Fig. 8.1. Irregular shape Al foil (50 µm thickness) samples; (right) L-shape and (left) U-shape before treatment using PEO process

The samples were cut to the required shapes, formed as appropriate, with all angles being around 90^{o}, and fixed on the holders by plastic fittings as described in section 3.1. The electrolytes prepared from different concentrations of potassium hydroxide (KOH), sodium pyrophosphate ($Na_4P_2O_7$), and sodium silicate (Na_2SiO_3), denoted E1 to E9 in Table 8.1.

The PEO processes were carried out in a 2.0 L cylindrical stainless steel cell, also served as the counter-electrode, equipped with a cooling coil. Figure 4.1 in **Chapter 4**, shows a schematic of PEO processing equipment, with details of electrical setup and the current mode used presented in Chapter 3. During the treatment, the electrolyte temperature was maintained below 35 ±5.0 ˚C, by cooling the electrolyte in the electrolytic cell. However, due to the relatively large area and irregular shape of the samples, the temperature was expected to rise during the PEO process. The samples were treated for 6 min. To maintain similar distribution of electric field on the surface of the working electrode during the PEO process, the samples were suspended and positioned centrally in the middle of the steel tank using an isolated metal holder and plastic holders. SEM images were taken with an InspectF50 SEM. The images were generated using 15kV accelerating voltage, 10.8 mm working distance and 1000× and 2000x magnification.

8.4. Optical emission spectroscopy

The OES study was carried out using a FloTron XHR spectrometer to collect the spectra over the period of 6 min in the wavelength range from 300 to 900 nm. To ensure that the maximum light is collected by the optical fiber, the lens was located at around 5 mm in front of the sample for both inner and outer surfaces. Collected OES spectra were monitored and analysed as a function of time. Fig. 8.2 shows a schematic diagram of the sample geometries used in the experiments and position during PEO process for the measurements of optical emission spectra.

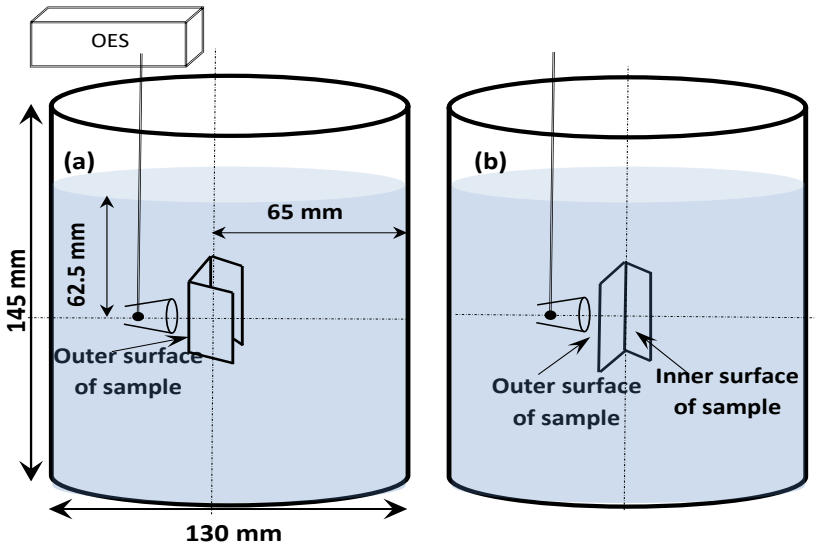

Fig. 8.2 Schematic diagram shows the position of samples (U and L) shapes inside the cell.

8.5. Sample analysis

In this study, we investigated the effects of current density distribution on the growth behaviour and properties of PEO coatings formed on complex geometry samples. The characteristics of PEO coatings such as thickness and phase composition were studied in different regions on the samples – in central parts of inner and outer surfaces and near the edges. The surface SEM images were analysed using ImageJ and MountainsMap 7.2 software to determine the characteristics of PEO coating. In addition, characteristics of microdischarges that appear at the surfaces of irregular shape substrates during PEO process were studied using OES to determine plasma composition and electron temperature. A more detailed description of the experimental equipment used and how the samples were positioned in the electrolyser is provided in **Chapter 3**.

8.6. Modelling of electric field and current density distribution in the electrolyser

Numerical simulation provides a capability for evaluation of the current distribution in a particular configuration of electrolyser and coating conditions. However, for predictive design and scale-up analytical models that represent the dependence of the current distribution on the process parameters are more advantageous.

PEO coatings can have different thickness and morphologies at the surface of the aluminium foil, which means that the current density during the process varies from place to place on the sample surface [187, 195] due to the sample shape, size and position in respect to the counter-electrodes. Substrate geometry of is one of the key factors that affect the current density values in the electrochemical cells [196, 197]. Although a brief review provided in this study does not allow a comprehensive explanation of electrochemical theory, a discussion of the electric field distribution in the electrolyser during the PEO treatments of complex shape samples may offer sufficient understanding of how it affects the current density distribution in the electrolyser, which, in turn, influences the formation of PEO coatings on such substrates.

To achieve better insights into the current density distribution at the edges and on the inner surfaces of the working electrode during the PEO treatment and corresponding effects on the coating formation, a numerical model was developed based on a COMSOL-Multiphysics software [121].

8.6.1. COMSOL model generation

When building up a model in the COMSOL environment, several aspects need to be considered [121, 198]. The following guidelines have been followed when building up the model of current density and potential distribution in the electrolyser during the PEO process. The most important is model simplification due to system symmetry should be used as much as possible to reduce the simulation run time. Fig. 8.3 shows the 2D geometry of the L and U shapes samples model. In this illustration, we used L-shape substrate as an example, with similar considerations being also applied to the U-shape.

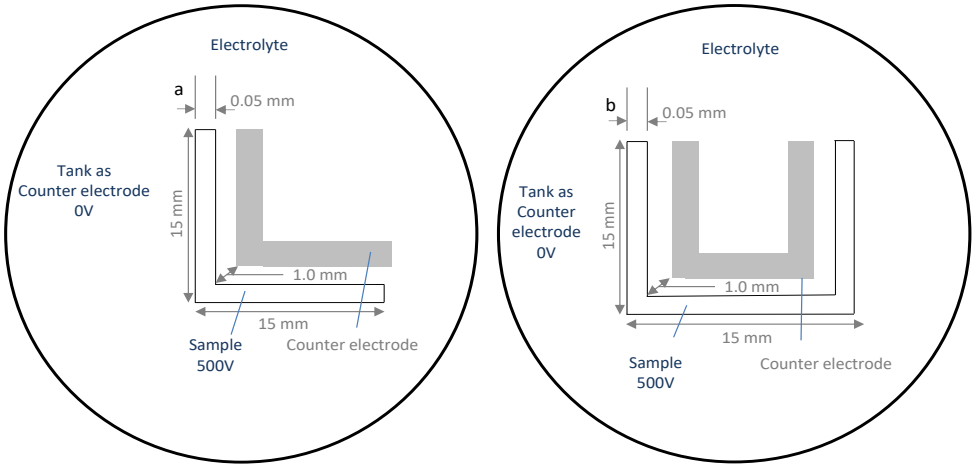

Fig. 8.3 2D geometry of working electrodes (L and U) shapes.

Definition of geometry. In 2D or 3D, the geometry of the structures can be defined in the CAD window. Due to the symmetry along the samples, the 3D geometry can be reduced to a 2D cross section. The main objects, such as the L- shape Al foil, the stainless steel tank and the electrolyte, were drawn using a SolidWorks software and imported in 2D CAD as show in Fig. 8.3.

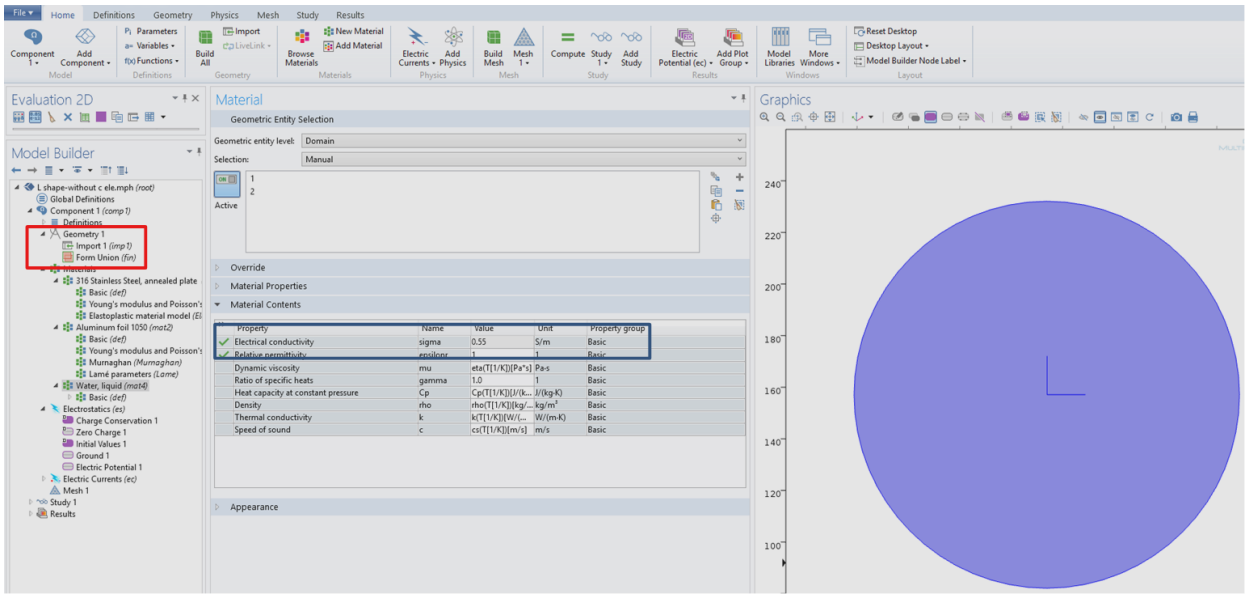

Fig. 8.4 Screen shot showing how the geometry of a simulation is defined and how the material parameters can be adjusted.

The red box in Fig. 8.4 outlines the definition of cell geometry in the model builder. The circle and the L-shape represent the stainless steel tank cathode and the Al foil sample anode respectively, separated by the electrolyte highlighted by the light blue colour.

Assignment of materials properties. In this step, we used predefined materials which properties were stored in the COMSOL library and then adjusted as necessary. The electrolyte domain of was assigned to water from the material library with electrical conductivity changed to 0.55 S/m to reflect the actual property. The highlighted blue box in Fig. 8.4 shows that the conductivity was changed for this model. AISI 304 stainless steel and A1050 Al alloy were chosen for the boundaries representing the tank (cathode) and the sample (anode) respectively.

Definition of components and selection of appropriate conditions. Prior to solving the model, it is necessary to define domains (volumes in 3D, surfaces in 2D) and the boundaries (surfaces in 2D, edges in 2D) on the geometry used. The boundary conditions used are electric insulation, ground, and electric potential. The two-dimensional numerical model used in this study is incorporated from the AC/DC module with the following built-in equations:

$$-\nabla . J = Q_j \qquad (7.1)$$

$$J = \sigma E + J_e \qquad (7.2)$$

$$E = -\nabla V \qquad (7.3)$$

Where J is current density, Q_j, is current source, σ is electric conductivity of electrolyte, E is electric field, J_e is external current density, and V is voltage. In this work, the tank surface was set to the electric ground and the electric potential of Vo = 500 V was imposed on the sample.

Mesh. The finite element mesh is shown in Fig. 8.5. At the domain area (electrolyte) the mesh consists of 18224 elements and the mesh area 17660.0 mm^2. It was generated by using the automatic mesh creator with option [fine].

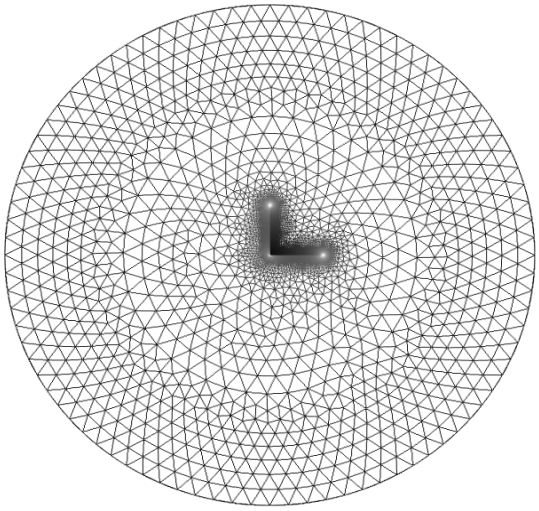

Fig. 8.5 Finite element mesh for the boundaries on the sample (anode)/electrolyte boundary

In the primary current distribution, it was assumed that no overpotential accompanies the activation of the reaction. The cell can be presented as a simple circuit model for the PEO process. A constant resistance represents the electrolyte which is a conductive medium with constant conductivity and the current distribution is controlled by the resistivity of the electrolyte between the working electrode and the cathode (Fig.8.3).

To take into account the fact that the non-uniform electric field distribution around the working electrode causes the local current density at the edges to increase, which may according to the current–voltage diagram, lead to the redistribution of the coating growth rate along the sample surface, we suggested to apply a floating potential electrode for a boundary condition with the same shape as the working electrode but positioned 1 mm beside it (Fig. 8.3). The floating potential electrode (Qo=0) was chosen from the (COMSOL library) for applying a boundary condition, and it has same material type of the cathode.

8.7. Electric field and current density distribution

Fig. 8.6 (a) and 8.7 (a) display the distributions of electric field and current density on the surface of L and U shape working electrodes respectively. The contour lines represent the distribution of electric field and the arrows – the distribution and direction of current density that clearly show differences between the outer and inner sides on the working electrodes. Irrespective of the working electrode shape, the electric field strength is the highest near the edges and between the working electrodes and the floating potential electrode for all conditions.

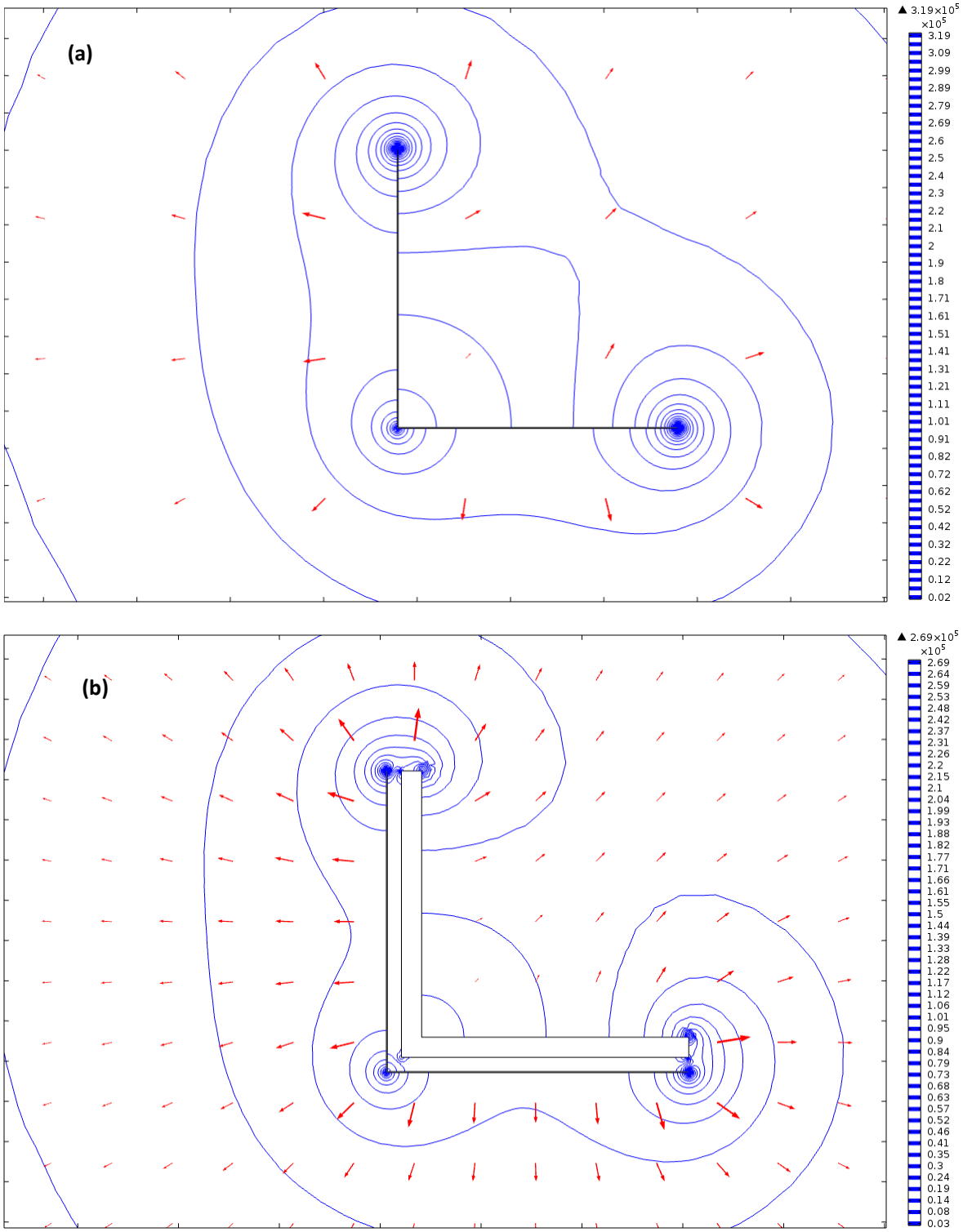

Fig. 8.6 COMSOL modelling results of current density (A/m2; arrows) and electric field (V/m; contour lines) distributions in the electrolyser for the PEO treatments of L-shape electrode (a) without floating potential electrode (b) with floating potential

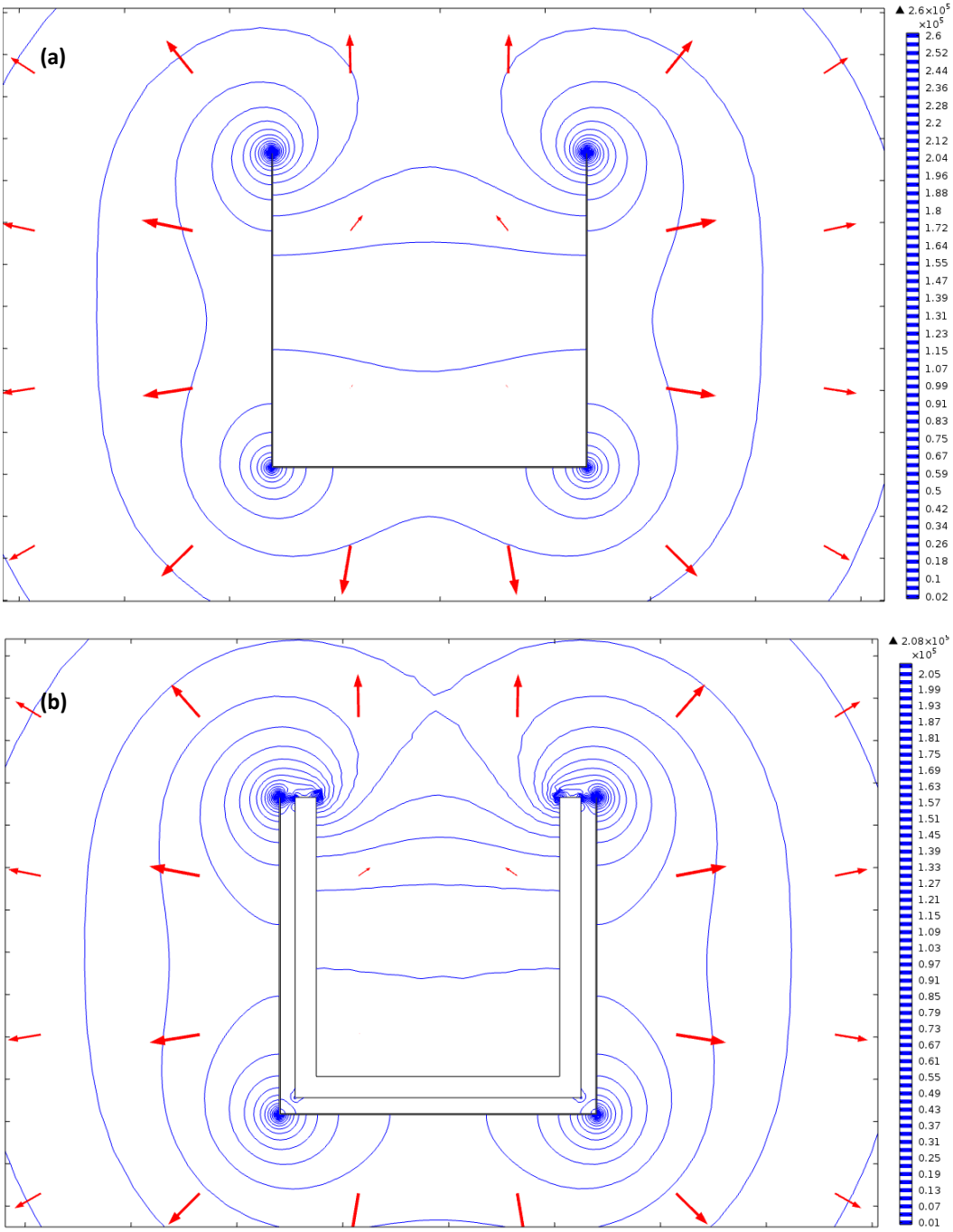

Fig. 8.7 COMSOL modelling results of current density (A/m^2; arrows) and electric field (V/m; contour lines) distributions in the electrolyser for the PEO treatments of U- shape electrode (a) without floating potential electrode (b) with floating potential electrode.

The electric field strength at the surfaces of L and U shape electrodes in the cell arrangements with floating potential electrodes is higher than in those without them. In both cases, the values of current density at edges are nearly 6 times higher than at the middle (Fig.(8.5)(8.6)). This difference is due to the effect of electrode edges and corners (outside angles) on electric field distribution. The arrows indicate that the current density at edges and

outside angles of the samples in the cells with floating potential electrodes is higher than in those without them. The difference in the distribution of electric field between the inner and outer surfaces around L and U shapes can be visualised from the modelling results, which is another way that may provide a knowledge to investigate the coating thickness.

Fig. 8.8. Shows the appearance of the coated samples (L and U) shapes after PEO treatment.

Uneven electric field and current density in the electrolyser induced by the shape of electrodes causes different in thickness along the samples. This was explained why the thickness of PEO coatings at edges was higher than that near the edges or at middle of samples as well as why poor coatings were formed at the corners. Examples of PEO treatment of samples with poor coating at the corners and in the edges are presented in Fig. 8.8. Therefore, solving the problem of current density distribution at the edges would help increasing coating uniformity.

On the other hand, the electrolyte compositions studied in **Chapter 5** have considerable influence on the characteristics of produced coatings. For instance, the introduction of sodium silicate in the electrolyte leads to the increase in the thickness of the coatings, with the increase in the thickness of the outer layer being higher than that of the dense inner layer. This was clearly observed in the PEO coatings produced in electrolytes (1-1-1) and (1.25-2-2) (see Fig 8.8 and 8.13). In addition, increase of potassium hydroxide (KOH) into the electrolyte leads to increases in the electrolyte conductivity which leads to the raise of the current density during the PEO process and resulting coating thickness.

In order to visualise the simulated distribution of current density (A/m^2) across the sample surface, a cross-section was considered between two points of sample adjacent its outer and inner surfaces (Fig. 8.9 (a)(b)).

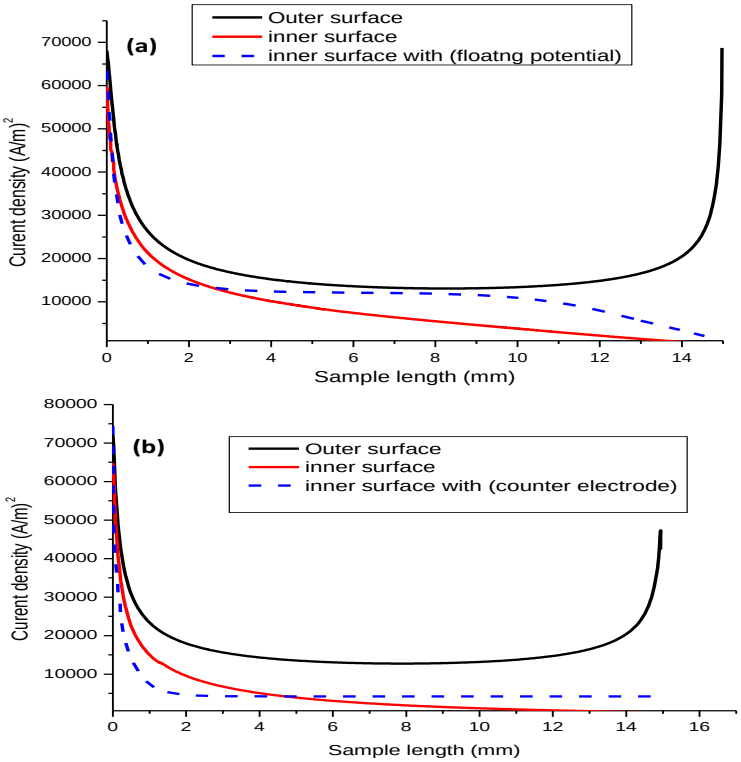

Fig. 8.9 Simulation results of current density as a function of sample length for PEO process at inner and outer surface, with and without floating potential electrode (a) L-shape and (b) U-shape.

It is clear that when the floating potential electrode was used beside the working electrode in both cases, the current density along the inner surfaces increased and became more uniform. Thus, the simulation of electric field and current density distributions over irregular shape working electrodes during PEO process can help understanding the reasons behind the differences in coating morphology and thickness. Moreover these results provide a guideline on how to improve coating thickness uniformity and morphology at the edges and in the corners of irregular shape substrates to enable their use in specific applications that might require a higher coating thickness on one side.

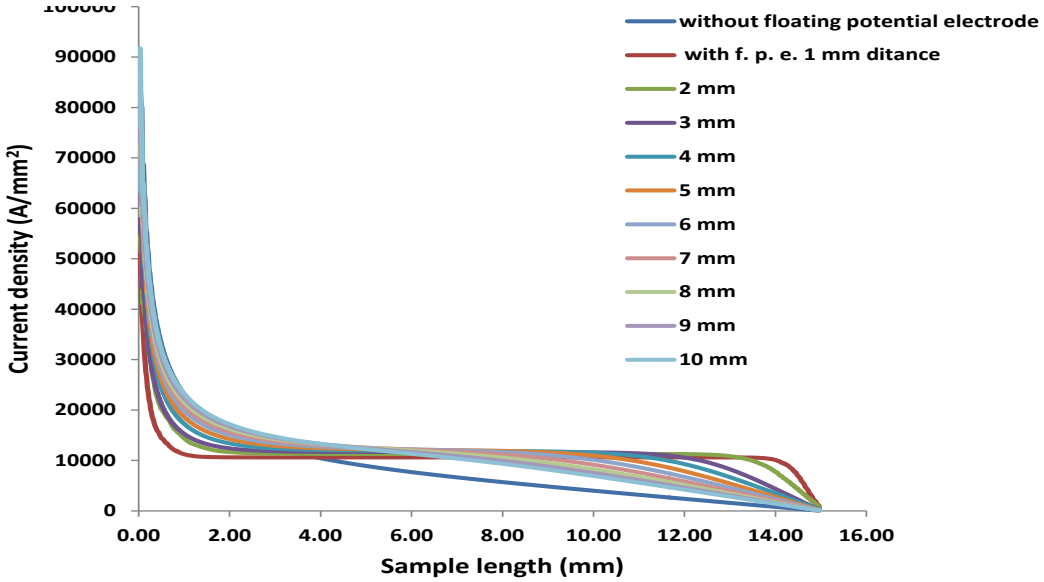

Fig. 8.10. Calculated current density distributions across the length of L-shape working electrode when a floating potential electrode was placed at various distances from it.

For further understanding of current density distribution during the PEO process, an application of the floating potential counter-electrode was considered at various distances from the L- shape working electrode. Results of calculation of the current density distribution along the inner surface of the L-shape electrode presented in Fig. 8.10 show how the values of current density change with changing distance between the floating potential electrode and working electrode. In general, the current density increases when the distance decreases due to the effect of increasing potential resulted from the application of the floating electrode.

8.8. Current transient behaviour during plasma electrolytic process

The variations of current density with the time of potentiostatic PEO treatments of irregular shape samples in different electrolytes are shown in Fig. 8.10. For the in L-shape samples, the current density initially increases sharply to reach the maximum of 0.3 A/cm^2 to 0.6 A/cm^2 depending on the type of electrolyte solution. While for U-shape samples, these values decrease to 0.18 A/cm^2 to 0.3 A/cm^2, also depending on the type of electrolyte used. Then for both types of samples, the current density asymptotically converges to the steady state values with some fluctuations observed for the samples treated in the silicate electrolyte.

From the experimental observations, the PEO process can be divided into three stages. In all conditions, the current density increases at the first stage according to the voltage increase to the pre-set values of 530 V and -180 V. Then, at stage two, a significant drop in current density occurs because of rapid formation of the PEO coating which increases the system resistance, restricting the current flow. Within this stage, the white sparks are sparse and local coarse arcs are occasionally produced. After that, in the third stage, only fine micro arcs occur on the surface of the samples and the reactions proceed steady with some distinctive changes in current density. These results are consistent with previous observations [4, 12, 52, 55, 125, 126, 199, 200]. The current density-time curves were different from each other at the stages due to the different electrolyte concentrations (see **Chapter 4**). Comparing transient behaviour of current density during PEO treatments of L and U shape samples (Fig.8.11), it can be seen that, in spite of the clear symmetry in current density curves between the two conditions, the values of current density at the three stages of U-shape treatment are less than those in L-shapes. This is due to the sample geometry effect, where shielding of the substantial fraction of inner surface area of the U shape electrode affects the net current density.

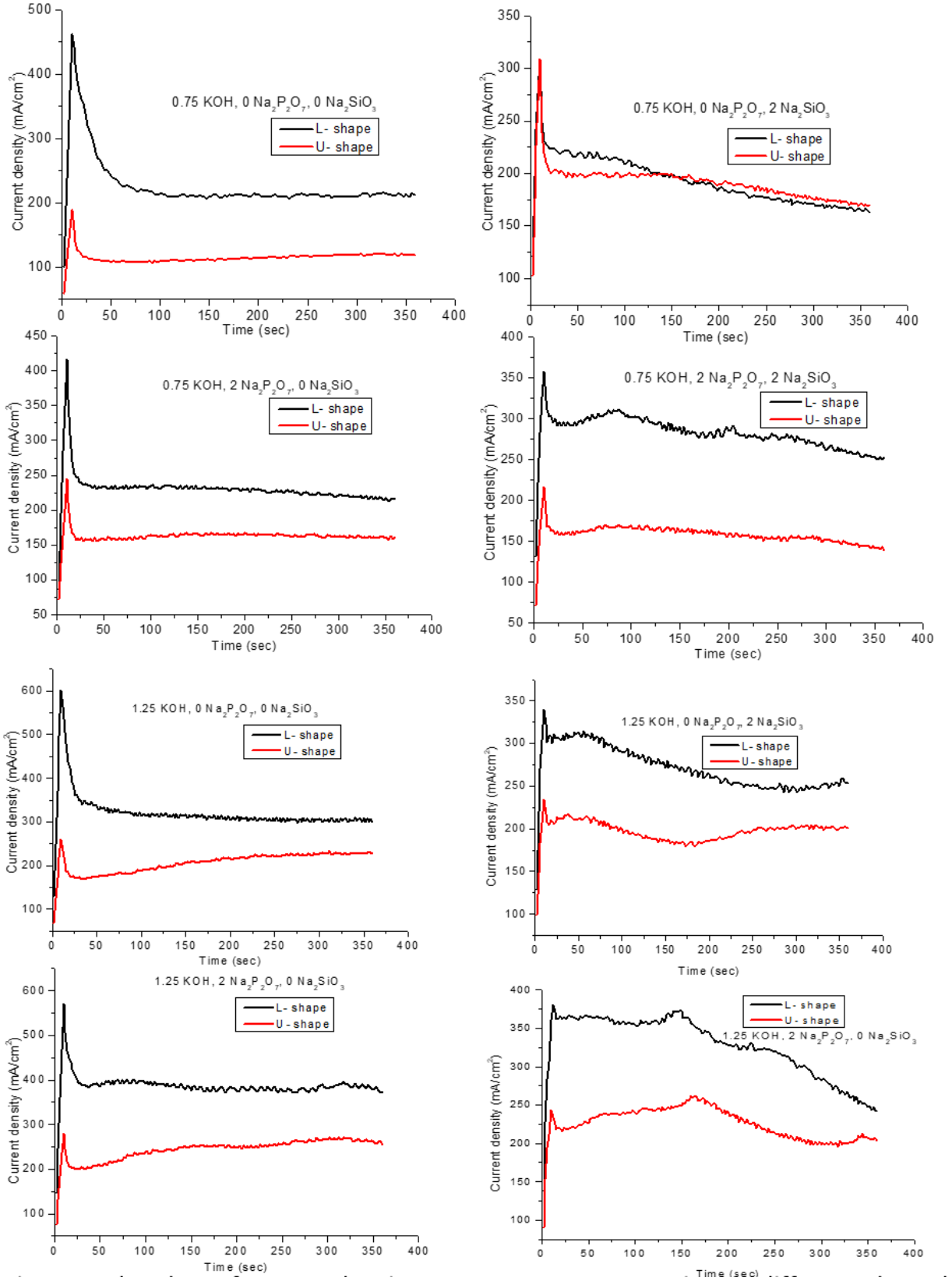

Fig. 8.11. The plots of current density versus PEO treatment time in different electrolyte compositions for L and U shapes

8.9. Coating thickness distribution

Coating thickness is one of the important factors that influence the micromechanical and tribological behaviour in both regular and irregular shapes. In certain applications, a relatively soft coating can assist sample bending and enhance its flexibility. This means a substantial value of residual aluminium may play a crucial role for the stuffiness of the composite material.

To obtain better knowledge about the nature of PEO coatings and their thickness distribution on or near edges and corners of irregular shape substrates (see Fig. 8.10), the coating thickness was evaluated using MountainMap7.4 software using SEM images of sample cross-sections prepared in these regions (Fig 8.12).

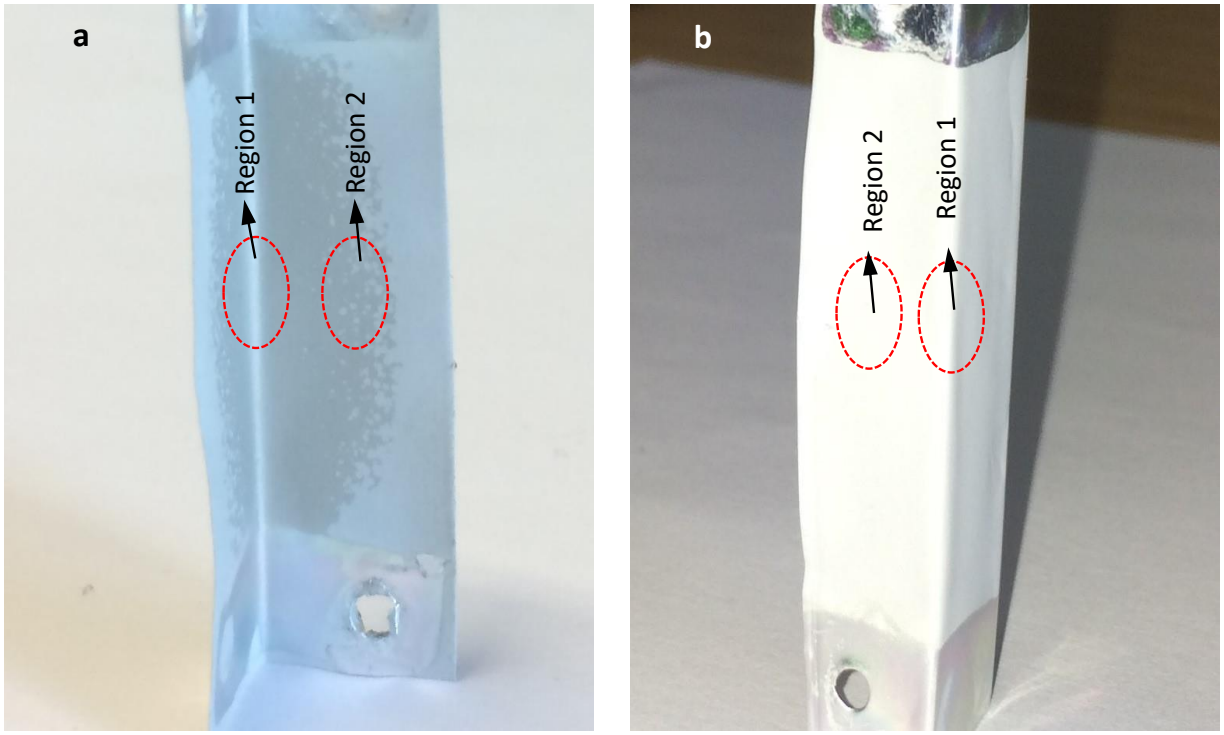

Fig. 8.12 Regions selected to measure thicknesses of PEO coatings for (a) L-shape sample, (b) U-shape sample treated in different electrolytes.

The thicknesses of coatings formed in outer and inner sides at different regions on the working electrodes are shown in Table 8.2. The thickness of PEO coatings produced from different electrolytes in different regions of irregular shape substrates, is presented in Table 8.2. It is clear that for both shapes there is a disparity values of coatings thickness measured on inner and outer surfaces.

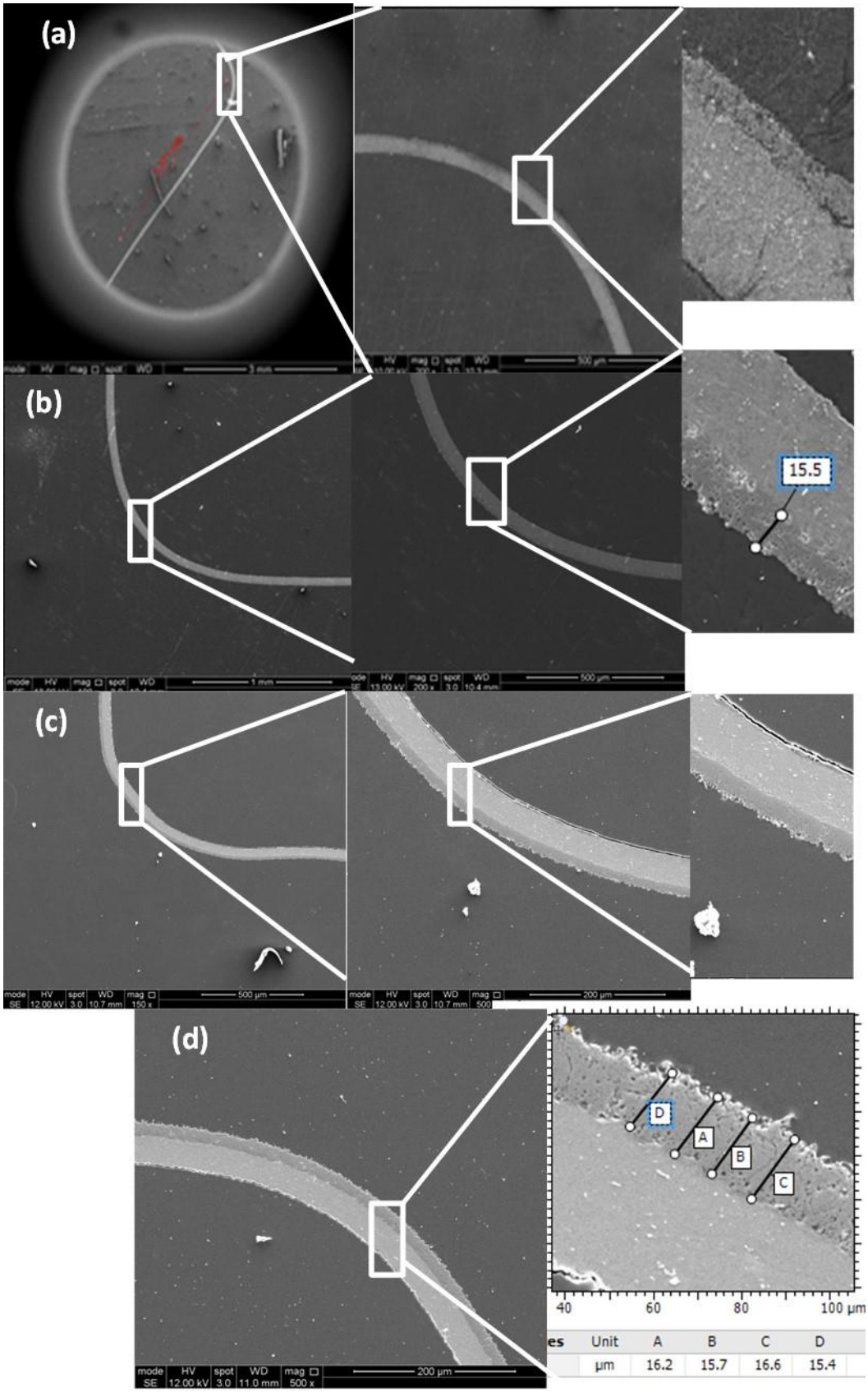

Fig. 8.13 Details of PEO coating thickness measurement using SEM cross-sections of the corner regions of samples treated in the electrolyte E2 and E6 for (a) and (b) L-shape and E4 and E8 (c) and (d) U-shape.

Table. 8.2. Different solutions of electrolytes used for PEO coating process of irregular Al foil samples.

Electrolyte composition g/l	L-shape Outer surface		U-shape Outer surface	
	Region 1- On corner	Region 2	Region 1- On corner	Region 2
0.75 KOH (E1)	10.1 ± 0.7	10 ± 0.8	10.0 ± 0.7	9.2± 0.8
0.75 KOH, 2.0 Na_2SiO_3 (E2)	9.1 ± 0.8	8 ± 0.7	11.0 ± 1.3	9.0 ± 0.9
0.75 KOH, 2.0 $Na_4P_2O_7$ (E3)	12.3 ± 1.2	11.55 ± 0.9	13.3 ± 1.2	11.55 ± 0.9
0.75 KOH, 2.0 Na_2SiO_3,2.0 $Na_4P_2O_7$ (E4)	17.8 ± 1.9	15.0 ± 1.9	14.4 ± 1.2	13.1 ± 1.7
1.0 KOH, 1.0 Na_2SiO_3,1.0 $Na_4P_2O_7$ (E5)	16.6 ± 0.81	15.3 ± 0.9	15.1 ± 0.6	13.6 ± 0.8
1.25 KOH (E6)	12.6 ± 0.41	12.7 ± 0.7	11.5 ± 0.8	10.7 ± 0.9
1.25 KOH, 2.0 Na_2SiO_3 (E7)	16.4 ± 1.2	14.9 ± 1.2	13.7 ± 1.2	12.9 ± 1.3
1.25 KOH, $Na_4P_2O_7$ (E8)	13.2 ± 0.9	13.8 ± 0.8	15.9 ± 0.9	14.5 ± 0.2
1.25 KOH, 2.0 Na_2SiO_3,2.0 $Na_4P_2O_7$ (E9)	32.3 ± 1.3	29.3 ± 1.1	29.3 ± 1.3	29.6 ± 1.1

As can be seen in Fig. 8.12 and 8.13, in region (1), the coatings thickness on outer corner is higher than that in the inner corner due to the edge effect. However, samples treated in electrolyte solutions with higher concentrations, such as E4 and E9, exhibit more uniform coverages and appreciable coating growth on inner surfaces (Fig 8.14). While in the flat area (region 2), the coating thickness on the outer surfaces is mainly the same as that produced on regular shapes. This is consistent with the results of modelling of electric field and current density distributions on the surfaces of such working electrodes discussed in section 8.7.

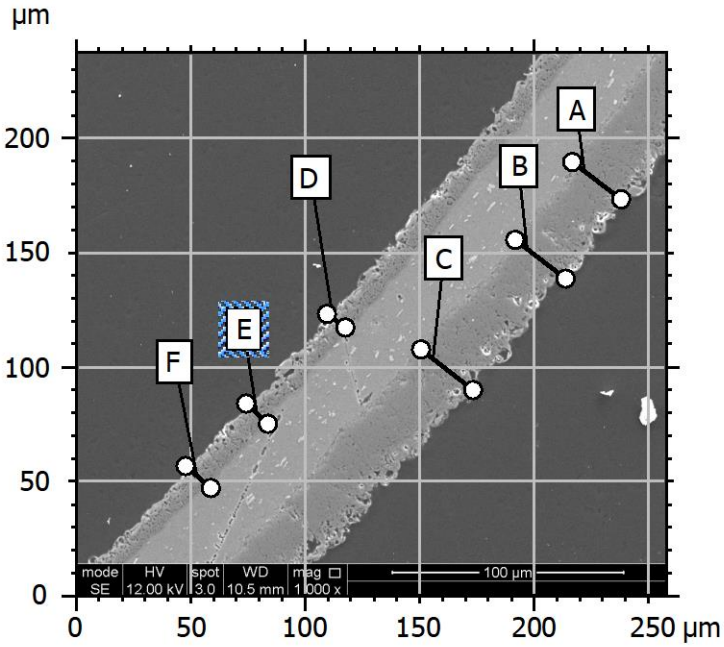

Distances	Unit	A	B	C	D	E	F
HDist	µm	26.8	27.8	28.8	10.0	13.0	14.6

Fig. 8.14 SEM image of a cross section of the PEO coating formed on inner and outer surfaces of the corner region of a U-shape Al foil sample treated for 6 min in electrolyte (1.25-2-2).

Considering the effects of other factors such as electrolyte concentrations and treatment time type, the more irregular shape the more difference there is in current density. Edges and corners are cites of high current density that attract additional current and therefore more developing thicker coatings. While central areas of flat walls exhibit lower current densities and will have thinner coatings. In modelling, we suggested to use a floating potential electrode beside the internal surfaces and inner corners to increase the current density, thus promoting thicker coatings. However, in real systems this would require further studies due to the difficulties of placing the counter electrode near the working electrode. It is obvious that in practice, irregular shapes are unavoidable due to the function of the parts; however, components with less sharp angles would facilitate PEO treatments and provide uniform coating growth. Many other factors would also have to be considered for surface finishing of irregular shapes using PEO process to reconcile requirements from design and processing aspects.

8.10. Optical emission characterisation

Owing to the involvement of electrochemical and thermal reactions, the mechanisms of oxide layers formation by PEO treatment are complex [10, 55]. Throughout the PEO process,

a large amount of sparks moves quickly on the surface of the working electrode. However, there are many parameters such as treatment time, electrolyte compositions and current mode affecting the evolution and characteristics of sparks. The emission intensity signals of the species can be used to specify whether the plasma generates conditions required for a certain coating process. Although the amount of experimental data on microdischarge phenomena is rapidly expanding, there are still many uncertainties [201]. The geometrical shapes of samples and their dimensions is a crucial issue for understanding the coating growth mechanisms during PEO processing. This section of the work is focused on the study of the behaviour of the plasma micro-discharges during PEO treatments of irregular shape samples, in particular the effects of internal and external surfaces.

Fig.8.13 and 8.14 display the typical optical emission spectra of microdischarges at inner and outer surfaces of an L-shape aluminium foil substrate during PEO processing carried out in different electrolytes, collected in the wavelength range from 300 nm to 900 nm at the processing time of 6 min. For both inner and outer surfaces, it is found that PEO plasma contains aluminium from the substrate and sodium, potassium and hydrogen β Balmer lines from the electrolyte. Spectral lines recorded at 486.1 nm (H_β), 589.5 nm (Na I), 765 nm (K I) correspond the electrolyte species and lines from the sample substrate are 304.1 nm (Al I), 396.1 nm (Al I), as identified by NIST atomic spectra database are collected in Table 8.3 [202].

Table 8.3 Observed spectral lines with wavelength, transition, statistical weights of the upper and lower states gk, and gi respectively, energy difference and the transition probabilities (Aki).

Line	λ (nm)	Transition	g_k	g_i	Energy (eV)	A_{ki} (10^8 S^{-1})
H_β	486.1	4d 2D → 2p 2P	4	2	2.55	0.172
Na I	589.5	3p 2P → 3s 2S	3	3	1.36	0.64
K I	765	$3p^6$4S → $3p^6$ 4P	-	-	-	3.2
Al I	304.1	3s23d 2D → 3s23p 2P	6	4	4.0	0.732
Al I	396.1	$3s^2$4s ^{2}S → $3s^2$3p ^{2}P	2	4	3.13	0.982

It is clear that, for both inner and outer surfaces of the samples treated in all electrolytes except E6 containing only KOH, the most intense line belongs to sodium. The active species in the plasma may give the high temperature condition needed to melt and sinter the oxides produced by the electrochemical reactions, thus forming the ceramic layers.

Figures 8.15 and 8.16 show optical emission spectra of plasma discharge recorded from inner and outer surfaces during PEO treatments of L-shale Al foil samples. The general trend

of the emission spectral lines of all species at the inner surfaces are stronger than those at the outer surfaces, although the difference in emission intensity not high. This appears to be consistent with the modelling and the experimental results of current density, which in turn is reflected in thicknesses and morphology of PEO coatings.

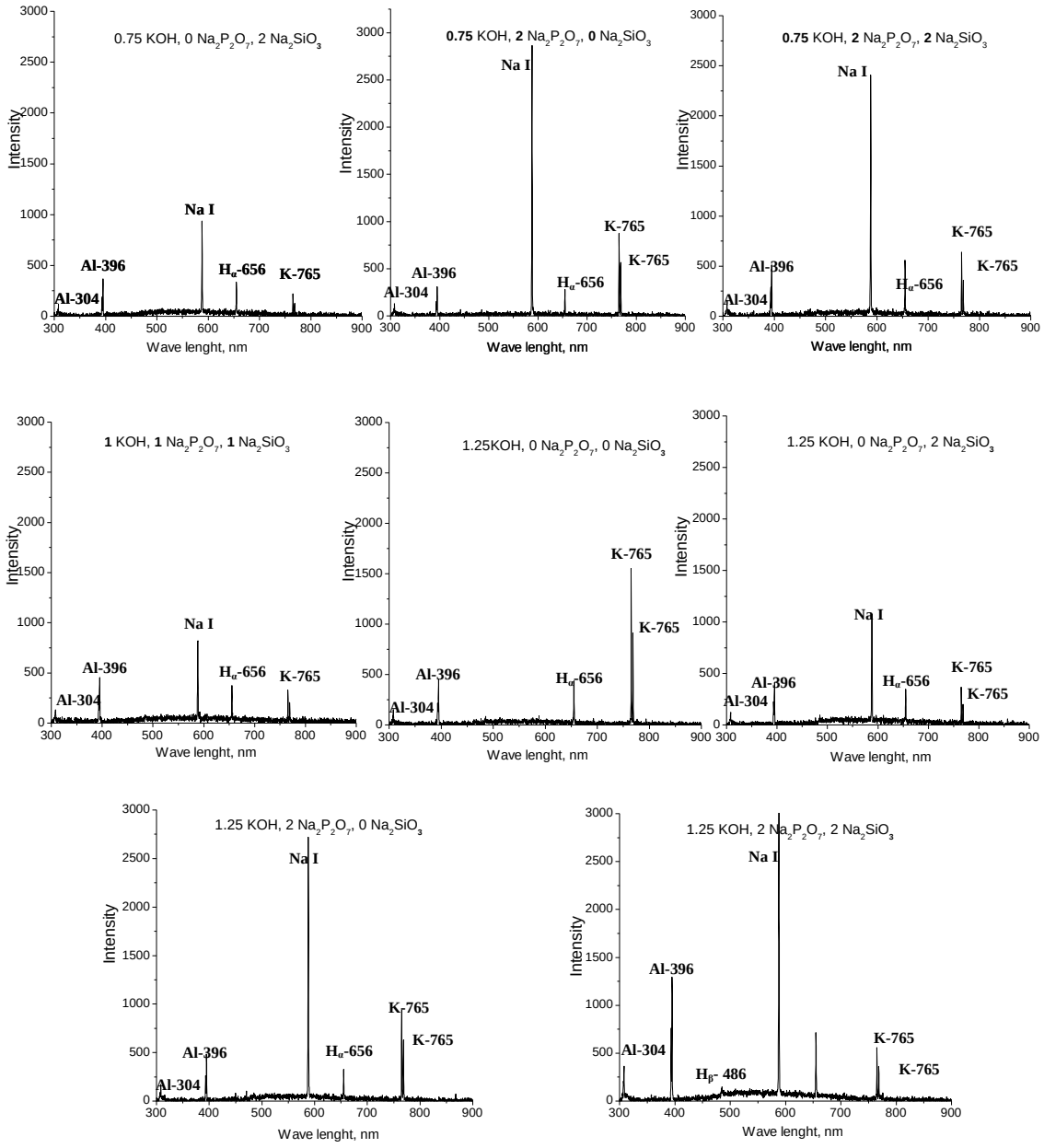

Fig. 8.15 Emission spectra of microdischarges during PEO of Al-foil (L-shape) at inner surface in different electrolyte compositions.

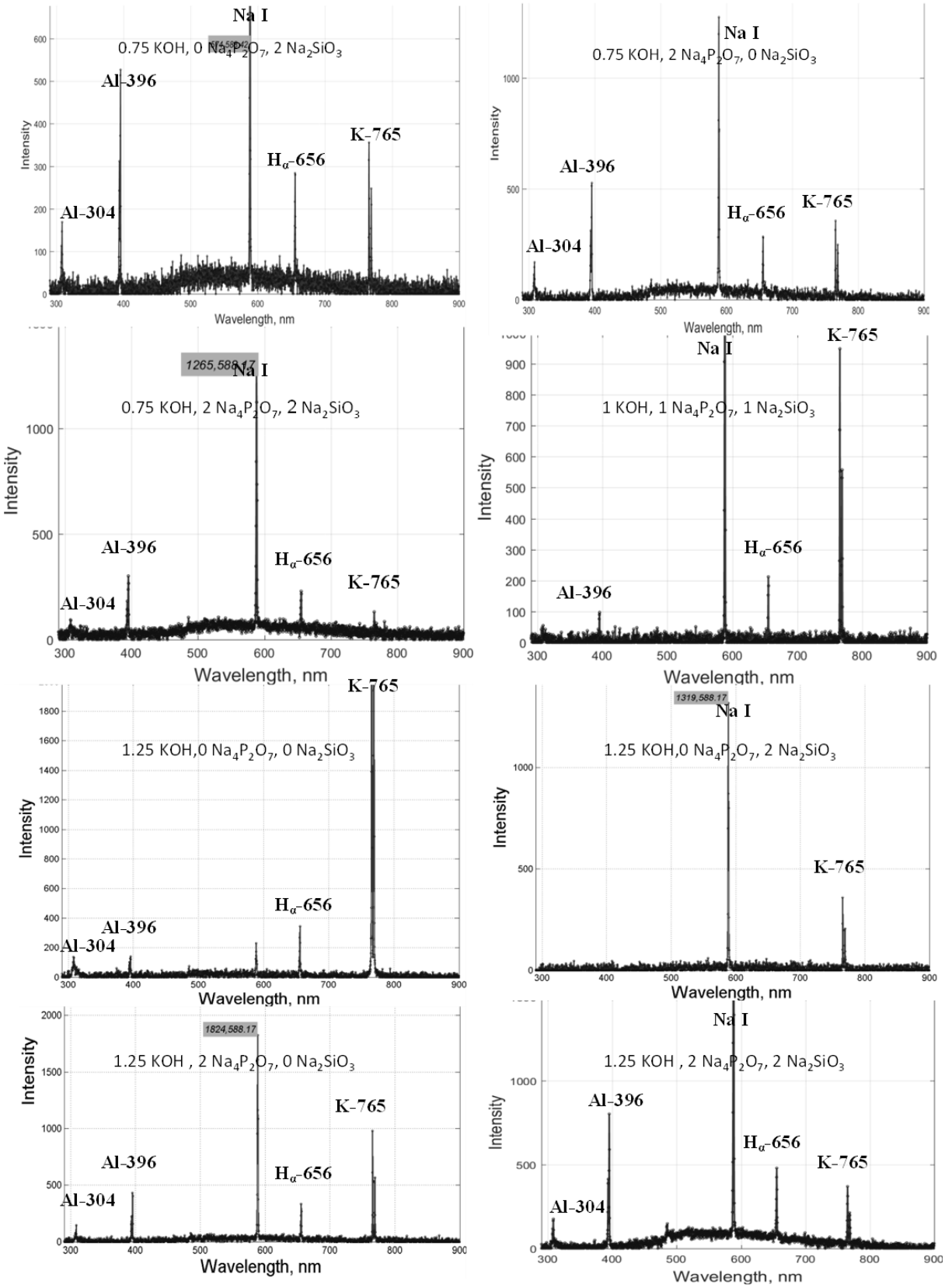

Fig. 8.16 Emission spectra of microdischarges during PEO of Al-foil (L-shape) at outer surface in different electrolyte compositions.

The geometrical shapes of samples and their dimensions play an important role in current density distribution during PEO process. However the discharges can be influenced by many other factors such as treatment time and type of electrolyte [109]. In our experiments, if we drew attention at the inner surfaces of L shape samples by positioning focusing lens of the OES system in front of them as shown in (Fig 8.17 a). The inner surface consists of two internal faces two longitudinal edges, four transverse edges and the corner, while the outer surface consists of just two longitudinal edges and two transverse edges. These edges and corners may contribute to the output spectrum produced [65, 203]. Effects of edges and corners in complex shapes on thickness distribution and morphology of PEO coatings can be demonstrated in (Fig 8.17 b), which provides an example of the appearance of L-shape sample treated in electrolyte E2 (0.75 g/l KOH, 2.0 g/l $Na_4P_2O_7$). A thicker and more uniform white coating can be clearly observed at the edges and on the corner of the sample compared with the other regions on the sample. This is also confirmed by the results current density distribution modelling (Fig 8.5-8.6 and 7.8) and coating thickness measurements using cross-sectional SEM images (Table 8.2)

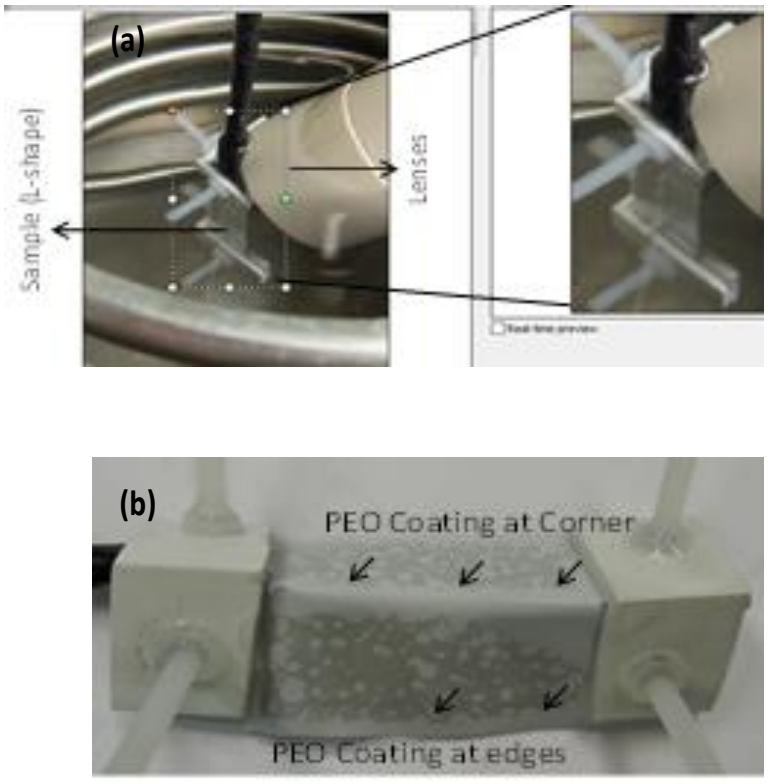

Fig. 8.17 (a) L-shape Al foil sample assembly and its position in the cell during the PEO process and (b) after treatment

The intensity variation of species emission lines with treatment time of Al-foil (L-shape samples) at inner (in front of lens) and outer surfaces in different electrolytes during the PEO processes presented in (Fig 8.18 (a) (b) (c)).

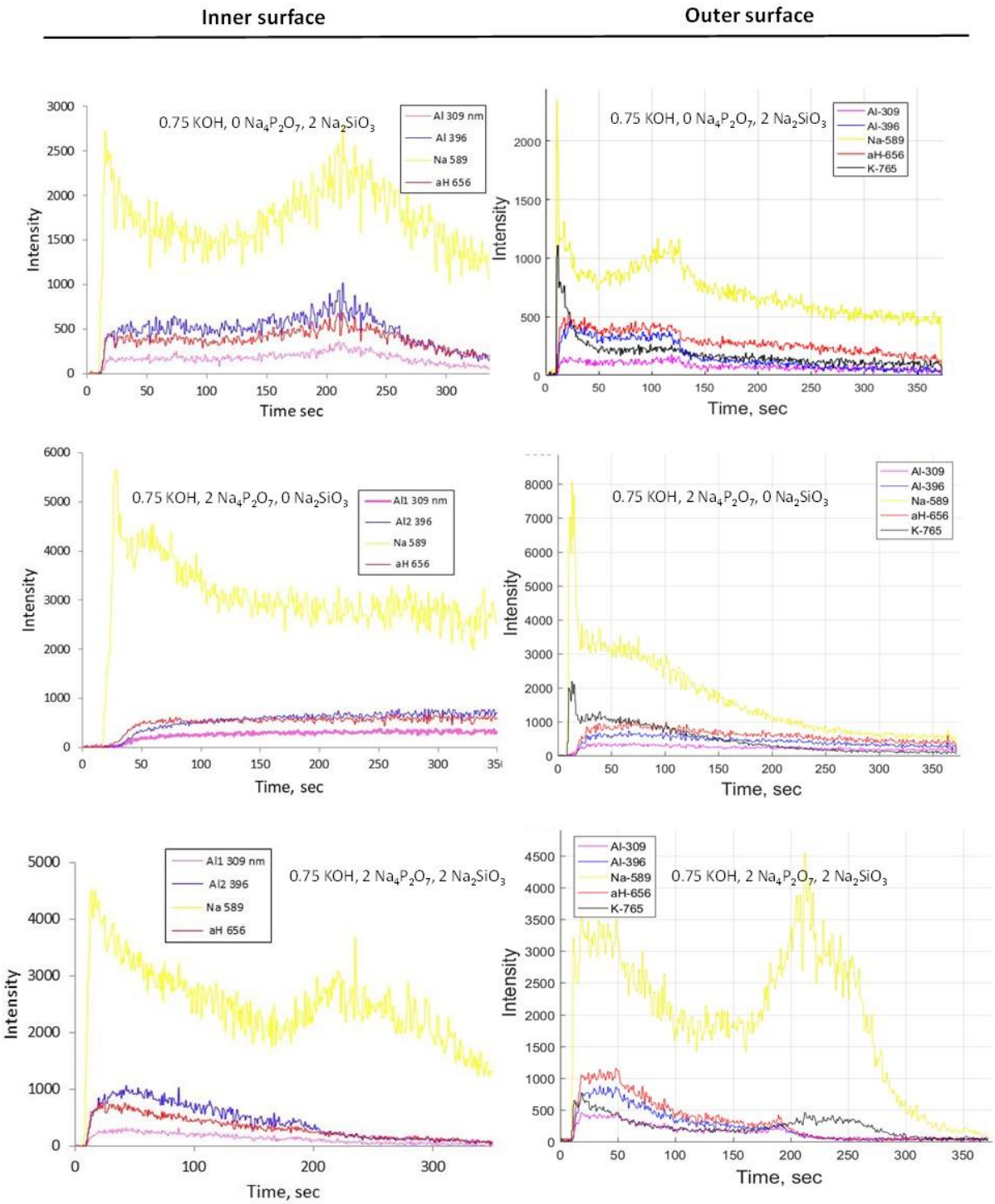

Fig 8.18 (a) Variations of the intensity of spectral lines during the PEO processing of L-shape Al foil sample at inner and outer surfaces in different electrolytes.

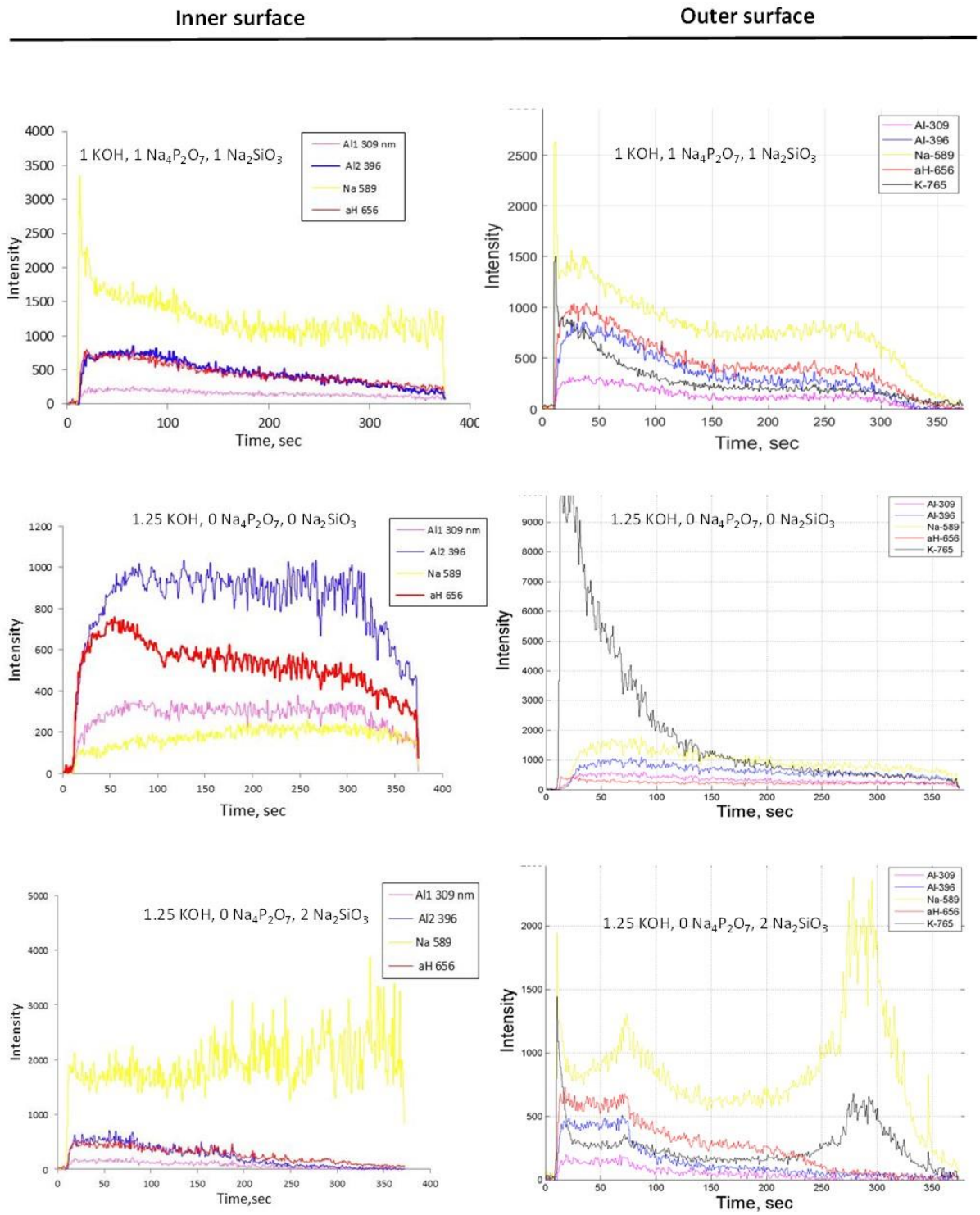

Fig. 8.18 (b) Variations of the intensity of spectral lines during the PEO processing of L-shape Al foil sample at inner and outer surfaces in different electrolytes

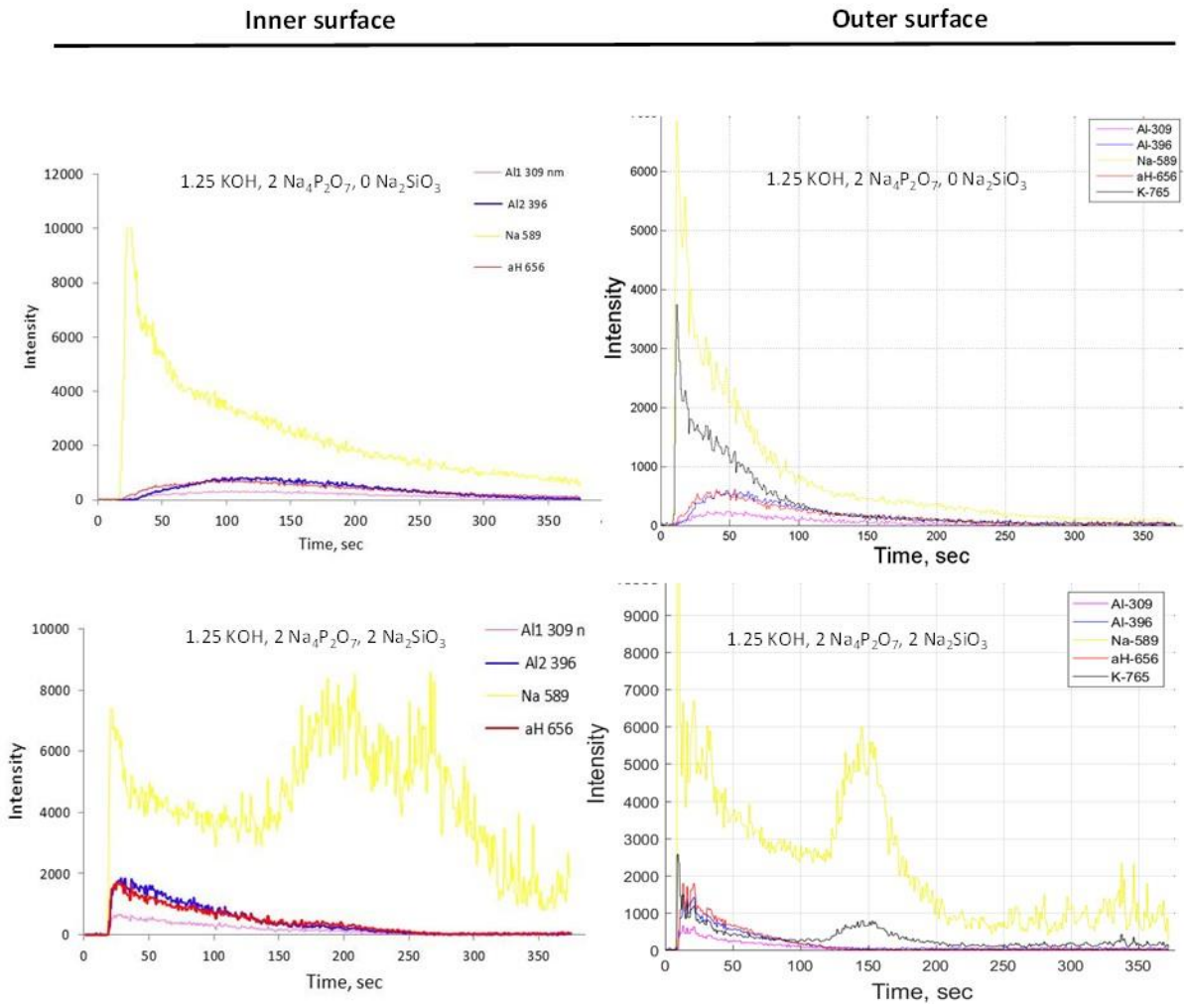

Fig. 8.18 (c) Variations of the intensity of spectral lines during the PEO processing of L-shape Al foil sample at inner and outer surfaces in different electrolytes.

As the PEO process continues, the discharge appearance varies and emission intensities of species in the plasma change for all conditions at both inner and outer surfaces. In both cases (inner and outer surfaces), Na-589 line shows strong intensity signals that have a similar trend. This also applies to other species, however in some cases, there are signal fluctuations at later stages, such as during treatments in electrolytes (0.75-2-2), (1.25-0-2) and (1.25-2-2). Hussein *et al.* [109] stated that strong discharge may cause irreversible damage to the coatings. In spite of the intensities of most lines at inner surfaces being stronger, the trends in their behaviour at both surfaces are mainly similar, however it is not quite true for the treatments in (125-0-2) and (125-0-0) electrolytes. For the sample treated in electrolyte (1.25-0-0) the signals recorded at the outer surface show Na-589, which is strange, the only reason may just be a noise in the system rather than a defined spectral line. In the other side, the location of plasma discharge concentrated around the edges due to the effects of high voltage and strong

electric field, which led to the higher current density. This influences the coating growth and could cause relatively uneven coating thickness distribution compared to the flat regions.

8.11. Electron concentration and temperature

The relative intensities of spectral lines of the same atomic species were applied to compute the plasma electron temperature (Te). Once relative intensities are known, the temperature corresponding to a given line ratio [203] then the following relation was used to determine the plasma electron temperature;

$$\frac{I\,(1)}{I\,(2)} = \frac{A_{mn}(1)g_m(1)\lambda_0(2)}{A_{mn}(2)g_m(2)\lambda_0(1)}\,exp - \left\{\frac{E_{(m2)}-E_{(m1)}}{kT}\right\}$$

Where kT is the thermal energy, $I\,(1)$and $I\,(2)$are relative line intensities of lines of the same species in question, $A_{mn}(i)$ are the transition probabilities, *m* the upper and *n* the lower level of the respective lines, $g_m(i)$ the statistical weight of the upper levels, $E_m(i)$ energies of the upper levels of lines and $\lambda_0(i)$ the wavelengths of the peak centres in vacuum. In this work, the intensity ratio of the lines of Al recorded at 396.1 nm and 304.1 were used to determine instantaneous values of plasma electron temperature. Fig. 8.19 ((a), (b), (c)) show the plasma electron temperature as a function of treatment time for different electrolytes. Hussein et al. [109] stated that the T_e profile during the PEO process depends strongly on the type of discharge. From the results presented, there appears to be no substantial differences in Te of discharge at the inner and outer surfaces of L-shape samples. For example, in the case of the sample treated in electrolyte E2, (0.75 g/l KOH, 2.0 g/l $Na_4P_2O_7$) the plasma electron temperature increased from 4000 ± 300 K at the earlier stages to 5000 ± 450 K by the end of process, while in the outer surface it changed from 5500 ± 300 K to 5000 ± 450 K. The difference in temperature is significant at the earlier stages of the coating growth. However the outer surface shows higher electron temperature for most samples. At the initial stage of the process, the current rapidly reaches the set limit and as the resistance of the growing coating increases the current decreases. The discharges at this stage are characterised by optical emission with well-defined spectral lines. Gradually, soft sparking is initiated on the edges of the samples where local current density is higher. This means that the samples which have more edges are exposed a significant amount of discharges than less edges which leads to higher electron plasma temperature. This is consistent with the data of Fig. 8.18-8.19.

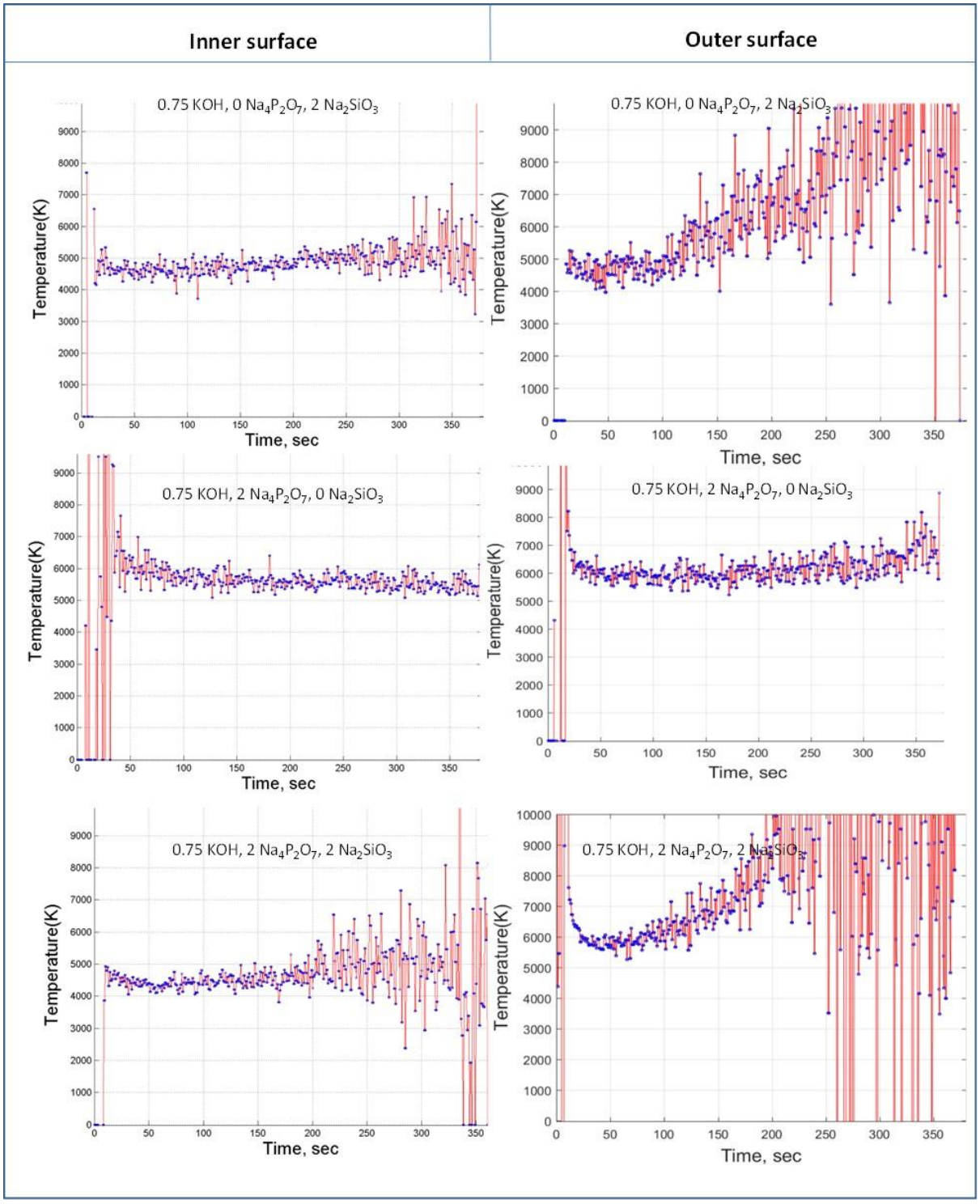

Fig 8.19 (a) Plasma electron temperature as a function of PEO process time at the inner and outer surfaces of L-shape Al-foil samples treated in different electrolytes

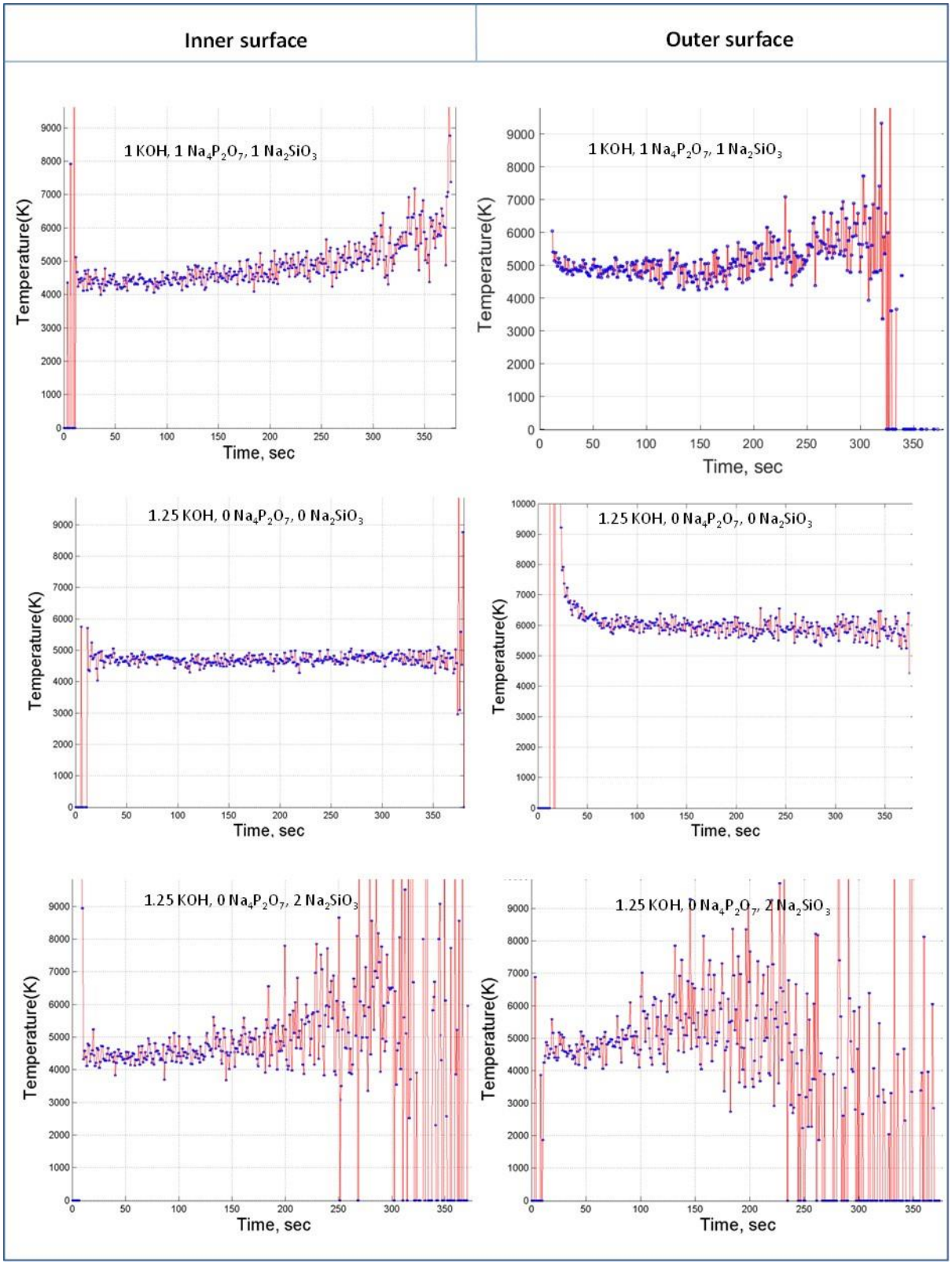

Fig 8.19 (b) Optical emission spectroscopy of plasma discharge and current density during PEO treatments in electrolytes E4 and E9

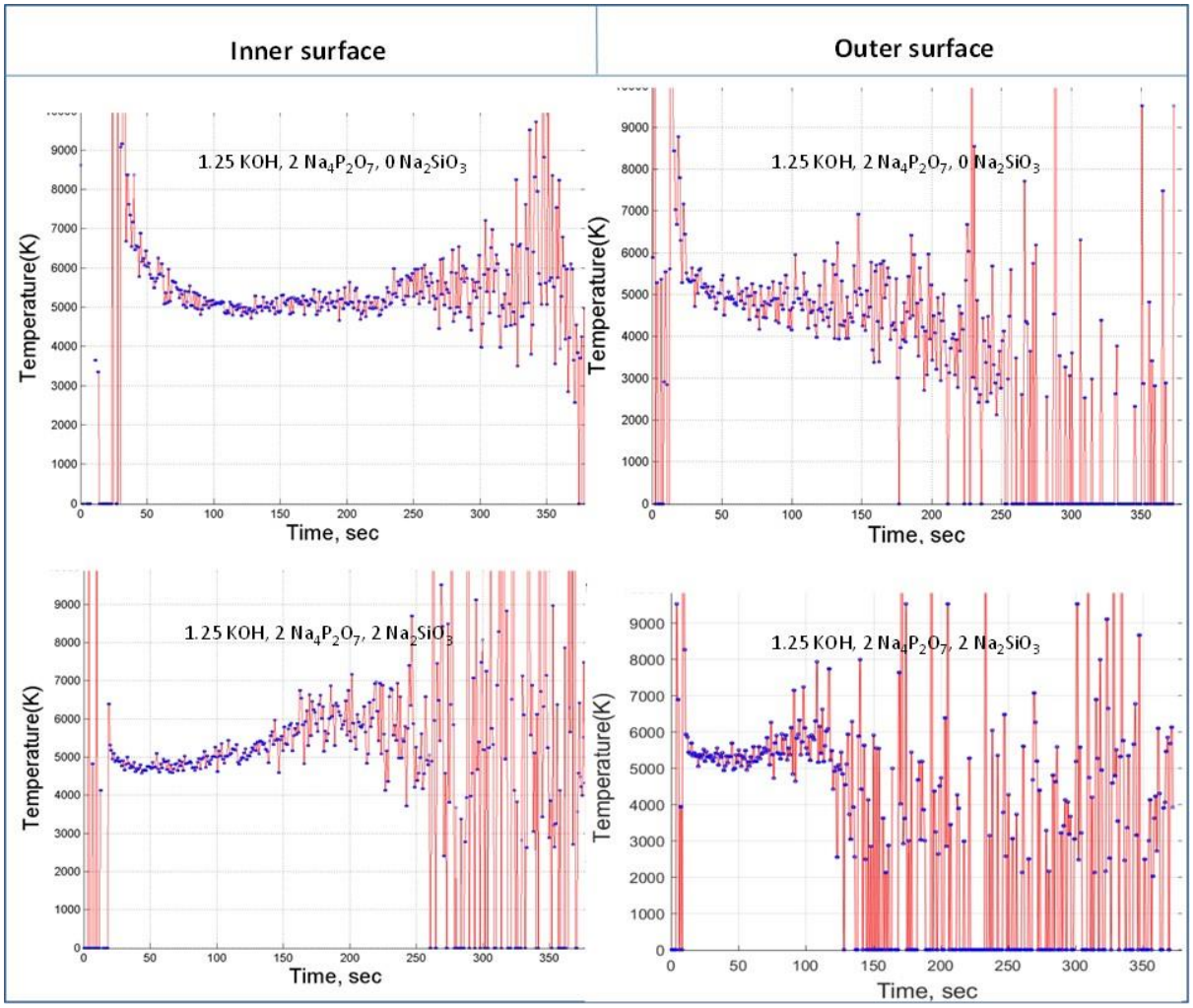

Fig. 8.19 (c) Optical emission spectroscopy of plasma discharge and current density during PEO treatments in electrolytes E4 and E9

To achieve better understanding about how discharge appearance changes and the plasma intensities vary during PEO treatments of irregular shape samples and monitor the evolution of the main treatment parameters, Fig 8.20 presented evolutions of absolute and relative emission intensities as well as plasma electron temperature on the outer surfaces of samples in comparison with current density evolution during PEO treatments in electrolytes E4 and E5.

As discussed in Section 8-6, the current distribution is among the most significant parameters characterising the operation of the electrochemical cell. The current density on the electrodes is directly proportional to the reaction rates and its distribution critically affects the electrochemical process. [185].

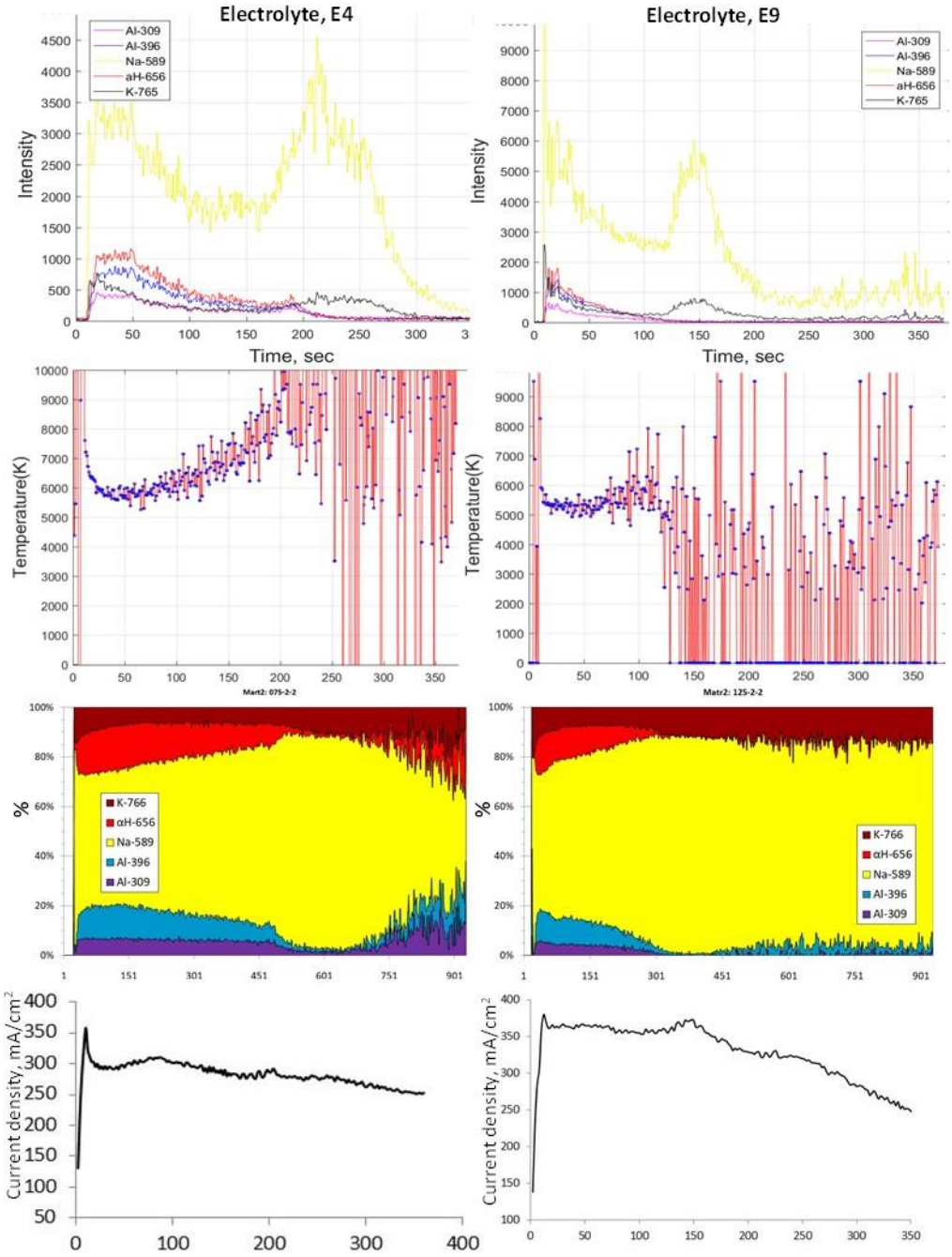

Fig. 8.20 Optical emission spectroscopy of plasma discharge and current density during PEO treatments in electrolytes E4 and E9

As can be seen from Fig. 8.20, the higher extinction of Al lines occurred between 4 and 5 min in sample treated in electrolyte E4 and between around 2 and 5 min in electrolyte 9. During these periods of time, the current density decreased to the steady state stage in both electrolytes and the plasma temperature showed high fluctuation. The thicknesses of these two layers change relatively each other with the potassium hydroxide concentration.

Increasing the KOH as discussed in **Chapter 5** leads to an increase the coating thickness. The thickness of the coating produced in electrolyte E9 was around 29.0 µm while that in E4 was 15.0 µm. Fig. 8.20 shows the amount of consumed aluminium during the treatment in electrolyte E9 is more than that in electrolyte E4.

8.12. Summary

Distribution of electric field in the electrolyser is an important factor, affecting formation of PEO coatings on complex shape substrates. To study effects of electric field on current density distribution on the surface of the working electrode at various electrolyser layouts, numerical modelling was used.

The modelling results showed that the shape of sample strongly influences the current density due to the primary electric field distribution in the electrolyser. Numerical solutions indicated that the electric field strength and current density at the edges and on the outer corners of L and U shape electrodes are higher than in the flat surfaces. In both cases, the values of current density at edges are nearly 6 times higher than those at the middle.

The L and U shaped thin-walled 3D ceramic-metal composite structures were successfully fabricated using PEO treatments in electrolytes containing 0.75 to 1.25 g/l KOH, 2.0 Na_2SiO_3 and 2.0 g/l $Na_4P_2O_7$, with uniform PEO coatings without cracks grown on the edges and corners at outer surfaces of L and U shape Al foil samples. However, the coating thickness at the inner surfaces was around 30 % lower.

The PEO process is capable of forming a uniform coating at the edges and around sharp corners, with typical coating thickness ranging from about 10 to 30 µm for both L and U shape substrates, depending on the electrolyte composition used.

Chapter 9
Conclusions and future work

9.1. Conclusions

In this research, ceramic alumina films were produced by conversion of different shapes aluminium foil substrate using PEO technique. The key point is that the Plasma electrolytic oxide coatings are formed by substrate oxidation in an aqueous electrolyte via a series of localized electrical discharge events which allow oxide growth to proceed so as to produce ceramic films.

Control of PEO process parameters such as current regime, treatment time and electrolyte composition and understanding current distribution in the electrolyser help avoiding poor composite performance, such as mechanical and dielectric response, caused by differential thicknesses of ceramic and residual Al layers. So, the degree of conversion of the Al foil into its oxide and the limitations to create uniform coatings on regular and complex shapes were studied after a series of different analyses. Based on these studies, the following conclusions could be drawn from this research.

1. In first stage of analyses, treatment time was the only variable parameter during the PEO process. The findings of this part are summarised as follows:

   a) In general the PEO coatings grow thicker with longer process time and higher current densities, however it is crucial to select the appropriate setting for current density and treatment time according to the application.

   b) Complete conversion of Al foil specimen to alumina ceramic with thickness of 75 ± 1.5 µm successfully achieved, except a very small area that does not exceed 1 % of the sample volume. However such sample showed high brittleness.

   c) The highest degree of surface roughness and coating growth rate were observed in the later stages of the PEO process. While the minimum porosity was observed after 10 min of the PEO treatment.

d) Treatment time strongly affected the gamma to alpha alumina transformation. Both γ and α - alumina are observed after 6 min varying in relative proportion through the coating thickness.

e) Alumina films created after 6 min of process time with thickness 17 ± 1.4 μm from one side show a good degree of flexibility compared with other produced oxide films. The nanoindentation yields an elastic modulus was 182 ± 30 GPa which is consistent with the measured phase proportion and porosity percentage.

f) The current efficiency of the oxide layer growth ranges from 19-36 %, and increasing with treatment time. Similarly, the aluminium loss increases with treatment time. While the oxygen evolution was the main electrochemical process for all treatment times and the current efficiency of oxygen evolution decreases with time.

g) According to the results achieved, regions on the Al foil surfaces (edge, centre and near the metal part) affected the coatings growth rate. The edges regions had undergone higher coating growth than in centre regions.

2. Electrolyte constituents in any electrolysis process is an important factor because it is able to influence with the included chemical reaction such as anodic oxidation and hydrogen evolution the structure of the coatings. A series of different electrolytes compositions are used to study these influences on the coatings characteristics during the PEO process. The conclusions of these studies are listed as follow:

a) The electrolyte solution with addition of potassium hydroxide provides the conductivity and raise the rate of anodic dissolution and oxygen evolution which causes to increase the current density of PEO process and coating thickness. Multiple linear regression modelling confirms the strongest effect of KOH on coating thickness and roughness. Whilst porosity is most strongly affected by $Na_4P_2O_7$.

b) Among the three components investigated, potassium hydroxide is found to be the predominant factor effecting on thickness and roughness, followed by sodium pyrophosphate and sodium silicate.

c) The thickest coating achieved in electrolyte E9 (1.25 g/l KOH, 2.0 g/l $Na_4P_2O_7$, 2.0 g/l Na_2SiO_3) corresponds to conversion of about 70 % of Al foil to alumina ceramics, with residual aluminium foil thickness around 20 µm. This may enhance the flexibility of foil after treatment as explained in last chapter.

d) The coatings include mainly γ-Al_2O_3 and an amorphous component. Octahedral and tetrahedral coordination of alumina are affected by additions of silicate and pyrophosphate to the electrolyte.

3. For further investigations of mechanisms and kinetics of the electrochemical processes, alkaline silicate/phosphate electrolytes are selected over a range voltage during cyclic voltammetry analysis. The CV method provided us a useful information about the oxide film formation, dissolution and dielectric breakdown which is very helpful in clarifying the mechanisms of the coatings formation and the main conclusions are outlined as follow:

   a) The non-linear behaviour of the current – voltage curve was observed when using electrolyte without silicate/phosphate. It reflects a combination of three processes, including dissolution, passivation and formation of PEO coating under discharge conditions.

   b) Silicate addition obstruct anodic dissolution of Al, which enhanced the oxide growth. While phosphate, in addition of promoting α-Al2O3 phase formation it is also enhancing strong metal passivation and allow the breakdown voltage to be easily obtained.

c) Under the studied conditions, we can also conclude that the sparking voltage decreases when electrolyte resistivity decrease which is consistent with Ikonopisov equation. However which's more surprising and unexpected in K electrolyte, is the earlier emission starting prior to the current starts increasing.

4. A simulation of the electric field and current density using a COMSOL Multiphysics package has provided us beneficial information about the magnitudes and directions of the current density and electric field in the electrolyser during the PEO process, taking into account the shapes and positions of the working electrodes.

5. Thin-walled 3D ceramic structures were successfully produced using PEO method for samples treated in electrolytes (0.75 g/l KOH, 2.0 Na_2SiO_3 2.0 g/l $Na_4P_2O_7$) and (1.25 g/l KOH, 2.0 Na_2SiO_3 2.0 g/l $Na_4P_2O_7$). Inner and outer uniform PEO coatings at edges and corners were created, however the coating thickness at inner surface was less than the outer by around 30 %.

9.2. Future work

- In the short term future, new experiments using controlled processing parameters, e.g. current regime, type, shape and thickness of working electrodes and understanding current distribution in the electrolyser help avoiding poor composite performance, such as mechanical and dielectric response, caused by differential thicknesses of ceramic and residual Al layers.
- Electrochemistry module has been added recently to COMSOL Multiphysics which is a finite element software designed for a wide range of physical phenomena. This model focuses on electroanalysis and demonstrates the modelling of mass transport, current density and electrochemical reactions. This will give a direct support for investigation of the chemistry at the electrode-electrolyte interface during PEO.
- A study should be directed towards current and prospective future applications suitable for thin ceramic-metal composites produced using PEO technique.

Activities during PhD Study

Conferences attendance

1) 14th International Conference on Plasma Surface Engineering (PSE 2014), Germany, September, 2014, Poster presentation.
2) Department Poster Competition, Sheffield University, May 2015, Poster presentation.
3) 42nd International Conference on Metallurgical Coatings and Thin Films (ICMCTF 2015), USA, April 2015, Oral presentation.
4) Department 3rd Year PhD Student Seminar, Sheffield University, March 2016, Oral presentation.
5) "Sustainable Functional Materials" conference- Scarborough-UK, poster presentation.
6) 5th International Conference "Electrochemical and Plasma Electrolytic Modification of Metal Surfaces", Russia, May 2016, oral presentation

References

[1] B. C. Gündüz, M Yakuphanoğlu,, "Production of Al_2O_3 Thin films for FET and MOSFET Transistor Gate Applications," presented at the 6th International Advanced Technologies Symposium 2011.

[2] J. Poortmans and V. Arkhipov, *Thin film solar cells : fabrication, characterization and applications*. Chichester: Wiley, 2008.

[3] L. F. Miller, *Thick film technology and chip joining*. New York: Gordon and Breach, 1972.

[4] C.-J. Liang, "In-situ Impedance Spectroscopy Studies of the Plasma Electrolytic Oxidation Coating Process," Phd, Materials Science and Engineering, The University of Sheffield, UK, 2013.

[5] C. C. Koch, *Nanostructured materials : processing, properties, and applications*. Norwich, NY: William Andrew Pub., 2007.

[6] C. amazing. (2008). *Thick – film ceramic substrates design guide* [PDF]. Available: http://www.coorstek.com/resource-library/library/8510-1537_thick-film_design_guide.pdf.

[7] P. Auerkari, *Mechanical and Physical Properties of Engineering Alumina Ceramics*. Technical Research Centre of Finland, 1996.

[8] A. L. Yerokhin, X. Nie, A. Leyland, A. Matthews, and S. J. Dowey, "Plasma electrolysis for surface engineering," *Surface and Coatings Technology,* 1999.

[9] R. H. U. Khan, A. Yerokhin, X. Li, H. Dong, and A. Matthews, "Surface characterisation of DC plasma electrolytic oxidation treated 6082 aluminium alloy: Effect of current density and electrolyte concentration," *Surface and Coatings Technology,* vol. 205, no. 6, pp. 1679-1688, 2010.

[10] R. O. Hussein, X. Nie, and D. O. Northwood, "An investigation of ceramic coating growth mechanisms in plasma electrolytic oxidation (PEO) processing," *Electrochimica Acta,* vol. 112, pp. 111-119, 2013.

[11] G. Sundararajan and L. Rama Krishna, "Mechanisms underlying the formation of thick alumina coatings through the MAO coating technology," *Surface and Coatings Technology,* vol. 167, no. 2–3, pp. 269-277, 2003.

[12] M. M. S. Al Bosta, K.-J. Ma, and H.-H. Chien, "The effect of MAO processing time on surface properties and low temperature infrared emissivity of ceramic coating on aluminium 6061 alloy," *Infrared Physics & Technology,* vol. 60, pp. 323-334, 2013.

[13] S. V. Gnedenkov *et al.*, "Production of hard and heat-resistant coatings on aluminium using a plasma micro-discharge," *Surface and Coatings Technology,* vol. 123, no. 1, pp. 24-28, 2000.

[14] A. Y. R. Khan, X. Li , H. Dong, A. Matthews, "Surface characterisation of DC plasma electrolytic oxidation treated 6082 aluminium alloy: Effect of current density and electrolyte concentration," *Surface and Coatings Technology,* vol. 205, pp. 1679-1688, 2010.

[15] P. Boch and J. C. Nièpce, *Ceramic Materials: Processes, Properties, and Applications*. Wiley, 2010.

[16] M. Bruce A. (2003). *Cooling Issues for Automotive Electronics*. Available: http://www.electronics-cooling.com/2003/08/cooling-issues-for-automotive-electronics/

[17] M. A. Aswad, "Residual Stress and Fracture in High Temperature Ceramics," Doctor of Philosophy, School of Materials, The University of Manchester, Manchester- UK, 2012.

[18] H. Dong, *Surface engineering of light alloys : aluminum, magnesium and titanium Alloys*. Oxford, UK; Boca Raton, FL: Woodhead Publishing ; CRC Press, 2010.

[19] J. F. Shackelford and R. H. Doremus, *Ceramic and Glass Materials: Structure, Properties and Processing*. Springer, 2008.

[20] W. Gitzen, *Alumina as a ceramic material* . Columbus, Ohio: American Ceramic Society, 1970.

[21] Kyocera. (2013). *Electronic fine ceramics* [PDF]. Available: http://americas.kyocera.com/kicc/pdf/Kyocera%20(substrates)%20Electronic%20Fine%20Ceramics.pdf.

[22] R. Jamaati and M. R. Toroghinejad, "Manufacturing of high-strength aluminum/alumina composite by accumulative roll bonding," *Materials Science and Engineering: A,* 2010.

[23] C. Tek, "Thick - film substrates ceramic design guide," ed. USA: TMMA, 2011, p. 16.

[24] Y. El Hafiane, A. Smith, Y. Abouliatim, T. Chartier, L. Nibou, and J. P. Bonnet, "Calcium aluminate cement tapes – Part I: Structural and microstructural characterizations," *Journal of the European Ceramic Society,* vol. 34, 2014.

[25] D. Thomas, P. Abhilash, and M. T. Sebastian, "Casting and characterization of LiMgPO4 glass free LTCC tape for microwave applications," *Journal of the European Ceramic Society,* 2013.

[26] G. Blugan, K. Morawa, S. Koebel, T. Graule, and J. Kuebler, "Development of a tape casting process for making thin layers of Si3N4 and Si3N4 + TiN," *Journal of the European Ceramic Society,* vol. 27, no. 16, pp. 4789-4795, 2007.

[27] A. C. E. Kristoffersson, "Tape Casting of Alumina in Water with an Acrylic Latex Binder," (in English), *Journal of the European Ceramic Society.,* vol. 17, 1997.

[28] M. N. Rahaman, *Ceramic Processing and Sintering*. Taylor & Francis, 2003.

[29] A. B. F. K. M. Tok, "Tape casting of high dielectric ceramic substrates for microelectronics packaging," (in English), *Journal of Materials Engineering and Performance,* vol. 8, no. 4, pp. 469-472, 1999.

[30] J. V. Rushton, "Anodic Oxidation of Aluminium and its Alloys," *Transactions of the IMF,* vol. 14, no. 1, pp. 191-206, 1938.

[31] J. A. Curran, "Plasma electrolytic oxidation for surface protection of aluminium, magnesium and titanium alloys," *Transactions of the IMF,* vol. 89, no. 6, pp. 295-297, 2011.

[32] N. S. a. J. Russ., " Phys. Chem. Soc., vol. 12, no. 1-2, p. 193, 1880."

[33] A. G. a. H. Betz, "Electrolytkondensatoren," *Berlin: Krayn.,* 1937.

[34] G. M. a. G. Markova, "A method of forming anodes of electrolytic condensers," vol. 32, p. 63 1976.

[35] V. E. Gnedenkov Sergej, J. Koval' Sergej, G. E. Chizhikov Roman, L. Sinebrjukhov Sergej, and V. E. Mashtaljar Dmitrij, "Method of plasmaelectrolytic oxidation of metals and alloys," ed, 2012.

[36] F. H. Lu, J. L. Zeng, and H. P. Teng, "Method for forming oxide film by plasma electrolytic oxidation," ed: Google Patents, 2014.

[37] Hisamoto, Jun, Tanaka, Toshiyuki, Yanagawa, and Masahiro, "Al material excellent in thermal crack resistance and corrosion resistance," S. Kabushiki Kaisha Kobe Seiko, Ed., ed, 2000.

[38] J. Sun, W. Qian, W. Qu, and S. Hui, "Pulsed power supply for plasma electrolytic deposition and other processes," ed: Google Patents, 2015.

[39] J. Curran, S. Hutchins, and O. Dunkin, "Corrosion and erosion-resistant mixed oxide coatings for the protection of chemical and plasma process chamber components," ed: Google Patents, 2014.

[40] A. Yerokhin, "Method of forming a bioactive coating," ed: Google Patents, 2014.

[41] L. K. Mirelman, J. A. Curran, and T. W. Clyne, "The production of anatase-rich photoactive coatings by plasma electrolytic oxidation," *Surface and Coatings Technology,* vol. 207, no. 0, pp. 66-71, 2012.

[42] A. L. Y. L O Snizhko, , N L Gurevina, A Leyland, A Pilkington and A Matthews "Discharge characterization in plasma electrolytic oxidation of aluminium," (in English), *Journal of Physics D: Applied Physics,* 2003.

[43] S. M. K. Abuali Galedari, S. M., "Effect of pulse frequency on microstructure and surface properties of Ck45 steel treated by plasma electrolysis method," *Journal of Alloys and Compounds,* vol. 551, no. 0, pp. 415-421, 2013.

[44] M. M. S. Al Bosta, K.-J. Ma, and H.-H. Chien, "Effect of Anodic Current Density on Characteristics and Low Temperature IR Emissivity of Ceramic Coating on Aluminium 6061 Alloy Prepared by Microarc Oxidation," (in English), *Journal of Ceramics Journal of Ceramics,* vol. 2013, no. 2, pp. 1-14, 2013.

[45] G. N. Alisch, D. Lampke, T., "Simultaneous plasma-electrolytic anodic oxidation (PAO) of Al–Mg compounds," *Surface and Coatings Technology,* vol. 206, pp. 1085-1090, 2011.

[46] A. Y. L.Snizhko, A. Pilkington, N. Gurevina, D. Misnyankin, A. Leyland , A. Matthews, "Anodic processes in plasma electrolytic oxidation of aluminium in alkaline solutions," *Electrochimica Acta,* vol. 49, pp. 2085-2095, 2004.

[47] C. L. F. Walsh, R. Wood, K. Stevens, J. Archer, A. Poeton & A. Ryder,, "Plasma electrolytic oxidation (PEO) for production of anodised coatings on lightweight metal (Al, mg, Ti) alloys," (in English), 2009.

[48] A. G. Rakoch, I. V. Bardin, V. L. Kovalev, and T. G. Avanesyan, "Microarc oxidation of light constructional alloys: Part 1. Main notions on the microarc oxidation of light constructional alloys," (in English), 2013.

[49] A. D. B. ABDULLAH, "Mechanical properties of dissimilar aluminium-based alloy Joints by MIG welding," Academic, 2012.

[50] C. S. C. Dunleavy, J. A. Clyne, T. W., "Plasma electrolytic oxidation of aluminium networks to form a metal-cored ceramic composite hybrid material," *Composites Science and Technology,* 2011.

[51] F. Jaspard-Mécuson *et al.*, "Tailored aluminium oxide layers by bipolar current adjustment in the Plasma Electrolytic Oxidation (PEO) process," *Surface and Coatings Technology,* vol. 201, no. 21, pp. 8677-8682, 2007.

[52] C. E. V.-R. Barchiche, D. Rocca, E., "A better understanding of PEO on Mg alloys by using a simple galvanostatic electrical regime in a KOH–KF–Na3PO4 electrolyte," *Surface and Coatings Technology,* vol. 205, no. 17–18, pp. 4243-4248, 2011.

[53] M. E. Achhab and K. Schierbaum, "Structure and Hydrogen Sensing Properties of Plasma Electrochemically Oxidized Titanium Foils," *Procedia Engineering,* 2012.

[54] I. Apachitei, B. Lonyuk, L. E. Fratila-Apachitei, J. Zhou, and J. Duszczyk, "Fatigue response of porous coated titanium biomedical alloys," *Scripta Materialia,* 2009.

[55] A. L. Yerokhin *et al.*, "Oxide ceramic coatings on aluminium alloys produced by a pulsed bipolar plasma electrolytic oxidation process," *Surface and Coatings Technology,* vol. 199, no. 2, pp. 150-157, 2005.

[56] L. Zhen-Wei and D. Shi-Chun, "Effect of Anode Pulse-Width on the Microstructure and Wear Resistance of Microarc Oxidation Coatings," *Metals,* vol. 7, no. 7, p. 243, 2017.

[57] R. O. Hussein, X. Nie, and D. O. Northwood, "Influence of process parameters on electrolytic plasma discharging behaviour and aluminum oxide coating microstructure," *Surface and Coatings Technology,* vol. 205, no. 6, pp. 1659-1667, 2010.

[58] Y. Guangliang, L. Xianyi, B. Yizhen, C. Haifeng, and J. Zengsun, "The effects of current density on the phase composition and microstructure properties of micro-arc oxidation coating," *Journal of Alloys and Compounds,* vol. 345, no. 1–2, pp. 196-200, 2002.

[59] Z. Li and S. Di, "Preparation and properties of micro-arc oxidation self-lubricating composite coatings containing paraffin," *Journal of Alloys and Compounds,* vol. 719, no. Supplement C, pp. 1-14, 2017.

[60] R. H. U. Khan, A. L. Yerokhin, T. Pilkington, A. Leyland, and A. Matthews, "Residual stresses in plasma electrolytic oxidation coatings on Al alloy produced by pulsed unipolar current," *Surface and Coatings Technology,* vol. 200, no. 5–6, pp. 1580-1586, 2005.

[61] J. A. Curran and T. W. Clyne, "Porosity in plasma electrolytic oxide coatings," *Acta Materialia,* vol. 54, no. 7, pp. 1985-1993, 2006.

[62] J. A. U. o. C. Curran, *Thermal and mechanical properties of plasma electrolytic oxide coatings*. 2006.

[63] U. Malayoglu, K. C. Tekin, U. Malayoglu, and S. Shrestha, "An investigation into the mechanical and tribological properties of plasma electrolytic oxidation and hard-anodized coatings on 6082 aluminum alloy," *Materials Science and Engineering: A,* vol. 528, pp. 7451-7460, 2011.

[64] X. A. Nie, "Thickness effects on the mechanical properties of micro-arc disch arge oxide coatings on aluminium alloys," (in English), *SURFACE AND COATINGS TECHNOLOGY,* vol. 116-119, no. 3, pp. 1055-1060, 1999.

[65] C. Wei, Chen, "A Novel Method of Inner Surface Modification by Plasma Electrolytic Oxidation," *National High Technology Research,* 2002.

[66] S. Shrestha, A. Merstallinger, D. Sickert, and B. D. Dunn, "Some preliminary evaluations of black coating on aluminium AA2219 alloy produced by plasma electrolytic oxidation (PEO) process for space applications," (in English), *EUROPEAN SPACE AGENCY -PUBLICATIONS- ESA SP,* vol. 540, pp. 57-66, 2003.

[67] J. Liu, W. Zhang, H. Zhang, X. Hu, and J. Zhang, "Effect of Microarc Oxidation Time on Electrochemical Behaviors of Coated Bio-compatible Magnesium Alloy," *Materials Today: Proceedings,* vol. 1, no. 1, pp. 70-81, 2014.

[68] K. Venkateswarlu, J. Hari, D. Sreekanth, M. Sandhyarani, A. Bose, and N. Rameshbabu, "Effect of Micro Arc Oxidation Treatment Time on In-Vitro Corrosion Characteristics of Titania Films on Cp Ti," *International Journal of Bioscience, Biochemistry and Bioinformatics,* vol. 2, no. 6, p. 421, 2012.

[69] E. Matykina, A. Berkani, P. Skeldon, and G. E. Thompson, "Real-time imaging of coating growth during plasma electrolytic oxidation of titanium," *Electrochimica Acta,* vol. 53, no. 4, pp. 1987-1994, 2007.

[70] B.-H. A. Dong-Gun Lee, Uk-Rae Cho, "Effects of time variation on formation of oxide layers of Al7075 aluminum alloy by Electrolytic plasma processing (EPP)," presented at the Fracture & Strength of Solids, Jeju, Korea, 2013.

[71] J. B. Bajat, R. Vasilić, S. Stojadinović, and V. Mišković-Stanković, "Corrosion Stability of Oxide Coatings Formed by Plasma Electrolytic Oxidation of Aluminum: Optimization of Process Time," vol. 69, no. 7, pp. 693-702, 2013.

[72] J. G. Miao, R. Wu, Q. R. Chen, K. D. Hao, and Z. L. Wei, "Effects of Electrolyte Parameters on Properties of Ceramic Coatings Formed on Aluminum Alloy 7075 by Plasma Electrolytic Oxidation," *Advanced Materials Research,* vol. 668-668, pp. 875-879, 2013.

[73] I. V. R. Lukiyanchuk, V. S. Tyrina, L. M. Chernykh, I. V., "Plasma electrolytic oxide coatings on valve metals and their activity in CO oxidation," *Applied Surface Science,* 2009.

[74] K. Wang, B.-H. Koo, C.-G. Lee, Y.-J. Kim, S.-H. Lee, and E. Byon, "Effects of electrolytes variation on formation of oxide layers of 6061 Al alloys by plasma electrolytic oxidation," *Transactions of Nonferrous Metals Society of China,* vol. 19, no. 4, pp. 866-870, 2009.

[75] Y. J. Liu, J. Y. Xu, C. Gao, J. C. Zhang, X. H. Chen, and W. Lin, "Effects of different electrolyte systems on the formation of micro-arc oxidation ceramic coatings of 6061 aluminum alloy," (in English), *Rev. Adv. Mater. Sci. Reviews on Advanced Materials Science,* vol. 33, no. 2, pp. 126-130, 2013.

[76] A. Polat, M. Makaraci, and M. Usta, "Influence of sodium silicate concentration on structural and tribological properties of microarc oxidation coatings on 2017A aluminum alloy substrate," *Journal of Alloys and Compounds,* vol. 504, no. 2, pp. 519-526, 2010.

[77] A. Fattah-Alhosseini, M. Vakili-Azghandi, and M. Keshavarz, "Influence of Concentrations of KOH and Na 2 SiO 3 Electrolytes on the Electrochemical Behavior of Ceramic Coatings on 6061 Al Alloy Processed by Plasma Electrolytic Oxidation," *Acta Metall. Sin. (Engl. Lett.),* vol. 29, no. 3, pp. 274-281, 2016.

[78] L. Jung-Hyung and K. Seong-Jong, "Effects of silicate ion concentration on the formation of ceramic oxide layers produced by plasma electrolytic oxidation on Al alloy," (in English), *Japanese Journal of Applied Physics,* vol. 56, no. 1S, 2017.

[79] G. Lv *et al.*, "Characteristic of ceramic coatings on aluminum by plasma electrolytic oxidation in silicate and phosphate electrolyte," *Applied Surface Science,* vol. 253, no. 5, pp. 2947-2952, 2006.

[80] B.-H. Ahn *et al.*, "Effect of Na2SiO3 concentration on the properties of AZ31 magnesium alloy prepared by electrolytic plasma processing," *Electronic Materials Letters,* vol. 9, no. 6, pp. 813-815, 2013.

[81] M. M. S. Al Bosta and K.-J. Ma, "Influence of electrolyte temperature on properties and infrared emissivity of MAO ceramic coating on 6061 aluminum alloy," *Infrared Physics & Technology,* vol. 67, pp. 63-72, 2014.

[82] D. S. Doolabi, M. Ehteshamzadeh, and S. M. M. Mirhosseini, "Effect of NaOH on the Structure and Corrosion Performance of Alumina and Silica PEO Coatings on

Aluminum," *Journal of Materials Engineering and Performance,* journal article vol. 21, no. 10, pp. 2195-2202, 2012.

[83] I. J. Hwang, D. Y. Hwang, Y. M. Kim, B. Yoo, and D. H. Shin, "Formation of uniform passive oxide layers on high Si content Al alloy by plasma electrolytic oxidation," *Journal of Alloys and Compounds,* vol. 504, Supplement 1, no. 0, pp. S527-S530, 2010.

[84] D. Salehi Doolabi, M. Ehteshamzadeh, and S. M. M. Mirhosseini, "Effect of NaOH on the structure and corrosion performance of alumina and silica PEO coatings on aluminum," (in English), *J Mater Eng Perform Journal of Materials Engineering and Performance,* vol. 21, no. 10, pp. 2195-2202, 2012.

[85] K. Du, X. Guo, Q. Guo, F. Wang, and Y. Tian, "A monolayer PEO coating on 2024 Al alloy by transient self-feedback control mode," *Materials Letters,* vol. 91, no. 0, pp. 45-49, 2013.

[86] A. Polat, M. Makaraci, and M. Usta, "Influence of sodium silicate concentration on structural and tribological properties of microarc oxidation coatings on 2017A aluminum alloy substrate," (in English), *Journal of Alloys and Compounds Journal of Alloys and Compounds,* vol. 504, no. 2, pp. 519-526, 2010.

[87] Y. Guan, Y. Xia, and G. Li, "Growth mechanism and corrosion behavior of ceramic coatings on aluminum produced by autocontrol AC pulse PEO," (in English), *Surface and Coatings Technology Surface and Coatings Technology,* vol. 202, no. 19, pp. 4602-4612, 2008.

[88] "Residual stresses in plasma electrolytic oxidation coatings on Al alloy produced by pulsed unipolar current," (in Undetermined).

[89] H. Duan, C. Yan, and F. Wang, "Effect of electrolyte additives on performance of plasma electrolytic oxidation films formed on magnesium alloy AZ91D," *Electrochimica Acta,* vol. 52, no. 11, pp. 3785-3793,2007.

[90] X. Guo, K. Du, Q. Guo, Y. Wang, C. Wang, and F. Wang, "Experimental study of densification effect on Al 2024 plasma electrolytic oxidation film," (in English), *Int.J.Electrochem.Sci. International Journal of Electrochemical Science,* vol. 11, no. 9, pp. 7960-7975, 2016.

[91] M. M. S. A. Bosta and K.-J. Ma, "Suggested mechanism for the MAO ceramic coating on aluminium substrates using bipolar current mode in the alkaline silicate electrolytes," *Applied Surface Science,* no. 0.

[92] W. H. Gitzen and S. American Ceramic, *Alumina as a ceramic material*. Columbus, Ohio: American Ceramic Society, 1970.

[93] H. S. S. S. Santos, S.P. Toledo, "Standard transition aluminas. Electron microscopy studies," (in English), vol. Vol. 3, pp. 104-114, 2000.

[94] J. Congleton, N. J. Petch, and S. A. Shiels, "The brittle fracture of alumina below 1000°C," *Philosophical Magazine,* vol. 19, no. 160, pp. 795-807, 1969.

[95] J. Congleton and N. Petch, "Dislocation movement in the brittle fracture of alumina," (in English), *Acta Metallurgica Acta Metallurgica,* vol. 14, no. 10, pp. 1179-1182, 1966.

[96] R. Hussein, D. O. Northwood, and X. Nie, *Coating growth behavior during the plasma electrolytic oxidation process*. 2010.

[97] G. G.-H. Wei-Chao, Lv Huan, Chen Guang-Liang, Chen, "Investigation of morphology and composition of plasma electrolytic oxidation coatings in systems of Na2SiO3–

NaOH and (NaPO3)6–NaOH," *Journal of Materials Processing Technology,* vol. 182, pp. 28-33, 2007.

[98] S. Z. Liu, Jianmin Wang,, "Preparation and Characterization of Plasma Electrolytic Oxidation Coating on 5005 Aluminum Alloy with Red Mud as an Electrolyte Additive," *Metallurgical and Materials Transactions B,* vol. 48, pp. 2223-2231, 2017.

[99] J. A. Curran and T. W. Clyne, "Thermo-physical properties of plasma electrolytic oxide coatings on aluminium," *Surface and Coatings Technology,* vol. 199, no. 2–3, pp. 168-176, 2005.

[100] X. Nie, E. I. Meletis, J. C. Jiang, A. Leyland, A. L. Yerokhin, and A. Matthews, "Abrasive wear/corrosion properties and TEM analysis of Al2O3 coatings fabricated using plasma electrolysis," *Surface and Coatings Technology,* vol. 149, no. 2, pp. 245-251, 2002/01/15/ 2002.

[101] C. B. Wei, X. B. Tian, S. Q. Yang, X. B. Wang, R. K. Y. Fu, and P. K. Chu, "Anode current effects in plasma electrolytic oxidation," *Surface and Coatings Technology,* vol. 201, pp. 5021-5024, 2007.

[102] Y. Guan, Y. Xia, and G. Li, "Growth mechanism and corrosion behavior of ceramic coatings on aluminum produced by autocontrol AC pulse PEO," *Surface and Coatings Technology,* vol. 202, pp. 4602-4612, 2008.

[103] C. S. Dunleavy, I. O. Golosnoy, J. A. Curran, and T. W. Clyne, "Characterisation of discharge events during plasma electrolytic oxidation," *Surface and Coatings Technology,* vol. 203, pp. 3410-3419, 2009.

[104] H. Duan, Y. Li, Y. Xia, and S. Chen, *Transient Voltage-Current Characteristics: New Insights into Plasma Electrolytic Oxidation Process of Aluminium Alloy*. 2012, pp. 7619-7630.

[105] T. Young, "Optical Emission Spectroscopy (OES)," ed, 2014, pp. 767-767.

[106] H. G. Mecuson F, Czerwiec T, Belmonte T, Dujardin L, *Abstracts of ICEPAM (Oslo, Norway),* 2004.

[107] S. J. Moon, Y., "Generation mechanism of microdischarges during plasma electrolytic oxidation of Al in aqueous solutions," *Corrosion Science,* vol. 51, no. 7, pp. 1506-1512, 2009.

[108] G. Y. I. Kharitonov D Yu, Novikov G I and Fridman A A "On the Mechanism of Impulse Electrolytic Spark Oxidation of Aluminium in Concentrated Sulphuric Acid, (Moscow: TcNIIAtomInform)," 1988.

[109] R. O. Hussein, X. Nie, D. O. Northwood, A. Yerokhin, and A. Matthews, "Spectroscopic study of electrolytic plasma and discharging behaviour during the plasma electrolytic oxidation (PEO) process," (in English), *J Phys D Journal of Physics D: Applied Physics,* vol. 43, no. 10, 2010.

[110] X. Yang, L. Chen, Y. Qu, R. Liu, K. Wei, and W. Xue, "Optical emission spectroscopy of plasma electrolytic oxidation process on 7075 aluminum alloy," *Surface and Coatings Technology,* vol. 324, pp. 18-25, 2017.

[111] N. V. M. V.N. Malyshev, "Proceedings of Russian Conference 'Anode'88',," *KAI, Kazan, 1988, p. 88, in Russian.*

[112] S. Durdu and M. Usta, "Characterization and mechanical properties of coatings on magnesium by micro arc oxidation," *Applied Surface Science,* vol. 261, pp. 774-782, 2012.

[113] S. Durdu, S. Bayramoğlu, A. Demirtaş, M. Usta, and A. H. Üçışık, "Characterization of AZ31 Mg Alloy coated by plasma electrolytic oxidation," *Vacuum,* vol. 88, pp. 130-133, 2013.

[114] R. Morrell, "Mechanical properties of engineering ceramics: Test bars versus components," *Materials Science & Engineering A,* vol. 109, no. 1-2, pp. 131-137, 1989.

[115] W. D. Z. L. Y. C. R. Xue, "Analysis of Phase Distribution for Ceramic Coatings Formed by Microarc Oxidation on Aluminum Alloy," (in English), *JACE Journal of the American Ceramic Society,* vol. 81, no. 5, pp. 1365-1368, 1998.

[116] C.-H. Hsu, H.-P. Teng, and F.-H. Lu, "Effects of addition of Al(NO3)3 to electrolytes on alumina coatings by plasma electrolytic oxidation," *Surface and Coatings Technology,* vol. 205, pp. 3677-3682, 2011.

[117] H. Wu *et al.*, "Ultra-hard ceramic coatings fabricated through microarc oxidation on aluminium alloy," *Applied Surface Science,* vol. 252, no. 5, pp. 1545-1552, 2005.

[118] D. Hasselman and R. Spriggs, "Kinetics of the Gamma-to-Alpha Alumina Phase Transformation," *Journal of the American Ceramic Society,* vol. 54, p. 412, 1971.

[119] R. W. James, *The optical principles of diffraction of x-rays*. Woodbridge: Ox Bow Press, 1993.

[120] W. C. Oliver and G. M. Pharr, "Measurement of hardness and elastic modulus by instrumented indentation: Advances in understanding and refinements to methodology," *J. Mater. Res.,* vol. 19, no. 01, pp. 3-20, 2004.

[121] E. J. F. Dickinson, H. Ekström, and E. Fontes, "COMSOL Multiphysics®: Finite element software for electrochemical analysis. A mini-review," *Electrochemistry Communications,* vol. 40, pp. 71-74, 2014.

[122] Z. Wang, H. Hu, and X. Nie, "Preparation and characterization of highly flexible Al hybrid composite," (in English), *J. Nanomater. Journal of Nanomaterials,* vol. 2015, 2015.

[123] C. S. Dunleavy, J. A. Curran, and T. W. Clyne, "Self-similar scaling of discharge events through PEO coatings on aluminium," *Surface and Coatings Technology,* vol. 206, no. 6, pp. 1051-1061, 2011.

[124] A. I. Sonova and O. P. Terleeva, "Morphology, structure, and phase composition of microplasma coatings formed on Al-Cu-Mg alloy," *Protection of Metals,* journal article vol. 44, no. 1, pp. 65-75, 2008.

[125] C. S. Dunleavy, J. A. Curran, and T. W. Clyne, "Time dependent statistics of plasma discharge parameters during bulk AC plasma electrolytic oxidation of aluminium," *Applied Surface Science,* vol. 268, no. 0, pp. 397-409, 2013.

[126] J. Martin *et al.*, "Effects of electrical parameters on plasma electrolytic oxidation of aluminium," *Surface and Coatings Technology,* vol. 221, no. 0, pp. 70-76,2013.

[127] R. O. Hussein, X. Nie, and D. O. Northwood, "An investigation of ceramic coating growth mechanisms in plasma electrolytic oxidation (PEO) processing," *Electrochimica Acta,* vol. 112, no. 0, pp. 111-119, 2013.

[128] V. Dehnavi, B. L. Luan, X. Y. Liu, D. W. Shoesmith, and S. Rohani, "Correlation between plasma electrolytic oxidation treatment stages and coating microstructure on aluminum under unipolar pulsed DC mode," *Surface & Coatings Technology,* vol. 269, pp. 91-99, 2015.

[129] E. V. Parfenov, A. L. Yerokhin, and A. Matthews, "Frequency response studies for the plasma electrolytic oxidation process," *Surface and Coatings Technology,* vol. 201, no. 21, pp. 8661-8670, 2007.
[130] E. V. Parfenov, A. Yerokhin, and A. Matthews, "Small signal frequency response studies for plasma electrolytic oxidation," *Surface and Coatings Technology,* vol. 203, no. 19, pp. 2896-2904, 2009.
[131] C. Y. Chao, "A Point Defect Model for Anodic Passive Films," (in English), *J. Electrochem. Soc. Journal of The Electrochemical Society,* vol. 129, no. 9, p. 1874, 1982.
[132] T. Wei, F. Yan, and J. Tian, "Characterization and wear- and corrosion-resistance of microarc oxidation ceramic coatings on aluminum alloy," *Journal of Alloys and Compounds,* vol. 389, no. 1–2, pp. 169-176, 2005.
[133] L. Rama Krishna, K. R. C. Somaraju, and G. Sundararajan, "The tribological performance of ultra-hard ceramic composite coatings obtained through microarc oxidation," *Surface and Coatings Technology,* vol. 163–164, no. 0, pp. 484-490, 2003.
[134] N. P. S. Narayanan, S. Lee, Min Ho, "Surface modification of magnesium and its alloys for biomedical applications.," (in English), 2015.
[135] "Standard transition aluminas. Electron microscopy studies," (in English), 2000.
[136] W. Xue, Z. Deng, R. Chen, and T. Zhang, "Growth regularity of ceramic coatings formed by microarc oxidation on Al–Cu–Mg alloy," *Thin Solid Films,* vol. 372, no. 1–2, pp. 114-117, 2000.
[137] L. A. S. V. Chernenko, I. Papanova, "Coating by Anodic Spark Electrolysis," *Khimiya, Leningrad, (in Russian, ISBN 5-7245-0588-6).* 1991.
[138] W.-C. Gu, G.-H. Lv, H. Chen, G.-L. Chen, W.-R. Feng, and S.-Z. Yang, "Characterisation of ceramic coatings produced by plasma electrolytic oxidation of aluminum alloy," *Materials Science and Engineering: A,* vol. 447, no. 1–2, pp. 158-162, 2007.
[139] Z. Gorgin Karaji, R. Hedayati, B. Pouran, I. Apachitei, and A. A. Zadpoor, "Effects of plasma electrolytic oxidation process on the mechanical properties of additively manufactured porous biomaterials," *Materials Science and Engineering: C,* vol. 76, no. Supplement C, pp. 406-416, 2017.
[140] R. Morgenstern, M. Sieber, T. Grund, T. Lampke, and B. Wielage, "Plasma electrolytic oxidation of titanium aluminides," *Plasma electrolytic oxidation of Titanium Aluminides,* vol. 118, no. 1, p. 012025, 2016.
[141] R. Kamal Jayaraj, S. Malarvizhi, and V. Balasubramanian, "Optimizing the micro-arc oxidation (MAO) parameters to attain coatings with minimum porosity and maximum hardness on the friction stir welded AA6061 aluminium alloy welds," (in English), *Defence Technology Defence Technology,* 2017.
[142] M. JK, *Proc Phys Soc 1950;B63:2–11*.
[143] S. Bisgaard and D. M. Steinberg, "The Design and Analysis of 2k-p× s Prototype Experiments," *Technometrics,* vol. 39, no. 1, pp. 52-62, 1997.
[144] D. surf. (2014, 17/06/2014). *Surface imaging metrology software*. Available: http://www.digitalsurf.fr/en/mntkey.html
[145] Blogfast. (2011, 11/08/2015). *The art and science of amateur experimentalism*. Available: http://www.sciencemadness.org/talk/viewthread.php?tid=320

[146] G. Wirtz, U. Univ. of Illinois, and M. Conference: 78. annual meeting of the American Ceramic Society, "Mechanism of anodic spark deposition," (in English), *Am. Ceram. Soc. Bull.,* vol. 56:6, pp. 563-566, 1977.

[147] N. C. Wardlaw and M. McKellar, "Mercury porosimetry and the interpretation of pore geometry in sedimentary rocks and artificial models," (in English), *PTEC</cja:jid> Powder Technology,* vol. 29, no. 1, pp. 127-143, 1981.

[148] V. Dehnavi, B. L. Luan, X. Y. Liu, D. W. Shoesmith, and S. Rohani, "Correlation between plasma electrolytic oxidation treatment stages and coating microstructure on aluminum under unipolar pulsed DC mode," *Surface and Coatings Technology,* vol. 269, pp. 91-99, 2015.

[149] S. M. Shrestha, A. Sickert, D. Dunn, B. D., "Some preliminary evaluations of black coating on aluminium AA2219 alloy produced by plasma electrolytic oxidation (PEO) process for space applications," (in English), *ESA SP,* vol. 540, pp. 57-66, 2003.

[150] A. Y. L. Snizhko, A. Pilkington, N. Gurevina, D. Misnyankin, A. Leyland , A. Matthews, "Anodic processes in plasma electrolytic oxidation of aluminium in alkaline solutions," *Electrochimica Acta,* vol. 49, no. 13, pp. 2085-2095, 2004.

[151] F. C. Walsh *et al.*, "Plasma electrolytic oxidation (PEO) for production of anodised coatings on lightweight metal (Al, mg, Ti) alloys," (in English), *Trans Inst Met Finish Transactions of the Institute of Metal Finishing,* vol. 87, no. 3, pp. 122-135, 2009.

[152] L. Wang, W. Fu, S. Wang, and J. Li, "Plasma electrolytic oxidation coatings in KOH electrolyte and its discharge characteristics," *Journal of Alloys and Compounds,* vol. 594, pp. 27-31, 2014.

[153] L. Rama Krishna, K. R. C. Somaraju, and G. Sundararajan, "The tribological performance of ultra-hard ceramic composite coatings obtained through microarc oxidation," *Surface and Coatings Technology,* vol. 163–164, pp. 484-490, 2003.

[154] R. McPherson, "Formation of metastable phases in flame- and plasma-prepared alumina," (in English), *Journal of Materials Science,* vol. 8, no. 6, pp. 851-858, 1973.

[155] D. Apperley, "Solid-state NMR spectra were obtained at the EPSRC UK National Solid-state NMR Service at Durham," Durham University (UK) 1225, 2015.

[156] H. Li and J. Zhang, "Preparation of microarc oxidation ceramic layer on Ti6Al4V titanium alloy and its oxidation resistance property," (in English), *INTERNATIONAL HEAT TREATMENT AND SURFACE ENGINEERING,* vol. 8, no. 2, pp. 51-54, 2014.

[157] M. M. S. Al Bosta, K.-J. Ma, and H.-H. Chien, "The effect of MAO processing time on surface properties and low temperature infrared emissivity of ceramic coating on aluminium 6061 alloy," (in English), *INFPHY Infrared Physics and Technology,* vol. 60, pp. 323-334, 2013.

[158] D. C. Montgomery and E. A. Peck, *Introduction to linear regression analysis*. New York: Wiley, 1982.

[159] N. A. Weiss and M. J. Hassett, *Introductory statistics*. Reading, Mass.: Addison-Wesley Pub. Co., 1982.

[160] X. Zhan, X. Liang, G. Xu, and L. Zhou, "Influence of plant root morphology and tissue composition on phenanthrene uptake: Stepwise multiple linear regression analysis," (in English), *Environmental Pollution Environmental Pollution,* vol. 179, no. 5, pp. 294-300, 2013.

[161] A. L. Yerokhin, A. A. Voevodin, V. V. Lyubimov, J. Zabinski, and M. Donley, "Plasma electrolytic fabrication of oxide ceramic surface layers for tribotechnical purposes on

aluminium alloys," *Surface and Coatings Technology,* vol. 110, no. 3, pp. 140-146, 12/10/ 1998.

[162] M. Javidi and H. Fadaee, "Plasma electrolytic oxidation of 2024-T3 aluminum alloy and investigation on microstructure and wear behavior," *Applied Surface Science,* 2013.

[163] M. Schneider, K. Kremmer, and S. Höhn, "Corrosion protection of thickness reduced plasma electrolytic layers on AZ31," (in English), *MACO Materials and Corrosion,* vol. 67, no. 9, pp. 921-928, 2016.

[164] S.-I. Pyun and S.-M. Moon, "Corrosion mechanism of pure aluminium in aqueous alkaline solution," *Journal of Solid State Electrochemistry,* journal article vol. 4, no. 5, pp. 267-272, 2000.

[165] V. P. Parkhutik, J. M. Martinez-Duart, J. Perrière, A. Climent, Y. E. Makushok, and J. M. Albella, "Electrochemical and plasma anodic oxidation of CdxHg1 − xTe," *Thin Solid Films,* vol. 200, no. 1, pp. 129-138, 1991.

[166] P. Deepa and R. Padmalatha, "Corrosion behaviour of 6063 aluminium alloy in acidic and in alkaline media," *Arabian Journal of Chemistry*.

[167] Z. Han, J. Tian, J. Lao, G. Li, and J. Dai, "Effects of thickness and substrate on the mechanical properties of hard coatings," (in English), *Journal of Coatings Technology and Research,* vol. 1, no. 4, pp. 337-341, 2004.

[168] A. L. H. W. S. X. Nie, A. Yerokhin, S.J. Dowey, A. Matthews, "Thickness effects on the mechanical properties of micro-arc discharge oxide coatings on aluminium alloys," (in English), *Surface and Coatings Technology,* pp. 1055-1060, 1999.

[169] C. Xiaozhou, W. Chao, X. Xiangxin, and C. Gongjin, "Effect of ti addition on the residual aluminium content and mechanical properties of the B4C-al composites produced by vacuum infiltration," (in English), *Arch. Metall. Mater. Archives of Metallurgy and Materials,* 2015.

[170] D. V. Heyd and D. A. Harrington, "Platinum oxide growth kinetics for cyclic voltammetry," *Journal of Electroanalytical Chemistry,* vol. 335, no. 1, pp. 19-31, 1992.

[171] B. Liu *et al.*, "The redox behavior of vanadium in alkaline solutions by cyclic voltammetry method," *Electrochimica Acta,* vol. 76, pp. 262-269, 2012/08/01/ 2012.

[172] O. Makhotkina and P. A. Kilmartin, "The use of cyclic voltammetry for wine analysis: Determination of polyphenols and free sulfur dioxide," *Analytica Chimica Acta,* vol. 668, no. 2, pp. 155-165, 2010.

[173] R. L. Doyle, I. J. Godwin, M. P. Brandon, and M. E. G. Lyons, "Redox and electrochemical water splitting catalytic properties of hydrated metal oxide modified electrodes," *Physical Chemistry Chemical Physics,* 10.1039/C3CP51213D vol. 15, no. 33, pp. 13737-13783, 2013.

[174] H. Duan, Y. Xia, S. Chen, and Y. Li, "Transient voltage-current characteristics: New insights into plasma electrolytic oxidation process of aluminium alloy," (in English), *Int.J.Electrochem.Sci. International Journal of Electrochemical Science,* vol. 7, no. 8, pp. 7619-7630, 2012.

[175] S. Ikonopisov, *Electrochimica Acta,* vol. 20, no. 783, 1975.

[176] R. K. Nigam, K. C. Singh, and S. Maken, "Electrical breakdown phenomenon and electronic conduction during the anodic growth of Nb 2 O 5," *Can. J. Chem.,* vol. 65, no. 3, pp. 512-517, 1987.

[177] G. J. Williams and J. G. Drummond, "Preparation of Large Sections for the Microscopical Study of Paper Structure," (in English), *JOURNAL OF PULP AND PAPER SCIENCE,* vol. 26, pp. 188-193, 2000.
[178] R. Allem, "Characterization of Paper Coatings by Scanning Electron Microscopy and Image Analysis," (in English), *JOURNAL OF PULP AND PAPER SCIENCE,* vol. 24, no. 10, pp. 329-336, 1998.
[179] G. Chinga, & Norges Teknisk-Naturvitenskapelige Universitet, Fakultet For Naturvitenskap Og Teknologi, Institutt For Kjemisk Prosessteknologi. (2002). Structural Studies of LWC Paper Coating Layers Using SEM and Image Analysis Techniques.
[180] X. Ma, C. Blawert, D. Höche, M. L. Zheludkevich, and K. U. Kainer, "Investigation of electrode distance impact on PEO coating formation assisted by simulation," *Applied Surface Science,* vol. 388, pp. 304-312, 2016.
[181] R. R. Nevyantseva, S. A. Gorbatkov, E. V. Parfenov, and A. A. Bybin, "The influence of vapor–gaseous envelope behavior on plasma electrolytic coating removal," *Surface and Coatings Technology,* vol. 148, no. 1, pp. 30-37, 2001.
[182] E. V. Parfenov, R. G. Farrakhov, V. R. Mukaeva, A. V. Gusarov, R. R. Nevyantseva, and A. Yerokhin, "Electric field effect on surface layer removal during electrolytic plasma polishing," *Surface & Coatings Technology,* vol. 307, pp. 1329-1340, 2016.
[183] W. Zimmerman, Multiphysics Modeling with Finite Element Methods, 2006.
[184] W.-C. Gu, G.-H. Lv, H. Chen, G.-L. Chen, W.-R. Feng, and S.-Z. Yang, "PEO protective coatings on inner surface of tubes," *Surface and Coatings Technology,* vol. 201, no. 15, pp. 6619-6622, 4/23/ 2007.
[185] E. Dickinson, "Theory of Current Distribution," in *Comsol web log [online]*, ed, 2014.
[186] R. O. Hussein, D. O. Northwood, and X. Nie, "The effect of processing parameters and substrate composition on the corrosion resistance of plasma electrolytic oxidation (PEO) coated magnesium alloys," *Surface and Coatings Technology,* vol. 237, no. 0, pp. 357-368, 2013.
[187] K. Popov, P. Zivkovic, and N. Nikolic, "A mathematical model of the current density distribution in electrochemical cells," (in English), *J. Serb. Chem. Soc. Journal of the Serbian Chemical Society,* vol. 76, no. 6, pp. 805-822, 2011.
[188] V. S. Bagockij, V. S. Bagockij, V. S. Bagockij, and V. S. Bagockij, *Fundamentals of electrochemistry*. Hoboken, N.J: John Wiley, 2006.
[189] J. O. Dukovic, "Computation of current distribution in electrodeposition, a review," (in No Linguistic Content), *IBM J. Res. & Dev. IBM Journal of Research and Development,* vol. 34, no. 5, pp. 693-705.
[190] R. Arrabal, E. Matykina, P. Skeldon, and G. E. Thompson, "Coating formation by plasma electrolytic oxidation on ZC71/SiC/12p-T6 magnesium metal matrix composite," *Applied Surface Science,* vol. 255, no. 9, pp. 5071-5078, 2009.
[191] S. V. Gnedenkov *et al.*, "Formation and electrochemical properties of the superhydrophobic nanocomposite coating on PEO pretreated Mg–Mn–Ce magnesium alloy," *Surface and Coatings Technology,* vol. 232, no. 0, pp. 240-246, 2013.
[192] P. Huang, K.-W. Xu, and Y. Han, "Preparation and apatite layer formation of plasma electrolytic oxidation film on titanium for biomedical application," *Materials Letters,* vol. 59, no. 2–3, pp. 185-189, 2005.

[193] P. Zhang, X. Nie, H. Henry, and J. Zhang, "Preparation and tribological properties of thin oxide coatings on an Al383/SiO2 metallic matrix composite," *Surface and Coatings Technology,* vol. 205, no. 6, pp. 1689-1696, 2010.

[194] Y. S. Zou, K. Zhou, Y. F. Wu, H. Yang, K. Cang, and G. H. Song, "Structure, mechanical and tribological properties of diamond-like carbon films on aluminum alloy by arc ion plating," *Vacuum,* vol. 86, no. 8, pp. 1141-1146, 2012.

[195] C. T. J. Low, E. P. L. Roberts, and F. C. Walsh, "Numerical simulation of the current, potential and concentration distributions along the cathode of a rotating cylinder Hull cell," *Electrochimica Acta,* vol. 52, no. 11, pp. 3831-3840, 2007.

[196] U. M. F. Lima, and H. Reinecke, "Simulation of Current Density for Electroplating on Silicon Using a Hull Cell," *Conference: 2012 Comsol Conference in Milan,* October 2012.

[197] M.-H. Wang, "Effect of Electrode Shape on Impedance of Single HeLa Cell: A COMSOL Simulation," (in English), *Effect of Electrode Shape on Impedance of Single HeLa Cell: A COMSOL Simulation,* 2015. BioMed Research International

[198] C. M. v. 4.4. Available: www.comsol.com.

[199] Y. Gu, S. Bandopadhyay, C.-f. Chen, C. Ning, and Y. Guo, "Long-term corrosion inhibition mechanism of microarc oxidation coated AZ31 Mg alloys for biomedical applications," (in English), *JMAD Materials and Design,* vol. 46, pp. 66-75, 2013.

[200] A. L. Yerokhin, X. Nie, A. Leyland, A. Matthews, and S. J. Dowey, "Plasma electrolysis for surface engineering," *Surface and Coatings Technology,* vol. 122, no. 2–3, pp. 73-93, 1999.

[201] A. B. Rogov and V. R. Shayapov, "Correlations between the optical emission spectra and microstructure of microplasma coatings on aluminum 2024 alloy," (in English), *APSUSC Applied Surface Science,* vol. 258, no. 11, pp. 4871-4876, 2012.

[202] P. American Institute of, "Journal of physical and chemical reference data," (in English), *Journal of physical and chemical reference data.,* 2004.

[203] R. O. Hussein, X. Nie, and D. O. Northwood, "A spectroscopic and microstructural study of oxide coatings produced on a Ti–6Al–4V alloy by plasma electrolytic oxidation," *Materials Chemistry and Physics,* vol. 134, no. 1, pp. 484-492, 2012.